ABSTRACT

Title of Dissertation: INVESTIGATION OF VESICULAR-MEDIATED TRANSPORT OF INTERCELLULAR ADHESION MOLECULE-1-TARGETED CARRIERS FOR TREATMENT OF LYSOSOMAL STORAGE DISORDERS

Rachel Lee Manthe, Doctor of Philosophy, 2017

Dissertation directed by: Associate Professor, Silvia Muro
Fischell Department of Bioengineering &
Institute for Bioscience and Biotechnology Research

Numerous cellular processes and therapeutic interventions rely on vesicular-mediated endocytosis to gain entry into cells and sub-cellular compartments, as well as for transcellular transport across biological barriers such as found at the blood-brain interface. Yet, endocytic behavior can be altered in disease, representing an additional hurdle in the design of effective therapeutic strategies. Lysosomal storage disorders (LSDs), characterized by lysosomal accumulation of undigested substrates as a result of deficient enzymatic activity, illustrate this paradigm. Currently, intravenous infusion of recombinant lysosomal enzymes to replace those deficient is the standard clinical approach for these disorders. However, clathrin-mediated endocytosis utilized by replacement enzymes for cellular uptake and lysosomal trafficking is altered, thereby impacting treatment efficacy

as recently demonstrated in acid sphingomyelinase-deficient type A Niemann-Pick disease (NPD). Therefore, alternative means to bypass defunct routes is warranted. Therapeutic delivery via polymer nanocarriers targeting intercellular adhesion molecule-1 (anti-ICAM NCs), a cell-surface molecule overexpressed in endothelial and subjacent tissue cells during inflammation, such as in LSDs, represents a viable option since it permits uptake, intra- and transcellular transport via a unique endocytic route called the cell adhesion molecule (CAM) pathway. In this dissertation, cell culture and animal models were used to examine the (1) endocytic activity of the CAM pathway and other clathrin-independent routes in type A NPD, (2) role of targeting valency (*i.e.*, density of ICAM-1-targeting molecules on the NC surface) in regulating the CAM pathway, and (3) effects induced via engagement of ICAM-1 on cells by anti-ICAM NCs. The results herein demonstrate the CAM pathway is more active in diseased cells compared to other classical endocytic pathways, making it the most amenable route for therapeutic enzyme replacement. Further, modulating targeting valency of NCs optimized this strategy for enhanced enzyme delivery to the brain, a target organ for type A NPD. Lastly, anti-ICAM NCs attenuated endothelial release of soluble ICAM-1, an inflammatory regulator, representing a secondary benefit of this system. Overall, this work validates utility of anti-ICAM NCs for enzyme replacement to treat NPD and likely other LSDs, and provides insight into biological processes and design parameters that influence the therapeutic efficacy of targeted drug carriers.

INVESTIGATION OF VESICULAR-MEDIATED TRANSPORT OF INTERCELLULAR ADHESION MOLECULE-1-TARGETED CARRIERS FOR TREATMENT OF LYSOSOMAL STORAGE DISORDERS

by

Rachel Lee Manthe

Dissertation submitted to the Faculty of the Graduate School of the
University of Maryland, College Park, in partial fulfillment
of the requirements for the degree of
Doctor of Philosophy
2017

Advisory Committee:
Professor Silvia Muro, Chair
Professor Peter Kofinas
Professor Daniel Nelson
Professor Wenxia Song
Professor Kimberly Stroka

Dedication

This work is dedicated to my parents, Kent and Barbara Manthe, for their unwavering love and support, and for teaching me by example the values of hard work, integrity, and perseverance.

Acknowledgements

First and foremost, I would like to acknowledge my mentor and advisor, Dr. Silvia Muro. Thank you for exuding a contagious passion for research, for providing continuous support and encouragement over the years, for sharing your immense expertise in the fields of cell biology and drug delivery, and for intellectually challenging me, while also providing great mentorship and guidance during completion of my dissertation research. It is because of your tremendous efforts and dedication that has ultimately cultivated my skills and knowledge as an independent researcher. I am also incredibly thankful for all the wonderful past and present members of the Muro Laboratory that I've had the pleasure of working alongside over the past six years. I would especially like to thank those who assisted in completion of this work, Jeff Rappaport, Dr. Daniel Serrano, and Dr. Melani Solomon. I also thank Dr. Steven Jay (Fischell Department of Bioengineering; University of Maryland, College Park) for use of the Nanosight LM10 instrument.

I am unbelievably fortunate to have also developed a number of great friendships during my time in graduate school. To Dr. Rasa Ghaffarian and Dr. Janet Hsu in particular, I am truly grateful for the life-long friendships we have developed during and outside of lab. I respect and admire you both in so many ways, and my life has been enriched professionally and personally by our friendship. I look forward to sharing many more experiences and memories together in the years ahead. As well, to Dr. Melani Solomon, you are truly an inspiration as a researcher, mother, and friend. Your boundless generosity and patience in helping others is unmatched, and your positive attitude, infectious smile and laughter were incredibly uplifting during even the most chaotic of times. Lastly, to

Nikša Roki, I hope you always stay curious. Along with your hard work and passion for research, you will do great things in the future.

Most importantly, I am truly blessed to have such an amazing support system in my parents, grandmother, and the entire Gross family. My achievements are a reflection of all your unconditional love and encouragement. Further, I cannot put into words how appreciative I am to have shared this journey with my amazing husband, Tyson Gross. Thank you for always being there to celebrate the good times and for being a crutch during the rough patches, for putting up with lost time spent together between late nights and weekends working, and for the other countless sacrifices you made in pursuit of my goal. I love you dearly and I cannot imagine anyone else by my side.

My graduate work was supported by the National Science Foundation Graduate Research Fellowship Program, the University of Maryland Flagship Fellowship and Future Faculty Program, and by the Ruth L. Kirschstein NRSA Individual Pre-Doctoral Fellowship of the National Institutes of Health.

Table of Contents

List of Tables

List of Figures

List of Abbreviations

Anti-ICAM…….Antibody targeted to intercellular adhesion molecule-1
ASM…….....Acid sphingomyelinase
BBB……....Blood-brain barrier
CAM……...Cell adhesion molecule
CNS……Central nervous system
CPM……..... Counts per minute
CTB……Cholera toxin B
EEA-1…….Early endosome antigen-1
EGF……Epidermal growth factor
ER…….....Endoplasmic reticulum
ERT…….Enzyme replacement therapy
HBMECs…….....Human brain microvascular endothelial cells
HUVECs…….....Human umbilical vein endothelial cells
^{125}I…….....Iodine-125
ICAM-1…….....Intercellular adhesion molecule-1
IgG…….....Immunoglobulin G
LAMP-1…….....Lysosome-associated membrane protein-1
LFA-1…….....Lymphocyte function-associated antigen-1
LSDs…….....Lysosomal storage disorders
M6P…….....Mannose-6-phosphate
Mac-1…….....Macrophage-1 antigen
MDC…….....Monodansylcadaverine
MMP…….....Matrix metalloproteinase
NCs…….....Nanocarriers
NHE1…….....Na^+/H^+ exchanger 1
NPD……Niemann-Pick disease
PKC…….....Protein kinase C
PLGA…….....Poly(lactic-co-glycolic acid)
RES…….....Reticuloendothelial system
SEM…….....Standard error of the mean
sICAM-1…….....Soluble ICAM-1
TCA…….....Trichloroacetic acid
Tf……...…….Transferrin
TGN…….....*trans*-Golgi network
TNFα…….....Tumor necrosis factor alpha
Wt…….....Wild-type

Chapter 1: Introduction and Overview

1.1. Motivation and Goals

Lysosomal storage disorders (LSDs) are a rare class of approximately 60 genetic diseases most commonly caused by dysfunctional acid hydrolases found within the lysosomal lumen [1]. As a result of this defect, undigested metabolites accumulate within lysosomes and, secondarily, within compartments of the endo-lysosomal and autophagic pathways [1-4]. Due to the role of functional lysosomal activity in maintaining cellular homeostasis [1, 5-8], such aberrant storage leads to pathology in peripheral organs, and often times the central nervous system (CNS) as well [1, 4, 9-13].

A number of therapies currently exist for LSDs, each having benefits and disadvantages depending on the particular LSD and its associated symptoms [9, 11, 12, 14-20]. Intravenous infusion of wild-type recombinant lysosomal enzymes to replace those deficient, known as enzyme replacement therapy (ERT), is the current clinical standard [11, 12, 16, 18-36]. In this approach, the replacement enzymes bind to mannose-6-phosphate (M6P) receptors on the surface of cells, followed by clathrin-mediated endocytosis and subsequent trafficking to lysosomes to degrade the storage material [9, 11, 16, 37]. While ERT has been successful for treatment of peripheral organs, this approach is still significantly hindered by rapid clearance from the circulation, potential for immunogenicity, inactivation by proteases, and the inability of these enzymes to cross the blood-brain barrier (BBB) [9, 12-16, 19, 25, 38-40]. Hence, neurological disorders that associate with at least half of all LSDs remain untreated with conventional ERT [9, 13, 15].

In order to circumvent the BBB, recombinant enzymes have been fused to affinity moieties (*e.g.*, proteins, peptides, etc.) that are recognized by receptors involved in clathrin-

mediated transport across this barrier, such as the insulin receptor, transferrin (Tf) receptor, low-density lipoprotein, and others [27, 41-44]. However, such approaches do not provide protection against enzyme degradation or offer control over delivery in the context of cellular uptake, lysosomal trafficking, enzyme release in lysosomes, transcytosis, etc. As an alternative strategy, nano-scale drug carriers (NCs) have tunable physiochemical properties and can be additionally functionalized with stealth polymers and/or biological agents to overcome these challenges [45-50]. Most commonly, NCs are targeted to cell-surface receptors involved in vesicular-mediated endocytic uptake, which is often accompanied by lysosomal trafficking, and in certain cases, transcytosis across cellular barriers [47, 51-56]. Consequently, lysosomal enzyme delivery via NCs has shown promise for treatment of LSDs [9, 16, 19].

Depending on the receptor targeted, endocytosis can occur via classical routes (*e.g.*, clathrin- or caveolae-mediated), or independent pathways that are currently less understood [47, 51, 53, 54]. However, recent work by our laboratory has shown altered clathrin-mediated endocytosis of acid sphingomyelinase (ASM) deficient in type A Niemann-Pick disease (NPD), resulting in diminished therapeutic efficacy [57]. Therefore, better understanding of the status of such vesicular-mediated pathways in LSDs is imperative to improve delivery of lysosomal enzymes or other therapeutics that rely on these routes for entry into and across cells.

Targeting enzyme-loaded NCs to intercellular adhesion molecule-1 (ICAM-1), a transmembrane glycoprotein expressed on the vascular endothelium and other cell types, is a particularly attractive strategy for LSD treatment [58-65]. Due to role of ICAM-1 in mediating leukocyte adhesion and extravasation into sites of inflammation, its expression

is upregulated during pathological states (*e.g.*, in LSDs) [66, 67], making it amenable for enhanced enzyme delivery to peripheral organs and the CNS. Importantly, multivalent NCs targeted to ICAM-1 (anti-ICAM NCs) induce cellular uptake via the cell adhesion molecule (CAM) pathway [68], a unique endocytic route that enables enzyme trafficking to lysosomes with enhanced degradation of the stored substrate [60-64, 69], as well as delivery across cellular barriers (*e.g.*, BBB) in cell culture and animal models [58-61, 65, 70-72]. Hence, utilization of the CAM pathway represents a viable treatment option for LSDs, especially those characterized by neurological defects. Interestingly, the CAM pathway is even functional when classical pathways are inhibited [57]. In fact, delivery of recombinant ASM via anti-ICAM NCs markedly increased enzyme uptake in type A NPD cells compared to free ASM, resulting in significant reduction of lysosomal storage and, consequently, restoration of the clathrin pathway [57, 62, 63]. Therefore, anti-ICAM NCs may provide an alternative route for therapeutic delivery in LSDs that associate with dysfunctional endocytic behavior.

In light of this information, the **overall goal** of this dissertation is to enhance our understanding of vesicular-mediated transport in LSDs and apply this knowledge to improve the design and efficacy of therapeutic strategies for these disorders. These goals are addressed in the following three specific aims:

Aim 1: Probe the status of vesicular-mediated transport in type A NPD.

Aim 2: Elucidate regulation of the CAM pathway in order to optimize therapeutic enzyme delivery via anti-ICAM NCs for type A NPD.

Aim 3: Examine potential effects of anti-ICAM NCs that may exacerbate inflammation in type A NPD.

First in **Chapter 3**, we build off our laboratory's recent finding of impaired clathrin-mediated endocytosis in type A NPD by examining potential alterations in caveolae-mediated endocytosis, macropinocytosis, and non-classical CAM-mediated endocytosis, followed by exploration of aberrancies in transcytosis via the clathrin, caveolar, and CAM pathways in this disease.

Based on the preliminary evidence described above, it appears exploiting the CAM pathway for enzyme delivery via anti-ICAM NCs is an advantageous strategy over conventional clathrin-mediated ERT. While we have learned much regarding the CAM pathway over the last decade, better understanding of its regulation is still needed in order to further optimize the design of anti-ICAM NCs for therapeutic applications. As such, in **Chapter 4** we focus on how anti-ICAM targeting valency (*i.e.*, number of targeting molecules per carrier) influences the CAM pathway, including anti-ICAM NC binding and associated cell-signaling, endocytic uptake, lysosomal trafficking, and transendothelial transcytosis, along with examination of the implications of targeting valency on therapeutic ASM delivery to the brain in cell culture and mice. In this work, we also paid particular attention to understanding the relationship between lysosomal trafficking and transcytosis, as well as how NCs dissociate from their bound receptor on the basolateral cell-surface after transcytosis, a phenomenon poorly studied for any given targeted drug carrier.

Lastly, an important consideration in the design of any drug carrier is the potential for effects that may hinder treatment efficacy or further exacerbate disease. Since ICAM-1 is a critical player in inflammation [73, 74], a condition found in many pathologies including LSDs [66], effects of blocking this receptor via anti-ICAM NCs warrants consideration in order to assess the safety of this treatment strategy. Therefore, **Chapter 5**

explores the effect of ICAM-1 engagement by anti-ICAM NCs on the release of an inflammatory regulator, soluble ICAM-1 (sICAM-1) [75, 76].

1.2. Significance and Novelty

Through completion of the aforementioned aims, this dissertation renders knowledge on vesicular-mediated transport in LSDs, NC design parameters, and cellular mechanisms regulating transport of anti-ICAM NCs via the CAM pathway, as well as potential side effects of utilizing anti-ICAM NCs for LSD therapy, which altogether will aid in guiding translational drug delivery for improved treatment of these disorders.

Given the reliance of many therapeutics on vesicular-mediated transport, understanding potential alterations in the pathways regulating these processes is paramount for rationale therapeutic design. Currently, clathrin-mediated endocytosis is known to be impacted in type A NPD [21, 57]. However, potential aberrancies in other routes that could be exploited for therapeutic delivery have not been investigated. Hence, the work presented herein along with present literature will help define the most amenable pathways for treatment of LSDs.

Delivery of recombinant lysosomal enzymes via anti-ICAM NCs has shown to be a viable and promising alternative to current ERT strategies [58-65, 69-72]. As mentioned in the prior section, the widespread distribution and overexpression of ICAM-1 in LSDs permits enhanced enzyme delivery to all peripheral organs affected [58, 60, 61]. Moreover, no treatment currently exists for neurological LSDs due to the tight barrier at the blood-brain interface [9]. Yet, our laboratory has demonstrated in several works that anti-ICAM NCs can be transported across cell culture models of the BBB and into the brains of mice

following intravenous administration [59-61, 65, 71, 72], offering for the first time a means to treat these particular LSDs, and perhaps other neurological disorders (*e.g.*, Alzheimer's, Parkinson's, Huntington's, etc.). In contrast to the classical clathrin and caveolar routes, the CAM pathway also permits uptake and intracellular trafficking of carriers with various sizes and geometries [62, 77-79], which offers flexibility in the design of enzyme carriers and represents a novel strategy in the field of drug delivery. As well, after anti-ICAM NC uptake, ~ 50% of the internalized ICAM-1 receptor recycles back to the plasma membrane within 1 h [80], permitting binding of anti-ICAM NCs left in the circulation or binding by a subsequent dose. Of great therapeutic potential, anti-ICAM NCs may also provide a means to circumvent defunct pathways in LSDs, such as recently found in the case of altered clathrin-mediated endocytosis in type A NPD [57].

To better understand regulation of the CAM pathway, we chose to study modulation of valency since it is an important design parameter of drug carriers that influences their targeting and overall avidity [47]. However, the effects of valency on associated cell-signaling and uptake, and more specifically lysosomal trafficking and transcytosis have not been extensively explored; yet, both are critical processes for successful treatment of LSDs, especially those associated with neurological impairments. Therefore, this work is significant because investigation into the effects of targeting valency will enable optimization of anti-ICAM NCs that permit sufficient binding and cellular uptake, while also providing maximum transport across the BBB for enhanced lysosomal enzyme delivery to the brain.

Another particularly interesting aspect of this work is our examination of the relationship between lysosomal trafficking and transcytosis of anti-ICAM NCs,

particularly whether they are independent pathways or sequential events, which is currently not well-known for any targeted drug carriers. Therefore, understanding these mechanisms is critical for development of carriers that can be tailored for intracellular accumulation and/or transcellular delivery to subjacent tissues, which are both desirable for treatment of LSDs, and may need to be differentially tuned for other applications.

Due to the multivalent nature of anti-ICAM NCs, they strongly bind to ICAM-1 receptors expressed on the surface of cells [81]. Yet, how these ligand-receptor complexes dissociate from their bound receptor on the basolateral cell-surface after transcytosis is another poorly understood process. In this dissertation, we provide preliminary work demonstrating a mechanism for basolateral detachment of transcytosed anti-ICAM NCs, while also shedding light on how targeting valency impacts this process. Altogether, this work will provide better understanding of ICAM-1 biology and the cellular events regulating transport, associated with ICAM-1 engagement of not only drug carriers but natural ligands (*i.e.*, leukocytes) as well, which holds great significance to the fields of vascular biology and drug delivery.

Lastly, little information is currently available regarding how carrier binding to their target receptor affects the receptor's physiological function. We explore this concept by examining the release of sICAM-1 in the absence and presence of anti-ICAM NCs. In doing so, this work will provide insight into the development of novel approaches using ligand-targeted drug carriers to exploit or modulate the function of a receptor in order to obtain a desired outcome.

Chapter 2: Background[1]

2.1. Lysosomes and Lysosomal Storage Disorders

Constituting approximately 5% of the intracellular volume of mammalian cells, lysosomes are acidic, membrane-bound organelles that play a crucial role in a number of cellular processes required to maintain homeostasis [6]. Therefore, any lysosomal aberration could potentially lead to disease. The most well-known class of diseases caused by dysfunctional lysosomes are the lysosomal storage disorders (LSDs), a group of approximately 60 different diseases characterized by lysosomal accumulation of non-degraded metabolites [1]. Although each particular LSD is relatively rare, the combined prevalence of these diseases is estimated to be 1 in every 2,000 live births, while the prevalence of some LSDs is much higher in certain populations, such as the case of Gaucher disease in the Ashkenazi Jewish population (1 in 855 births) [82].

2.1.1. Lysosome Structure and Function

Lysosomes are heterogeneous in size and morphology, and contain more than 50 acid hydrolases that function at a pH between 4.5-5.0 maintained by vacuolar H^+-ATPases [1, 6, 83, 84]. Along with activator molecules, these hydrolases are responsible for the degradation of different substrates (*e.g.*, proteins, lipids, sugars, nucleic acids) taken up

[1]Chapter 2 contains text, tables, and figures reproduced in part with permission from: (1) Manthe, R.L. and Muro. S., *Lysosomes and nanotherapeutics: diseases, treatments, and side effects.*, in *Handbook of Nanobiomedical Research*, V. Torchilin, Editor. 2014, World Scientific Publishing Co.: Singapore. Vol. 2, Chapter 8: p. 261-305; © 2014 World Scientific Publishing Co. (2) Rappaport, J., Manthe, R.L., et al., *Altered clathrin-independent endocytosis in type A Niemann-Pick disease cells and rescue by ICAM-1-targeted enzyme delivery.* Mol Pharm, 2015. 12(5): p. 1366-76; © 2015 American Chemical Society. (3) Manthe, R.L.* and Rappaport, J.*, et al., *A comparative study on the alterations of endocytic pathways in multiple lysosomal storage disorders.* Mol Pharm, 2016. 13(2): p. 357-68; © 2015 American Chemical Society.

from the extracellular environment via endocytosis [8]. Lysosomes also offer protection against foreign substances and pathogens that invade the cell, and contribute to the disposal of intracellular components that are no longer needed through a process called autophagy, where degradation of intracellular macromolecular assemblies render monomeric units that may be returned to the cytosol and recycled as new building blocks [1, 6, 8]. In addition, lysosomes play an important role in removing plasmalemma lipids and proteins, and repairing this structure after injury (*e.g.*, due to mechanical stress in muscle cells) [5, 7]. Plasmalemma disruption leads to increased intracellular calcium, which triggers targeted fusion of lysosomes to the plasmalemma for addition of a new phospholipid membrane to repair the damaged area [5, 7].

With regard to lysosomal hydrolases, these enzymes enter the rough endoplasmic reticulum (ER) during their synthesis [6, 16]. Oligosaccharides containing mannose residues are then added to these enzymes, followed by transport to the Golgi apparatus where phosphorylation of the mannose residues yields enzymes tagged with M6P [85, 86]. Binding of M6P residues to their respective receptors in the *trans*-Golgi network (TGN) mediates intracellular trafficking of these enzymes to lysosomes, where they dissociate from M6P receptors due to the acidic luminal pH in this compartment [85, 86]. Delivery occurs via multiple fusion and fission cycles with late endosomes, with M6P receptors being recycled back to the TGN [6]. In addition, a fraction of the lysosomal enzymes are secreted to the extracellular milieu via exocytosis [86, 87]. Secreted enzymes that contain M6P bind to M6P receptors on the surface of nearby cells, inducing clathrin-mediated endocytosis that results in transport to lysosomes [86, 87]. Some secreted enzymes contain mannose instead of M6P and can be taken up by mannose receptors on monocytes and

macrophages [87]. Lastly, lysosomes also contain highly glycosylated integral proteins in their membrane, including LAMP-1, LAMP-2, tetraspanin CD63 or LAMP-3, LIMP-2, etc. [8, 88]. These proteins assist in maintaining lysosome stability and integrity, transport of soluble metabolites out of lysosomes, and chaperone-mediated autophagy and macroautophagy [1, 88]. LIMP-2 also acts as a receptor for sorting several lysosomal proteins in an M6P-independent manner [6].

2.1.2. Lysosomal Storage Disorders

LSDs consist of about 60 different diseases affecting humans and several animal species [1]. Most of these disorders are caused by dysfunctional lysosomal enzymes, resulting in lysosomal accumulation of unmetabolized substrates, including lipids, glycoproteins, and glycosaminoglycans [1] (**Figure 1**). However, several LSDs are caused by defective integral membrane proteins, such as LAMP-2A in Danon disease and NPC1 in type C Niemann-Pick disease (NPC) [1]. Also in a number of LSDs, the primary defects affect proteins in the ER, Golgi, and endosomal pathways involved in the synthesis, modification, and trafficking of lysosomal proteins [1, 12, 89]. This is the case in mucolipidosis (ML) type II (I Cell disease) and ML type III (pseudo-Hurler polydystrophy), which cause lysosomal enzymes to be secreted from the cell [1]. Certain LSDs also associate with a more neutral lysosomal pH [90, 91] that affects hydrolase and vesicle maturation, intracellular trafficking, recycling of M6P receptors back to the Golgi, secretion, signaling, and other functions [9, 92, 93].

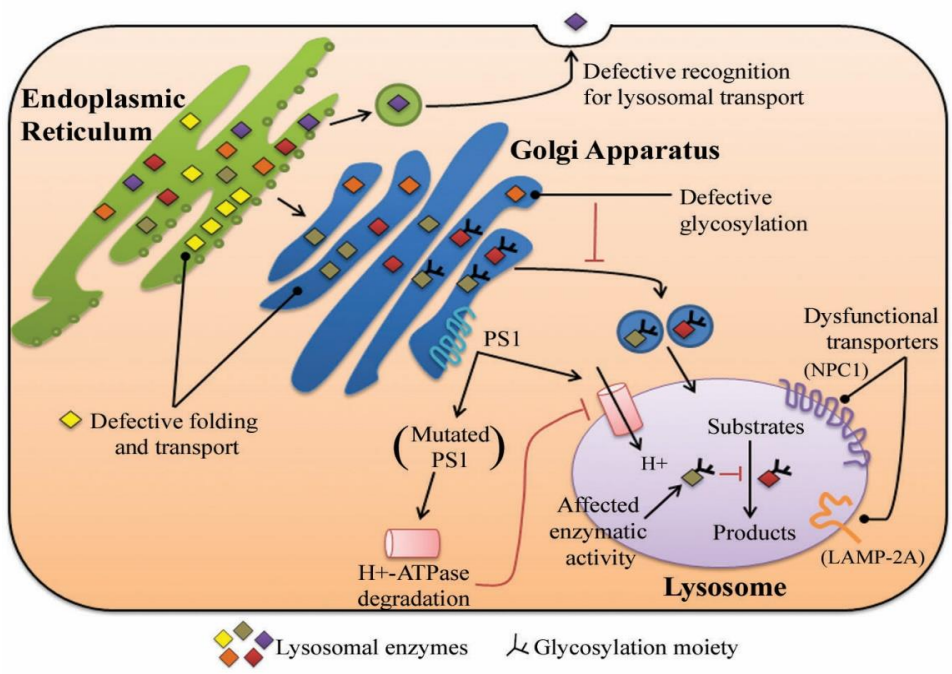

Figure 1. Overview of some aberrations identified in LSDs. Genetic mutations associated with LSDs cause dysfunctions in upstream compartments, lysosomal membrane components, and lysosomal enzymes, all of which affect lysosome function. Defects include incorrect folding of lysosomal enzymes in the ER, dysfunctional trafficking due to defective recognition or defective glycosylation, insufficient lysosomal acidification, and dysfunctional integral membrane proteins of the lysosome. Consequently, LSDs are characterized by aberrant accumulation of undigested substrates in the lysosome. Figure reproduced from [19].

All LSDs are monogenic diseases inherited as autosomal recessive traits, with the exception of Fabry disease, mucopolysaccharidosis (MPS) type II (Hunter disease), and Danon disease [12, 94]. In some cases, although only one gene is defective, the enzyme it encodes may modify the activity of several other enzymes [1], leading to multiple enzyme deficiencies such as in the case of multiple sulphatase deficiency (MSD) [95]. Depending on the age when clinical symptoms begin to develop, LSDs are classified as infantile, juvenile, or adult forms [1]. Since lysosomes are essential components of almost all cell types, the primary and secondary affects associated with LSDs manifest into a wide range of phenotypic symptoms in multiple tissues and organs [1]. Infantile forms are the most severe and involve dysfunction of the CNS [1]. CNS involvement is not limited to

newborns though, as late onset of LSDs characterized by neurological symptoms are also seen in juvenile and adult forms [1, 96]. Overall, at least half of all LSDs associate with severe CNS disorders (*e.g.*, seizures, dementia, ataxia, brainstem dysfunction, vision loss, movement disorders, etc.) that result in early death [1, 9]. Less severe LSDs manifest in infancy and progress slowly into adulthood, mainly causing peripheral disease, including damage to the liver, spleen, striated muscle, kidneys, lungs, bone, immune system, etc. [1, 9, 82]. Regardless, inflammation caused by oxidative stress and leukocyte activation from biochemical and metabolic stresses often causes the initial pathology to further spread and increase in severity [9, 20]. Moreover, multiple epigenetic and environmental factors contribute further to the phenotypic variability of LSDs [1, 82].

The prevalence and location of gene mutations frequently differ in patients with the same LSD and can lead to varying degrees of severity in patients [1]. For example, both types A and B Niemann-Pick disease (NPD) are caused by deficiency of acid sphingomyelinase (ASM), a lysosomal enzyme responsible for hydrolysis of sphingomyelin to ceramide, which results in aberrant sphingomyelin storage [97]. Despite both disorders being caused by ASM deficiency, patients with type A NPD suffer from severe neurodegeneration and have additional complications associated with visceral organs such as the lungs, liver, and spleen [97]. Consequently, most patients with type A NPD often do not survive past the age of three years old [97]. In contrast, type B NPD is less severe than type A and these patients have minimal or no neurological impairments; instead, they develop problems associated with visceral organs in early childhood, particularly hepatosplenomegaly and pulmonary dysfunction [97]. Deficiency of ASM activity in NPD has been found to be caused by more than 180 different mutations in the

SMPD1 gene that encodes this enzyme [97]. However, development of either type A or B NPD often depends on the particular genetic mutation and the level of remaining ASM activity in cells, which along with patho-physiological examination is used for diagnosis of either type of NPD [97-99]. Type A NPD associates with lower residual ASM activity and specific mutations (*e.g.*, R496L) have been linked to this disorder [97, 100-102]. In contrast, type B NPD associates with greater (yet still inadequate) ASM activity and common mutations (*e.g.*, deltaR608) causing this disorder have been identified as well [97, 100, 103, 104]. Epigenetic factors also seem to influence the correlation between genotype and phenotype for types A and B NPD [97, 103-105]. For example, just three mutations are known to account for nearly 90% of type A NPD in the Ashkenazi Jewish population [97], and a single mutation has been linked to more than 90% of patients with type B NPD in Chile [104]. As such, the relationship between genotype and phenotype are beginning to be made, as well as genetic screening for these disorders [97, 106]. Overall, in this work we particularly focused on type A NPD since this disorder is a good model to study both disease and therapies relative to CNS and peripheral LSDs.

Lastly, lysosomal substrate accumulation in LSDs also causes secondary accumulation in compartments of the endo-lysosomal and autophagic pathways [1-4]. For example, lysosomal storage can delay the rate at which autophagic vacuoles are processed or affect autophagosome-lysosome fusion, resulting in retention of materials in autophagosomes, as shown in Pompe disease, ML type IV, MPS type IIA, and MSD [2, 3, 107]. In cell culture models of MPS type IIIA and MSD, this effect associates with abnormal distribution of SNARE proteins in cholesterol-rich regions of the lysosomal

membrane, which locks the SNAREs in place and inhibits their capacity to assist in autophagosome-lysosome fusion [108].

Some of these systems, particularly autophagy components, are also impaired in non-LSD diseases, including neurodegenerative disorders, inflammatory diseases, and a variety of cancers [3, 109-113]. In the case of neurodegenerative diseases such as Alzheimer's, Huntington's, and Parkinson's diseases, patients progressively lose cognitive and motor abilities due to neuronal death resulting from protein accumulation in autophagic vacuoles, which is similar to the neurological effects of LSDs described above [110-112, 114]. In Alzheimer's disease, as an interesting example, dysfunction of the autophagic pathway, resulting in amyloid plaques, is caused by defective lysosomal proteolysis [114], leading to the accumulation of undigested substrates in lysosomes and autophagic vacuoles within dystrophic axons and dendrites [111]. The cause of this dysfunction is mutated presenilin-1 (PS1), which affects proper glycosylation and transport of vacuolar H^+-ATPases, resulting in poor lysosome acidification and, hence, poor activation of lysosomal hydrolases (see **Figure 1**) [111].

Apart from the autophagic pathway, several groups including our laboratory have also observed alterations in the behavior of endocytic receptors and their associated pathways in LSDs [21, 57, 115-121]. Consequently, these alterations impact intracellular delivery and effects of therapeutic lysosomal enzymes [21, 57, 121], such as the case of ASM required for NPD treatment [21, 57]. Alterations in vesicular-mediated transport are further explored in **Chapter 3**.

2.1.3. Clinical and Experimental Treatments for LSDs

A number of strategies have been proposed to treat LSDs and are summarized in **Table 1** [9, 11, 12, 14-20]. Organ or cell transplantation has been clinically implemented to alleviate phenotypic symptoms in several LSDs, such as Gaucher, Pompe, and Krabbe diseases, among others [16, 20]. Organ transplantation, commonly of the liver and kidneys, is performed in severe cases of organ failure [1]. Alternatively, cell therapy involves transplantation of healthy bone marrow or mesenchymal stem cells [122], which can then secrete normal or wild-type lysosomal enzymes and be endocytosed with transport to lysosomes in neighboring diseased cells for repair of the defective enzyme activity (cross correction effect) [16, 37]. These options alleviate LSD symptoms in organs of the reticuloendothelial system (RES), but are limited in scope due to lack of suitable donors and graft rejection [122].

Table 1. Examples of different treatment modalities for LSDs.

Treatment	Goal	LSD Examples	Bottlenecks	Refs.
Organ transplantation	Replacement of damaged organ(s) (*e.g.*, liver and kidneys)	Fabry and Cystinosis	Limited to treatment of peripheral organs; graft rejection; lack of suitable donors	1, 16, 137
Cell therapy	Transplantation of normal cells from a healthy donor	Sandhoff; GM1 gangliosidosis; Tay-Sachs; Pompe; Gaucher; Krabbe; Hurler; others	Limited to treatment of peripheral organs; graft rejection; lack of suitable donors	16, 20, 122
Gene therapy	Use of viral vectors to deliver exogenous lysosomal gene sequences to restore functional enzyme activity	Sanfilippo; Pompe; Fabry; Sandhoff; NPC; Gaucher; MPS type VII; other MPS types	Often limited to treatment of peripheral organs; safety concerns (potential for immunogenicity and random insertion into host gene)	20, 123-132
Substrate reduction therapy	Block synthesis of accumulating substrates	Gaucher; Fabry; Tay-Sachs; NPC; Cystinosis; others	Lack of complete inhibitor specificity; potential side effects of depleting substrate	12, 133-136
Use of chemical chaperones	Assist in correct folding of lysosomal enzymes	Gaucher; Fabry; GM1 gangliosidosis	Requires knowledge of the particular mutation(s); limited to LSDs caused by incorrect enzyme folding	141-143
Use of cytosolic molecules	Reduce substrate storage by increasing levels of cytosolic molecule(s) involved in vesicle trafficking	NPC	Limitations associated with use of gene therapy or protein transduction to increase levels of the cytosolic molecule(s)	16, 144
Enhanced lysosome exocytosis	Lysosomal exocytosis to reduce substrate accumulation	NPC; Wolman; Batten; Fabry; Farber; several others	Loss of lysosomes with functional enzymes; disruption of autophagic processing	145-149
Enzyme replacement therapy	Replacement of defective lysosomal enzyme(s) with recombinant enzyme(s)	Hurler; Hunter; Sanfilippo type A; MPS type VI and VII; Fabry, Gaucher type I-III; Pompe; Krabbe; Sandhoff; others	Rapid clearance from the circulation; inactivation by proteases; reduced access through tissue and cellular barriers; immunogenicity	11, 12, 16, 18-36

Table adapted from [19].

Gene therapy is a treatment option with great promise in terms of therapeutic efficacy [20, 123, 124]. Various viral vectors (*e.g.*, adenovirus, adeno-associated virus, retrovirus, and lentivirus) have been utilized for delivery of wild-type cDNA sequences into diseased cells to restore functional enzymes and tested in clinical trials for several LSDs [20, 123-126]. The efficacy of this approach is greater in peripheral organs, especially those of the RES, while CNS treatment remains elusive and, hence, intracerebral administration and alternative approaches are being explored [9, 124, 127-132]. The overall safety of gene therapy (*e.g.*, immunogenicity, random insertion in the host genome) is also being investigated [9, 124].

Small molecule therapies have also been explored, including substrate reduction, chemical chaperones, and cytosolic molecules [9]. In substrate reduction therapy, inhibitory molecules reduce the biosynthesis of accumulating substrates, such as *N*-butyldeoxynojirimycin (Miglustat or Zavesca®), which has been tested for Fabry and Tay-Sachs [133, 134], and is clinically approved for Gaucher disease [135]. Cysteamine is another substrate inhibitor successfully used to treat Cystinosis [136, 137], and genistein is currently in clinical trials for treatment of MPS [135]. However, lack of complete specificity and long-term effects of impairing anabolic routes need to be fully investigated. Certain accumulated metabolites can be removed using small molecules such as cyclodextrins, which have been shown to remove excess cholesterol and glycosphingolipids in a mouse model of NPC disease [138] and are currently in clinical trials for treatment of this disorder [139, 140]. In addition, some of these inhibitors act as chemical chaperones that assist in lysosomal protein folding and are being explored in clinical trials for treatment of Gaucher, Fabry, and GM1 gangliosidosis [141-143]. This is

helpful in the case of mutations that cause incorrect enzyme folding (not affecting the catalytic site) and facilitates transport into lysosomes since misfolded enzymes often accumulate in upstream compartments [143].

Other approaches have focused on lysosomal-associated transport. When substrate accumulation is due to defective lysosomal transport, storage can be reduced by increasing intracellular levels of the molecules controlling intracellular vesicle trafficking [9]. This is the case of Rab9 overexpression, which reduces cholesterol and sphingolipid storage in NPC disease [144]. However, increasing intracellular levels of cytosolic molecules requires gene therapy or protein transduction and, therefore, is bound to the limitations of these methods. Alternatively, inducing lysosome exocytosis helps release non-degraded metabolites extracellularly, which can be achieved through use of cyclodextrins, δ-tocopherol, or by overexpression of transcription factor EB (TFEB) [145-149].

Lastly, ERT is the most widely used clinical therapy for LSDs with several products currently FDA-approved or in different phases of clinical trials for treatment of Gaucher, Fabry, Pompe, several types of MPS, and a few other LSDs [18, 30-36]. In this approach, wild-type recombinant lysosomal enzymes are intravenously infused in patients to replace those absent in the disease [16]. Glycosylation motifs on these enzymes bind to cell-surface M6P receptors, or the enzymes can be modified to target other clathrin-associated receptors [9, 11]. In principle, cells then take up the enzymes via clathrin-mediated endocytosis and deliver them to lysosomes to clear stored substrates [9, 11]. ERT relies on the cross correction effect and the fact that relatively low amounts of the ‘correcting enzyme’ (≤ 10-20% of endogenous levels) are needed for therapeutic effects [37]. Although this therapy has proven valuable with regard to treatment of peripheral tissues, several limitations

reduce its efficacy, including rapid clearance from the circulation, inactivation by proteases, immunogenicity with production of antibodies against recombinant enzymes, and the inability of recombinant lysosomal enzymes to cross the blood-brain barrier (BBB) [9, 12-16, 19, 25, 38-40]. Several approaches have focused on overcoming these caveats, including optimization of enzyme glycosylation, modification of said residues, or enhancement of mannose or M6P receptor expression to improve enzyme targeting [21, 22, 29, 87].

ERT via glycosylation-independent mechanisms is another option achieved by designing fusion proteins that contain the enzyme fused to an affinity peptide for recognition by cell-surface receptors [16]. Examples of this strategy have been shown to improve delivery of several LSD enzymes through use of insulin-like growth factor II (ILF-II) peptides to target M6P receptors, receptor-associated protein that binds to low-density lipoprotein receptors, or others, all of which result in clathrin-dependent endocytosis and lysosomal transport [9, 23, 27, 41-44]. Chimeras containing protein transduction domains (*e.g.*, HIV Tat) have also been used to improve charge-mediated binding to the plasma membrane, followed by passive endocytic uptake and/or penetration through the plasmalemma [24, 26, 28].

Although certainly valuable, most these approaches are suboptimal, which has resulted in a limited number of clinically-approved ERT for peripheral organ treatment in a small fraction of LSDs [11, 13, 150]. As such, ERT is advantageous for type B NPD and, in fact, a recombinant form of ASM (Olipudase Alfa®) is currently in phase II/III of clinical trials for this disease after phase Ib studies showed minimal adverse reactions and decreased sphingomyelin levels, which resulted in reduction in the volumes of the spleen

and liver, and improved patient quality of life [151]. However, there are currently no treatments approved nor under investigation in clinical trials for the majority of LSDs that are characterized by neurological dysfunctions, such as in the case of type A NPD [9, 13, 15, 97]. Hence, there is a compelling need for more effective approaches for enzyme replacement to adequately address these diseases.

2.2. Nanocarriers for Drug Delivery

Nanotechnology has had a profound impact on the medical field, including delivery of therapeutic agents such as small chemicals, and protein- and nucleic acid-based therapeutics [45, 50]. Nano-scale (< 1 μm) drug delivery systems (nanocarriers; NCs) can be fabricated from a wide array of materials including synthetic, semi-synthetic, and biological products to form structures with unique compositions and architectures [45, 50]. To improve the efficacy of therapeutic agents, NCs must be able to overcome the barriers that limit the efficacy of drugs in solution, such as issues with poor drug solubility and stability, rapid degradation and/or clearance from the circulation, systemic toxicity, poor accumulation in disease target sites, difficulty in maintaining drug concentrations within therapeutic windows, and subcellular transport to the molecular targets requiring therapeutic intervention [47, 48] (**Figure 2**). These factors can be controlled by the physicochemical properties of the NC, which can be modified by additional functionalization with polymers and biological compounds [46, 49].

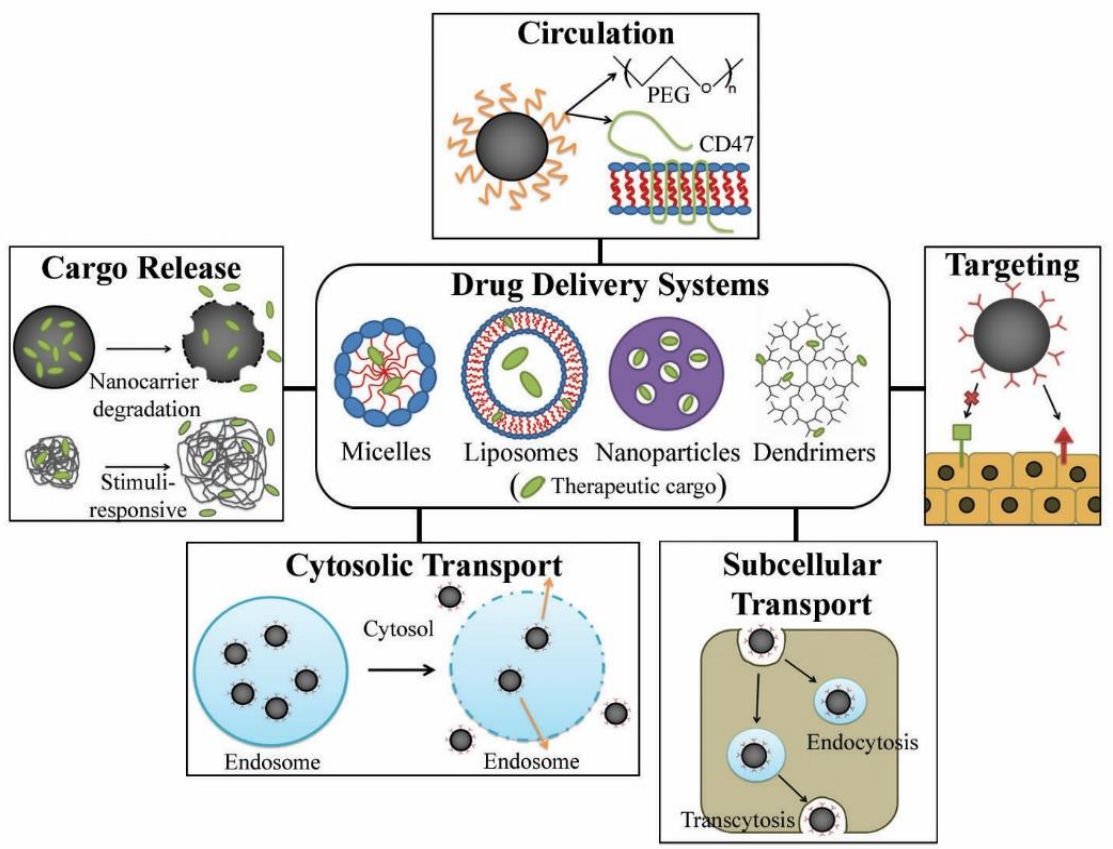

Figure 2. Structure and function of drug delivery systems. Various types of drug delivery systems currently exist and provide enhanced therapeutic efficacy compared to drugs in solution due to their ability to prolong circulation, bind to specific sites, and gain access to therapeutic targets of interest through enhanced transcellular, intracellular, and cytosolic transport, while also providing control over cargo release. Figure reproduced from [19].

2.2.1. Nanocarrier Types and Properties

Liposomes are the oldest and probably most investigated drug delivery system [152]. Based on natural phospholipids found in cellular membranes, liposomes self-assemble in aqueous solution into bilayered spherical vesicles with a diameter ranging from 50 nm to several μm [153, 154]. Their main advantage derives from the amphiphilic nature of phospholipids, allowing for hydrophilic molecules to be entrapped in the liposome inner aqueous lumen or onto its surface, while hydrophobic molecules partition into the bilayer [46]. Liposomes also have low toxicity and can be functionalized to improve their

circulation time and to provide site-specific targeting [49, 153]. They have modest drug-loading capacity and can tolerate a low degree of the aforementioned modifications, which affects their stability and clearance [155, 156].

Closely related to liposomes are polymersomes and polymeric micelles. Polymersomes are analogous to liposomes, but are composed of amphiphilic block copolymers as opposed to phospholipids [153, 157]. They also form bilayered vesicles of a comparable size range and can be loaded with hydrophilic and hydrophobic agents [153]. While polymersomes are more rigid and less permeable to drugs than liposomes [153], they allow for a higher degree of functionalization, chemical stability, and structural control [153, 157]. Amphiphilic block copolymers can also self-assemble into micelles (a few nm in diameter), which possess only an inner hydrophobic core and an outer hydrophilic layer [48, 153]. They can be functionalized for targeting, have low toxicity and high loading capacity for water-insoluble drugs, and offer advantages including simplicity of preparation, controlled release profile, and prolonged blood circulation time [48, 153].

NCs fabricated from biodegradable polymers (synthetic, natural, or hybrid) have become one of the most popular drug delivery systems due to their versatility as therapeutic carriers [48, 158, 159]. They can exist in a variety of shapes and sizes (10-1,000 nm) as hollow or solid structures with varying degrees of porosity [153, 160]. The therapeutic agent can be encapsulated, adsorbed onto the carrier surface, or dispersed throughout the polymer matrix [46, 48]. Control of drug release can be achieved via diffusion, surface erosion, or bulk degradation of the NC over a period of time [153, 160].

With regard to materials, some of the most commonly used biocompatible synthetic polymers are polyanhydrides, polyorthoesters, polycaprolactone, polylactides,

polyglycolides, poly(lactide-co-glycolides), poly(methyl methacrylate), poly(acrylic acid), poly(vinyl alcohol), and poly(ethylene glycol), which is commonly referred to as PEG [161, 162]. Poly(lactic-co-glycolic acid) (PLGA) is one of the most widely investigated polymers for NCs because of its FDA-approval (owing to its good biocompatibility) [163] and controllable rate of degradation (hence, controlled drug release) via modification of particle size and the ratio of lactic to glycolic acid [160]. PEG is also widely used in drug delivery systems because of its ability to solubilize hydrophobic drugs and its relatively low interaction with components of the immune system, thereby allowing for prolonged blood circulation [160, 164]. Since some synthetic polymers have somewhat poor batch-to-batch variability and residual chemicals from their fabrication may pose safety concerns [153], natural polymers such as chitosan, gelatin, albumin, natural gum, and sodium alginate are also utilized [162]. A number of polymers are also sensitive to biologically-relevant stimuli such as changes in pH, which results in swelling of the drug delivery system with concomitant drug release [165, 166]. These polymers include chitosan, polyethylenimine, poly(acrylic acid), poly(L-lysine), and others [165, 166].

Other nano-scale systems are based on inorganic materials, such as silica NCs, metal NCs, quantum dots, and carbon nanotubes [48]. While often used in diagnostic applications, these carriers are also advantageous for drug delivery due to their small size (< 50 nm) and ease of functionalization with targeting moieties, drugs, etc. [48]. However, they are still under investigation in regard to their safety. Some of these systems also possess inherent imaging capability, allowing for real-time monitoring of biodistribution and treatment efficacy [167-169]. One relevant example is that of 10-100 nm superparamagnetic iron-oxide NCs [48, 167, 169], which have become popular for drug

delivery applications because they are relatively biocompatible, biodegradable, can serve as an MRI contrast agent [48, 167], and their distribution can be manipulated by applying an external magnetic field over the desired area of accumulation [167].

2.2.2. Targeting Strategies

Regardless if therapeutic intervention is required at one localized site or at multiple sites throughout various organ systems in the body, targeting can enhance the efficacy of drug delivery systems by maximizing their bioadhesion [45, 47]. This can be achieved in a non-specific manner by targeting common elements (*e.g.*, negative charge of the cell-surface, affinity to ubiquitous macromolecules) or more specifically by taking advantage of physiological features unique to the diseased tissue, including increased vascular permeability (passive targeting) and specific cell/tissue markers that are overexpressed during the pathological state (active targeting) [47, 170]. Specific targeting helps maintain therapeutic levels of a drug at the diseased site(s) while minimizing potential side effects in healthy tissues [45, 47].

The most common passive targeting strategy is the enhanced permeability and retention (EPR) effect exploited in cancer therapy, which takes advantage of the leaky vasculature of tumor areas to enhance NC accumulation within the cancerous tissue [171]. NCs that rely on the EPR effect are approved clinically for the treatment of several cancers [48]. A representative example is Doxil, a PEGylated liposome that encapsulates the chemotherapeutic agent doxorubicin, used in the treatment of ovarian cancer, breast cancer, and Kaposi's sarcoma [48]. The EPR phenomenon also occurs in other diseases where inflammatory processes have disrupted the permeability barrier of the vascular

endothelium, such as in infection, infarction, rheumatoid arthritis, etc. [48, 164]. Similar to the EPR effect, NCs also accumulate within organs characterized by discontinuous blood vessels that do not present a barrier to diffusion of compounds, such as the liver and spleen [47]. By the first pass phenomenon, NCs can also be passively targeted to organs directly downstream of the administration site via normal blood flow [47].

In some disorders where multiple organ systems are affected, non-specific active targeting can enhance ubiquitous delivery of NCs throughout the body [9, 14]. This can be achieved by relying on non-specific interactions of NCs toward general biological features, such as in the case of positively-charged moieties in HIV Tat peptide, RGD counterparts, and other sequences that can provide affinity to the negatively-charged plasmalemma of cells [47, 172]. Coating NCs with cationic polymers, such as chitosan, serves a similar purpose [165].

Specific active targeting is typically employed when localized treatment is required [47]. This is achieved by addressing NCs to specific markers of diseased sites (including extracellular or cell-surface determinants) using affinity moieties such as proteins and peptides, antibodies and their fragments, sugars, and aptamers [47, 173, 174]. Targeting moieties can be coupled to NCs via hydrophobic or electrostatic interactions, chemical conjugation, etc. [47]. This approach can also be designed to target specific cell-surface receptors involved in vesicular-mediated endocytic transport into or across cells as discussed below [47, 175]. As well, the number of targeting moieties per carrier (*i.e.*, valency) influences their avidity, binding, uptake, intracellular trafficking, transcytosis, and biodistribution, and can therefore be modulated to achieve a desired outcome [59, 79, 176-180].

2.2.3. Transport into Cells and across Cellular Barriers

In most cases, the targets for therapeutic action are intracellular; hence, once drug carriers reach the diseased tissues they must gain access to particular intracellular compartments to act on the molecular component(s) responsible for a given pathology [45, 47, 52, 174]. Most commonly, this requires drug delivery to the cell cytosol for action in this location or in order to gain access to other organelles [45, 47]. Physical mechanisms such as ultrasound or electroporation can be used to temporarily increase the permeability of the plasma membrane for entry into the cytosol, although these techniques are only applicable locally and/or are relatively toxic [47, 181]. Alternatively, some toxins or positively-charged cell-penetrating peptides that achieve cell-surface binding via forming pores or by electrostatic interactions, respectively, can facilitate translocation through the phospholipid bilayer [172, 182]. This route is typically restricted to molecular conjugates rather than larger NCs and also lacks site-specificity since it mainly exploits general plasmalemma features [47]. In order to improve these aspects, endocytosis is often used [47, 183].

Through endocytosis, cells internalize plasma membrane components, extracellular materials, and objects bound to the cell-surface in membrane-bound vesicles that pinch off into the cytosol [53]. This process occurs via distinct pathways, each having a different biological role and relevance to drug delivery [53, 54, 184]. The most common pathways are those that internalize fluid and dissolved solutes, termed pinocytosis, some of which also concentrate cell-surface receptors with affinity for specific extracellular ligands [53, 54, 184]. The most ubiquitous pinocytic pathway is clathrin-mediated endocytosis, which regulates receptors involved in cell-signaling and uptake of ligands such as low-density

lipoprotein, M6P, Tf, etc., as mentioned previously [185]. This route has been widely targeted for delivery of therapeutics, drug conjugates, and carriers bearing clathrin-associated ligands [51, 53, 185]. Another common pinocytic pathway is caveolae-mediated endocytosis, characterized by caveolin-1-rich vesicles that form in lipid raft domains of the plasma membrane [186]. Therapeutics bearing albumin, cholera toxin B (CTB), or antibodies to aminopeptidase P, PV1, GM1, and other caveolae components have been shown to internalize within caveolar vesicles [47, 51, 187]. Given the small size of endocytic vesicles resulting from these two pathways, commonly within 50-200 nm in diameter, pinocytosis via the clathrin- and caveolae-mediated routes is also referred to as micropinocytosis [51, 54]. Conversely, in the third classical pinocytic mechanism, macropinocytosis, vesicles do not concentrate specific receptors but instead internalize large volumes of fluid (vesicle diameter > 500 nm) to promote cell growth, sample antigens, etc. [188]. Hence, macropinocytosis is amenable for uptake of drug delivery systems with a variety of sizes and shapes [47, 175]. Although especially active in macrophages and dendritic cells, this pathway can be transiently induced by epidermal growth factor (EGF) in other cell types, therefore also playing a key role in biology and drug uptake [56, 188]. In addition to these classical pinocytic pathways, less common routes have been observed in association with certain cell-surface receptors, including CAM-mediated endocytosis induced by binding to ICAM-1 [68], as well as that of GPI-anchored proteins, IL-2β receptor, and bound growth factors [189].

Intracellular trafficking and the final destination of internalized material is often determined by the endocytic route targeted [47]. In some instances, clathrin- or CAM-mediated endocytosis can deliver contents back to the cell-surface via recycling endosomes

[80, 190, 191]. Instead, the caveolar pathway may lead to retrograde transport to the Golgi apparatus or the ER [47]. Most commonly though, materials internalized by endocytosis, including drugs and drug carriers, traffic to lysosomal compartments [47]. This can be an obstacle to therapy when drugs and/or their carriers get trapped and degraded in lysosomes, or an advantage when lysosomal features (enzymes, pH, etc.) can be exploited to control drug release or trigger escape to the cytosol [19, 54, 184]. In addition, endo-lysosomal trafficking is required in diseases where the therapeutic target is the lysosome itself, such as in LSDs [9, 19, 184].

Targeting of pathways associated with transport across cellular barriers is also necessary for NC accumulation in tissues and can be achieved by endocytosis in certain instances [9]. Prominent examples of such cellular barriers are the endothelial lining of the BBB and the epithelial lining of the gastrointestinal tract, where tight junctions between neighboring cells prevent free transport of substances between the blood and tissue [192, 193]. To overcome these permeability barriers, paracellular and transcellular pathways are utilized [9]. The paracellular route involves transport between neighboring cells via transient disruption of tight junctions, which can be induced by certain NCs (*e.g.*, small dendrimers) or by application of hyperosmotic solutions, vasoactive agents, ultrasound, solvents, or stabilizers [194-197]. Since this route is often associated with leakage of substances between the compartments separated by the barrier, the transcellular route is used as an alternative [9]. This involves NC binding to specific receptors located on the apical surface of cells that constitute the barrier, followed by endocytosis, trafficking across the cell body, and final exocytosis from the basolateral cell-surface [9]. This process is

called transcytosis and can be induced by targeting certain receptors associated with clathrin-, caveolae-, or CAM-mediated endocytosis [70, 71, 175, 198-200].

2.3. Lysosomal Delivery of Nanocarriers

To overcome the limitations posed by current LSD therapies, NC systems are being explored. During the 1970s and early 1980s, liposomes were utilized to improve ERT [201-206]. However, with the development of a greater variety of drug delivery systems in recent years [45, 50], new opportunities exist for the treatment of LSDs.

2.3.1. Nanocarriers for ERT

As discussed in **Section 2.1.3**, ERT is a promising treatment option for patients with LSDs and are clinically available for a small number of these diseases. However, delivery of 'naked' recombinant enzymes poses several limitations, including limited circulation, lack of protection from premature degradation, immunogenicity with production of antibodies, suboptimal targeting, lack of transport across cellular barriers such as the BBB, limited regulation over the subjacent endocytic uptake and lysosomal transport mechanism, and lack of control over enzyme release rate in lysosomes [9]. Unfortunately, the use of fusion proteins improves only aspects related to targeting and uptake [16]. Overall, these drawbacks make ERT a limited and expensive treatment averaging several hundred-thousand dollars per patient each year [36, 207-210].

To overcome these obstacles, recombinant lysosomal enzymes can be coupled to drug delivery carriers [9] (**Table 2**). Enzyme encapsulation can protect from degradation and offer control over the release rate [9]. Addition of 'stealth' polymers such as PEG to

the NC surface can help protect against degradation by proteases, immunological responses, and prolong systemic circulation [211, 212]. As well, targeting can be improved by coating NCs with multiple copies of affinity moieties, which enhances their overall avidity due to multivalency [81], thereby allowing selection over the mechanism of transport across cellular barriers and into cells [9]. Enzyme-carrying systems can also be co-loaded with small cell-permeable compounds so that lysosomal degradation of NCs releases these cargoes within the cell for combined therapeutic interventions (*e.g.*, using recombinant enzymes and small molecule treatments) [9].

Table 2. Advantages of using NCs in ERT for LSDs.

Challenges of ERT for LSDs	How NCs Overcome Challenges
Rapid clearance from the circulation	PEG or other stealth strategies; modification of NC physicochemical properties
Loss of enzyme activity by proteases or generation of blocking antibodies	NCs provide protection by encapsulation or by posing steric hindrance to proteases and the immune system
Glycosylation defects of lysosomal enzymes	Use of glycosylation-independent mechanisms for enzyme targeting
Preferential accumulation in the RES	Carrier functionalization for active targeting
Inadequate transport across tissue and cellular barriers	Carrier functionalization to enhance transport
Gaining cell entry	Targeting cell-surface receptors involved in various forms of endocytosis
Need frequent administrations due to inefficient delivery and lack of sustained release	NCs provide controlled release of cargo by modulation of NC composition

Table adapted from [19].

Liposomes were the first drug delivery systems investigated in the context of LSD treatments. Initial studies conducted during the 1970s and early 1980s tested the potential of liposomes for enzyme delivery of β-fructofuranosidase, α-mannosidase, β-glucuronidase, β-glucosidase, and β-galactosidase [201-206]. *In vivo* performance of each

formulation depends heavily on the physicochemical properties of the liposome, which can be influenced by the phospholipid composition, entrapped lysosomal enzyme, preparation method, etc. [202-204, 206]. For example, liposomal formulations showed enhanced uptake of β-glucuronidase (MPS type VII) in the liver, whereas negatively-charged liposomes accumulated in lysosomes more efficiently and positively-charged liposomes showed longer enzyme activity (11 versus 2 days) [204]. The addition of PEG to liposomal formulations also enhanced both enzyme delivery and prolonged activity in lysosomes [213]. In cases where lysosomal delivery is required to treat immune cells (*e.g.*, Batten disease) [214, 215], liposomes can be coated with autologous heat-aggregated IgG or apolipoprotein E to enhance accumulation in lysosomes of polymorphonucleocytes [214]. In a similar technique, phagocytes were targeted by liposomes coated with heat-aggregated isologous IgM [215]. More recently, liposomes modified with lysosomotropic agents (*e.g.*, octadecyl-rhodamine B (Rh)) and loaded with velaglucerase alfa (VPRIV™) for ERT of Gaucher disease type I were shown to improve uptake by monocytes and fibroblasts in culture, accumulation in lysosomes, and enzymatic activity [216-218]. As well, addition of RGD peptides to liposomes significantly enhanced the delivery of recombinant α-galactosidase, resulting in reduced lysosomal storage in a cell model of Fabry disease [219].

Apart from liposomes, limited work has been published on the use of other drug delivery systems for LSD enzyme replacement. At the micro-scale, calcium alginate microspheres loaded with glucocerebrosidase have been tested in cell culture to mimic local implantation in Gaucher disease type I [220]. This would achieve prolonged enzyme release in areas of the body that are difficult to access from the circulation, as current ERT

by intravenous administration is suboptimal at alleviating bone pathologies characteristic of this disease [220]. Immobilization of lysosomal enzymes on magnetic microparticles has also been reported [221].

At the sub-micrometer scale, several NC modalities have been used for endocytic uptake in cells other than those of the immune system. With regard to inorganic particles, quantum dots with surface-immobilized enzymes resulted in lysosomal transport with sufficient enzyme delivery to restore normal substrate levels in a cell culture model [222]. Gold NCs (13 nm) coated with cell-penetrating peptides (penetratin and Tat) and lysosomal sorting proteins (L1 and L2) showed targeted localization into lysosomes in cell cultures and have been proposed to be applicable for delivery of lysosomal enzymes [223]. As per polymer-based carriers, polyelectrolyte-based complexes (< 200 nm) of trimethyl chitosan displayed pH-dependent dissociation of α-galactosidase with enzyme release within the lysosomal compartment in a cell culture model [224]. Moreover, biodegradable PLGA NCs modified with a small glycopeptide appear promising for therapeutic enzyme delivery across the BBB in mouse models of MPS type I and II [225]. Lastly, delivery of α-galactosidase (deficient in Fabry disease) via NCs comprised of human serum albumin and silk worm-derived 30Kc19 protein have also recently been shown to have enhanced cellular uptake, stability, and degradation of the accumulated lysosomal substrate in patient fibroblasts [226].

Overall, these approaches have shown enhanced enzyme circulation and accumulation in the CNS and RES organs *in vivo*, or improved enzyme stability with lysosomal transport and activity in cell cultures.

2.3.2. ICAM-1-Mediated ERT

Long after the liposomal studies of the 1970s and 1980s, the first strategy that attempted delivery of recombinant lysosomal enzymes using NCs was published in 2004 and focused on targeting ICAM-1 using model polymer NCs (~200-250 nm) coated with anti-ICAM antibodies (anti-ICAM NCs) [63]. ICAM-1 is a transmembrane, immunoglobulin-like glycoprotein involved in inflammation [66, 67] and was selected for targeting because of several reasons. ICAM-1 is expressed on most cell types in the body, which is amenable for targeting both peripheral organs and the CNS via different modes of administration (*e.g.*, intravascular, intrathecal, and others) [66]. It is particularly overexpressed during pathology, including inflammation associated with LSDs, which can provide preferential targeting to most affected sites [66]. ICAM-1 is abundant on endothelial cells lining the vasculature, in direct contact with lysosomal enzymes injected into the circulation, and is uniquely involved in mediating transcellular extravasation of leukocytes from the bloodstream to tissues without opening of the cell junctions, which may facilitate transport across cellular barriers [66, 67].

In addition, ICAM-1 has been found to mediate endocytosis with transport to lysosomes via CAM-mediated endocytosis [68] (**Figure 3**). This is a unique mechanism different from classical macropinocytosis, phagocytosis, and clathrin- or caveolae-mediated endocytosis, and has been shown in all cell types tested to date, including endothelial, epithelial, mesothelial, fibroblasts, skeletal muscle, neurons, cells of the RES, etc. [66, 68, 227]. Further, the CAM pathway provides uptake of drug carriers within an ample range of sizes (100 nm to a few μm) in non-immune cells [62, 77-79]. This is possible due to specific ICAM-1-mediated activation of the sodium-proton exchanger

protein NHE1 and the sphingomyelin/ceramide pathway, which regulate the physicochemical properties of the cell-surface and reorganization of the cytoskeleton into actin stress fibers, facilitating engulfment and endocytosis of micron-sized objects targeted to ICAM-1 [68, 78, 227].

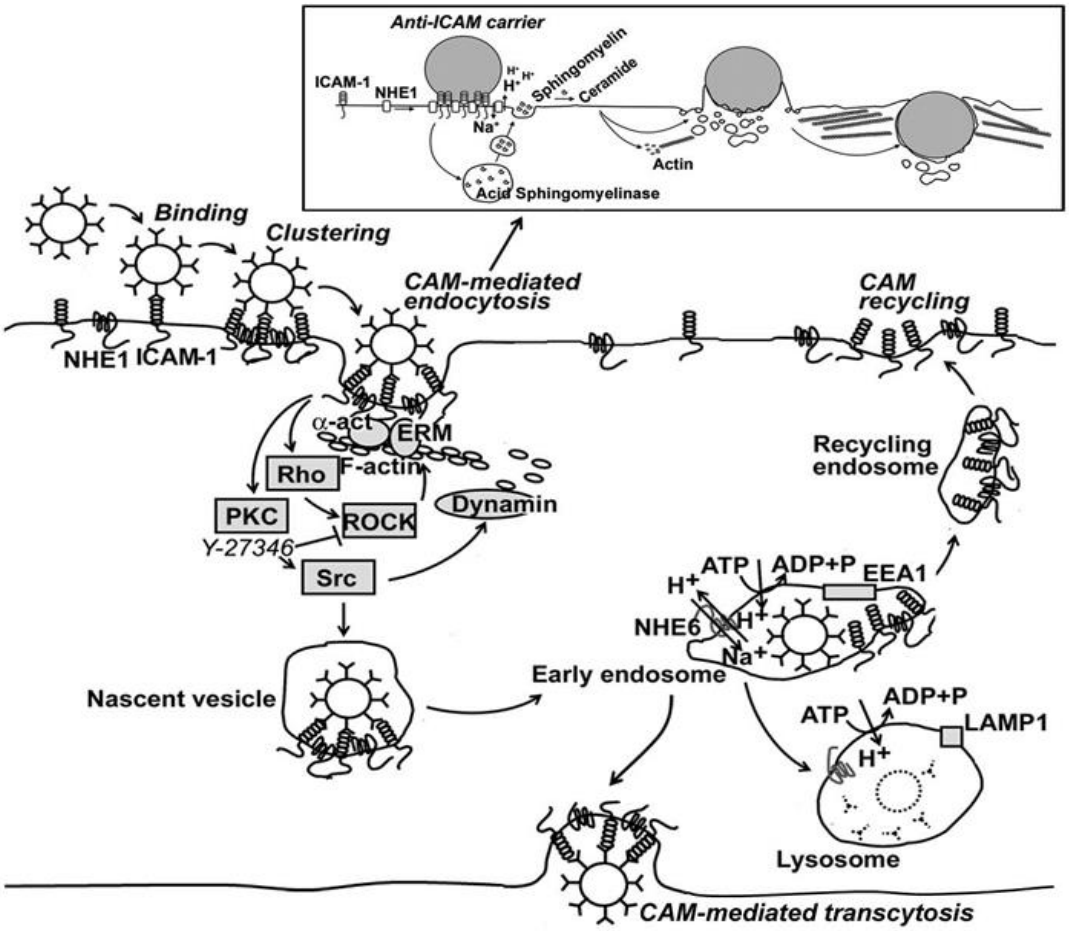

Figure 3. Mechanism of CAM-mediated endocytosis and transcytosis. The cartoon shows the regulatory elements subjacent to CAM-mediated endocytosis (induced upon ICAM-1 engagement by anti-ICAM NCs) and the associated subcellular (lysosomal or transcytotic) trafficking. Figure reproduced from [19] (Figure originally modified from [78, 191] with permission).

Several studies used model polystyrene NCs or biocompatible PLGA counterparts to improve delivery of recombinant lysosomal enzymes by targeting ICAM-1, including ASM deficient in NPD [58, 62, 64, 65, 72], α-galactosidase deficient in Fabry disease [59,

61, 70], and α-glucosidase deficient in Pompe disease [60]. This strategy reduced the circulation time of lysosomal enzymes (preferable to avoid immunogenicity and other side effects), while providing enhanced enzyme accumulation in most LSD target organs after intravenous administration in mouse models, as compared to free enzyme [58-61, 65, 72]. For instance, anti-ICAM NCs enhanced enzyme accumulation by ~200-fold in the lungs and ~15-fold in the liver, which are target organs in type B NPD [58]. As well, there were ~5-fold and ~1.5-fold increases in the heart and kidneys that are primarily affected in Fabry disease [61], and in Pompe, enzyme accumulation was enhanced by ~10-fold in the heart and ~6-fold in the skeletal muscle, both of which are major targets in this disease [60].

Importantly, it has recently been found that anti-ICAM NCs can also undergo transcytosis across transwell models of the BBB [71] and gastrointestinal epithelium [70], as well as transport lysosomal enzymes across the BBB in mice [59-61, 65, 72]. As a result, this strategy markedly enhanced accumulation of lysosomal enzymes compared to free counterparts in the brains of mice after a single intravenous injection: ~7-fold increase for ASM, ~4-fold increase for α-galactosidase, and ~6-fold increase for α-glucosidase [60, 61].

Similar to clathrin-mediated transport via the Tf receptor and low-density lipoprotein receptor [51, 175, 199, 200], targeting ICAM-1 permits not only transcellular delivery, but lysosomal trafficking as well [9, 16]. Specifically, anti-ICAM NCs tested in cell cultures improved uptake, lysosomal transport, and lysosomal degradation of the intended substrate compared to free enzymes [60-64, 69]. As well, recent work demonstrated ASM delivery via anti-ICAM NCs can restore altered clathrin-mediated endocytosis in type A NPD by attenuating lysosomal storage, suggesting this pathway can circumvent disabled routes in LSDs [57]. The rate of CAM-mediated endocytosis and

lysosomal transport can also be controlled by modulation of several design parameters, such as carrier size and shape [62, 79], targeting valency [79], the molecular epitope to which carriers bind [228], and pharmacological agents that impact the cell machinery involved in regulation of endocytic transport [227, 229].

Overall, targeting ICAM-1 permits rapid and enhanced enzyme accumulation throughout multiple tissues and organs, which is preferable to avoid immunogenicity and other unintended side effects associated with prolonged enzyme circulation and the need for frequent dosing. Although several studies suggest that no acute toxicity associates with this strategy [61, 230-235], given the importance and complexity of ICAM-1 signaling and function [66, 75], additional examination into potential side effects is necessary to clearly define the potential benefits and limitations of this strategy for therapeutic applications.

Chapter 3: Status of Vesicular-Mediated Transport in Type A NPD[2]

3.1. Introduction

Vesicular-mediated endocytic uptake, intracellular trafficking, and transcellular delivery of therapeutics are critical processes that impact the success of many treatment modalities, such as in the case of ERT for LSDs discussed in **Chapter 2.** However, it has become increasingly apparent that these processes are altered in disease, including LSDs [21, 57, 115-120]. Specifically, lysosomal accumulation of non-degraded substrates in LSD cells affects not only metabolic flux, but also causes intracellular "traffic jams" that interfere with fusion of pre-lysosomal compartments (*e.g.*, autophagosomes and endosomes), biosynthetic and secretory activity, cytoskeletal rearrangement, compartment transport, and other homeostatic processes) [1, 10, 21, 108, 236-238]. Consequently, therapeutic delivery may be impaired in these diseases, representing an important question of great fundamental and translational interest.

In particular, lysosomal accumulation of lipids in certain LSDs has been linked with aberrant trafficking of plasma membrane components and ligands associated with clathrin and caveolar pathways [21, 108, 118, 119, 238]. This is the case for cells from patients with type A NPD, which is characterized by ASM deficiency leading to sphingomyelin and, secondarily, cholesterol storage [239]. As a consequence of this storage, patients

[2]Chapter 3 contains text and figures reproduced in part with permission from: (1) Rappaport, J., Manthe, R.L., et al., *Altered clathrin-independent endocytosis in type A Niemann-Pick disease cells and rescue by ICAM-1-targeted enzyme delivery.* Mol Pharm, 2015. 12(5): p. 1366-76; © 2015 American Chemical Society. (2) Manthe, R.L.* and Rappaport, J.*, et al., *A comparative study on the alterations of endocytic pathways in multiple lysosomal storage disorders.* Mol Pharm, 2016. 13(2): p. 357-68; © 2015 American Chemical Society.

suffer severe neurological defects that often result in death at a young age [97]. In type A NPD cells, our laboratory recently demonstrated a link between lysosomal storage and altered clathrin-mediated endocytosis [57]. Compared to healthy wild-type cells, type A NPD cells exhibited reduced uptake of Tf [57], a model ligand known to undergo clathrin-mediated endocytosis [51]. Further supporting this finding, there was a reduction in the formation of clathrin-coated pits in these cells, as well as abnormal distribution of intracellular clathrin heavy chain and recruitment to sites of Tf binding [57]. Similarly, dextran uptake via bulk fluid-phase pinocytosis was also reduced in this disease [57]. As a direct result of altered clathrin-mediated endocytosis in these cells, our laboratory also observed diminished uptake of therapeutic ASM [57], which again targets the clathrin route via the M6P receptor [21, 239]. This finding was supported by prior work demonstrating reduced ASM uptake by alveolar macrophages from a mouse model of NPD [21].

As an alternative to clathrin-mediated endocytosis, other pathways could be exploited for therapeutic delivery, including caveolae-mediated endocytosis, macropinocytosis, and CAM-mediated endocytosis as described in **Section 2.2.3**. As a brief reminder, caveolae-mediated endocytosis occurs in most cell types [53, 56, 240] and is characterized by caveolin-1-rich invaginations of ~50-100 nm that form in lipid raft regions of the plasmalemma [186, 240]. Uptake via this route has been achieved by exploiting caveolar ligands, such as CTB, simian virus 40, albumin, or antibodies to caveolar markers such as GM1 [47, 51, 56, 187, 241, 242]. Alternatively, macropinocytosis is characterized by constitutive uptake of fluids in large vesicles (> 500 nm in diameter) and can be transiently induced in non-hematopoietic cells by EGF [56, 188]. Lastly, the CAM pathway is a unique clathrin- and caveolae-independent route [68] recently found to

enhance ASM delivery by coupling the enzyme to ICAM-1-targeted NCs, resulting in greater degradation of the associated lysosomal storage compared to free ASM and restoration of the clathrin pathway [57].

However, potential aberrancies in each of these routes have not been investigated. Hence, the goal of this chapter was to provide a thorough investigation into alterations in endocytic uptake and trafficking via these three pathways. As well, additional analysis was performed to further probe abnormalities associated with the clathrin pathway that were not previously examined. Since targeting certain receptors of the clathrin, caveolar, and CAM pathways can also induce transcytosis across biological barriers [70, 71, 175, 198-200], the chapter concludes with examination of altered transcytosis via these routes, which is required to transport therapeutic ASM across the BBB. Together, these results will aid rationale design of therapeutics by providing insight into strategies to bypass or restore defunct pathways for enhanced efficacy.

3.2. Materials and Methods

3.2.1. Antibodies and Reagents

Alexa Fluor 488-, Alexa Fluor 594-, and fluorescein-labeled Tf or CTB, fluorescent secondary antibodies, and Texas Red-labeled dextran (10,000 MW) were from Invitrogen (Carlsbad, CA). Non-fluorescent human Tf and CTB were from Sigma-Aldrich (St. Louis, MO). Antibodies to Tf and CTB were from Calbiochem (La Jolla, CA), and those against markers of early endosomes (EEA-1) and lysosomes (LAMP-1) were from Calbiochem (La Jolla, CA) or Santa Cruz Biotechnology (Dallas, TX), respectively. Antibody to ganglioside GM1 was obtained from the Developmental Studies Hybridoma Bank, created

by the NICHD of the NIH and maintained by The University of Iowa, Department of Biology (Iowa City, IA). Mouse monoclonal anti-human ICAM-1 (clone R6.5) [243] was from American Type Culture Collection (Manassas, VA). Green Fluoresbrite® 100 nm diameter polystyrene beads were from Polysciences (Warrington, PA). Cell culture reagents were from Gibco-BRL (Grand Island, NY) or Cellgro (Manassas, VA). Porous transwell inserts (1.0 μm-pore) were from Thermo Fisher Scientific (Waltham, MA). Iodine-125 (^{125}I) and Iodogen pre-coated tubes were from Perkin Elmer (Waltham, MA) and Thermo Fisher Scientific (Waltham, MA), respectively. Unless otherwise noted, all other reagents were from Sigma-Aldrich (St. Louis, MO).

3.2.2. Cell Cultures

Primary skin fibroblasts obtained from wild-type and type A NPD patients (homozygous for the R496L mutation) were kindly provided by Dr. Edward Schuchman (Department of Genetics and Genomic Sciences, Mount Sinai School of Medicine, New York, NY). Cells were seeded on glass coverslips and incubated at 37°C, 5% CO_2, and 95% relative humidity in Dulbecco's Modified Eagle Medium supplemented with 10% fetal bovine serum (FBS), 2 mM glutamine, 100 U/mL penicillin, and 100 μg/mL streptomycin. Alternatively, human brain microvascular endothelial cells (HBMECs) from Applied Cell Biology Research Institute (Kirkland, WA) were cultured in RPMI 1640 basal medium supplemented with 20% FBS, 2 mM L-glutamine, 30 μg/mL endothelial cell growth supplement (ECGS), 100 μg/mL heparin, 100 U/mL penicillin, and 100 μg/mL streptomycin. HBMECs were grown to confluence at 37°C, 5% CO_2, and 95% relative humidity on either 1% gelatin-coated glass coverslips or uncoated 1.0 μm-pore transwell

inserts, both in 24-well plates. To mimic intracellular lipid storage that is characteristic of type A NPD, HBMECs were incubated for 48 h prior to assay with 20 μM imipramine, which degrades endogenous ASM and renders it inactive [244]; hence, creating ASM deficiency and intracellular lipid storage characteristic of this disease [57]. Where indicated, cells were incubated overnight with 10 ng/mL tumor necrosis factor alpha (TNFα) to mimic inflammatory activation typical of NPD and other LSDs [9, 239].

3.2.3. Ligand Uptake by Caveoli

Wild-type and type A NPD fibroblasts were incubated in medium containing 33.3 μg/mL red Alexa Fluor-594 CTB for varying periods of time (15 min to 5 h) at 37°C to measure the kinetics of uptake by caveolar endocytosis. Cells were then washed, fixed with 2% paraformaldehyde, and incubated with goat anti-CTB followed by green FITC-labeled rat anti-goat IgG. This protocol renders CTB bound to the cell-surface double stained in red and green (red + green = yellow) versus internalized CTB, which appears only red, as previously described [68]. To verify that CTB uptake was mainly contributed by caveolae-relative to clathrin-mediated endocytosis, similar experiments were conducted in the presence of 1 μg/mL filipin (inhibits caveolar uptake [245]), 50 μM monodansylcadaverine (MDC; inhibits the clathrin pathway [246]), or a mixture of both inhibitors. All samples were washed, mounted on slides, and analyzed by fluorescence microscopy. This was done using an Olympus IX81 microscope with a UPlanApo 60x objective (Olympus, Inc.; Center Valley, PA) and filters optimized for red, green, and blue fluorescence (Semrock, Inc.; Rochester, NY). Images were taken with an ORCA-ER camera (Hamamatsu; Bridgewater, NJ) and SlideBook 4.2 software (Intelligent Imaging Innovations; Denver,

CO), and analyzed using Image-Pro 6.3 (Media Cybernetics, Inc.; Rockville, MD). To facilitate analysis using a customized algorithm that detects both fluorescent pixels and endosomal-sized vesicles, both surpassing a background threshold fluorescence [57, 247], CTB was pseudocolored green and the additional stains were pseudocolored red. Therefore, surface CTB appears yellow relative to green internalized counterparts. The percentage of internalized green fluorescent pixels over the total cell-associated fluorescence and the absolute number of green fluorescent vesicles were quantified. Where indicated, these parameters were expressed per cell area (in mm^2), which was obtained from observation of the cell borders by phase-contrast microscopy. Regression analysis was performed with SigmaPlot 11.0 (Systat Software Inc.; San Jose, CA).

3.2.4. Fluid-Phase Uptake and Validation via Selected Pathways

To quantify bulk fluid-phase pinocytosis, wild-type and type A NPD fibroblasts were incubated at 37°C for varying periods of time (30 min to 8 h) with 1 mg/mL Texas Red-labeled dextran (10,000 MW), a fluid-phase marker for endocytosis. Cells were washed, fixed with 2% paraformaldehyde, and the number of fluorescent dextran-filled compartments was quantified by fluorescence microscopy using the customized algorithm described in **Section 3.2.3**. Where indicated, this parameter was expressed per cell area (in mm^2).

To validate dextran uptake via selected pathways, wild-type fibroblasts were incubated for 30 min at 37°C with Texas Red-labeled dextran in the presence of 200 µg/mL Tf or 33.3 µg/mL of CTB, ligands of clathrin- or caveolae-mediated endocytosis, respectively, conjugated to green fluorescein or Alexa Fluor 488. Cells were washed and

fixed with 2% paraformaldehyde. Alternatively, cells incubated with Texas Red-labeled dextran alone were washed, fixed, and permeabilized for 5 min with 0.2% Triton X-100 followed by immunostaining of ganglioside GM1 detected using a green Alexa Fluor 488-labeled secondary antibody. Cell samples were examined by fluorescence microscopy using the algorithm previously described. In merged-channel images, uptake of red dextran within green Tf-, CTB-, or ganglioside GM1-containing vesicles was visualized as colocalization of these colors (yellow), indicating co-uptake via clathrin- or caveolae-mediated endocytosis. The percentage of colocalization was calculated for each cell using the total fluorescence area occupied by each label and the total number of endosome-size vesicles occupied by each label.

Additionally, macropinocytosis was evaluated by incubating wild-type or type A NPD cells for varying periods of time (15 min to 8 h) at 37°C with 1 mg/mL Texas Red-labeled dextran in medium containing 100 ng/mL EGF, which stimulates formation of membrane ruffles and macropinocytosis [188]. Cell samples were washed, fixed with 2% paraformaldehyde, and the number of fluorescent dextran-filled compartments was quantified and expressed per cell area (in mm^2) as described above.

Specific inhibition of macropinocytosis was also verified by incubating wild-type fibroblasts at 37°C for 30 min with 200 µg/mL red Alexa Fluor 594-conjugated Tf (clathrin route), 1 h with 33.3 µg/mL red Alexa Fluor 594-conjugated CTB (caveolar route), or co-incubation for 30 min with 1 mg/mL Texas Red-labeled dextran and 100 ng/mL EGF (macropinocytosis) in the absence (control condition) versus presence of 3 mM amiloride, which is known to inhibit macropinocytosis [248, 249]. Cells were washed, fixed with 2% paraformaldehyde, and surface-bound (non-internalized) Tf or CTB were immunostained

using antibodies conjugated to green FITC. All samples were analyzed by fluorescence microscopy using the customized algorithm described earlier, which required Tf or CTB to be pseudocolored green, while the additional cell-surface stains were pseudocolored in red. Therefore, in merged-channel images, surface Tf or CTB appear yellow versus internalized counterparts that appear green. The percentage of internalized green fluorescent pixels over the total cell-associated fluorescence was quantified and compared between control and amiloride conditions. Similarly, the total number of endocytic vesicles occupied by dextran was quantified and compared between the two conditions.

Regression analysis for bulk fluid-phase uptake and macropinocytosis was performed with SigmaPlot 11.0.

3.2.5. Intracellular Trafficking of Ligands

Wild-type and type A NPD fibroblasts were incubated for 30 min at 37°C with 200 µg/mL of Tf or 33.3 µg/mL of CTB, both conjugated to red Alexa Fluor 594. Samples were then washed, fixed, and permeabilized as described in **Section 3.2.4**. Early endosomal compartments were then labeled using anti-EEA-1 followed by a secondary antibody conjugated to green Alexa Fluor 488. Alternatively, lysosomes were labeled using green Alexa Fluor 488-conjugated anti-LAMP-1. Cells were visualized by fluorescence microscopy, where colocalization of red-labeled ligands (Tf or CTB) with green-labeled compartment markers appear yellow in merged-channel images, and were analyzed using the algorithm described. This colocalization was expressed as a percentage of the total ligands present in cells, and the number of EEA-1 or LAMP-1-possitive vesicles were also quantified.

3.2.6. Preparation and Characterization of Anti-ICAM NCs

Model polymer NCs were prepared by adsorbing R6.5 antibody (anti-ICAM) onto the surface of 100 nm, green fluorescent polystyrene beads [57, 64]. Briefly, ~5 μM total antibody was incubated with ~10^{13} NCs/mL for 1 h at room temperature, followed by washing and centrifugation at 12,000 rpm for 3 min to remove non-bound antibody. NCs were resuspended at a final concentration of ~7 x 10^{11} NCs/mL in phosphate buffered saline containing 1% bovine serum albumin, followed by sonication at low power to mitigate aggregates. The diameter of the resulting anti-ICAM NCs was 258 ± 7 nm with a polydispersity index (PDI) of 0.15 ± 0.03, as measured by dynamic light scattering (Zetasizer Nano-S90, Malvern Instruments; Westborough, MA). Although not intended for clinical use, these prototype carriers have been demonstrated to render coating efficacy, *in vivo* targeting, and intracellular transport comparable to anti-ICAM NCs made of biodegradable PLGA [58, 81], and are therefore a valid model.

3.2.7. Anti-ICAM NC Uptake via the CAM Pathway

TNFα-activated healthy (control) and imipramine-treated (diseased) HBMECs were exposed for 1 h at 37°C to green fluorescent anti-ICAM NCs, then washed and fixed with 2% paraformaldehyde. Samples were incubated with a secondary antibody labeled with Texas Red, which is only accessible to anti-ICAM on the coat of cell-surface located NCs (not internalized ones), as demonstrated [247]. This allows differential staining of cell-surface bound (green + red = yellow) and internalized (green alone) NCs. The absolute number of NCs internalized per cell and the percentage of NCs internalized from the total

cell-associated (surface-bound + internalized) NCs were quantified by fluorescence microscopy, as described [247].

3.2.8. Transcytosis of Model Ligands

Healthy (control) and imipramine-treated (diseased) HBMECs were cultured on 1.0 μm-pore transwell inserts. For assessment of the CAM pathway, both healthy and diseased cells were activated overnight with TNFα. ^{125}I-labeled Tf (clathrin pathway), CTB (caveolar pathway), or free anti-ICAM (CAM pathway) were then added to the apical chamber of transwell inserts (2-3 μg) and incubated for 30 min at 37°C to allow binding to cells. Afterwards, the non-bound fraction or ligand that leaked across the cell monolayer was removed by washing both the apical and basolateral chambers. The bound cargo was then further incubated with cells in fresh medium at 37°C for additional time up to 24 h to permit transcytosis across the monolayer. At select time points, the ^{125}I content in the basolateral chamber was measured using a gamma counter (2470 Wizard^2, Perkin Elmer; Waltham, MA), and the amount of Tf, CTB, or anti-ICAM transcytosed was calculated based on their respective specific activities (CPM/mass).

3.2.9. Statistics

Fluorescence experiments involved two or three independent assays and microscopy analysis involved random selection of 8-15 regions located throughout the sample for image acquisition. Individual analysis of each cell contained in such images was pursued, where all vesicles contained per cell were included in the analysis (this represents a total between 1,000 and 3,000 vesicles per condition). For transcytosis

experiments, data were $n \geq 3$. Data were calculated as the mean ± standard error of the mean (SEM), where statistical significance was determined as $p < 0.05$ by Student's *t*-test.

3.3. Results

3.3.1. Endocytosis of Caveolar Ligands

To build upon our laboratory's recent study demonstrating altered clathrin-mediated endocytosis in type A NPD fibroblasts [57], here we focused on clathrin-independent routes. First, we examined uptake of fluorescent CTB, a molecule that associates with ganglioside GM1 on the plasmalemma and internalizes largely by caveolae-mediated endocytosis [250]. Over the course of 1 h, total CTB associated with wild-type (herein referred to as healthy) cells to a significantly greater extent than type A NPD (herein referred to as diseased) cells, and also localized to the perinuclear region versus an endosomal-punctate-like appearance as observed in the disease case (**Figure 4A**). Hence, CTB distribution in healthy cells was consistent with Golgi and ER trafficking, as expected for caveolar uptake of this toxin [240, 250]. Verifying this route (since clathrin-mediated endocytosis could also contribute to CTB uptake [251]), only treatment with filipin, a cholesterol-binding agent that inhibits caveolar endocytosis [245], but not MDC, an inhibitor of clathrin-coated pits [246], significantly diminished CTB endocytosis in healthy cells: 47% versus 81% of control, respectively (**Figure 4B**). Further, CTB uptake in the presence of both filipin and MDC did not differ from filipin alone (51% of control; **Figure 4B**). Importantly, total association of CTB with diseased cells was only 64% that of healthy cells (**Figure 4A**), indicating a defect in the caveolar route. In fact, filipin inhibition of CTB uptake, alone or in combination with MDC, was less acute in diseased cells (63% and

80% of control, respectively; **Figure 4B**) and no effect was found for diseased cells treated with MDC alone (111% of control), which is expected because these cells have impaired clathrin-mediated uptake [57].

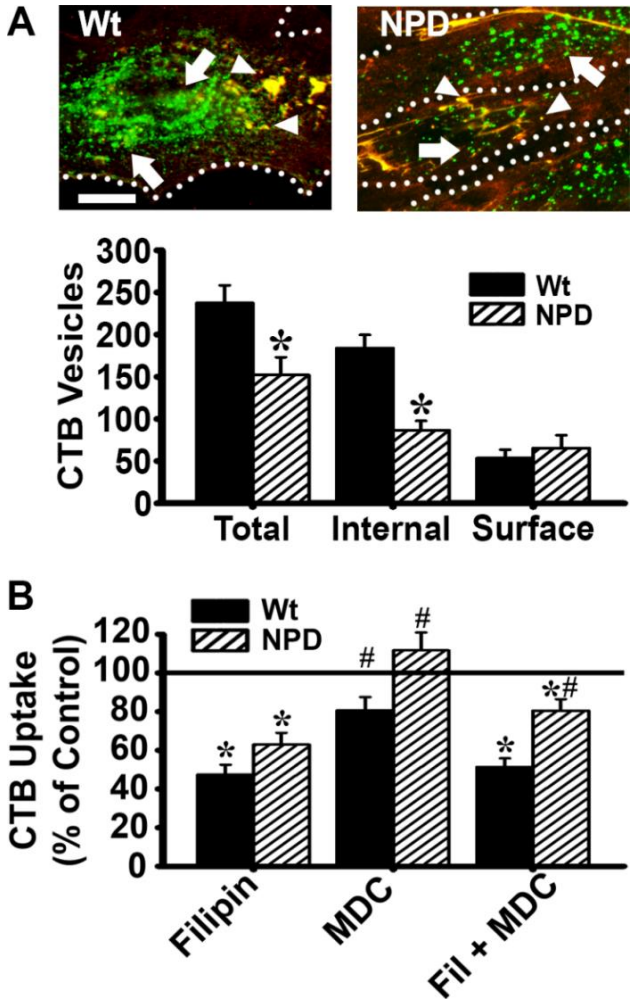

Figure 4. Binding and internalization of CTB in type A NPD fibroblasts. (A) Fluorescence microscopy of wild-type (Wt) and NPD fibroblasts incubated with fluorescent CTB (pseudocolored green) for 1 h at 37°C. Non-bound CTB was washed off, cells were fixed, and surface-bound CTB was immunostained (red + green = yellow, arrowheads) to distinguish it from internalized CTB (green, arrows). Dotted lines mark the cell borders, as observed by phase-contrast microscopy. Scale bar = 10 µm. Total, internal, and surface CTB (fluorescent objects over background) were quantified. (B) Uptake of CTB by Wt and NPD fibroblasts was assessed after 1 h as described in (A). Incubations were conducted in the presence of filipin (inhibits caveolae-mediated endocytosis), MDC (inhibits clathrin-mediated endocytosis), or a mixture of both inhibitors. The number of internalized vesicles containing CTB was quantified as in (A) and expressed as a percentage of the uptake found for their respective controls (absence of inhibitors; indicated by the solid horizontal line). Data are the mean ± SEM. (A) *Comparison to Wt cells. (B) *Comparison of inhibitor-treated cells versus control; #comparison of MDC or filipin + MDC mixture versus filipin alone ($p < 0.05$ by Student's *t*-test). Figure adapted from [252].

The endocytic differences observed between healthy and diseased cells mostly applied to the internalized fraction of CTB (47% that of healthy cells), whereas the amount of CTB bound to the cell-surface was similar in both cell types (**Figure 4A**), suggesting that the defect may lie in the uptake process. Examination of the kinetics of CTB uptake suggested this event was slower in diseased versus healthy cells: the half-time for maximal uptake was 26 and 12 min, respectively, when comparing the percentage of CTB that was internalized from the total cell-associated fraction (**Figure 5A**). With time, this parameter reached a similar saturation (95% uptake for healthy cells and 94% uptake for diseased cells; **Figure 5A**). When quantifying the number of internalized vesicles containing CTB, the uptake kinetics were even more affected (half-time of 20 min for healthy cells versus 134 min for diseased cells; **Figure 5B**), and when the number of internalized vesicles containing CTB was normalized to the cell-surface area (because different cell sizes would render different numbers of invaginating vesicles even if the rate of uptake was the same), a similar, yet more acute pattern was observed (**Figure 5C**). Overall, reduced CTB uptake supports caveolae-mediated endocytosis is altered in this disease.

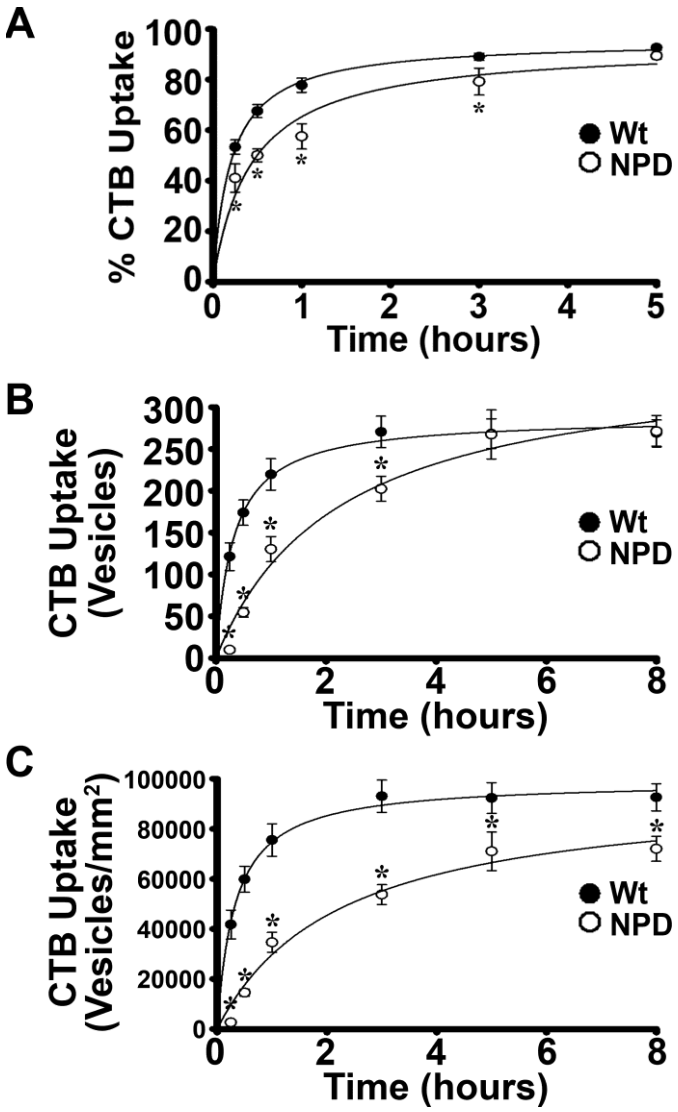

Figure 5. Kinetics of CTB uptake in type A NPD fibroblasts. Kinetics of CTB uptake in Wt versus NPD fibroblasts, examined as described in **Figure 4.** The graphs show the (A) percentage of internalized CTB from the total cell-associated CTB, (B) total number of CTB-positive vesicles internalized per cell, and (C) number of internalized vesicles normalized per cell area, to account for the difference in Wt and NPD cell sizes. Solid lines depict regression curves, with $R^2 \geq 0.94$ for all curves. Data are the mean ± SEM. *Comparison to Wt cells ($p < 0.05$ by Student's *t*-test). Figure adapted from [252].

3.3.2. Fluid-Phase Uptake in Bulk and via Clathrin or Caveolar Pathways

Next, we evaluated bulk fluid-phase uptake of fluorescent dextran. Diseased cells exhibited reduced dextran uptake at 60-70% compared to healthy cells (see 1 h time point in **Figure 6A**), which is similar to a previous report by our group [57]. As in the case of

altered uptake of CTB, diseased cells showed slower dextran uptake kinetics compared to that of healthy cells (half-time for maximal internalization was 67 versus 29 min, respectively), yet maximal uptake per cell was not diminished (**Figure 6A**). However, when the number of dextran-containing vesicles was normalized to cell size, maximal uptake at saturation seemed reduced for diseased cells (**Figure 6B**).

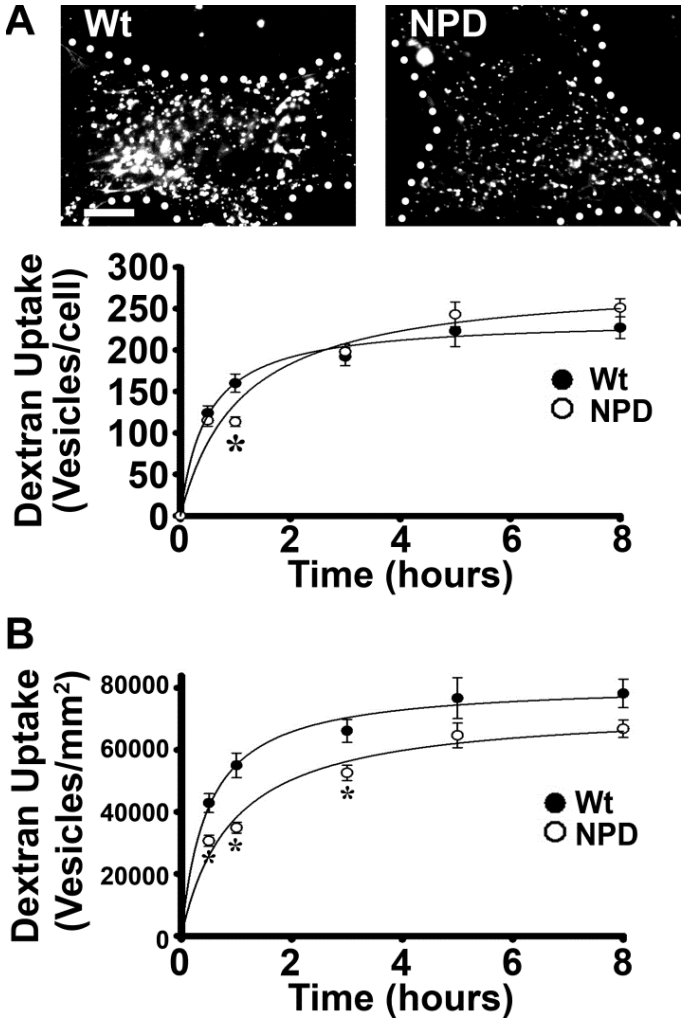

Figure 6. Kinetics of bulk pinocytosis in type A NPD fibroblasts. (A) Microscopy images and quantification of the number of dextran-filled vesicles (fluorescent objects over background) associated with Wt or NPD fibroblasts incubated for varying periods of time at 37°C with medium containing fluorescent dextran (microscopy images show 1 h as an example). Dotted lines mark the cell borders, as observed by phase-contrast microscopy. Scale bar = 10 µm. (B) The number of dextran-filled vesicles per cell area. Solid lines depict regression curves, with $R^2 \geq 0.95$ for all curves. Data are the mean ± SEM. *Comparison to Wt cells ($p < 0.05$ by Student's *t*-test). Figure adapted from [252].

The observed decrease in dextran uptake may be attributed to alteration in one or a combination of the pathways that contribute to bulk pinocytosis: clathrin-, caveolae-, and macropinocytic endocytosis [53]. For most cells, clathrin-coated pits and caveoli are the most likely uptake mechanisms since macropinocytosis is largely restricted to immune cells and cells transiently stimulated by growth factors [188]. To confirm this, fluorescent dextran internalized by healthy cells significantly colocalized with ligands that associate with the clathrin route [185] (41-48% colocalization with Tf) or the caveolar route [250, 252] (48-53% colocalization with CTB) (**Figure 7A**). As well, since a fraction of CTB may enter certain cells via the clathrin pathway [251], we further confirmed dextran uptake via caveoli in healthy cells by colocalization with a lipid raft domain constituent: the CTB target, ganglioside GM1 (40-55% colocalization; **Figure 7B**). The contribution of clathrin and caveolar pathways to endocytosis has been shown to differ between different cell types and culture conditions [253-256]. Yet in this case, the validation described above indicates that these two routes contributed similarly to dextran uptake in these cells, which parallels previous data [57, 252].

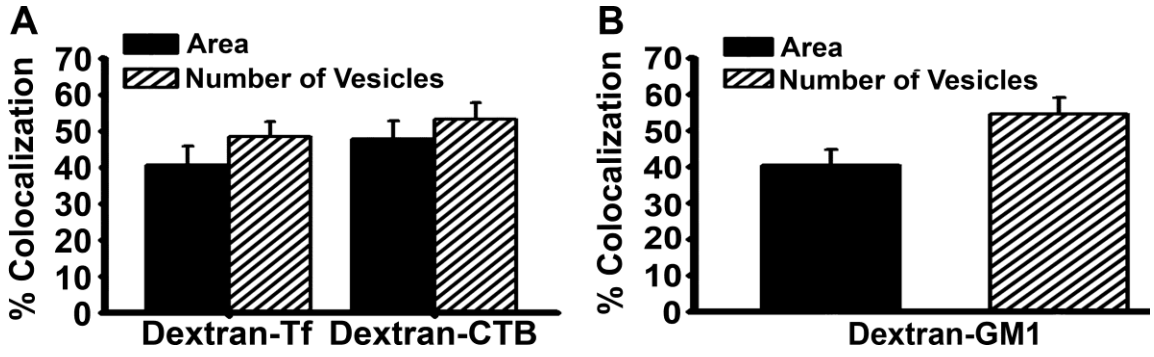

Figure 7. Fluid-phase uptake via clathrin- or caveolae-mediated endocytosis. (A) Quantification of the percent colocalization of red fluorescent dextran-filled vesicles internalized by Wt fibroblasts (30 min at 37°C) along with green fluorescent Tf or CTB. (B) Quantification of the percent colocalization of red fluorescent dextran-filled vesicles internalized by Wt fibroblasts (30 min at 37°C) with green fluorescent-immunostained ganglioside GM1. Colocalization area and number of vesicles are shown. Data are the mean ± SEM. Figure adapted from [257].

3.3.3. Fluid-Phase Uptake via Macropinocytosis

Since macropinocytosis is known to contribute to non-specific uptake of extracellular fluid, we also evaluated this route. Specifically, we examined dextran uptake in healthy and diseased cells under induction with EGF, a treatment that results in the formation of membrane ruffles on the cell-surface in non-immune cells and, hence, transiently induces macropinocytosis [188]. To first verify this premise, amiloride (an inhibitor of macropinocytosis [248, 249]) was found to inhibit dextran uptake in healthy cells, while it did not affect uptake of Tf (clathrin pathway) or CTB (caveolar pathway) (**Figure 8**).

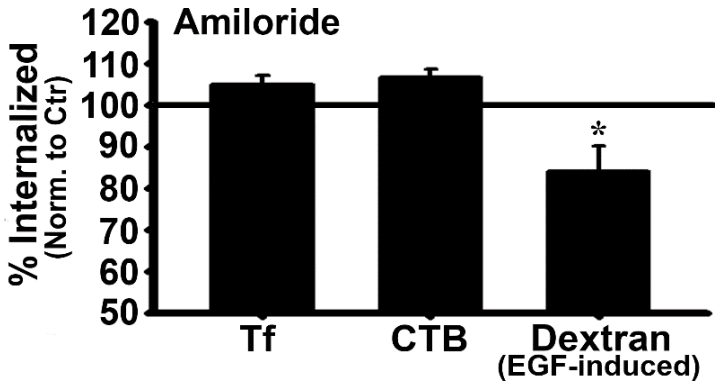

Figure 8. Specific inhibition of macropinocytosis. (A) Wt fibroblasts were incubated for 30 min at 37°C with fluorescent Tf (clathrin route), 1 h with fluorescent CTB (caveolar route), or co-incubated for 30 min with fluorescent dextran and EGF (macropinocytosis). Incubations were performed in the absence (control) versus presence of amiloride, an inhibitor of macropinocytosis. Uptake of Tf, CTB, and dextran were assessed and quantified as described previously. Data were normalized to control cells (absence of inhibitor), which is indicated by the solid horizontal line. Data are the mean ± SEM. *Comparison to control cells ($p < 0.05$ by Student's *t*-test). Figure reproduced from [257].

With this verification in place, we found diseased cells internalized only 72% as much dextran as healthy cells after 1 h (**Figures 9A-B**), demonstrating deficient macropinocytic activity. Both the kinetics associated with this endocytic route and the maximal uptake level were affected. The half-time for maximal internalization was 26 min

in diseased cells relative to 17 min in healthy cells, with diseased cells reaching only 86% of the maximal uptake observed in healthy samples **(Figure 9B)**. Further, a more altered result was found when the number of internalized vesicles was normalized to the cell size: maximal uptake per mm^2 in disease was 67% of healthy cells (**Figure 9C**).

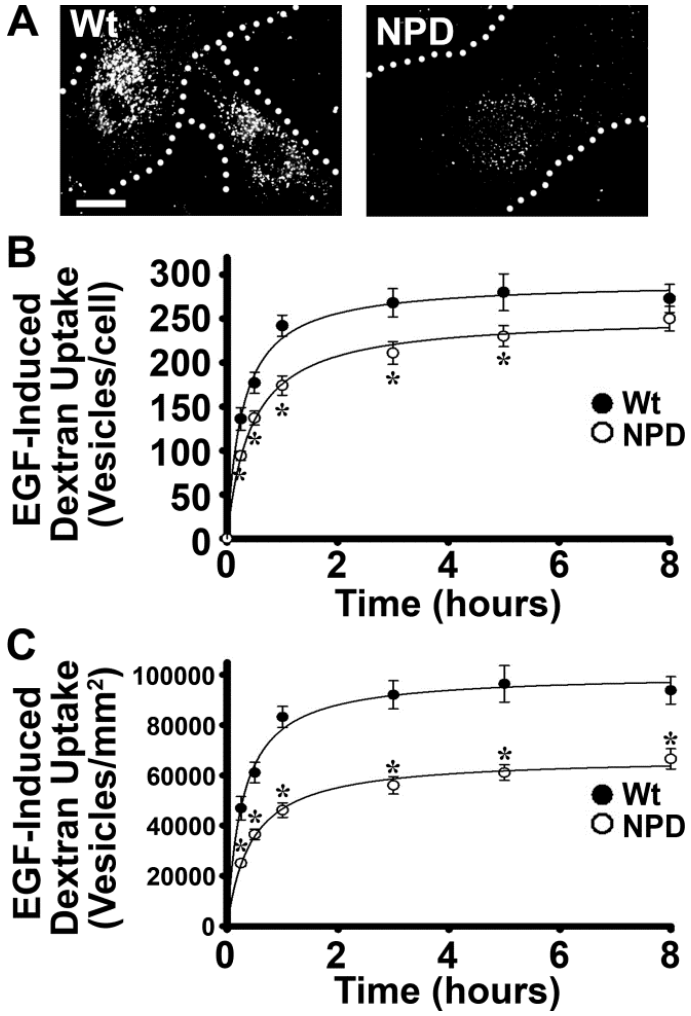

Figure 9. Macropinocytosis in type A NPD fibroblasts. (A) Microscopy images of Wt and NPD fibroblasts incubated for 1 h at 37°C in medium containing 100 ng/mL EGF (to stimulate macropinocytosis) and fluorescent dextran. Dotted lines mark the cell borders, as observed by phase-contrast microscopy. Scale bar = 10 µm. (B, C) Kinetics of EGF-induced uptake of dextran in Wt and NPD cells was assessed at the indicated times, as described in **Figure 6**. Panel (B) shows the number of dextran-filled vesicles per cell and (C) shows the number of dextran-filled vesicles per cell area. Lines depict regression curves, with $R^2 \geq 0.98$ for all curves. Data are the mean ± SEM. *Comparison to Wt cells ($p < 0.05$ by Student's *t*-test). Figure adapted from [252].

3.3.4. Intracellular Trafficking of Clathrin and Caveolar Ligands

With alterations being observed in diseased cells for both the clathrin pathway [57] and caveolar pathway (demonstrated herein), we next evaluated potential changes in the intracellular trafficking of ligands internalized via clathrin- or caveolae-mediated routes. For this purpose, we examined the colocalization of Tf or CTB with markers of early endosomes (EEA-1) or lysosomes (LAMP-1). Fluorescence microscopy visualization (**Figures 10A-B**) and quantification (**Figure 10C**) showed an enhanced number of both early endosomes and lysosomes in diseased cells compared to healthy cells (149% and 152% of healthy levels, respectively), which is expected in LSDs [1, 19]. Most importantly, a smaller fraction of Tf and CTB colocalized with endosomal compartments (67% and 78% of the healthy level; **Figures 10A** and **10D**), and this was also the case for colocalization of these ligands with lysosomes (23% and 70% of the healthy level; **Figures 10B** and **10E**). Therefore, intracellular trafficking subsequent to clathrin- and caveolae-mediated uptake also seems to be altered in LSDs, which may be a consequence of the lower rate of endocytosis.

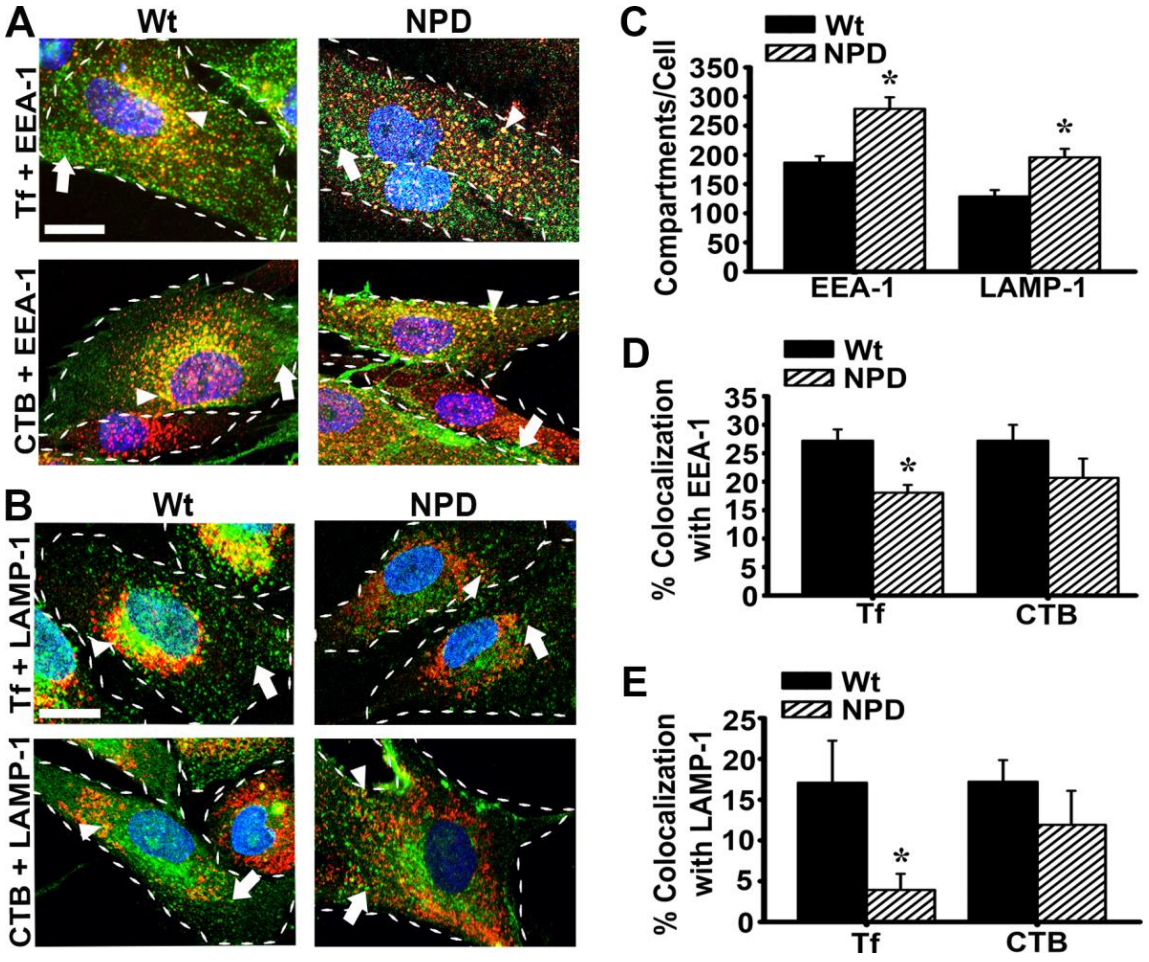

Figure 10. Intracellular trafficking of ligands in type A NPD fibroblasts. Wt or NPD fibroblasts were incubated for 30 min at 37°C with fluorescent Tf or CTB (pseudocolored green), followed by immunostaining of (A) early endosomes or (B) lysosomes using antibodies against EEA-1 or LAMP-1, respectively (pseudocolored red). Cell nuclei were stained blue with DAPI. Colocalization of Tf or CTB with EEA-1 or LAMP-1 appears yellow (red + green; arrowheads), while Tf or CTB localized in other areas are visualized as green (arrows). Dashed lines mark the cell borders, as observed by phase-contrast microscopy. Scale bar = 10 μm. (C) Quantification of the number of EEA-1- or LAMP-1-positive vesicles. (D) Colocalization of Tf or CTB with EEA-1, or (E) with LAMP-1, expressed as the percentage of the total Tf or CTB associated with cells. Data are the mean ± SEM. *Comparison to Wt cells ($p < 0.05$ by Student's *t*-test). Figure adapted from [257].

3.3.5. Anti-ICAM NC Uptake via the CAM Pathway

Since uptake via bulk fluid-phase, receptor-mediated pathways (clathrin or caveolar), and macropinocytosis is impaired in type A NPD as shown herein and in other work [57], approaches to bypass these routes or enhance endocytic signaling may help

improve therapeutic efficacy. As described previously, utilizing the CAM pathway for enzyme delivery via their coupling to anti-ICAM NCs represents an attractive and viable approach for enzyme replacement in LSDs. In fact, the specificity of anti-ICAM NCs to enhance binding, uptake, lysosomal enzyme delivery and activity, storage reduction in cell culture, and biodistribution in mouse models, relative to naked ASM or control IgG NCs has already been documented in several prior publications [57, 58, 60, 61, 68, 81, 258, 259]. Despite the apparent advantages of this strategy, it is still important to evaluate potential alterations in the CAM pathway. This applies especially in the case of NPD since these cells are deficient in ASM, which is required for CAM-mediated endocytosis [78].

At a time point (1 h) when caveolae-mediated uptake of CTB and clathrin-mediated uptake of Tf were significantly impaired (**Figures 4** and **5** for CTB, and [57] for Tf), a significant decrease in the absolute number of anti-ICAM NCs internalized by diseased cells was also observed compared to healthy, control cells (77% of control; **Figure 11A**). Similarly, the percentage of internalized NCs from the total cell-associated (surface-bound + internalized) NCs was slightly reduced (although not statistically significant) in diseased cells (88% of control; **Figure 11B**). Therefore, the CAM pathway is in fact also impaired in this disease.

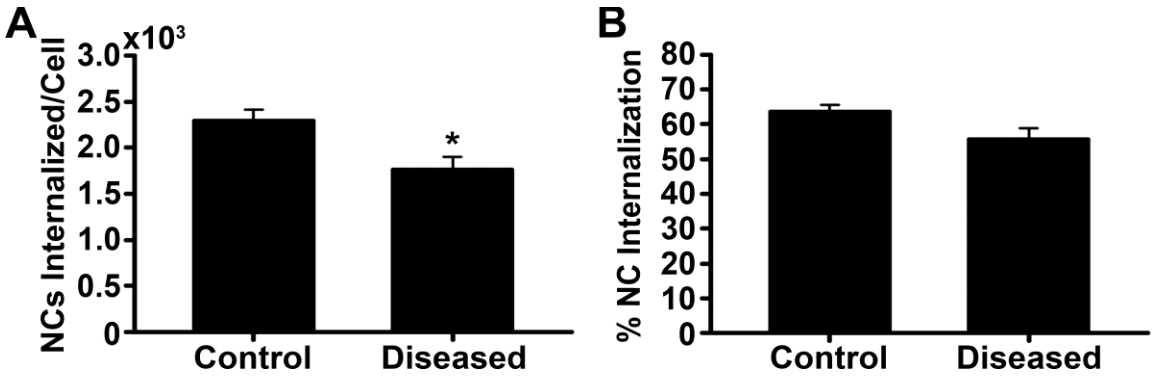

Figure 11. Anti-ICAM NC uptake in diseased cells. Healthy **(**Control) and imipramine-treated (diseased) brain endothelial cells were pre-treated with TNFα to mimic inflammation-like conditions typical in type A NPD. The cells were then incubated for 1 h at 37°C with green fluorescent anti-ICAM NCs. Surface-bound versus internalized NCs were distinguished using the immunolabeling technique described in **Section 3.2.7**. (A) The total number of NCs internalized per cell and (B) internalized NCs as a percentage of total cell-associated NCs. Data are the mean ± SEM. *Comparison to control ($p < 0.05$ by Student's *t*-test).

3.3.6. Comparison of Cargo Uptake by Receptor-Mediated Pathways

By comparing endocytic uptake of Tf, CTB, or anti-ICAM NCs at the 1 h time point in healthy and diseased cells, it is clear that all three pathways are altered in the disease scenario (**Figure 12**). However, the CAM pathway was least affected in diseased cells compared to the two classical endocytic routes (clathrin and caveolar) in terms of absolute cargo internalization and the percentage of cargo internalization (**Figures 12A-B**). Specifically, absolute cargo uptake in diseased cells relative to healthy controls was 36%, 47%, and 77% for the clathrin, caveolar, and CAM pathways, respectively (**Figure 12A**), while the percentage of cargo internalization relative to controls was 79%, 74%, and 88%, respectively (**Figure 12B**). Therefore, endocytic alterations in LSDs present an additional obstacle to sufficient enzyme delivery via the classical endocytic routes (clathrin and caveolar), as well as the non-classical CAM pathway. Nevertheless, the CAM pathway seems more amenable for therapeutic enzyme delivery.

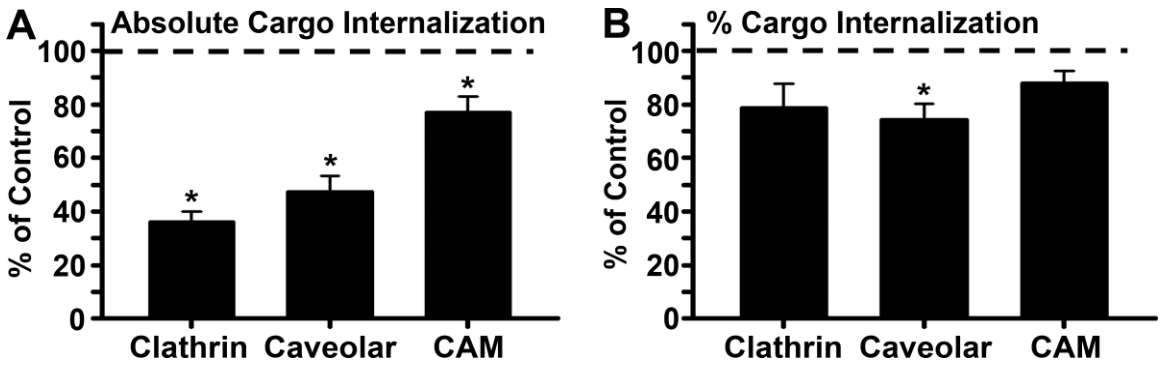

Figure 12. Comparison of cargo uptake by receptor-mediated pathways in diseased cells. Type A NPD fibroblasts or imipramine-treated (diseased) brain endothelial cells were incubated for 1 h at 37°C with fluorescent Tf (clathrin pathway), CTB (caveolar pathway), or anti-ICAM NCs (CAM pathway). Uptake of Tf, CTB, and anti-ICAM NCs was assessed and quantified as described previously. (A) Absolute cargo internalization and (B) the percentage of cargo internalization relative to that found for wild-type fibroblasts or control endothelial cells, respectively (indicated by the horizontal dashed lines). Data are the mean ± SEM. *Comparison to control ($p < 0.05$ by Student's *t*-test). *Tf data were extracted from previously published work [57].*

3.3.7. Transcytosis via Receptor-Mediated Pathways

Given that nearly half of all LSDs associate with neurological dysfunction [1, 9], we next examined whether transcytosis via the clathrin, caveolar, and CAM pathways is also impaired in diseased brain endothelial cells. Between 3 and 24 h of incubation, the absolute amount of Tf, CTB, or free anti-ICAM transcytosed across diseased cells ranged from 2.2-2.7 ng per well (**Figure 13A**). While the CAM pathway transcytosed the greatest amount of cargo, there was no statistical difference found between the three pathways, suggesting that each pathway may be unaffected or similarly impacted in the diseased cells. Interestingly though, when this amount of transcytosed cargo was expressed relative to the levels found in healthy cells between the same time frame, free anti-ICAM transcytosis via the CAM pathway was diminished (72% of healthy control), while CTB transcytosis via the caveolar pathway was unaffected (98% of healthy control), and Tf transcytosis via the clathrin pathway was slightly enhanced, although not statistically greater than that of the

control (122% of healthy control) (**Figure 13B**). However, looking at this same parameter (cargo transcytosed in diseased cells as a percentage of the healthy controls) over the entire 24 h incubation period, each pathway was in fact slightly impaired: 90%, 91%, and 81% of healthy controls for the clathrin, caveolar, and CAM pathways, respectively (**Figure 13C**). The discrepancy between the two data sets (**Figures 13B-C**) suggest that the kinetics of Tf transcytosis differ in healthy versus diseased cells. Specifically, the data indicate diseased cells had diminished Tf transcytosis during the initial 3 h time period, likely caused by diminished Tf uptake [57]. Then, between 3 and 24 h of incubation, internalized Tf in diseased cells was able to traverse the cell barrier, resulting in a greater amount of Tf transcytosed by 24 h. In contrast, healthy cells transcytosed the majority of cell-bound Tf during the initial 3 h, so that additional transcytosis of Tf between 3 and 24 h was minimal. As such, the fraction of Tf transcytosed between 3 and 24 h appears greater for diseased cells (**Figure 13B**). Yet, over the duration of the entire experiment, more Tf was actually transcytosed in healthy cells (**Figure 13C**). Interestingly, these differences did not apply to CTB transcytosis via the caveolar route or anti-ICAM transcytosis via the CAM pathway. Overall though, transcytosis was relatively unaffected in diseased cells via the three routes tested, and the reductions in transcytosis (if any) were much less acute than that observed for uptake in the case of the clathrin and caveolar pathways, while uptake and transcytosis via the CAM pathway were similarly impacted in diseased cells.

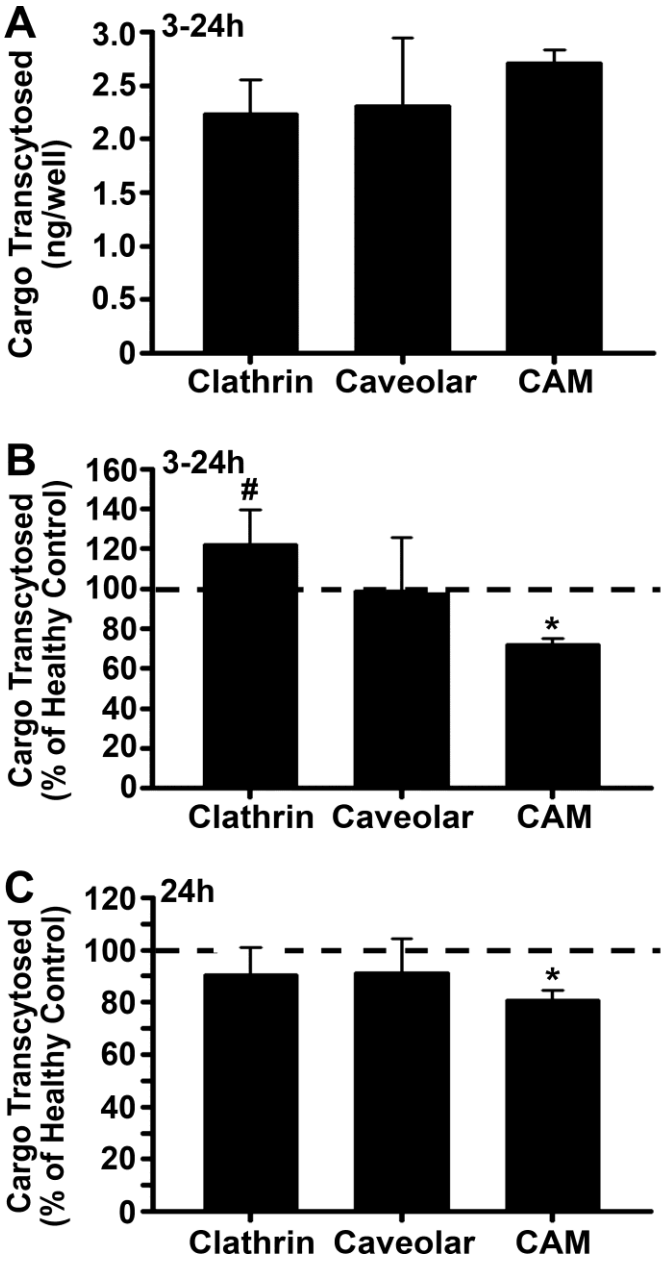

Figure 13. Comparison of transcytosis by receptor-mediated pathways in diseased cells. Healthy (control) or imipramine-treated (diseased) brain endothelial cells seeded on 1.0 μm-pore transwell inserts were incubated for 30 min at 37°C with ^{125}I-labeled Tf (clathrin pathway), CTB (caveolar pathway), or free anti-ICAM (CAM pathway) to allow binding to cells, followed by removal of the non-bound fraction via washing both apical and basolateral chambers, and incubation in fresh medium for additional time up to 24 h at 37°C. The absolute amount of cargo transcytosed (ng/well) was quantified as described in **Section 3.2.8**. (A) Absolute cargo transcytosed between 3 and 24 h of incubation in diseased cells. (B) Cargo transcytosed between 3 and 24 h of incubation in diseased cells as a percentage of that found in control endothelial cells (indicated by the horizontal dashed line). (C) Cargo transcytosed after 24 h incubation in diseased cells as a percentage of that found in control endothelial cells (indicated by the horizontal dashed line). Data are the mean ± SEM. *Comparison to control; $^{\#}$comparison to the CAM pathway ($p < 0.05$ by Student's *t*-test).

3.4. Discussion

Non-specific fluid-phase and receptor-mediated uptake, intracellular trafficking, and transcytosis are rather ubiquitous in mammalian cells, where they regulate a plethora of physiological functions and represent viable routes for drug delivery [47, 53, 260]. Therefore, altered endocytic transport may affect cell and tissue homeostasis, as well as delivery of therapeutics. Yet, information on the relative activity of individual endocytic pathways in diseased cells is still scarce. Recently, our laboratory reported aberrant clathrin-mediated endocytosis in type A NPD cells, which limited uptake of therapeutic ASM [57]. To evaluate alternative endocytic routes that may be amenable for LSD therapies, here we examined caveolae-, macropinocytic-, and CAM-mediated uptake in these diseased cells, as well as transcytosis via the clathrin, caveolar, and CAM pathways.

As previously found for the clathrin route [57], uptake of a model ligand (CTB) of the caveolar route was also impaired in type A NPD cells. Specifically, the rate of CTB uptake and the absolute number of CTB-positive vesicles was reduced in diseased cells compared to healthy controls (**Figures 4A** and **5**). Yet, because CTB levels at the cell-surface were comparable to those of healthy cells (**Figure 4A**) and because fluid-phase caveolar uptake does not associate with specific receptors, the observed defect seems to be due to an aberrant capability for internalization rather than an abnormal availability of caveolar receptors, as described for receptors of the clathrin route [21, 57]. Nevertheless, we have not compared the GM1 levels (to which CTB binds) on these cells, and it is possible that altered biosynthesis, trafficking to the cell-surface, and/or recycling of plasma membrane components could also contribute to these effects.

Additional work by our laboratory also found that the cellular distribution of the machinery regulating caveolar vesicle formation (*e.g.*, caveolin-1) is disrupted in diseased cells [252], which may have contributed to decreased uptake via this pathway. Briefly, caveolin-1 was found to locate proximal to the nucleus in diseased cells and there was very minimal colocalization of CTB with caveolin-1 [252], suggesting alterations in endogenous trafficking and/or recruitment to caveolar-binding ligands, as was also the case for clathrin heavy chain recruitment to sites of Tf binding [57]. Notably though, we still observed CTB uptake by diseased cells at a level that was 47% of healthy levels after 1 h (**Figure 4A**), which seems high considering the drastic alteration in caveolin-1 distribution observed by our group [252]. This difference may be due to uptake contributed by compensatory pathways. For example, small fractions of GM1 could be taken up in clathrin-coated vesicles [250, 251]. However, this route is altered in this disease [57] and would contribute only minimally to CTB uptake, as shown using single and combination inhibitors for the clathrin and caveolar routes (**Figure 4B**). An alternative pathway involves dynamin-independent vesicles formed in lipid rafts and trafficked to the ER, as observed for CTB and simian virus 40 [261]. Whether this pathway compensates for CTB uptake in these diseased cells remains to be determined. Nevertheless, finding aberrant caveolar uptake is supported by previous studies that suggest abnormal intracellular trafficking via this route in LSD cells [116, 119]. In agreement, we observed that internalized CTB distributed differently in healthy and diseased cells: localizing to perinuclear versus more punctate and widespread compartments, which is consistent with the Golgi versus endosomes, respectively (**Figure 4A**).

In conjunction with diminished CTB uptake, lower uptake of dextran in diseased cells was observed relative to healthy cells (**Figure 6B**), suggesting a generalized defect in fluid-phase pinocytic activity. Further, dextran uptake via the clathrin and caveolar routes were similar in diseased cells, indicating these two routes contribute equally to uptake (**Figure 7A**). Hence, the endocytic defect may stem from a common cause (*e.g.*, aberrant lysosomal storage and/or particular lipid accumulation). Recent work demonstrated endocytic dysfunction despite having genetic and lysosomal profiles that differ from type A NPD [115, 120]. Therefore, numerous factors may play a role, such as cytoskeletal abnormalities, impaired cytosolic diffusion of molecules, and/or altered lipid metabolism [10, 116, 117, 119, 236, 238]. In particular, NPD-associated changes of the lipid composition (sphingomyelin and cholesterol [239]) in membranes along the biosynthetic and endocytic routes could disrupt the biophysical properties of lipid raft domains and other regions, altering the association of integral and peripheral proteins that act as receptors, adaptors, signaling molecules, and others in both the caveolar and clathrin pathway. This may cause a disturbance in elements associated with vesicular fusion/fission, sorting, trafficking, and so forth [108, 120, 262]. In fact, our results showed reduced colocalization of internalized ligands of the clathrin (Tf) and caveolar (CTB) pathways with early endosomes and lysosomes (**Figure 10**). Others have also reported defects in other vesicular trafficking mechanisms, such as lysosomal exocytosis, which is required for plasmalemma recycling and proper display of membrane proteins, including endocytic receptors [262].

EGF-induced macropinocytosis was also reduced in diseased cells (**Figure 9**). Although there is less information on this direction, several reports have suggested alteration in related functions. For instance, several pathogens, such as the Ebola virus and

some intracellular bacteria, exploit macropinocytosis-like routes to invade cells [263-268], where ASM activity (deficient in type A NPD) modulates such pathogen-host cell interactions [264-267]. Further, ASM increases the ceramide content of the plasmalemma, providing both the biophysical properties and actin reorganization required to sustain formation of large macropinocytic engulfment structures [263-265, 267, 269]. Macropinocytosis is also linked to the formation of foamy macrophages in lipid metabolic alterations [270], both of which are observed to occur in NPD [239]. Hence, it is plausible that ASM deficiency leading to lipid storage in NPD results in altered macropinocytic uptake, as observed here.

Approaches to bypass altered routes may help improve the therapeutic efficacy of ERT. As described in **Section 2.3.2**, ICAM-1 is an attractive target due to its widespread expression and activation during inflammation (a hallmark of NPD and other LSDs [66, 239]), because it undergoes uptake via a clathrin- and caveolae-independent pathway [64, 68], and because ICAM-1 has no endocytic ligands endogenous to the body; thus, there are no competitors for the induction and progress of this pathway. However, uptake of anti-ICAM NCs was also diminished in diseased cells (**Figure 11**), most likely because secreted ASM activity is required for ceramide enrichment and derived signaling events upon carrier binding on the cell-surface [78]. However, previous work by our group has demonstrated that coupling recombinant ASM to anti-ICAM NCs provides the necessary activity to restore full function of this pathway [77, 78].

In comparing the endocytic uptake of all three pathways, it is clearly evident that the CAM pathway is least impacted in diseased cells (**Figure 12**). Multivalent binding of anti-ICAM NCs displaying multiple copies of anti-ICAM to the cell-surface may be more

efficient in receptor clustering and inducing endocytic signals than classical non-multivalent binding strategies [271]. However, uptake of NCs coated with antibodies against the Tf receptor (anti-TfR NCs) was found to be significantly reduced compared to anti-ICAM NCs in prior work [65]. In fact, monomeric Tf is more readily internalized than anti-TfR NCs, while the opposite is observed in the case of anti-ICAM [65, 271]. Therefore, the observed differences here are not solely due to an effect of valency, but are more likely influenced by the biological function of the targeted receptor [47]. Furthermore, although the clathrin and caveolar pathways share some commonalities (*e.g.*, use of dynamin and actin [53]), there are also major differences between these pathways that may account for the slight variance observed between these two routes. For instance, the caveolar pathway is not directly involved in the biosynthetic or endocytic transport of lysosomal enzymes as is the clathrin pathway [272], and caveolar trafficking is known to bypass the lysosome in many cases in favor of Golgi and ER targets [273]. Therefore, the caveolar pathway may be somewhat less affected by lysosomal alterations, as we observed.

In contrast to uptake, the impact of disease on transcytosis (if any) was less acute for the clathrin, caveolar, and CAM pathways, and there was little difference between the three routes (**Figure 13**). This suggests the transcytosis route may bypass defects associated with impaired uptake and/or intracellular trafficking associated with the endo-lysosomal pathway. Although, it is also possible minimal differences were observed between these three pathways due to the relative affinities of the respective ligands used. For example, lowering the affinity of an antibody targeting the Tf receptor was found in the literature to enhance transcytosis across the BBB with increased accumulation in the brain parenchyma of mice, while high affinity counterparts remained associated to the brain endothelium

[274]. Here, we evaluated clathrin-mediated transcytosis using human Tf ligand, which is likely to have much lower affinity than in the case of the monoclonal antibody against ICAM-1 used for assessment of the CAM pathway. Since ICAM-1 has no endogenous ligands that are specific, monomolecular and soluble (in contrast to the Tf receptor), anti-ICAM was utilized for the CAM pathway so we could comparatively test transcytosis of monomeric binding to receptors for all three routes. Therefore, it is possible that transcytosis via the clathrin and caveolar pathways was minimally reduced due to lower ligand affinity, in contrast to the CAM pathway which showed a greater reduction in transcytosis due to the higher affinity associated with antibodies.

Currently, no work has been published regarding the status of receptor-mediated transcytosis in LSDs. Although we only observed slight alterations in transcytosis via each of the three pathways tested, this finding is in tune with other studies showing diminished transcytosis across endothelial cells in conditions such as hyperlipidemia and hyperglycemia [275, 276]. Interestingly, inhibition of endogenous ceramide production, which also occurs in NPD due to the inactivity of ASM, significantly decreased transcytosis of oxidized low-density lipoprotein across vascular endothelial cells by reducing the expression of membrane proteins involved in the transcytosis process [275]. Consequently, there was a reduction in lipoprotein accumulation in the vascular wall, a feature known to cause atherosclerosis [275]. While this contradicts the high prevalence of arthrosclerosis found in NPD patients [277], due to the complexity and numerous pathological changes that associate with this disorder, the development of atherosclerosis cannot be minimalized to the relationship between ceramide and lipoprotein transcytosis alone. Moreover, other work demonstrated transcytosis of CTB-GM1 complexes across

epithelial cells is dependent on the structure of the ceramide domain, and this pathway is independent from that of retrograde transport through the TGN or ER [278]. Therefore, ceramide seems to play an important role in transcytosis via all three pathways [78, 275, 278, 279]. As such, alteration in ceramide production, activity, structure, distribution, etc. as a result of ASM deficiency could reduce transcytosis via each route.

3.5. Conclusions

Variations in uptake, intracellular trafficking, and transcytosis in healthy versus diseased cells represent important considerations for therapeutic delivery targeted to endocytic routes that regulate these processes. A summary of the findings presented in this chapter are depicted in **Figure 14**. While clathrin activity is essential for conventional ERT via the M6P receptor [11] and several other strategies targeted to clathrin-dependent receptors [9], uptake via this pathway was most affected in diseased cells (**Figure 12**) and not significantly better than the other two pathways in regard to transcytosis (**Figure 13**). Therefore, it may not be the best route for ASM delivery across the BBB and uptake into cells of the CNS. Targeting the caveolar route could be an alternative, but uptake via this pathway was also impaired and material internalized via this pathway often avoids lysosomes [51, 273]. As well, the caveolar route seems minimally involved in transport across the BBB [199, 280], making it unsuitable as a universal treatment for all LSDs. Strategies involving macropinocytosis may be possible using certain signaling molecules (*e.g.*, EGF), but because this is not a receptor-mediated pathway, cargo would remain dissolved in the fluid-phase, preventing specific or concentrated cargo from reaching the cell interior. In contrast to these other routes, the non-classical CAM pathway seems the

most amenable for therapeutic delivery since it rendered transcytosis across a diseased model of the BBB similar to the other routes (**Figure 13**) and had the greatest uptake by diseased cells (**Figure 12**). Although ASM activity is required, resulting in slight impairment of uptake and transcytosis, this pathway is a receptor-mediated process that allows for specific targeting and concentration of an enzyme cargo on the NC surface [64, 68, 78]. As well, coupling recombinant ASM to anti-ICAM NCs provides the necessary activity to recover this endocytic route [77, 78]. Hence, in the next chapter we focused on better understanding regulation of the CAM pathway in order to optimize therapeutic enzyme delivery via anti-ICAM NCs.

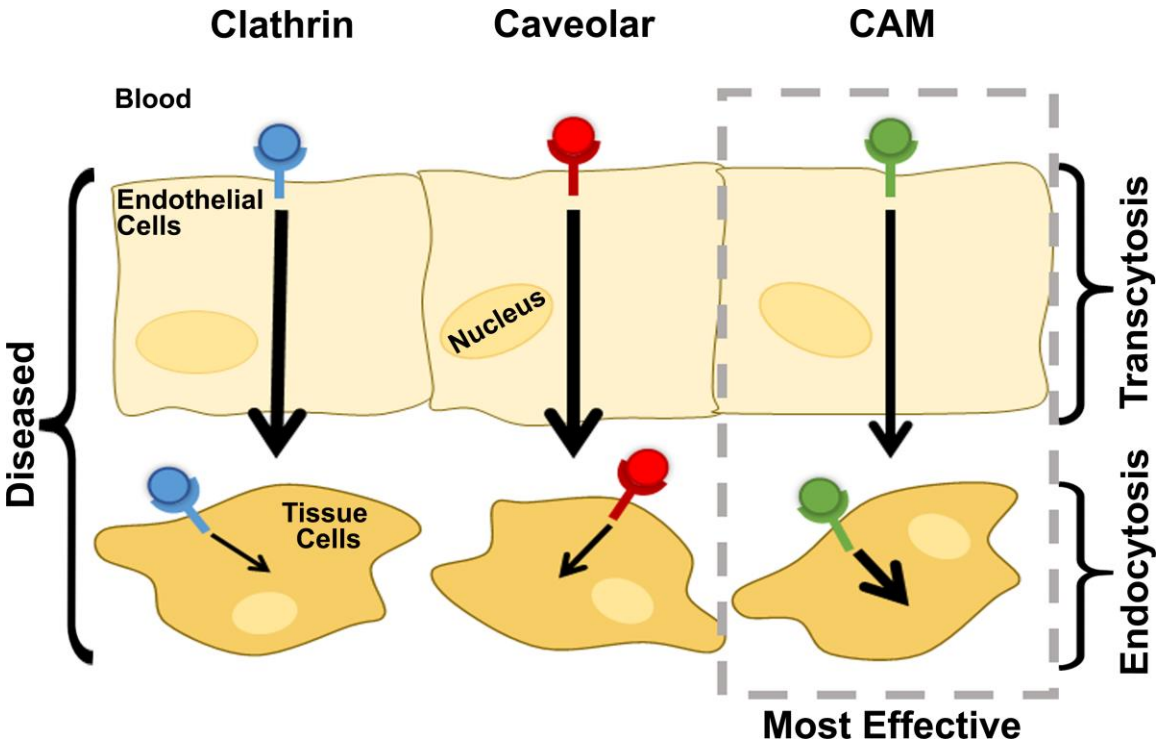

Figure 14. Relative efficiency of vesicular transport routes across and into cells in type A NPD. The cartoon depicts the efficiency of the clathrin, caveolar, and CAM pathways in regard to transcytosis across diseased endothelial cells and endocytic uptake by subjacent diseased tissue cells. The thickness of each black arrow represents the efficiency of transcytosis or endocytosis for each route, where increasing arrow thickness corresponds to greater efficiency. Taking into consideration both processes, the CAM pathway was found to be the most viable route in the disease scenario.

Chapter 4: Regulation of the CAM Pathway to Optimize Therapeutic Enzyme Delivery for Type A NPD[3]

4.1. Introduction

As described in **Section 2.2**, drug carriers targeted to endothelial cell-surface receptors involved in endocytic transport are broadly exploited for numerous therapeutic applications. In designing such carriers, selection of the endothelial cell-surface receptor for targeting must be carefully determined with consideration of a number of biological factors that impact their therapeutic efficacy, including competition by natural ligands for binding to the endothelial target, the expression level and distribution of the target receptor in the pathological condition requiring intervention, as well as the activity of the targeted endocytic pathway and the fate of the internalized material [47].

To improve treatment of type A NPD and other LSDs, which is the overall focus of this dissertation, delivery of lysosomal enzymes via anti-ICAM NCs is a viable option with great therapeutic potential. As described in prior sections, this is because ICAM-1 has widespread and enhanced expression in LSDs, and anti-ICAM NC binding permits transcytosis across cellular barriers with trafficking to lysosomes in tissue cells, both via the non-classical CAM pathway, resulting in enhanced enzyme delivery and reduction of substrate storage [57-72, 252, 257]. As well, the findings presented in **Chapter 3** and other work highlight the ability of this pathway to bypass classical routes (*e.g.*, clathrin and caveolar), whose endocytic activity was found to be impaired in type A NPD [57, 252,

[3]Chapter 4 contains text and figures reproduced in part with permission from: Manthe, R.L.* and Serrano, D.*, et al. *How carrier size and valency modulate receptor-mediated signaling: understanding the link between binding and endocytosis of ICAM-1-targeted carriers.* Biomacromolecules, 2016. 17(10): p. 3127-37; © 2016 American Chemical Society.

257]. Given these advantageous features, the goal of this chapter was to further elucidate regulation of the CAM pathway in order to optimize anti-ICAM NCs for this application.

Apart from selection of the endothelial cell-surface receptor for targeting, other design parameters also affect the success of therapeutic carriers, such as carrier size, shape, chemistry, and bulk concentration [47, 59, 62, 78, 79, 176, 259]. In regard to targeting ICAM-1, our laboratory has demonstrated the CAM pathway permits endothelial binding and uptake of carriers within a wide range of carrier sizes (from 100 nm to < few μm) and geometries (spherical, elongated, and irregular) in cell culture and mice [62, 78, 79]. This is in stark contrast to therapeutics and/or their carriers targeted to the clathrin or caveolar pathways, since they are restricted by the size of clathrin-coated pits (~100-200 nm in diameter) and caveoli invaginations (~50-100 nm in diameter) that form in these routes [51, 54]. For instance, spherical submicrometer (~200-250 nm in diameter) and 1 μm anti-ICAM carriers are both readily internalized by endothelial cells [79], although 1 μm carriers require a greater extent of cell-associated signaling for plasmalemma deformation and cytoskeletal remodeling during uptake [62, 68, 78, 79]. The great flexibility in carrier design likely stems from the physiological role of ICAM-1 in mediating the adhesion and extravasation of leukocytes, which are much larger entities [66, 67]. In fact, as in the case of multivalent leukocyte binding and extravasation, multivalent anti-ICAM carriers or conjugates are internalized more efficiently by vascular endothelial cells compared to monomeric counterparts [65, 271]. However, transcytosis of anti-ICAM was found to be similar to that of multivalent anti-ICAM NCs [281]. Therefore, in addition to carrier size, valency (*i.e.*, number of targeting molecules per carrier) is also likely to play an important role in regulation of the CAM pathway.

For clinical treatment of LSDs, NCs (~200-250 nm in diameter) are more relevant since they are trafficked more efficiently to lysosomes [62], and their small size does not impede delivery to capillaries and post-capillary venules, where carrier binding, intra- and transendothelial transport are most prominent due to minimal shear stress in these areas [176, 259]. The influence of valency using anti-ICAM NCs has been explored to some extent, although most work has focused primarily on valency effects pertaining to targeting and uptake [79, 176, 177, 180]. However, how valency influences cell-signaling events related to CAM-mediated uptake upon binding to ICAM-1 is not well-understood. Further, to our knowledge there is little information pertaining to the role of anti-ICAM valency on lysosomal trafficking and transcytosis across the BBB, which are two important processes for treatment of LSDs. Apart from the role of valency on these events, in general the relationship between lysosomal trafficking and transcytosis is not well-understood. While transcytosis most often implies avoidance of these compartments [198, 199], the CAM pathway permits both lysosomal trafficking and transcytosis [62-64, 70, 71]. Therefore, we investigated this caveat as well in order to better understand the mechanism(s) regulating the CAM pathway.

Lastly, whether mediated via classical or independent pathways, to the best of our knowledge there have been no studies on the mechanism(s) by which receptor-targeted drug carriers disengage from the basolateral endothelium after transcytosis across this lining. Some natural ligands, like iron-transporting Tf, dissociate from their receptors due to conformational changes occurring between the ligand-cargo in the bound versus unbound state (*i.e.*, iron-bound versus iron-unbound Tf) [282]. Yet, this has never been verified for the BBB or transcytosis events. As well, similar conformational changes do

not apply to ligands (*e.g.*, antibodies) used for targeting of drug carriers. Other natural ligands, including antibodies, can dissociate from their receptors due to changes in pH experienced during transit through endo-lysosomal compartments [283, 284]. However, as mentioned above, transcytosis most often implies avoidance of these compartments [198, 199]. Therefore, the multivalency of interaction and high avidity of targeted carriers may make it even more difficult to detach from a cell after transcytosis. This is of key importance since, even if transcytosis is efficient, a lack of detachment from the engaged receptor will result in carriers remaining bound to the basolateral side of the endothelium, thereby inhibiting carriers from being delivered to the underlining tissue.

In this context, proteolytic cleavage of the extracellular region of receptors, which has been observed in other instances [285], may permit basolateral detachment of targeted carriers after transendothelial transcytosis. In particular, matrix metalloproteinases (MMPs), zinc-dependent endopeptidases secreted by numerous cell types [286] are implicated in the shedding of cell-surface molecules to regulate a number of cellular events, including leukocyte-endothelial interactions and interactions between cells and the extracellular matrix [286-290]. Among MMPs, the gelatinases (MMP-9 and MMP-2) are implicated in cell migration across endothelial barriers [287-290]. Moreover, MMP-9 localized at the cell-surface has been shown to cleave the extracellular domain of ICAM-1 resulting in release of sICAM-1 [288, 291]. In fact, it has been speculated that shedding of ICAM-1, other endothelial CAMs, and their leukocyte co-receptors may help disengage both cell types after extravasation [292]. Although MMP-2 is not known to cleave ICAM-1, it may indirectly play a role in this process since MMP-2 is involved in cleavage of pro-MMP-9 into MMP-9, the active form of the proteinase [293, 294].

As such, in this chapter we explored how valency impacts anti-ICAM NC binding and associated cell-signaling, uptake, lysosomal trafficking, and transcytosis. As proof-of-concept, we also examined the therapeutic implications of valency in regard to anti-ICAM NC delivery of recombinant ASM (deficient in type A NPD) across the BBB in cell culture and mice. Moreover, we made significant efforts to decipher the link between lysosomal trafficking and transcytosis, as well as investigated the potential for proteolytic cleavage of surface ICAM-1 by MMP-9 or MMP-2 for anti-ICAM NC detachment from the basolateral cell-surface following transcytosis, along with speculation about the role of valency in mediating this process. Ultimately, this work will guide optimization of anti-ICAM NCs for treatment of type A NPD and other LSDs, as well as additional disorders requiring delivery across the BBB.

4.2. Materials and Methods

4.2.1. Antibodies and Reagents

Mouse monoclonal anti-human ICAM-1 (clone R6.5) [243] and rat monoclonal anti-mouse ICAM-1 (clone YN1) [295] were from American Type Culture Collection (Manassas, VA). Non-specific mouse IgG was from Jackson ImmunoResearch (West Grove, PA). Mouse IgM anti-ceramide was from Sigma-Aldrich (St. Louis, MO). Rabbit anti-human PKC (H-300), rabbit anti-human GAPDH, and FITC-labeled goat anti-mouse IgM were from Santa Cruz Biotechnology (Dallas, TX), Rabbit anti-phosphorylated human PKCα (phospho T638) was from Abcam (Cambridge, United Kingdom). Horseradish peroxidase (HRP)-linked anti-rabbit IgG was from GE Healthcare (Pittsburgh, PA). Texas Red-labeled secondary antibodies, Texas Red-labeled dextran (10,000 MW), and Alexa

Fluor 350-labeled secondary antibodies were from Invitrogen (Carlsbad, CA). Recombinant human ASM was kindly provided by Dr. Edward Schuchman (Department of Genetics and Genomics Sciences, Mount Sinai School of Medicine, New York, NY). Polystyrene beads were from Polysciences (Warrington, PA). Cell culture reagents were from Gibco-BRL (Grand Island, NY) or Cellgro (Manassas, VA). Porous transwell inserts (1.0 μm-pore) were from Thermo Fisher Scientific (Waltham, MA). ^{125}I and Iodogen pre-coated tubes were from Perkin Elmer (Waltham, MA) and Thermo Fisher Scientific (Waltham, MA), respectively. H-7 dihydrochloride, an inhibitor of protein kinase C (PKC), MMP-9 Inhibitor I (MMP-9i), and MMP-2 Inhibitor I (MMP-2i) were from EMD Millipore (Billerica, MA). Recombinant human MMP-9 (67 kDa) and MMP-2 (62 kDa) were from EMD Millipore (Billerica, MA) and Sigma-Aldrich (St. Louis, MO), respectively. Pre-cast 4-15% polyacrylamide gels were from Biorad (Hercules, CA) and PVDF membranes were from Pall Life Sciences (Port Washington, NY). Unless stated otherwise, all other reagents were from Sigma-Aldrich (St. Louis, MO).

4.2.2. Cell Cultures

HBMECs from Applied Cell Biology Research Institute (Kirkland, WA) were cultured in RPMI 1640 basal medium supplemented with 20% FBS, 2 mM L-glutamine, 30 μg/mL ECGS, 100 μg/mL heparin, 100 U/mL penicillin, and 100 μg/mL streptomycin. HBMECs were grown to confluence at 37°C, 5% CO_2, and 95% relative humidity on either 1% gelatin-coated coverslips or uncoated 1.0 μm-pore transwell inserts, both in 24-well plates. Alternatively, human umbilical vein endothelial cells (HUVECs) from Lonza (Walkersville, MD) were cultured in M-199 basal medium supplemented with 15% FBS,

2 mM L-glutamine, 15 µg/mL ECGS, 100 µg/mL heparin, 100 U/mL penicillin, and 100 µg/mL streptomycin. Cells were grown at 37°C, 5% CO_2, and 95% relative humidity on 1% gelatin-coated coverslips. Where indicated, cells were stimulated overnight with 10 ng/mL TNFα to induce endothelial activation, as found in LSDs [9, 239].

4.2.3. Preparation and Characterization of Anti-ICAM Carriers

Model polymer carriers were prepared by coating polystyrene beads (100 nm or 1 µm in diameter) via surface adsorption with anti-ICAM or non-specific IgG alone, mixtures containing different anti-ICAM to IgG mass ratios (100:0 versus 50:50 versus 25:75), or mixtures containing different anti-ICAM to ASM mass ratios (95:5 versus 50:50 anti-ICAM/ASM NCs) as described in **Section 3.2.6** and in prior work [64, 79]. For the antibody or ASM coat to be characterized, either anti-ICAM, IgG, or ASM were conjugated to ^{125}I, and the amount of radiolabeled antibody or enzyme per carrier was determined using a gamma counter (2470 Wizard^2, Perkin Elmer; Waltham, MA), as described [247]. The size of carriers was measured by dynamic light scattering or particle tracking (Nanosight LM10, Malvern Instruments; Westborough, MA), and the PDI and ζ-potential were obtained by dynamic light scattering and electrophoretic mobility, respectively (Zetasizer Nano-S90, Malvern Instruments; Westborough, MA).

Again, while non-degradable polystyrene carriers are not clinically relevant, they are used in this work to avoid potential confounding effects of concomitant NC degradation during intracellular trafficking and transcytosis. However, as mentioned in **Section 3.2.6**, these carriers have been shown to be comparable to biodegradable PLGA counterparts [58, 81]. As well, the addition of ASM to anti-ICAM NCs has not been found to affect their

physical properties or the ability of anti-ICAM to target cells [58, 81]. Prior work by our laboratory has also demonstrated minimal release of therapeutic enzymes from the NC surface under mechanical stress and physiological-like conditions [60, 61], while providing release in lysosomes for reduced accumulation of substrate storage [57, 60-62, 64].

4.2.4. Avidity and Binding Specificity of Anti-ICAM NCs

To test the avidity and binding specificity of green fluorescent anti-ICAM NCs with different valencies (~200 nm in diameter; 2,058 to 7,703 anti-ICAM molecules/μm^2 carrier surface) while avoiding confounding effects associated with NC uptake, TNFα-activated HBMECs seeded on coverslips were first fixed with 2% paraformaldehyde. To assess avidity, cells were then incubated with anti-ICAM NCs at different concentrations (from 22.5 to 3,780 pM) for 1 h at room temperature, followed by removal of non-bound NCs by washing. Similarly, binding specificity was examined by incubating anti-ICAM NCs with fixed, TNFα-activated HBMECs for 15 min to 24 h at room temperature using an intermediate NC concentration (113 pM). All samples were then washed, stained with DAPI to label cell nuclei, and mounted on slides for analysis by fluorescence microscopy as described in **Section 3.2.3**. Using a customized algorithm in Image-Pro 6.3 that detects fluorescent pixels over a background threshold, the number of NCs was then computed based on the number of pixels that theoretically correspond to the size of a single particle. Regression analysis was performed with SigmaPlot 11.0 (Systat Software Inc.; San Jose, CA) for each valency.

4.2.5. Ceramide Enrichment at Sites of Carrier-Cell Binding

Red or non-fluorescent anti-ICAM carriers of different sizes (250 nm or 1 μm in diameter) and valencies (from 800 to 30,000 anti-ICAM molecules/μm^2) were incubated for 15 or 30 min at 37°C with TNFα-activated HUVECs seeded on coverslips. Non-bound carriers were washed off, cells were fixed with 2% paraformaldehyde, and surface-bound carriers were immunostained blue with an Alexa Fluor 350-labeled secondary antibody. The cells were then permeabilized with 0.2% Triton X-100, and ceramide, a signaling molecule associated with the CAM pathway [77, 78] was immunostained in green. Cells were then visualized using fluorescence microscopy. Image-Pro 6.3 was used to determine ceramide fluorescence at sites of carrier binding, as described previously [77, 78]. Briefly, ceramide fluorescence intensity at the plane of a carrier "equator" was determined around the carrier circumference (membrane engulfment area) and outside the region of carrier binding (background), from which the ceramide enrichment associated with carrier binding was calculated (*i.e.*, engulfment - background).

4.2.6. PKC Signaling Upon Cell Binding of Targeted Carriers

Green or non-fluorescent anti-ICAM carriers of different sizes (250 nm or 1 μm in diameter) and valencies (8,000 to 13,000 anti-ICAM molecules/μm^2) were incubated for 10 or 30 min at 37°C with TNFα-activated HUVECs seeded on coverslips. Non-bound carriers were washed off, cells were fixed with 2% paraformaldehyde, and surface-bound carriers were stained blue with an Alexa Fluor 350-labeled secondary antibody. In parallel experiments, the cells were then permeabilized with 0.2% Triton X-100 and either total PKC or activated (phosphorylated)-PKCα were immunostained in red and visualized using

fluorescence microscopy, from which total PKC and pPKCα enrichment at sites of carrier-cell binding were calculated as described above for ceramide enrichment. In addition, pPKCα present in the lysate of cells incubated in the absence versus presence of anti-ICAM carriers (250 nm or 1 μm in diameter; 10,000 to 30,000 anti-ICAM molecules/μm^2) was separated by sodium dodecyl sulfate polyacrylamide gel electrophoresis (SDS-PAGE). This was followed by Western blot to immunodetect and normalize the level of pPKCα to that of the housekeeping protein GAPDH. For both fluorescence and Western blot assays testing PKC signaling, two different times (10 and 30 min) were analyzed and averaged to estimate signal enrichment. This is because PKC is involved in both endocytosis upon carrier binding to ICAM-1 and also subsequent intracellular trafficking [62, 68], events that occur sequentially. Since the uptake and intracellular trafficking kinetics of submicrometer carriers is slightly different from that of micrometer carriers, averaging the signal at two different time points minimizes potential confounding effects of a dual (uptake and trafficking) signal.

4.2.7. Uptake of Anti-ICAM NCs

To evaluate the effect of valency on NC internalization, green fluorescent anti-ICAM NCs (~200 nm in diameter; 2,058 to 7,703 anti-ICAM molecules/μm^2) were incubated with TNFα-activated HBMECs seeded on coverslips at 37°C for 5 min, 15 min, or 30 min to permit NC binding. After 30 min (pulse), non-bound NCs were removed by washing and further incubated in fresh medium at 37°C for additional time up to 24 h to allow uptake of surface-bound NCs (chase). At select time points, cells were fixed with 2% paraformaldehyde. As in **Section 3.2.7**, surface-bound NCs were immunostained using a

Texas Red-labeled secondary antibody, which recognizes both the anti-ICAM and mouse IgG coated on the NCs. Since NCs contain a green-fluorescent label, this renders yellow surface-bound NCs (red + green = yellow) versus green internalized NCs, as previously described [247]. Similar experiments were performed in the presence of 25 μM MMP-9 inhibitor (MMP-9i) or 25 μM MMP-2 inhibitor (MMP-2i).

Alternatively, uptake of green fluorescent anti-ICAM NCs (~200 nm in diameter; 7,703 anti-ICAM molecules/μm^2) was quantified in TNFα-activated HBMECs seeded on 1.0 μm-pore transwell inserts following a 30 min binding period at 37°C (pulse), and uptake for an additional 30 min or 1.5 h in carrier-free medium (chase). As in the coverslip model, cells were then washed, fixed, and immunostained to distinguish surface-bound versus internalized NCs. Cells were visualized using a LSM 710 confocal laser scanning microscope with a 100x Plan-APOCHROMAT objective and 405, 488, and 555 lasers (Zeiss; Oberkochen, Germany). Z-stacks were obtained starting from the basolateral cell-surface in contact with the transwell membrane and moving up to the apical cell-surface at a width of 0.37 μm per z-section. Then, z-stacks of the entire cell body (apical to basolateral surface) or z-stacks corresponding to only the basolateral cell-surface (1.11 μm width) were converted into three-dimensional color composites using Image J software.

For both the coverslip and transwell models, the algorithm described in **Section 4.2.4** was used to quantify the number of internalized NCs per cell based on the green fluorescent pixels, and the percentage of NC internalization was quantified as the green fluorescent pixels over the total cell-associated fluorescence. Where loss of total fluorescence over time occurred (as a result of three-dimensional stacking of internalized NCs that cannot be resolved with microscopy), the total number of cell-associated NCs at

the 30 min binding period was multiplied by the percentage of NC internalization to quantify the respective number of internalized NCs at each subsequent time point. Regression analysis was performed for each valency in the coverslip model using SigmaPlot 11.0.

4.2.8. Transcytosis of Anti-ICAM NCs or Anti-ICAM/ASM NCs

^{125}I-labeled anti-ICAM NCs (~200 nm in diameter; 2,058 to 7,703 anti-ICAM molecules/μm^2) were added to the apical chamber of 1.0 μm-pore transwell inserts above a monolayer of TNFα-activated HBMECs. NCs were incubated with cells for 30 min (pulse) at 37°C to allow binding to cells. NCs that did not bind to cells or those that leaked across the HBMEC monolayer were then removed by washing both the apical and basolateral chambers. Bound NCs were then incubated with cells in fresh medium at 37°C for additional time up to 30 h to allow transcytosis across the cell monolayer (chase). At select time points, the ^{125}I content in the cell fraction (bound and internalized NCs) and in the basolateral chamber below cells (transcytosed NCs) was measured using a gamma counter, and the number of NCs in each fraction was then calculated based on the CPM/NC. Further, the number of anti-ICAM NCs was corrected by subtraction of free ^{125}I in each fraction as determined by trichloroacetic acid (TCA) precipitation [247]. Regression analysis was performed for each valency using SigmaPlot 11.0. As well, similar experiments were performed in the presence of one of the following: 25 μM MMP-9i; 25 μM MMP-2i; 800 pg/mL recombinant MMP-9; 114 ng/mL recombinant MMP-2. To observe the effect of valency on delivery of a model therapeutic cargo, ^{125}I-labeled anti-ICAM/ASM NCs (95:5 versus 50:50 mass ratio) were also assessed in the same manner.

Lastly, the relationship between lysosomal trafficking and transcytosis was evaluated in two ways. First, ^{125}I-labeled anti-ICAM NCs (7,703 anti-ICAM molecules/μm^2) were added to the apical chamber of 1.0 μm-pore transwell inserts above a monolayer of TNFα-activated HBMECs. NCs were incubated with cells for 30 min at 37°C to allow binding to cells, non-bound NCs were removed by washing both chambers, and the cells were incubated for an additional 30 min in fresh medium to allow NC uptake. Afterwards, the cells were washed again and incubated in fresh medium supplemented with 10 μM H-7 (inhibits lysosomal trafficking) for another 4 h at 37°C. Alternatively, non-radiolabeled anti-ICAM NCs were added to cells and incubated for 30 min at 37°C to allow NC binding, followed by washing both chambers to remove non-bound NCs, and incubation for an additional 1.5 h at 37°C in fresh medium to allow NC uptake and trafficking to lysosomes. Afterwards, ^{125}I-labeled anti-ICAM NCs were added to cells for 30 min at 37°C for NC binding, followed by washing, and additional incubation for 4.5 h in fresh medium. The same procedure and corrections described above were then performed.

4.2.9. Lysosomal Trafficking of Anti-ICAM NCs

To examine lysosomal trafficking, TNFα-activated HBMECs seeded on coverslips were first incubated with Texas Red-labeled dextran (10,000 MW) for 45 min at 37°C, followed by washing and additional incubation at 37°C for 45 min to allow dextran trafficking to lysosomes. Anti-ICAM NCs (~200 nm in diameter; 2,058 to 7,703 anti-ICAM molecules/μm^2) were then added to cells for 30 min (pulse), followed by washing to remove non-bound NCs, and incubated in fresh medium for additional time up to 24 h

at 37°C to allow trafficking of NCs to lysosomes (chase). At select time points, cells were fixed with 2% paraformaldehyde. Green NCs colocalized with red lysosomes appear yellow in color versus NCs that are not in lysosomes which appear single-labeled in green [64]. Alternatively, colocalization of anti-ICAM NCs (7,703 anti-ICAM molecules/μm^2) with lysosomes was quantified in TNFα-activated HBMECs seeded on 1.0 μm-pore transwell inserts using the same procedure described above for the coverslip model. Imaging was performed via confocal microscopy in the same manner as described in **Section 4.2.7**.

For both models, the number of NCs colocalized with lysosomes per cell was quantified based on the yellow (green + red) fluorescent pixels, and the percentage of either total cell-associated or internalized NCs (as indicated) colocalized with lysosomes was quantified as the yellow fluorescent pixels over the total or internalized fluorescence, where the internalized fraction was quantified by multiplying the total cell-associated fluorescence by the percent internalization at each respective time point. Similar to NC uptake, where loss of total fluorescence over time occurred, the internalized fluorescence at the 30 min binding period was multiplied by the percentage of NC colocalization with lysosomes to quantify the respective number of NCs colocalized with lysosomes per cell at each subsequent time point. Regression analysis was performed for each valency in the coverslip model using SigmaPlot 11.0. Further, the total number of dextran-occupied lysosomes per cell was counted, as well as the number of NCs located within the pores of the transwell membrane.

4.2.10. Biodistribution of Anti-ICAM/ASM NCs in Mice

Wild-type C57Bl/6 mice from Jackson Laboratory (Bar Harbor, ME) were anesthetized by intraperitoneal injection of a ketamine/xylazine cocktail. Once under anesthesia, ^{125}I-labeled anti-ICAM/ASM NCs (95:5 versus 50:50 mass ratios) were injected into the jugular vein (~1.5 x 10^{13} NCs/kg of body weight). These antibody to enzyme ratios yield high valency NCs (~7,703 anti-ICAM molecules/μm^2 and 28 ± 2 ASM molecules/NC) and intermediate valency NCs (~4,145 anti-ICAM molecules/μm^2 and 203 ± 5 ASM molecules/NC). The total ASM injected was ~52 µg/kg for the high valency and ~378 µg/kg for the intermediate valency. Blood samples were collected 1, 15, and 30 min post-injection via the retro-orbital sinus, and organs of interest (brain, liver, and spleen) were collected after euthanasia at 30 min post-injection. The weight and ^{125}I content of all samples were measured to calculate the following: percent injected dose (% ID), percent injected dose per gram of tissue (% ID/g), and number of ASM molecules. Experiments were conducted following IACUC protocols with humane care guidelines, as approved by the University of Maryland, College Park.

4.2.11. Statistics

Fluorescence microscopy experiments encompassed a total sample size of $n \geq 12$. Western blot data were $n = 6$. For transcytosis studies, data were $n \geq 4$. Animal data were $n \geq 5$. Data were calculated as the mean ± SEM, where statistical significance was determined as $p < 0.05$ by Student's *t*-test.

4.3. Results

4.3.1. Characterization of Anti-ICAM NCs with Different Valencies

For most of the work presented below, the effect of targeting valency on the CAM pathway was assessed using 100 nm polystyrene beads coated with anti-ICAM and non-specific IgG in three different mass ratios (100:0, 50:50, and 25:75) as shown in **Table 3**. Each formulation had similar physical properties with diameters ranging from 178 to 182 nm, PDI of 0.17 to 0.19, and ζ-potential (surface charge) of -27.4 to -28.1 mV. By antibody radiolabeling, we also verified that only the targeting valency varied, while the total number of antibodies (anti-ICAM + IgG) on the NC surface remained similar (**Table 3**). Covering the NC surface with saturating levels of anti-ICAM rendered 7,703 anti-ICAM molecules/μm^2 of NC surface (valency 1), while addition of IgG to the coating mixture in increasing amounts resulted in 4,145 anti-ICAM molecules/μm^2 (valency 2; 55% anti-ICAM), and 2,058 anti-ICAM molecules/μm^2 (valency 3; 30% anti-ICAM) (**Table 3**).

Table 3. Characterization of anti-ICAM NCs with different valencies.

				Coating		Binding Avidity	
	Size (nm)	**PDI**	**Zeta Potential (mV)**	**Total Antibody Molecules/μm^2**	**Anti-ICAM Molecules/μm^2**	**B_{max} (NCs/Cell)**	**K_d (pM)**
Uncoated NCs	113 ± 2	0.06 ± 0.01	-38.5 ± 2.1	-	-	-	-
Valency 1							
Mouse IgG NCs	169 ± 4	0.19 ± 0.01	-27.4 ± 0.5	6,190 ± 286	-	-	-
Anti-ICAM NCs	178 ± 4	0.19 ± 0.00	-27.4 ± 0.2	7,703 ± 244	7,703 ± 244	14,681 ± 859	177.2 ± 37.7
Valency 2							
Anti-ICAM/IgG NCs	182 ± 2	0.18 ± 0.01	-28.1 ± 0.3	7,493 ± 240	4,145 ± 240	13,141 ± 766	218.7 ± 44.8
Valency 3							
Anti-ICAM/IgG NCs	181 ± 2	0.17 ± 0.01	-28.1 ± 0.5	6,792 ± 110	2,058 ± 110	12,465 ± 592	401.4 ± 59.8

Data are the mean ± SEM.

The reduction in valency among the three formulations correlated well with a decrease in their respective avidities toward fixed, activated brain endothelial cells: the binding constant (K_d) was 177, 219, and 401 pM for valencies 1, 2, and 3, respectively (**Table 3**). However, the absolute number of NCs bound at saturation was similar among all three valencies tested (**Table 3** and **Figure 15**), suggesting the number of cell-surface ICAM-1 accessible for NC binding is the limiting factor.

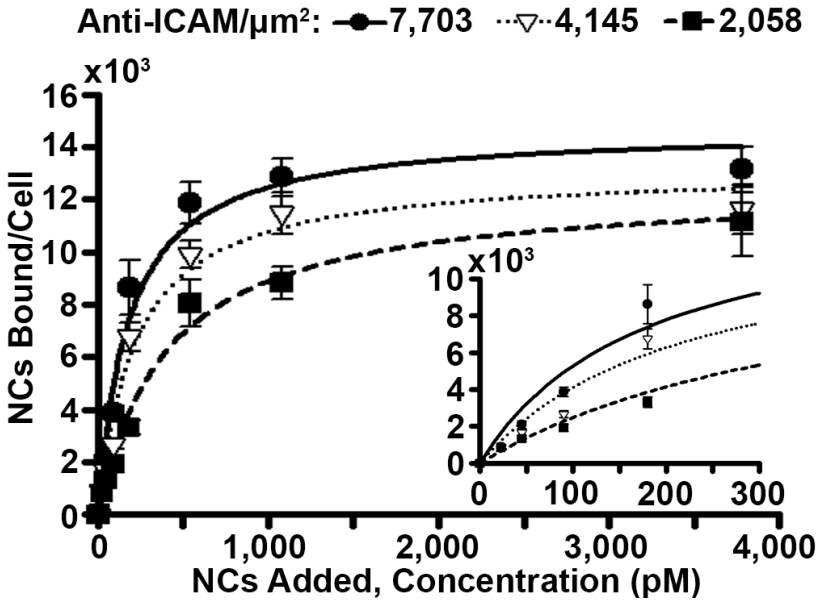

Figure 15. Role of valency on anti-ICAM NC avidity toward brain endothelial cells. Fixed, TNFα-activated HBMECs were incubated for 1 h at room temperature with varying concentrations (22.5 to 3,780 pM) of anti-ICAM NCs with different valencies, where the inset shows NC binding up to 300 pM. NC binding per cell was quantified by fluorescence microscopy as described in **Section 4.2.4**. Data are the mean ± SEM, for which regression curves were fitted. Statistical significance is not shown for simplicity, but it was obtained and considered in the description of the results.

4.3.2. Endothelial Binding of Anti-ICAM NCs with Different Valencies

Next, we used fixed, activated brain endothelial cells to assess anti-ICAM NC binding without concomitant uptake. As shown in **Figure 16**, NCs bound faster as anti-ICAM valency increased, which was expected based on the aforementioned avidity data.

Specifically, anti-ICAM NCs with high valency (7,703 anti-ICAM/μm^2) had a half-time ($t_{1/2}$) to maximal binding of 1.4 h, while the intermediate valency (4,145 anti-ICAM/μm^2) was 2.4 h, and the low valency (2,058 anti-ICAM/μm^2) rendered a $t_{1/2}$ of 6.6 h (**Table 4**). Yet again, all three valencies reached similar saturation levels and were comparable to those found for NC avidity (**Tables 3** and **4**), providing additional support that the number of accessible ICAM-1 receptors on the cell-surface limits NC binding.

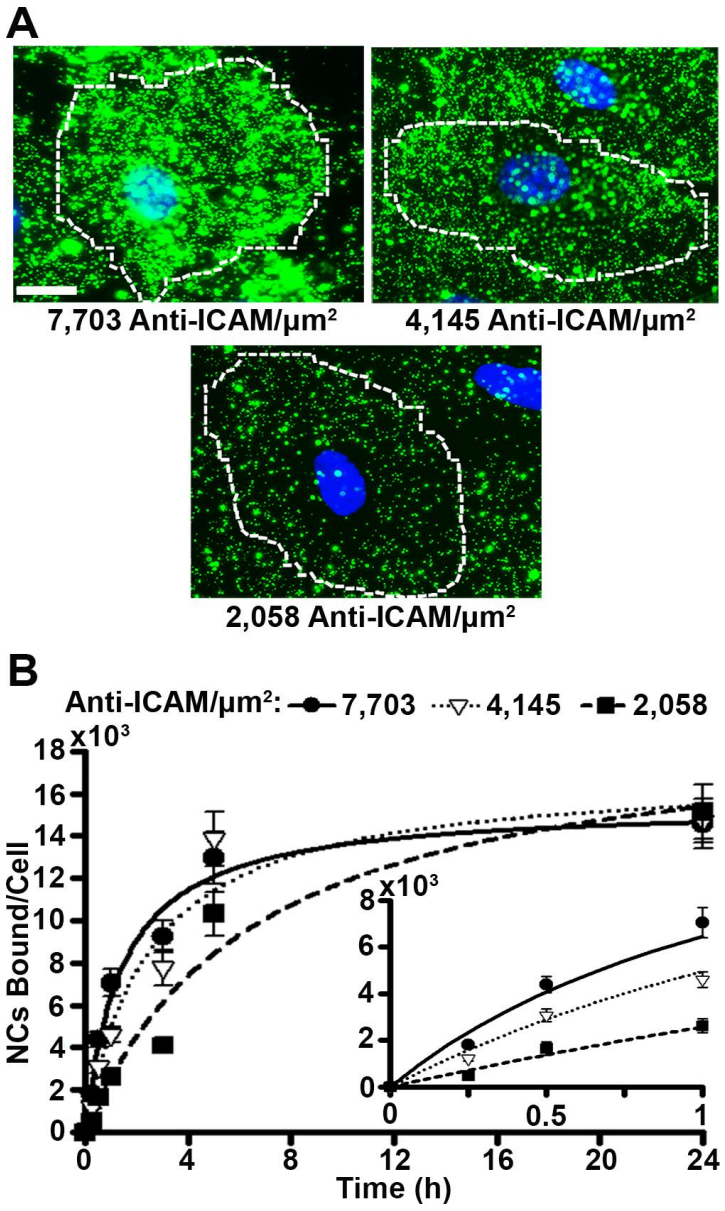

Figure 16. Role of valency on anti-ICAM NC binding to brain endothelial cells. (A) Fluorescence microscopy images showing binding of green fluorescent anti-ICAM NCs with different valencies to fixed, TNFα-activated HBMECs after 1 h incubation at room temperature. Cell nuclei were stained blue with DAPI and dashed lines mark the cell borders, as observed by phase-contrast microscopy. Scale bar = 10 μm. (B) Anti-ICAM NC binding to cells was quantified over a period of 24 h at room temperature, where the inset shows the first 1 h of incubation. Data are the mean ± SEM, for which regression curves were fitted. Statistical significance is not shown for simplicity, but it was obtained and considered in the description of the results.

Table 4. Summary of regression curve data for anti-ICAM NCs with different valencies.

	Valency 1	Valency 2	Valency 3
Anti-ICAM Molecules/NC μm²:	7,703 Ab/μm²	4,145 Ab/μm²	2,058 Ab/μm²
Binding			
$t_{1/2}$ (h)	1.40 ± 0.26	2.43 ± 0.76	6.62 ± 2.16
B_{max} (NCs Bound/Cell)	15,486 ± 837	17,003 ± 1,754	19,629 ± 2,615
Internalization			
$t_{1/2}$ (h)	0.47 ± 0.11	0.65 ± 0.16	0.80 ± 0.16
I_{max} (NCs Internalized/Cell)	2,292 ± 101	2,413 ± 126	1,674 ± 71
Transcytosis			
$t_{1/2}$ (h)	3.30 ± 0.60	1.66 ± 0.56	2.98 ± 1.00
T_{max} (NCs Transcytosed/Cell)	10,081 ± 508	7,129 ± 519	9,094 ± 821
Lysosomal Colocalization			
$t_{1/2}$ (h)	1.65 ± 0.38	2.12 ± 0.53	1.84 ± 0.40
L_{max} (NCs Colocalized/Cell)	1,803 ± 102	1,942 ± 128	1,258 ± 69

Data are the mean ± SEM. All $R^2 > 0.95$.

4.3.3. Endothelial Cell-Signaling Induced by Binding of Anti-ICAM Carriers with Different Valencies

Upon anti-ICAM carrier binding to cell-surface ICAM-1, there is a cascade of signaling events induced through the sodium proton exchanger 1 (NHE1) and ASM (see **Figure 3**) [68, 78, 227]. Briefly, ASM hydrolyzes sphingomyelin to ceramide at the cell-surface, causing modification of the lipid composition and biophysical properties of the plasma membrane at regions of anti-ICAM carrier binding [78]. Protein kinase C (PKC) has also been reported to contribute to this signaling, which along with the ceramide signal culminates in rearrangement of actin into stress fibers and carrier uptake [62, 68, 73, 77, 78, 227]. Here, we examined the correlation between anti-ICAM valency on carriers and induction of ceramide and PKC signaling in activated endothelial cells. To do so, we

prepared model anti-ICAM carriers of different sizes (250 nm versus 1 μm in diameter) and valencies (800 to 30,000 anti-ICAM molecules/μm^2).

First, we found a linear correlation between ceramide enrichment and anti-ICAM valency regardless of carrier size or concentration of carriers added to cells (**Figure 17**). Specifically, ceramide enrichment increased with a greater density of ICAM-1 engagement, which was calculated as the number of anti-ICAM molecules/μm^2 multiplied by a factor of two, since anti-ICAM is bivalent and each antibody molecule can theoretically engage two ICAM-1 molecules on a cell. In the case of micrometer carriers, decreasing anti-ICAM valency from 30,000 to 13,000 anti-ICAM molecules/μm^2 significantly reduced ceramide enrichment (2-fold decrease; points indicated by red arrows in **Figure 17**). Similarly, submicrometer carriers (12,000 versus 1,600 anti-ICAM molecules/μm^2) showed a 1.5 fold-reduction in ceramide enrichment (points indicated by purple arrows and circles in **Figure 17**). Despite having lower ceramide enrichment, submicrometer carriers with saturating valency had an enhanced rate of uptake compared to the larger carriers (data not shown, presented in [79]). Therefore, submicrometer carriers require less signal for uptake to occur. Interestingly, ceramide enrichment was comparable for anti-ICAM carriers (1 μm and 30,000 anti-ICAM molecules/μm^2) incubated with activated endothelial cells at different concentrations (1.2-fold difference; circled in blue in **Figure 17**), despite having significantly different levels of binding (19-fold difference; data not shown, presented in [79]). As such, ceramide enrichment is mediated by each one carrier as opposed to being dependent on the total number of carriers bound. Furthermore, carriers of different sizes (1 μm versus 250 nm) but similar valencies (13,000 versus 12,000 anti-ICAM molecules/μm^2) and concentration added to cells were comparable (1.2-fold

difference; points circled in green in **Figure 17**) even though submicrometer anti-ICAM NCs bind to a significantly greater extent (12-fold difference; data not shown, presented in [79]). Therefore, it is the valency density (*i.e.*, targeting molecules per carrier surface area) that regulates cell-signaling upon anti-ICAM NC binding, and not the absolute valency (*i.e.*, targeting molecules per carrier). However, for carriers of identical size, the surface area is the same and, therefore, only changes in absolute valency are possible. Since NCs of the same size are evaluated in the other sections of this chapter, valency is equivalent to valency density in this case.

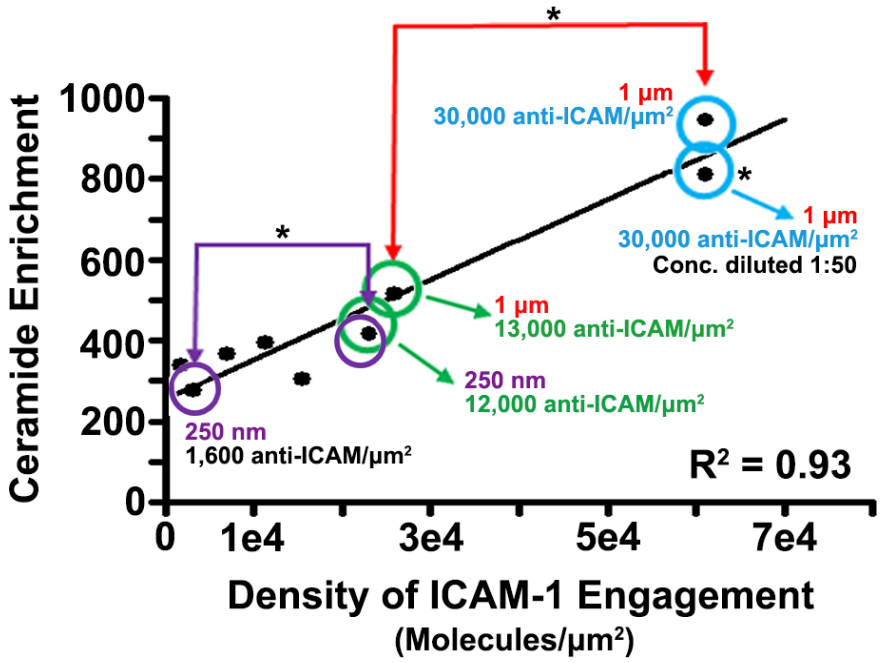

Figure 17. Role of valency on ceramide enrichment induced by anti-ICAM carrier binding to endothelial cells. Anti-ICAM carriers of different sizes (250 nm versus 1 µm in diameter) and valencies (800 to 30,000 anti-ICAM molecules/µm^2) were incubated with TNFα-activated HUVECs at 37°C for 15 min or 30 min and the enrichment of ceramide at sites of carrier-cell binding was measured as described in **Section 4.2.5**. The graph shows the relationship between ceramide enrichment and the density of ICAM-1 engagement, which was calculated as the number of anti-ICAM molecules/µm^2 multiplied by a factor of two, since anti-ICAM is bivalent and each antibody molecule can theoretically engage two ICAM-1 molecules on a cell. The line represents a linear regression, for which R^2 = regression coefficient. Data are the mean. *Comparison between the carriers indicated ($p < 0.05$ by Student's *t*-test). *Micrometer carrier data were collected by Dr. Daniel Serrano, former member of the Muro Laboratory.* Figure adapted from [79].

To further validate that valency density rules signaling upon carrier binding, we then examined PKC recruitment and activation at anti-ICAM carrier binding sites using an immunofluorescence approach similar to that for ceramide enrichment. Using an antibody capable of detecting all PKC isoforms regardless of their activation status, we found that total PKC enrichment at carrier binding sites depended on valency density, but not carrier size (**Figure 18A**; black bars). For instance, carriers with similar valencies (13,000 and 12,000 anti-ICAM molecules/μm^2) but very different sizes (1 μm versus 250 nm) rendered similar total PKC enrichment (1.05-fold difference; two left black bars in **Figure 18A**). Instead, for carriers of the same size (250 nm), lowering the valency from 12,000 to 8,000 anti-ICAM molecules/μm^2 decreased total PKC recruitment by 1.5-fold (two right black bars in **Figure 18A**). This pattern persisted when we evaluated a more specific marker of PKC signaling: active (phosphorylated)-PKCα (pPKCα), the main form related to ICAM-1 signaling [73]. As in the case of total PKC, very different sizes (1 μm versus 250 nm) but comparable valencies (13,000 versus 12,000 anti-ICAM molecules/μm^2) generated similar pPKCα enrichment (1.1-fold difference; two left white bars in **Figure 18A**), while carriers with the same size (250 nm) but different valencies (8,000 versus 12,000 anti-ICAM molecules/μm^2) rendered different enrichment (1.4-fold difference; two right white bars in **Figure 18A**). Western blot analysis of pPKCα, to confirm this result by a different method, suggested a similar trend when comparing carriers of the same size (1 μm) and different valencies (30,000 versus 13,000 anti-ICAM molecules/μm^2), which rendered different signal (1.24-fold; two left bars in **Figure 18B**). Carriers with different sizes (1 μm versus 250 nm) but more similar valencies (13,000 and 10,000 anti-ICAM molecules/μm^2) rendered a similar signal (1.08-fold difference; two right bars in **Figure 18B**). This is

despite Western blot not being ideal for this type of analysis, since it does not allow distinction between surface-bound and internalized carriers (in contrast to fluorescence visualization), and the goal is to relate binding valency to signals preceding endocytosis. Hence, the fact that Western blot results paired relatively well with fluorescence imaging strengthens our conclusion.

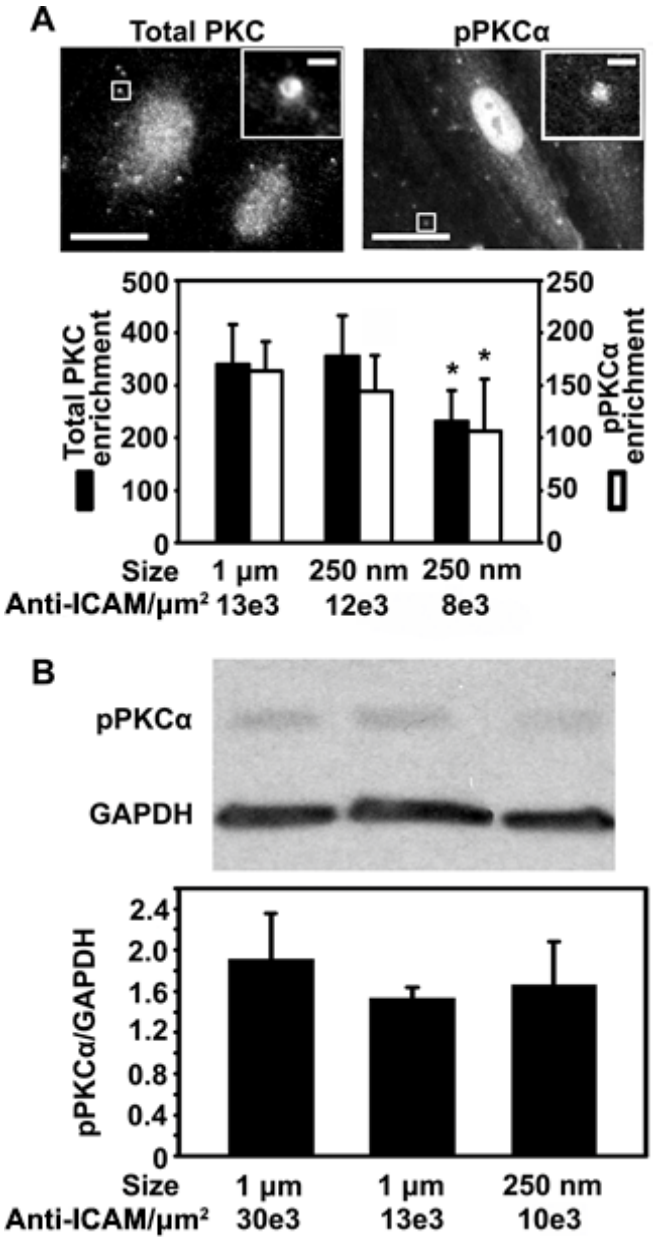

Figure 18. Role of valency on PKC signaling induced by anti-ICAM carrier binding to endothelial cells. (A) Fluorescence microscopy (top panel, with magnified insets showing 1 μm anti-ICAM carriers) and image quantification (bottom panel) of the enrichment of either total PKC or pPKCα upon incubation of anti-ICAM carriers with TNFα-activated HUVECs at 37°C (enrichment at 10 min and 30 min was averaged). Different carrier sizes (250 nm versus 1 μm in diameter) and anti-ICAM valencies (8,000 to 13,000 anti-ICAM molecules/μm^2) are shown. Scale bar = 10 μm (full) or 1 μm (inset). (B) Western blot (top panel) and densitometric quantification (bottom panel) showing pPKCα normalized to GAPDH levels, in cells incubated with anti-ICAM carriers (250 nm or 1 μm in diameter; 10,000 to 30,000 anti-ICAM molecules/μm^2) as in (A). Data are the mean ± SEM. *Comparison to carriers of the same size but different valencies ($p < 0.05$ by Student's *t*-test). Figure adapted from [79].

4.3.4. Endothelial Uptake of Anti-ICAM NCs with Different Valencies

Next, we examined the effect of valency on anti-ICAM NC uptake by activated brain endothelial cells (**Figure 19**). To do so, we utilized a pulse-chase method in which anti-ICAM NCs were permitted to bind to cells for 30 min, followed by washing to remove non-bound NCs, and incubation in fresh medium for additional time up to 24 h (chase) in order to track uptake of bound NCs. As seen in **Table 4** and **Figure 19B**, regardless of the difference in valencies, anti-ICAM NC uptake is a much faster process than binding: the half-time ($t_{1/2}$) for maximal NC uptake was less than 1 h for all valencies compared to the 1.4-6.6 h required for binding (**Table 4**). Hence, the data indicate that anti-ICAM NC binding is the rate limiting step in the CAM pathway. In accord, the half-time to maximal uptake increased along with a reduction in anti-ICAM valency: 28 min, 39 min, and 48 min for the high, intermediate, and low valencies, respectively, which was expected given the same trend in their binding rates (**Table 4**). However, maximal anti-ICAM NC uptake was approximately 30% less for the low valency (2,058 anti-ICAM molecules/μm^2) (**Table 4** and **Figure 19B**), despite having similar levels of binding at saturation (**Figure 16**). This could be attributed to a reduction in the total number of anti-ICAM NCs bound after the 30 min pulse (~1,600 NCs bound for the low valency versus ~2,200 NCs bound for the intermediate and high valencies; data not shown). Looking at **Figure 19C**, we also found a similar trend between valency and anti-ICAM NC uptake expressed as a percentage of total cell-associated NCs. Nevertheless, the differences between these valencies were much less acute than that of NC binding, and uptake via the CAM pathway was found to be a very efficient process, given there was 100% NC internalization at saturation for all three valencies tested (**Figure 19C**).

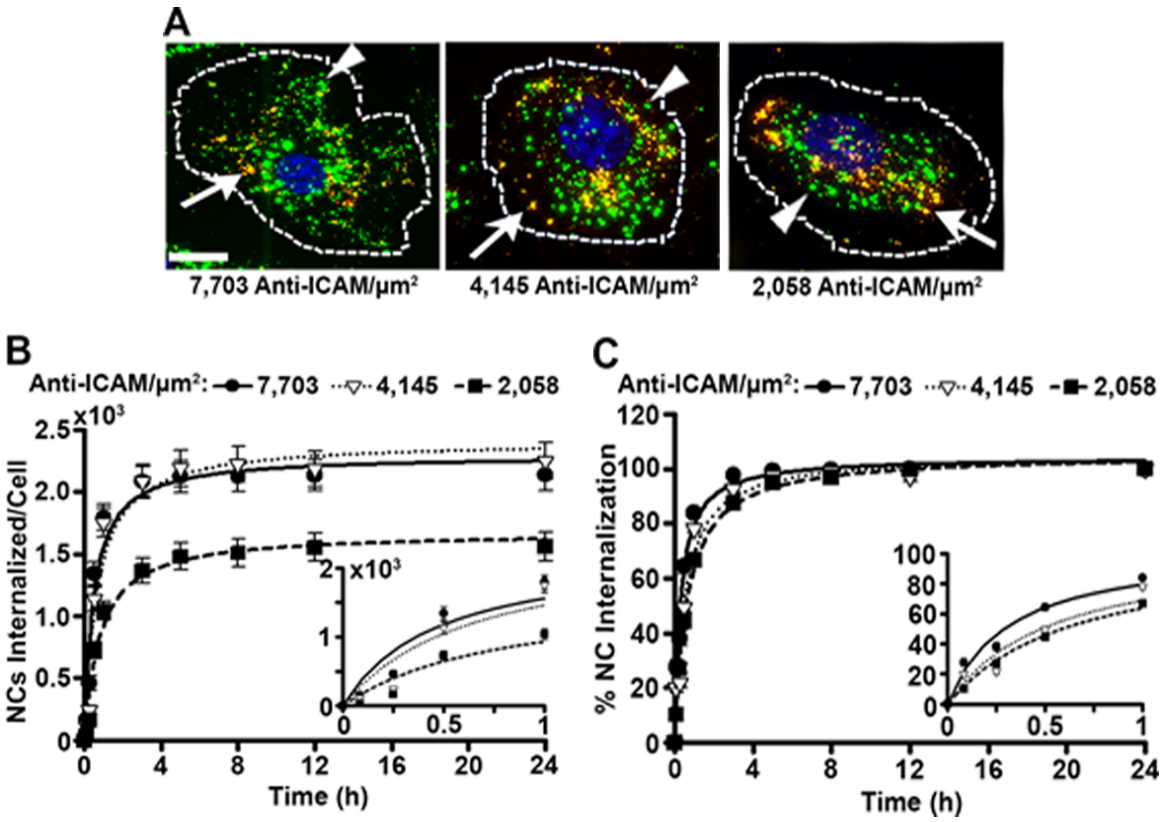

Figure 19. Role of valency on anti-ICAM NC uptake by brain endothelial cells. (A) Fluorescence microscopy showing internalization of green fluorescent anti-ICAM NCs with different valencies by TNFα-activated HBMECs after 30 min pulse at 37°C to permit NC binding, and an additional 30 min incubation in carrier-free medium to allow NC uptake (1 h total). Surface-bound versus internalized NCs were distinguished using an immunolabeling technique (see **Section 4.2.7**) that renders surface-bound NCs yellow (red + green; arrows) versus green internalized NCs (arrowheads). Cell nuclei were stained blue with DAPI and dashed lines mark the cell borders, as observed by phase-contrast microscopy. Scale bar = 10 μm. Anti-ICAM NC internalization by cells was assessed using this pulse-chase method up to a total time of 24 h. (B) Absolute number of anti-ICAM NCs internalized per cell over this time period. (C) Anti-ICAM NCs internalized as a percentage of total cell-associated (surface-bound + internalized) NCs over this time period. (B, C) Insets show the first 1 h of incubation. Data are the mean ± SEM, for which regression curves were fitted. Statistical significance is not shown for simplicity, but it was obtained and considered in the description of the results.

4.3.5. Transcytosis of Anti-ICAM NCs with Different Valencies

To subsequently investigate the influence of valency on anti-ICAM NC transcytosis across brain endothelial cells, we utilized the more physiologically-relevant transwell model that permits separation of the apical and basolateral compartments. First, we verified the specificity of anti-ICAM NC binding to activated brain endothelial cells in this model.

As seen in **Figure 20,** the total number of cell-associated anti-ICAM NCs was significantly higher compared to non-specific IgG NCs after only 30 min incubation, as expected (6.4-fold enhancement).

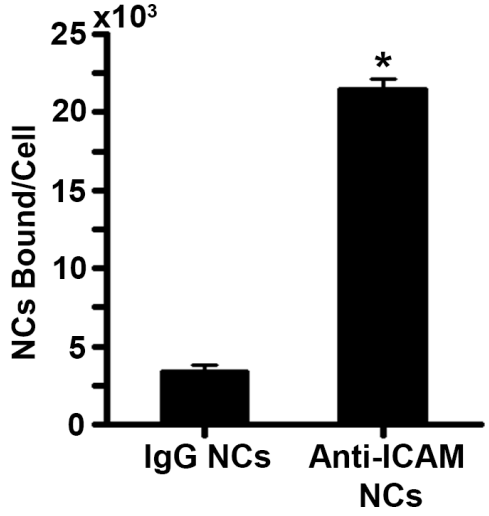

Figure 20. Specificity of anti-ICAM NC binding to brain endothelial cells on transwell inserts. Binding of ^{125}I-labeled anti-ICAM NCs or ^{125}I-labeled IgG NCs to TNFα-activated HBMECs grown on transwell inserts after 30 min incubation at 37°C. Data are the mean ± SEM. *Comparison to IgG NCs ($p < 0.05$ by Student's *t*-test).

With this validation in place, we assessed the role of valency on anti-ICAM NC transcytosis using the same pulse-chase technique described in the prior section to eliminate potentially confounding results due to NCs that may have passively leaked across the endothelial monolayer. Anti-ICAM NC transcytosis was found to be a very efficient process, as approximately 70-80% of all cell-associated NCs were transcytosed to the basolateral chamber at saturation (**Figure 21B**). As seen in **Figure 21A** and the corresponding data in **Table 4**, absolute anti-ICAM NC transcytosis was slower than NC uptake and within the same time range as NC binding. At first glance, it appears the efficiency of NC transcytosis was not linearly correlated with valency, but rather had a bell-shaped distribution. Specifically, the half-time for maximal transcytosis was 3.3 h

(7,703 anti-ICAM molecules/μm^2), 1.7 h (4,145 anti-ICAM molecules/μm^2), and 3 h (2,058 anti-ICAM molecules/μm^2) (**Table 4**). However, this is because the transcytosis process and data measured also encompasses binding and uptake. Therefore, since the intermediate and low valencies (4,145 and 2,058 anti-ICAM molecules/μm^2, respectively) had slower rates of NC binding and uptake (**Table 4** and **Figure 22A**), the data for transcytosis actually suggest this process was more efficient for lower valencies, indicating an inverted linear dependency between valency and NC transcytosis when considered as an independent event (**Figure 22B**). Overall then, given the opposite relationships between anti-ICAM valency and NC binding/uptake or transcytosis as isolated processes (**Figures 22A-B**), the efficiency of the entire transport process as a sequence of these events (binding → uptake → transcytosis) produces the bell-shaped curve described earlier (**Figure 22C**). As such, an intermediate valency seems to be the best for therapeutic delivery because it balances the efficiency of NC binding and uptake, along with the efficiency of transcytosis.

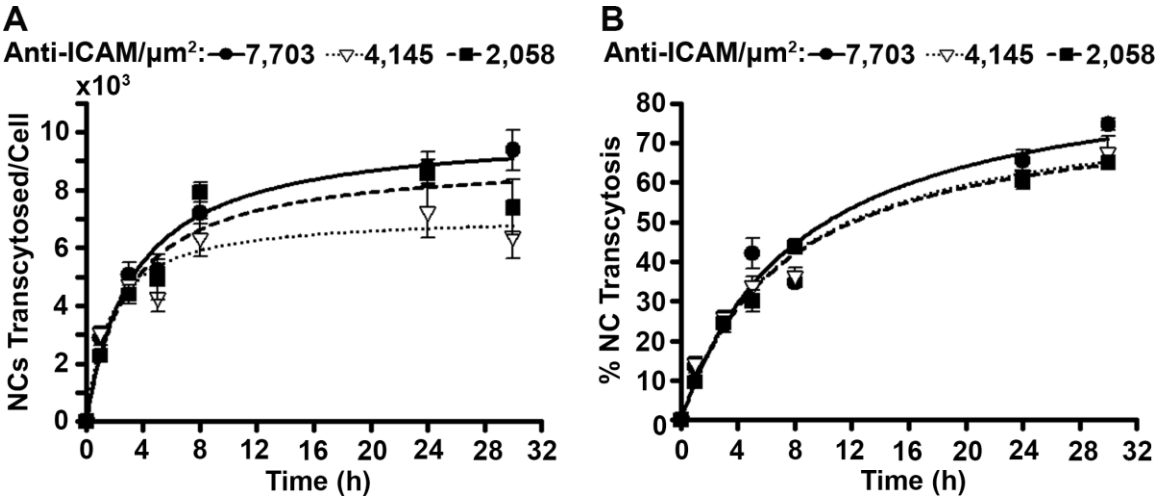

Figure 21. Role of valency on anti-ICAM NC transcytosis across brain endothelial cells. Transcytosis of ^{125}I-labeled anti-ICAM NCs with different valencies across a monolayer of TNFα-activated HBMECs after 30 min apical binding at 37°C, removal of non-bound NCs by washing both apical and basolateral chambers, and incubation in fresh medium at 37°C for additional time up to 30 h total. (A) Quantification of the absolute number of NCs transcytosed per cell to the basolateral chamber over time. (B) Percentage of NCs transcytosed with respect to the total number of NCs (cell-associated + transcytosed). Data are the mean ± SEM, for which regression curves were fitted. Statistical significance is not shown for simplicity, but it was obtained and considered in the description of the results.

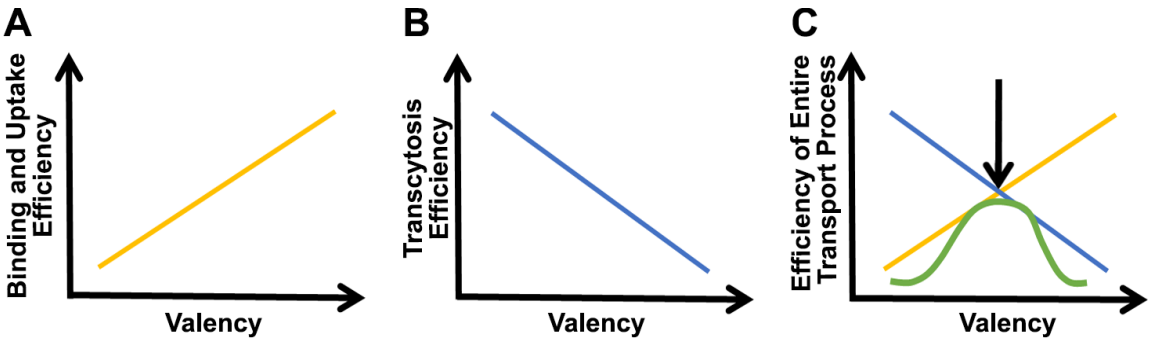

Figure 22. Model of dependence between targeting valency and NC transcytosis. (A) There is a direct linear correlation between increasing anti-ICAM valency and the efficiency of both NC binding and uptake. However, (B) considering NC transcytosis as an isolated event, there is an inverse linear relationship with valency. Therefore, (C) the entire transport process, encompassing sequential binding, uptake, and transcytosis, produces a bell-shaped curve (in green), resulting in an intermediate valency being the most efficient at the intersection of these processes (indicated by the black arrow).

4.3.6. Lysosomal Colocalization of Anti-ICAM NCs with Different Valencies

Based on the aforementioned findings, we questioned how anti-ICAM valency could modulate the efficiency of NC transcytosis. Given the propensity for anti-ICAM NCs and other drug delivery systems to traffic to lysosomes [47, 63, 64], we decided to examine whether valency impacts this process in brain endothelial cells using the same pulse-chase technique described previously (**Figure 23**). Using a coverslip model we observed that, regardless of valency, the colocalization of internalized anti-ICAM NCs with lysosomes was slower than NC uptake and faster than transcytosis (**Table 4** and **Figure 23B**): the half-time to maximal colocalization of anti-ICAM NCs with lysosomes was 1.7 h (7,703 anti-ICAM molecules/μm^2), 2.1 h (4,145 anti-ICAM molecules/μm^2), and 1.8 h (2,058 anti-ICAM molecules/μm^2). Upon examining the percentage of internalized anti-ICAM NCs colocalized with lysosomes (**Figure 23C**), we also found a similar trend.

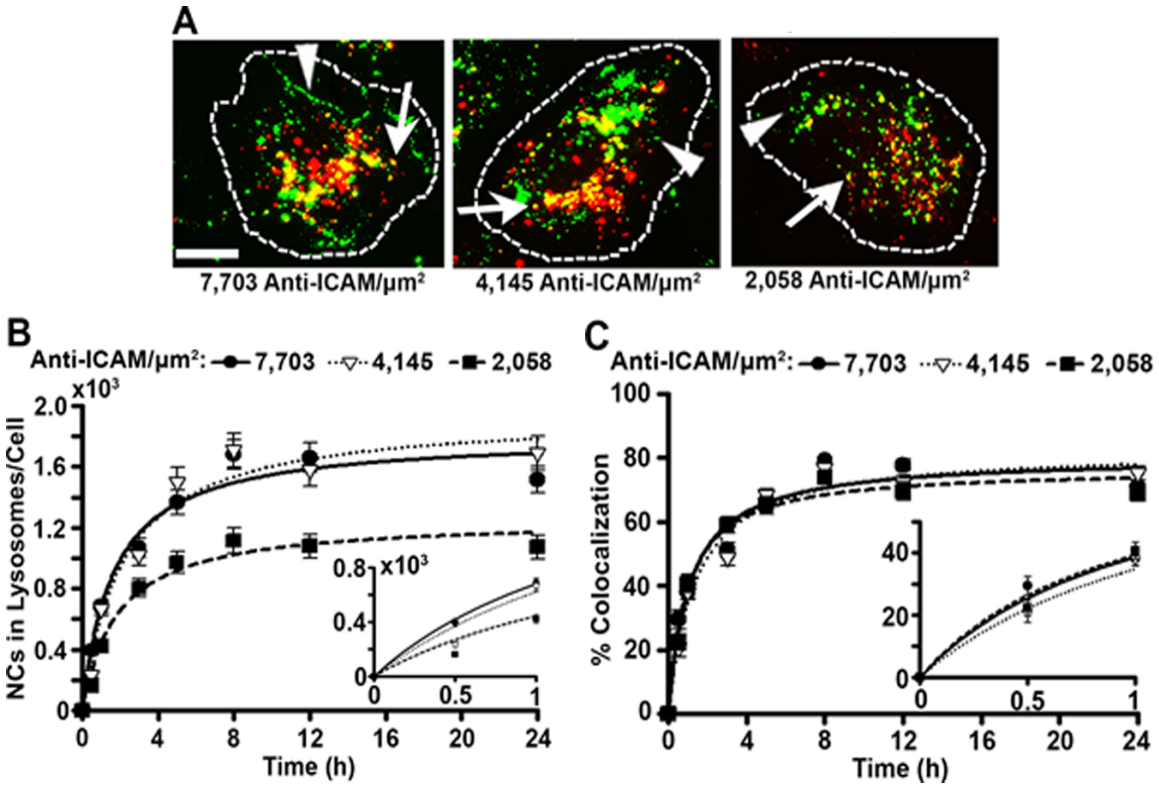

Figure 23. Role of valency on anti-ICAM NC trafficking to lysosomes in brain endothelial cells. (A) Fluorescence microscopy showing green fluorescent anti-ICAM NCs with different valencies colocalized with red lysosomes in TNFα-activated HBMECs on coverslips after 30 min pulse at 37°C to permit NC binding, and an additional 30 min incubation in carrier-free medium to allow NC uptake and trafficking to lysosomes (1 h total). Lysosomes were pre-loaded with Texas Red-labeled dextran, resulting in colocalization of internalized NCs with lysosomes to appear yellow (red + green; arrows) versus green (surface-bound + internalized) NCs (arrowheads). Dashed lines mark the cell borders, as indicated by phase-contrast microscopy. Scale bar = 10 μm. Anti-ICAM NC colocalization with lysosomes was assessed using this pulse-chase method up to a total time of 24 h. (B) Absolute number of anti-ICAM NCs colocalized with lysosomes per cell over this time period. (C) Internalized anti-ICAM NCs colocalized with lysosomes as a percentage of the total internalized NCs over this time period. (B, C) Insets show the first 1 h of incubation. Data are the mean ± SEM, for which regression curves were fitted. Statistical significance is not shown for simplicity, but it was obtained and considered in the description of the results.

As can be seen by the data for lysosomal colocalization (**Table 4**), although not statistically different among the valencies tested, the relationship between anti-ICAM NC valency and lysosomal colocalization was opposite to that found for transcytosis with slower lysosomal colocalization corresponding to the intermediate valency (**Figure 24**). Recalling the half-time for maximal transcytosis, the intermediate valency was the fastest

(most efficient), while the high and low valencies were slower (less efficient) and comparable to each other (**Table 4** and **Figure 24A**). However, for lysosomal colocalization, the intermediate valency had the slowest rate of lysosomal trafficking (least efficient) compared to the high and low valencies (more efficient) (**Table 4** and **Figure 24B**).

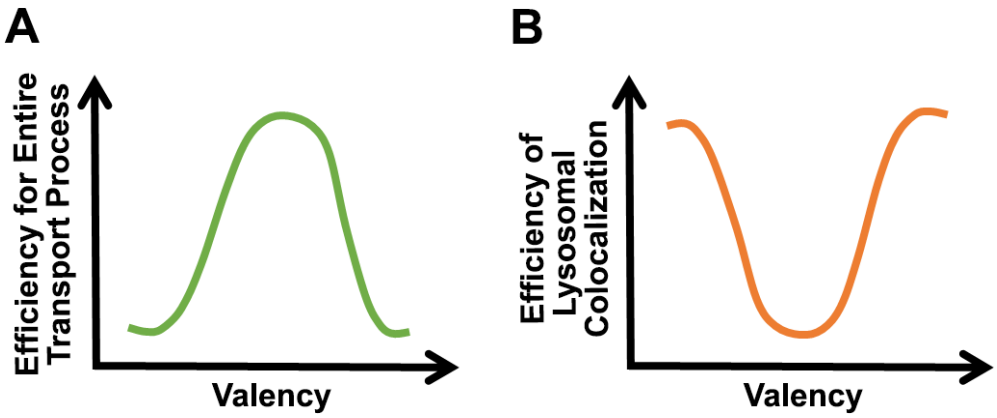

Figure 24. Relationship between valency and efficiency of NC transcytosis or lysosomal colocalization. (A) As presented in **Figure 22C**, the efficiency of transcytosis (considering the entire transport process) produced a bell-shaped curve due to the opposing trends in NC binding and uptake versus transcytosis when each process was independently evaluated. However, (B) the efficiency of NC lysosomal colocalization showed an inverse relationship with valency.

Moreover, maximal colocalization of anti-ICAM NCs with lysosomes at saturation was around 70% (**Figure 23C**), which is comparable to the maximal NC transcytosis at saturation (70-80%; **Figure 21B**). Altogether, these findings raised questions regarding the relationship between lysosomal trafficking and transcytosis, particularly whether they are independent processes or sequential events, as well as the role of valency in regulating these processes. Specifically, we postulated three scenarios of NC lysosomal trafficking and transcytosis that could be influenced by anti-ICAM valency (**Figure 25**). Each of these scenarios were explored in the more physiologically-relevant transwell model and are discussed in greater detail in subsequent sections.

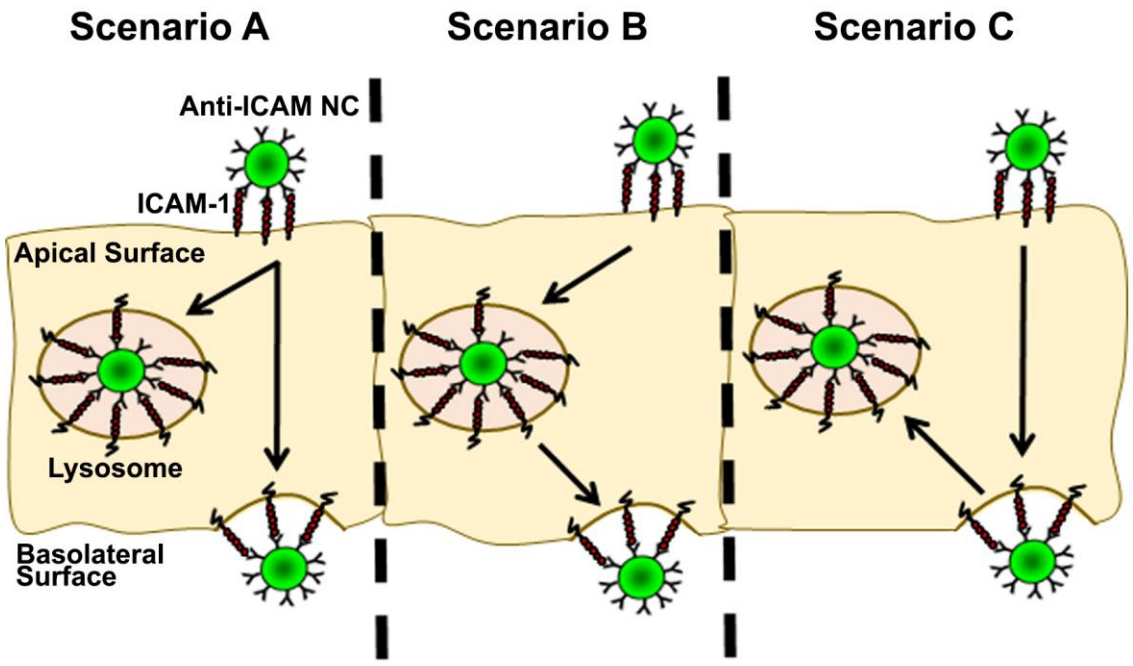

Figure 25. Models for the potential relationship between lysosomal trafficking and transcytosis of anti-ICAM NCs. In scenario (A), NCs undergo both lysosomal trafficking and transcytosis after uptake. These routes are independent from each other and valency may dictate the efficiency of each one independently. In scenario (B), NC trafficking to lysosomes or related compartments is a prerequisite for transcytosis, whereby the influence of valency on transcytosis is dictated by the preceding effect of valency on lysosomal trafficking. In scenario (C), NCs transcytosed to the basolateral cell-surface may be internalized again and trafficked to lysosomes, *e.g.*, if they are unable to dissociate from their bound receptors, and the influence of valency on lysosomal trafficking is dependent on the earlier effect of valency on transcytosis.

4.3.7. Uptake of Anti-ICAM NCs in the Transwell Model

Before examining lysosomal colocalization in the transwell system, we first sought to examine whether anti-ICAM NC uptake was similar between the coverslip and transwell models. To do so, we incubated high valency anti-ICAM NCs (7,703 anti-ICAM molecules/μm^2) with a monolayer of activated brain endothelial cells in transwell inserts using the same pulse-chase technique used for coverslips. Confocal microscopy was used to acquire z-stacks that were analyzed as color composites of either the whole cell body (apical to basolateral surface) or just the basolateral cell-surface (see **Section 4.2.7**). As in the coverslip model, anti-ICAM NCs were internalized by cells seeded on transwell inserts

and there was increased uptake over time (**Figure 26**). However, in comparison to coverslips, the percentage of total cell-associated NCs internalized was significantly less in the transwell model (1.6-2.3-fold difference). This finding was expected and does not mean NC uptake is less efficient in the transwell model compared to coverslips. Instead, it is because basolateral secretion of internalized NCs after transcytosis reduces the number of internalized NCs that contribute to this measurement and, hence, the percentage of internalized NCs with respect to total cell-associated NCs is reduced.

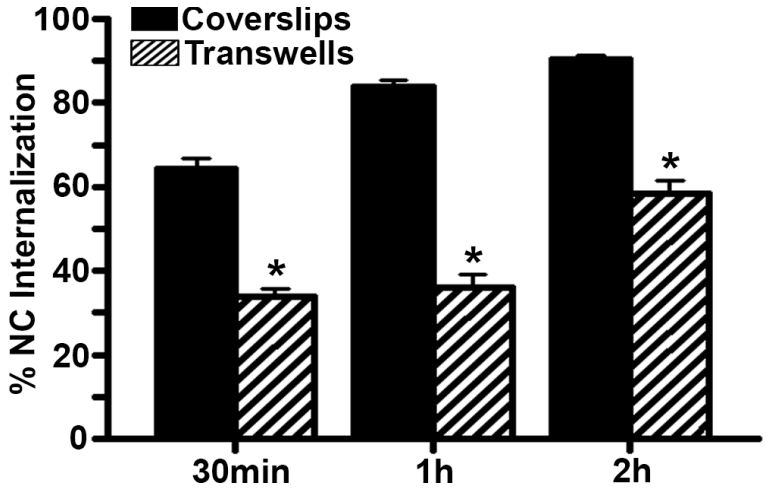

Figure 26. Anti-ICAM NC uptake by brain endothelial cells on coverslips versus transwell inserts. TNFα-activated HBMECs seeded on coverslips or transwell inserts were incubated with green fluorescent anti-ICAM NCs (7,703 anti-ICAM molecules/μm^2) for 30 min pulse at 37°C, followed by additional incubation in carrier-free medium up to 2 h total to allow NC uptake. Surface-bound versus internalized NCs were distinguished using the immunolabeling technique previously described. The graph shows anti-ICAM NCs internalized as a percentage of total cell-associated (surface-bound + internalized) NCs at each time point. Data are the mean ± SEM. *Comparison to coverslips at each time point ($p < 0.05$ by Student's *t*-test).

Upon examining the transwell data further, we observed the total number of NCs (surface-bound + internalized) in the whole cell was significantly greater (6-17-fold) than that of the basolateral cell-surface, as expected (**Figure 27A**). Over time, total NCs decreased in the whole cell with approximately a 30% reduction from 30 min to 2 h (**Figure**

27A), which is similar to the percentage of NCs transcytosed at this time (~20% NCs transcytosed; **Figure 21B**). In contrast, the total number of anti-ICAM NCs on the basolateral cell-surface remained relatively steady over time (**Figure 27A**), suggesting that the rate of transcytosis across the cell body is constant. Supporting this conclusion, the fraction of internalized anti-ICAM NCs in the whole cell was similar over time (212-262 NCs/cell; **Figure 27B**), while the number of surface-bound NCs significantly decreased in a linear fashion (R^2=0.991; regression curve not shown), which is likely a consequence of NCs being released from the basolateral cell-surface after transcytosis (50% reduction from 30 min to 2 h; **Figure 27B**). In fact, surface-bound NCs as a percentage of total cell-associated NCs on the basolateral surface also decreased with time in a similar manner (**Figure 27C**), thereby providing further evidence of anti-ICAM NC detachment from the basolateral cell-surface after transcytosis. Moreover, since surface-bound NCs could be distinguished on the basolateral endothelium via immunostaining, this provides verification that the targeting antibody (anti-ICAM) remains (to some degree) associated with the NC after transcytosis. This is imperative for subsequent NC binding and uptake by other cell types in the brain, which has been observed in co-culture models of the BBB (endothelial cells + astrocytes or pericytes) [71], as well as in the brains of mice with NPD (*unpublished data; Muro Laboratory*).

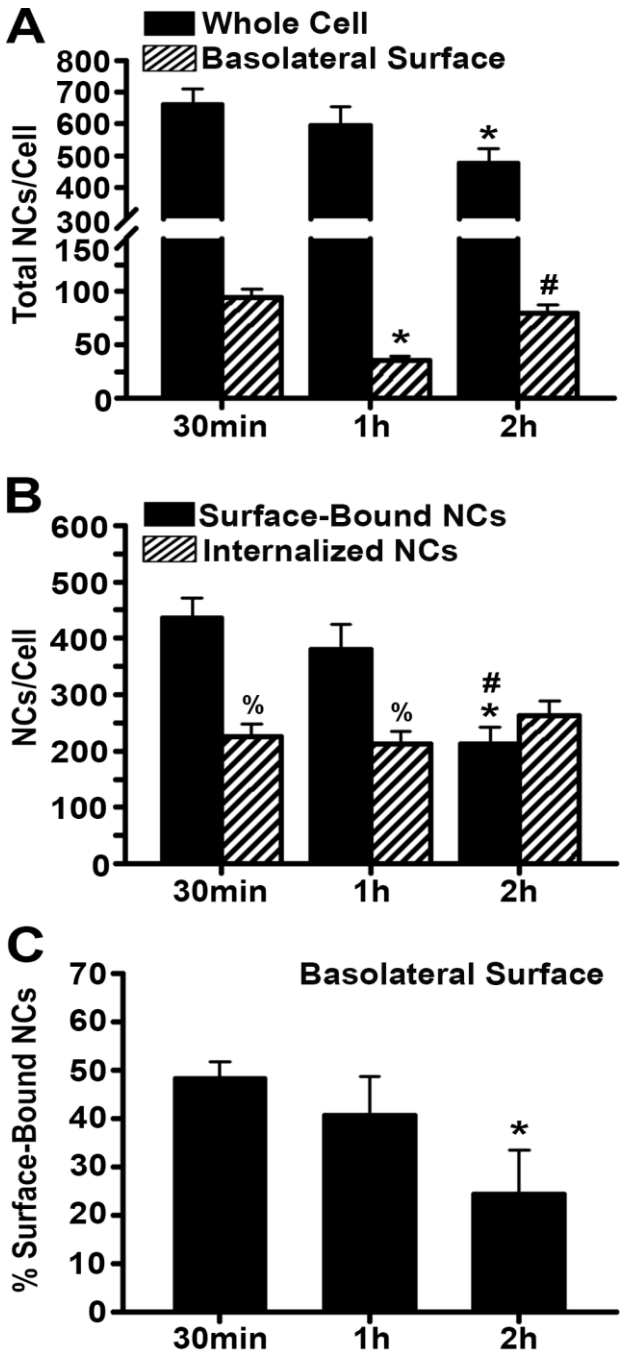

Figure 27. Anti-ICAM NC uptake by brain endothelial cells on transwell inserts. TNFα-activated HBMECs seeded on transwell inserts were incubated with green fluorescent anti-ICAM NCs (7,703 anti-ICAM molecules/μm^2) for 30 min pulse at 37°C, followed by additional incubation in carrier-free medium up to 2 h total to allow NC uptake. Surface-bound versus internalized NCs were distinguished using the immunolabeling technique previously described. (A) Total cell-associated NCs for the whole cell versus basolateral cell-surface (see **Section 4.2.7**). (B) Surface-bound versus internalized NCs for the whole cell. (C) Surface-bound NCs as a percentage of total cell-associated (surface-bound + internalized) NCs on the basolateral cell-surface. Data are the mean ± SEM. *Comparison to 30 min; $^{\#}$comparison to 1 h; $^{\%}$comparison to surface-bound NCs at each time point ($p < 0.05$ by Student's *t*-test).

4.3.8. Lysosomal Trafficking of Anti-ICAM NCs in the Transwell Model

Next, we examined lysosomal trafficking of anti-ICAM NCs in the transwell model by confocal microscopy (**Figure 28**). As found in coverslips, internalized anti-ICAM NCs colocalized with lysosomes in cells seeded on transwell inserts and there was increased colocalization over time (12-40% colocalization; **Figure 28B**). Although, similar to that of uptake, the degree of colocalization in transwells was reduced compared to coverslips (1.3-2.4-fold difference; **Figure 28B**). However, using the internalized NC fraction to calculate the percentage of lysosomal colocalization in the transwell model does not account for NCs that were internalized and subsequently transcytosed, since these NCs would be stained and quantified as basolateral surface-bound NCs. Therefore, using total cell-associated NCs in this quantification more accurately reflects lysosomal colocalization, and consequently, an even greater difference was observed between the two models (2.0-4.6-fold difference; **Figure 28C**). In accord with this finding, the absolute number of NCs colocalized with lysosomes per cell was significantly diminished in the transwell model, representing a 9-16-fold decrease from that found in coverslips (**Figure 28D**).

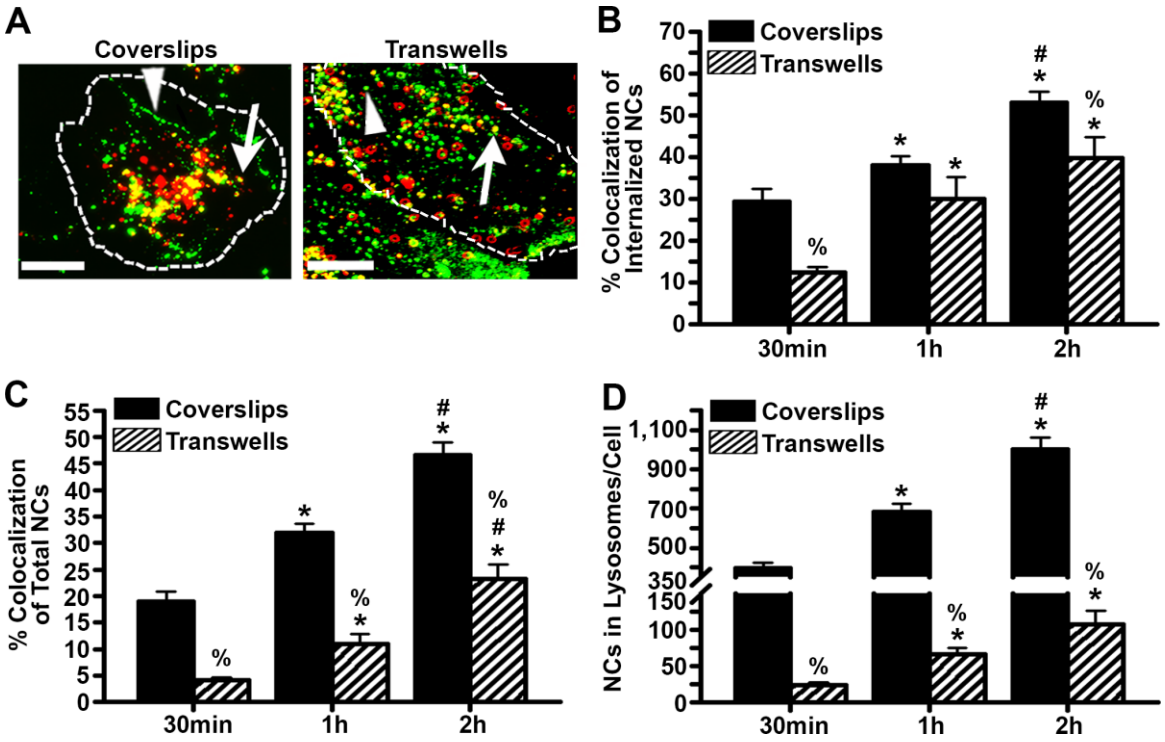

Figure 28. Lysosomal trafficking of anti-ICAM NCs in coverslips versus transwell inserts. (A) Fluorescence microscopy showing colocalization of green fluorescent anti-ICAM NCs (7,703 anti-ICAM molecules/μm^2) with red lysosomes in TNFα-activated HBMECs on coverslips versus transwell inserts after 30 min pulse at 37°C to permit NC binding, and an additional 30 min incubation in carrier-free medium to allow NC uptake and trafficking to lysosomes (1 h total). Lysosomes were pre-loaded with Texas Red-labeled dextran, resulting in colocalization of internalized NCs with lysosomes to appear yellow (red + green; arrows) versus green (surface-bound + internalized) NCs (arrowheads). Dashed lines mark the cell borders, as indicated by phase-contrast microscopy. Scale bar = 10 μm. Anti-ICAM NC colocalization with lysosomes was assessed using this pulse-chase method up to a total time of 2 h. (B) Percentage of internalized NCs colocalized with lysosomes. (C) Percentage of total cell-associated (surface-bound + internalized) NCs colocalized with lysosomes. (D) Absolute number of anti-ICAM NCs colocalized with lysosomes per cell. Data are the mean ± SEM. *Comparison to 30 min in each model; $^{\#}$comparison to 1 h in each model; $^{\%}$comparison to coverslips at each time point ($p < 0.05$ by Student's *t*-test).

Based on the data presented thus far, it appears nearly all anti-ICAM NCs were trafficked to lysosomes in the coverslip model because no apical versus basolateral polarization is possible, while both lysosomal trafficking and transcytosis are permitted in the transwell system. In agreement, the total number of lysosomes per cell was significantly greater in coverslips than transwells (268 versus 96 lysosomes per cell, respectively;

Figure 29A), which is likely given the prevalence of lysosomal trafficking in this model. Hence, it is possible that transcytosis versus lysosomal transport prevails in the BBB.

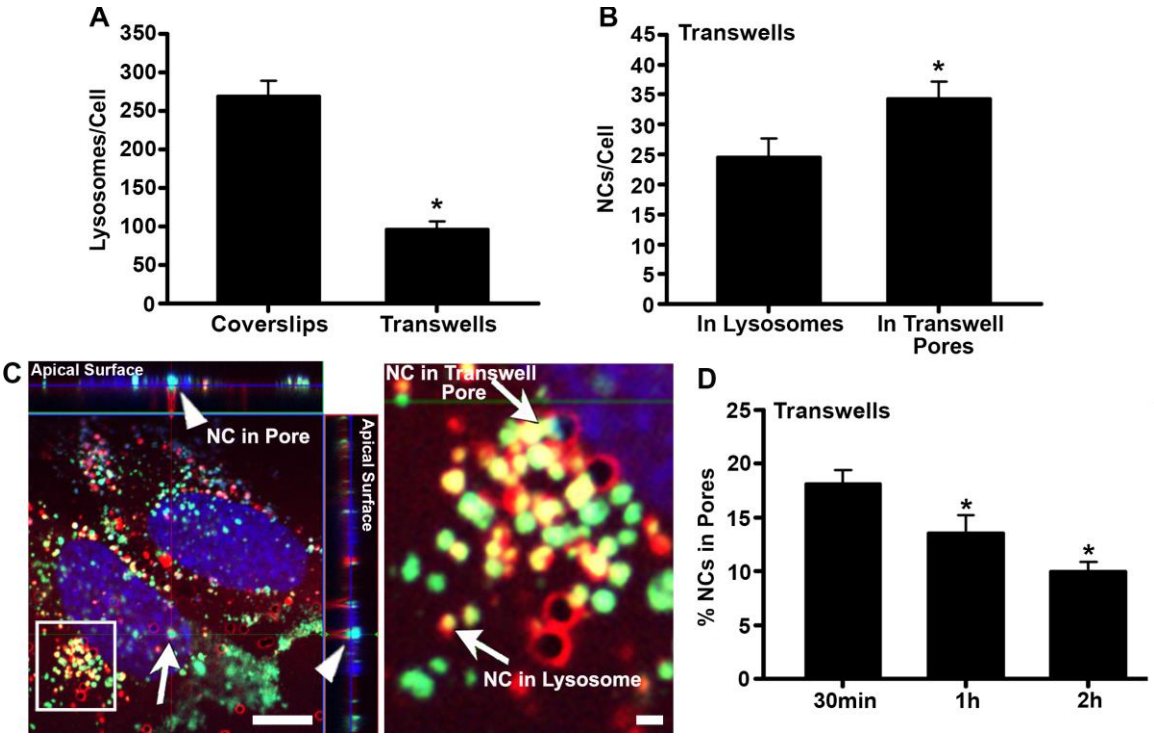

Figure 29. Anti-ICAM NC distribution in lysosomes and transwell pores. Lysosomes in TNFα-activated HBMECs seeded on coverslips or transwell inserts were pre-loaded with Texas Red-labeled dextran, followed by incubation with green fluorescent anti-ICAM NCs (7,703 anti-ICAM molecules/μm^2) for 30 min pulse at 37°C, and additional incubation in carrier-free medium up to 2 h total to allow NC uptake. (A) Total number of dextran-filled lysosomes per cell in either the coverslip or transwell model after 30 min. (B) Number of anti-ICAM NCs colocalized with dextran-filled lysosomes or the number of NCs found in the pores of transwell inserts after 30 min. (C) Confocal microscopy showing in the left panel a green fluorescent anti-ICAM NC (arrow) entering a transwell pore (arrowheads) after 1 h. Scale bar = 10 μm. The right panel is the magnified inset showing a green fluorescent anti-ICAM NC colocalized with a red dextran-filled lysosome and a NC in a transwell pore. Scale bar = 1 μm. (D) Anti-ICAM NCs in transwell pores as a percentage of total cell-associated NCs. Data are the mean ± SEM. (A) *Comparison to coverslips; (B) *Comparison to NCs in lysosomes; (D) *Comparison to 30 min ($p < 0.05$ by Student's *t*-test).

In scenario A (**Figure 25**), we speculated anti-ICAM NCs can be independently trafficked to both lysosomes and transcytosed across the cell body following uptake. The fact that NCs were detected in both lysosomes and transwell pores at early time points (**Figures 29B-C**) suggests this may be true. Disappearance of NCs from transwell pores

over time also indicates they are transcytosed into the basolateral chamber (**Figure 29D**), which validates the radiotracing data presented in **Figure 21**. Further, this is in contrast with increased NC colocalization with lysosomes over time (**Figure 28**), which is expected since these model NCs are non-biodegradable and, hence, will keep accumulating in lysosomes. Although we did not experimentally address the role of valency on lysosomal colocalization, because transport to lysosomes and transcytosis are independent processes in this scenario, they may also be independently modulated by valency. Hence, we cannot rule out scenario A (**Figure 25**).

4.3.9. Dependency between Lysosomal Trafficking and Transcytosis of Anti-ICAM NCs

As shown in **Figure 25**, it may be possible that lysosomal trafficking and transcytosis depend on each other. In scenario B, we postulated that transcytosis may require previous lysosomal (or related) trafficking where cells secrete materials to the basolateral space that were previously transported to lysosomes, while in scenario C lysosomal trafficking would follow transcytosis, *e.g.*, when anti-ICAM NCs are not able to detach from the receptor.

A priori, it seems that scenario B (**Figure 25**) may be ruled out, because if lysosomal trafficking preceded transcytosis then the influence of targeting valency on NC trafficking to lysosomes would be the same for transcytosis, yet they are in fact opposite (**Figure 24**). To confirm this, we tested whether anti-ICAM NC trafficking to lysosomes is a prerequisite to transcytosis using radiotracing techniques. First, we assessed if transcytosis of anti-ICAM NCs across activated brain endothelial cells would be decreased

in the presence of H-7, an inhibitor of PKC that hinders lysosomal trafficking [62, 68]. Briefly, since PKC inhibition can also hinder uptake [68], anti-ICAM NCs were first permitted to bind to and be internalized by cells using the pulse-chase technique described earlier. Then, cells were incubated in fresh medium supplemented with H-7 for another 4 h to assess the effect of inhibiting lysosomal trafficking on transcytosis. As seen in **Figure 30A**, inhibition of lysosomal trafficking did not affect NC degradation (measured as the percentage of free ^{125}I) in either the cell fraction or basolateral (*i.e.*, transcytosed) fraction as compared to the control condition (108% and 100% of control, respectively). As well, the absolute number of NCs associated with cells or those transcytosed to the basolateral chamber were not significantly impacted (109% and 86% of control, respectively), and this was the same case when expressed as the percentage of NCs in either fraction with respect to the total number of NCs present (cell-associated + transcytosed) (105% and 82% of control, respectively). Hence, it appears that transcytosis does not require pre-lysosomal transport.

In a parallel experiment, we attempted to pre-load lysosomes with an initial dose of non-radiolabeled anti-ICAM NCs, which would hinder transcytosis of a second dose of ^{125}I-labeled anti-ICAM NCs if passage through lysosomes was first required. However, as seen in **Figure 30B** this was not the case and the results showed a similar trend to that found in the case with H-7 treatment. More specifically, NC degradation was not significantly affected in both the cell and basolateral fractions (90% and 75% of control, respectively). As well, the absolute number of NCs associated with cells or those transcytosed were not affected (89% and 109% of control, respectively), nor was the percentage of NC distribution (96% and 109% of control, respectively). Therefore, both of

these findings confirm anti-ICAM NC transcytosis across brain endothelial cells is not dependent on passage through lysosomes, thereby ruling out scenario B.

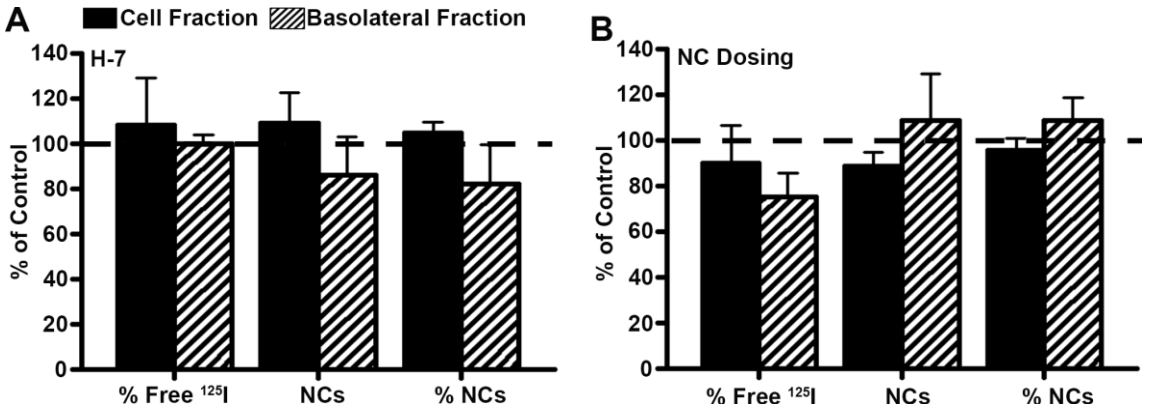

Figure 30. Effect of H-7 and dual NC dosing on anti-ICAM NC transcytosis. TNFα-activated HBMECs were grown to confluence on transwell inserts. (A) ^{125}I-labeled anti-ICAM NCs (7,703 anti-ICAM molecules/μm^2) were added to the apical chamber for 30 min at 37°C to permit binding, non-bound NCs were removed by washing both chambers, and the cells were incubated for an additional 30 min in fresh medium to allow uptake. Afterwards, the cells were washed again and incubated in fresh medium supplemented with H-7 for an additional 4 h at 37°C to inhibit lysosomal trafficking. (B) An initial dose of non-radiolabeled anti-ICAM NCs (7,703 anti-ICAM molecules/μm^2) was added to the apical chamber for 30 min at 37°C to allow NC binding, followed by washing both chambers to removed non-bound NCs, and incubated for an additional 1.5 h in fresh medium to allow uptake and trafficking to lysosomes. Then, ^{125}I-labeled anti-ICAM NCs were added to the apical chamber for 30 min, non-bound NCs were removed by washing, and cells were incubated for an additional 4.5 h in fresh medium. The data presented in (A) and (B) show NC degradation measured as the percentage of free ^{125}I, the number of NCs, and NC distribution as a percentage of total (cell-associated + transcytosed) NCs relative to their respective controls: (A) lack of H-7 and (B) no initial dose of non-radiolabeled NCs (indicated by the horizontal dashed lines). Data are the mean ± SEM. No statistical significance was found.

With respect to scenario C (**Figure 25**), this postulated that transcytosis occurs prior to lysosomal transport, *e.g.*, where NCs unable to effectively detach from their bound receptors may be removed by cells and trafficked to lysosomes. This hypothesis is examined in the following section.

4.3.10. Role of Valency on Lysosomal Trafficking and the Mechanism of Anti-ICAM NC Detachment after Transcytosis

Recalling the data presented in **Table 4**, the high and low valencies (7,703 and 2,058 anti-ICAM molecules/μm^2, respectively) had more efficient trafficking to lysosomes than the intermediate valency NCs (4,145 anti-ICAM molecules/μm^2) (summarized in **Figure 24B**). However, there was an inverse linear relationship between targeting valency and transcytosis when evaluated as an isolated process, where high valency NCs were least efficient and low valencies were more efficient (**Table 4** and **Figure 22B**). This could be due to either concomitant, yet independent NC trafficking to lysosomes and transcytosis, wherein targeting valency would independently impact either transport (scenario A; **Figure 25**), or lysosomal trafficking being subsequent to transcytosis (scenario C; **Figure 25**). This would be possible if NCs remained bound to receptors long enough after transcytosis, *e.g.*, if their high binding valency hinders their detachment from the cell after this process. In looking at the intracellular degradation of anti-ICAM NCs via radiotracing (**Figure 31**), there was very little intracellular degradation (< 20% degradation) and it was similar among the three valencies tested, which further supports transcytosis being largely independent of lysosomal trafficking. However, the high valency NCs had slightly greater degradation than the other two valencies (**Figure 31**), especially after 5 h when a large fraction of NCs are transcytosed across cells (**Figure 21A**). Hence, it appears there is a tendency for high valency NCs to be retained in the cell, which is consistent with enhanced anti-ICAM NC colocalization with lysosomes as observed for the high valency NCs (**Table 4**).

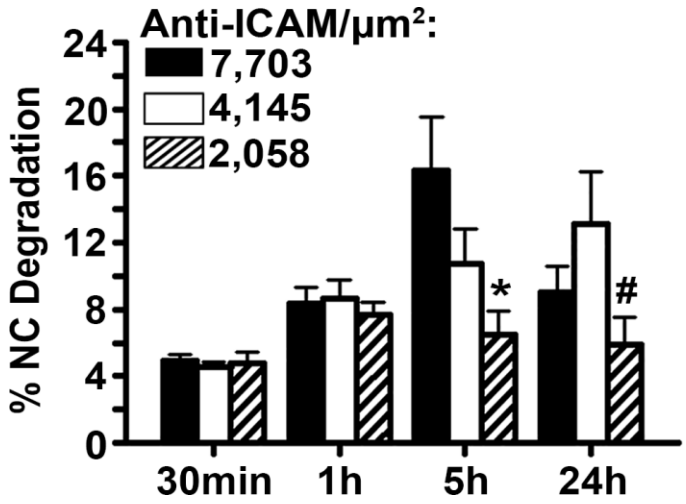

Figure 31. Intracellular degradation of anti-ICAM NCs in brain endothelial cells. ^{125}I-labeled anti-ICAM NCs with different valencies were added to the apical chamber of transwell inserts for 30 min at 37°C to permit binding to TNFα-activated HBMECs. Non-bound NCs were removed by washing both chambers, and cells were incubated in fresh medium for additional time up to 24 h total. At select time points, the cells were washed, and the percentage of free ^{125}I (representative of intracellular NC degradation) was measured in cells by TCA precipitation (see **Section 4.2.8**). Data are the mean ± SEM. *Comparison to 7,703 anti-ICAM molecules/μm^2; $^{\#}$comparison to 4,145 anti-ICAM molecules/μm^2 ($p < 0.05$ by Student's *t*-test).

In light of these findings, we began to speculate that multivalent interactions may also impact detachment of anti-ICAM NCs from the basolateral cell-surface after transcytosis, where NCs that cannot efficiently detach from their bound receptors are measured as cell-associated (not transcytosed) NCs, and those that effectively detach are measured as transcytosed (NCs recovered in the basolateral chamber). As such, the valency of anti-ICAM NCs could influence the efficacy of this detachment. Specifically, higher valency implies enhanced avidity to the receptor (**Table 3**) and, consequently, could hinder basolateral detachment following NC transcytosis. If this is the case, high valency NCs that are unable to detach from the basolateral cell-surface may be trafficked back to lysosomes (scenario C in **Figure 25**). Based on data presented in **Chapter 5** and [291], efficient detachment of NCs from the basolateral cell-surface may require cleavage of the ICAM-1 receptor. For example, we have observed that MMP-9 and MMP-2 are involved in the

cleavage of ICAM-1 as measured by the release of sICAM-1 (**Chapter 5** and [291]). Therefore, we tested the influence of these molecules on anti-ICAM transcytosis by either inhibition of these MMPs or by addition of recombinant MMPs. First, inhibition of either MMP-9 or MMP-2 (MMP-9i or MMP-2i, respectively) did not affect the interaction of anti-ICAM NCs with cells (99% and 95% of control, respectively; **Figure 32A**). However, inhibition of MMP-9 was found to markedly decrease anti-ICAM NC transcytosis in terms of absolute NCs transcytosed and the percentage of total cell-associated NCs transcytosed (80% and 47% of control, respectively; **Figure 32B**). In agreement with the role of MMP-9 in ICAM-1 cleavage, addition of recombinant, active MMP-9 also enhanced absolute NC transcytosis (138% of control; **Figure 32C**). In contrast, inhibition of MMP-2 or addition of recombinant, active MMP-2 did not significantly impact NC transcytosis (**Figures 32B-C**). Hence, based on the data obtained pertaining to modulating MMP-9 activity, valency may inversely influence anti-ICAM NC transcytosis based on the number of ligand-receptor complexes required to be cleaved for NC detachment from the basolateral cell-surface. Given that valency directly influences binding and uptake needed prior to transcytosis, this explains why the intermediate valency may be optimal for therapeutic delivery: the intermediate valency provides enough avidity for efficient binding and uptake, while not hindering basolateral detachment after NC transcytosis. Therefore, although scenario A may occur, scenario C (**Figure 25**) is the most plausible explanation or the highest contributor for the observed differences in lysosomal trafficking and transcytosis of anti-ICAM NCs with different valencies.

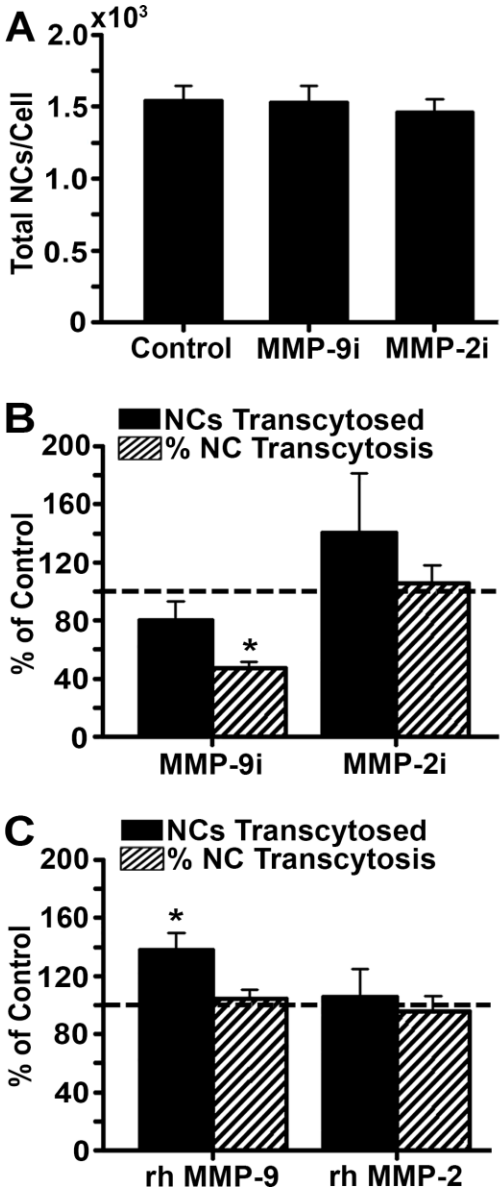

Figure 32. Anti-ICAM NC detachment from the basolateral cell-surface after transcytosis. (A) TNFα-activated HBMECs grown on coverslips were incubated with green fluorescent anti-ICAM NCs (7,703 anti-ICAM molecules/μm^2) for 30 min at 37°C, followed by washing to remove non-bound NCs, and incubation for an additional 30 min (1 h total). Incubations were done in control medium or medium supplemented with MMP-9 inhibitor (MMP-9i) or MMP-2 inhibitor (MMP-2i). The total number of cell-associated NCs was quantified by fluorescence microscopy as described in prior sections. (B, C) TNFα-activated HBMECs grown on transwell inserts were incubated for 30 min at 37°C with ^{125}I-labeled anti-ICAM NCs (7,703 anti-ICAM molecules/μm^2) to permit binding to cells, followed by washing both chambers to remove non-bound NCs, and incubation in fresh medium for an additional 4.5 h (5 h total). Incubations were done in control medium, or medium containing (B) MMP inhibitors or (C) recombinant (rh) MMPs. Data show quantification of the absolute number of NCs transcytosed to the basolateral chamber or NC transcytosis as a percentage of the total (cell-associated + transcytosed) NCs relative to the control condition, as indicated by the horizontal dashed lines. Data are the mean ± SEM. *Comparison to control ($p < 0.05$ by Student's *t*-test).

4.3.11. Effect of Valency on Therapeutic ASM Delivery in Cells and Mice

To further evaluate the efficiency of intermediate valency NCs, we examined delivery of therapeutic ASM coated on anti-ICAM NCs (anti-ICAM/ASM NCs) with high or intermediate valency across activated brain endothelial cells in a transwell model (**Figure 33**). In comparison to the high valency (7,703 anti-ICAM molecules/μm^2), transcytosis of anti-ICAM/ASM NCs with intermediate valency (4,145 anti-ICAM molecules/μm^2) was markedly enhanced in terms of the absolute number of NCs transcytosed per cell (1.5-fold increase, **Figure 33A**), as well as the percentage of NC transcytosis with respect to the total (cell-associated + transcytosed) number of NCs (1.8-fold increase; **Figure 33B**). Importantly, since an intermediate valency permits a greater number of ASM molecules to be coupled to the NC surface (203 ± 5 versus 28 ± 2 ASM molecules/NC for the intermediate versus high valency, respectively), there was further enhancement in the number of ASM molecules transported across the brain endothelial monolayer as compared to the high valency (11-fold increase; **Figure 33C**).

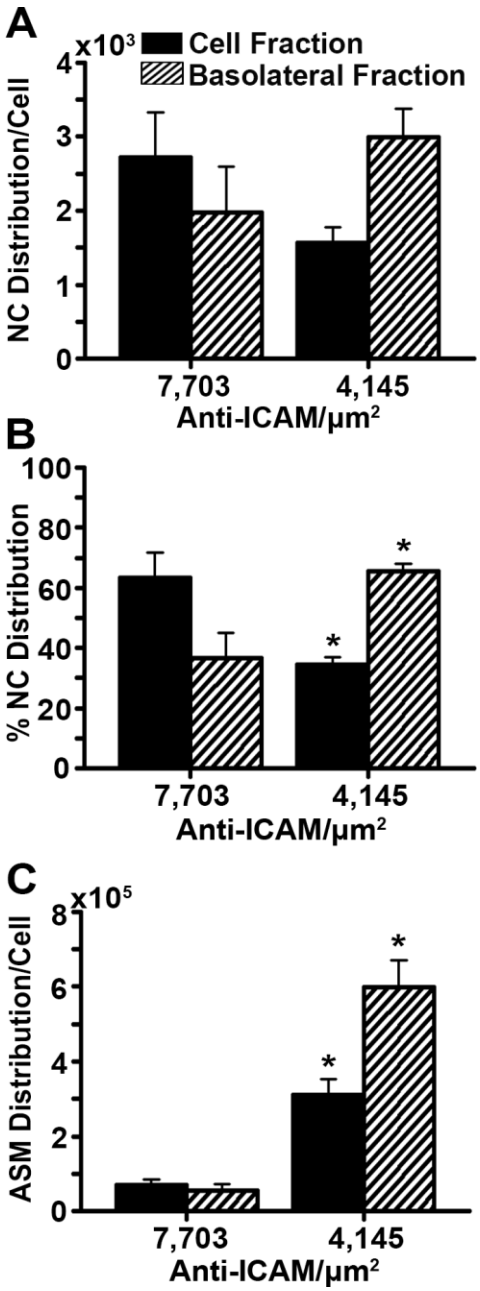

Figure 33. Role of valency on ASM delivery across brain endothelial cells by anti-ICAM NCs. ^{125}I-labeled anti-ICAM/ASM NCs with high or intermediate targeting valency (7,703 versus 4,145 anti-ICAM molecules/μm^2, respectively) were incubated with TNFα-activated HBMECs for 30 min to permit apical binding, followed by washing both chambers to remove non-bound NCs, and incubation in fresh medium for additional time up to 24 h total. The number of NCs associated with the cell fraction and those transcytosed to the basolateral chamber were measured using a gamma counter. (A) Quantification of the absolute number of NCs associated with the cell fraction (bound + internalized NCs) and basolateral fraction (transcytosed NCs). (B) NC distribution in each fraction as a percentage of the total number of NCs (cell-associated + transcytosed). (C) Distribution of ASM molecules in the cell and basolateral fractions. Data are the mean ± SEM. *Comparison to the high valency (7,703 anti-ICAM molecules/μm^2) for each fraction ($p < 0.05$ by Student's *t*-test).

Next, we evaluated ASM delivery in mice to ultimately prove the efficiency of intermediate anti-ICAM valency NCs in a complex physiological model. In agreement with the aforementioned cell culture findings, we observed a similar outcome following intravenous injection of anti-ICAM/ASM NCs with high or intermediate valency. For both valencies, anti-ICAM/ASM NCs were rapidly removed from the circulation: < 5% of the injected dose (% ID) remained in blood 15 min following administration (data not shown), which is important to avoid degradation and recognition by the immune system. However, the intermediate valency resulted in enhanced NC delivery to the brain compared to that found for the high valency in terms of both the % ID and the percent injected dose per gram of brain tissue (% ID/g) (**Figure 34A**). Specifically, anti-ICAM/ASM NCs with an intermediate valency showed 1.5-fold greater % ID and 1.6-fold greater %ID/g for the brain as compared to the high valency (**Figures 34A-B**). In accord with enhanced brain accumulation, NCs with intermediate valency had diminished non-specific clearance via the spleen (39% reduction in % ID and 33% reduction in % ID/g; **Figure 34B**); although, this same trend was not observed in the liver, which is another major clearance organ [58] (**Figure 34B**). This is possible given the liver is significantly larger in size than the spleen and, hence, a reduction in clearance will be less pronounced in this organ. Nevertheless, as in the case of the cell culture results shown above, the intermediate valency permitted a significant increase in the number of ASM molecules delivered to the brain (**Figure 34C**). In fact, there was an 11-fold increase in ASM molecules measured in the brain with the intermediate valency, which is the same enhancement found in the cell culture model. Therefore, therapeutic ASM delivery via anti-ICAM NCs with an intermediate valency represents a significantly improved means to treat type A NPD. Moreover, this strategy is

likely to improve enzyme replacement for other LSDs, as well as treatment of similar disorders that are currently hampered by insufficient transport across the BBB, which is of great significance to the field of drug delivery.

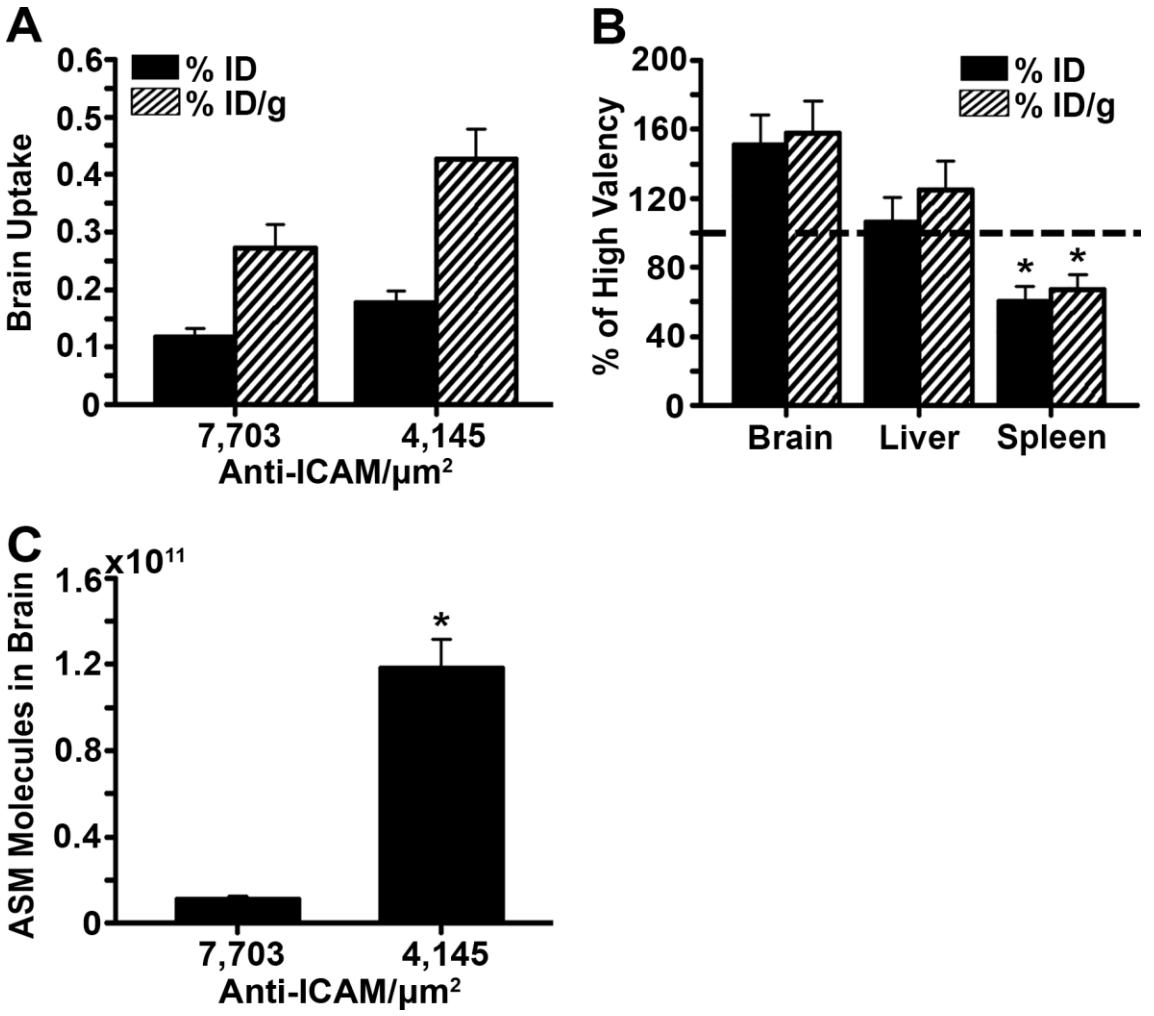

Figure 34. Role of valency on ASM delivery into the brains of mice by anti-ICAM NCs. Wild-type mice were intravenously injected with ^{125}I-labeled anti-ICAM/ASM NCs with high or intermediate targeting valency (7,703 versus 4,145 anti-ICAM molecules/μm^2, respectively). Organs were collected 30 min post-injection, weighed, and the ^{125}I content in each was measured using a gamma counter. (A) The percent injected dose (% ID) and percent injected dose per gram of tissue (% ID/g) in the brain. (B) The % ID and % ID/g for intermediate valency NCs in the brain, liver, and spleen as a percentage of that found for the high valency NCs. (C) Absolute number of ASM molecules distributed to the brain for both valencies. Data are the mean ± SEM. *Comparison to the high valency (7,703 anti-ICAM molecules/μm^2) ($p < 0.05$ by Student's *t*-test).

4.4. Discussion

Valency is a very important parameter in the design of targeted drug carriers. While the effect of valency has mainly been studied in regard to binding and uptake, subsequent processes (*i.e.*, uptake, lysosomal trafficking, and transcytosis) also warrant full consideration for optimal therapeutic efficacy. In this work, we examined the effect of valency on each of these events in order to optimize therapeutic delivery via anti-ICAM NCs for treatment of type A NPD and other disorders. To this end, we used anti-ICAM NCs with high, intermediate, or low targeting valency: 7,703 versus 4,145 versus 2,058 anti-ICAM molecules/μm^2, respectively. Based on the characterization data presented in **Table 3**, all three valencies were similar in size, PDI, ζ-potential, and the total number of antibodies (anti-ICAM + non-specific IgG) per NC surface area. Therefore, the findings presented herein are the result of valency alone and not due to the physiochemical properties of each carrier.

The rate of anti-ICAM NC binding to activated brain endothelial cells increased linearly with higher valency (**Table 4** and **Figure 16**), which was expected due to their enhanced avidity (**Table 3** and **Figure 15**). While higher valency seems optimal for targeting, it increases the likelihood of binding to off-site areas that may also express the targeted receptor, even if at low levels [47, 180]. While this possibility does not pose a significant problem for treatment of LSDs (since they are characterized by whole body dysfunction), this could be detrimental for treatment of more localized diseases or diagnostic applications [180]. High valency may also diminish targeting due to steric hindrances [47, 79, 177, 180]. This is especially relevant in the case of ICAM-1 since adequate clustering of this receptor is required for binding and CAM-mediated endocytosis

[68, 73, 79, 177]. Given sufficient time though, all three valencies reached similar binding levels at saturation (**Figure 16**), indicating that expression of ICAM-1 is a limiting factor.

In contrast to binding, NC uptake was a much faster process, rendering smaller differences in the rate of uptake among the three valencies tested (**Table 4** and **Figure 19**). Yet, there was also a linear correlation between increasing valency and faster uptake, which is in agreement with the linear relationship found between valency and enrichment of cell-signaling molecules associated with the CAM pathway, namely ceramide, PKC, and pPKCα (**Figures 17** and **18**). Therefore, at least for anti-ICAM NCs within this range of valencies, the cell-signaling induced upon binding to ICAM-1 was sufficient to induce rapid and efficient uptake of all cell-bound NCs. As well, additional analysis conducted in the Muro Laboratory verified there was no correlation when comparing ceramide enrichment to the total cell-surface area that all bound carriers occupied on a cell, the cell-surface area occupied by each single carrier, the estimated total ICAM-1 engaged by all carriers bound on a cell, or the estimated ICAM-1 engagement by each single carrier [79]. Therefore, it is the valency density (or absolute valency in the case of carriers of similar size) that regulates cell-signaling conducive to anti-ICAM NC uptake.

As mentioned in the introduction, the more pressing focus of this work was to examine the effect of valency on lysosomal trafficking and transcytosis, as well as whether these processes are linked. For instance, focusing on transcytosis, it appeared *a priori* that there was no linear relationship with valency. However, this was not the case after more detailed examination: transcytosis alone showed a linear, yet inverse relationship with valency, with lower valency NCs being more efficient at transcytosis (**Figure 22B**). However, due to the fact that transcytosis requires binding/uptake and both processes

depend directly on valency (**Figure 22A**), the combined effect produced a bell-shaped curve with intermediate valency NCs having maximal efficiency at the intersection of the binding/uptake and transcytosis plots (**Figure 22C**). In contrast, the opposite trend was observed in the case of lysosomal trafficking, resulting in an inverted bell-shaped curve (**Figure 24B**). Specifically, there was a trend toward enhanced lysosomal trafficking for the high valency NCs tested (**Table 4**), which paired well with slightly higher intracellular degradation for this valency (**Figure 31**).

To explain these findings, we speculated high valency NCs (*i.e.*, those with a greater number of ligand-receptor interactions) have impaired detachment from the basolateral endothelium after transcytosis, with transport back to lysosomes (scenario C in **Figure 25**). In support of this premise, high affinity antibodies targeting the Tf receptor (anti-TfR) were shown in the literature to have diminished transcytosis across the BBB, and in subsequent work was found to be due to enhanced lysosomal trafficking of high affinity anti-TfR as compared to low affinity counterparts [274, 296]. Similarly, gold NCs bearing human Tf ligands at a high valency showed reduced brain accumulation in mice compared to low valency particles due to their enhanced retention on or within the endothelium, which the authors speculated was due to inefficient detachment from the basolateral surface [179]. To investigate this aspect, we examined proteolytic cleavage via MMP-9 or MMP-2 as a potential mechanism for anti-ICAM NC detachment after transcytosis. Our findings presented in **Figure 32** suggest that MMP-9, which is secreted by endothelial cells upon ICAM-1 engagement [297], may contribute to this later stage of transcytosis by cleaving ICAM-1 from the basolateral endothelial surface [288, 291], thereby enabling detachment of transcytosed anti-ICAM NCs from cells.

In addition to scenario C, it is likely that scenario A (**Figure 25**) also occurs as discussed in **Section 4.3.8**, where NCs independently traffic to both lysosomes and are transcytosed. Therefore, lysosomal transport may occur via two routes, one from the apical surface following NC uptake (scenario A) versus from the basolateral surface after "frustrated" NC transcytosis (scenario C). The basolateral route depends on NC detachment after transcytosis, resulting in enhanced lysosomal transport of high valency NCs. In contrast, lysosomal transport from the apical surface is likely more efficient for lower valency, perhaps because these carriers take longer to be internalized or trafficked through the cell. However, since the bell-shaped curves for lysosomal transport and transcytosis are inverted seems to indicate that scenario C is the dominating process. In agreement, anti-ICAM NCs with intermediate valency were found to be optimal since they have sufficient targeting valency to provide both effective binding and uptake (limiting steps for low valency NCs), while it is not high enough to impair anti-ICAM NC detachment from the basolateral cell-surface after NC transcytosis (the limiting step for high valency NCs). Consequently, therapeutic ASM coated on anti-ICAM NCs with intermediate valency had significantly enhanced transcytosis across a cell culture model of the BBB as compared to high valency NCs (**Figure 33**).

In accord with the cell culture results, anti-ICAM/ASM NCs with intermediate valency showed enhanced brain accumulation in mice following intravenous injection (**Figure 34**), which is in agreement with recent work demonstrating lower anti-ICAM NC valency improved brain delivery of α-galactosidase deficient in Fabry disease [59]. Although the percent injected dose found in the brain was very low (< 1%), ASM delivery via anti-ICAM NCs is still significantly better compared to delivery of the free enzyme (7-

fold enhancement [60]) or when coupled to other targeted NCs, such as in the case of anti-TfR NCs (2.5-fold enhancement [65]). Importantly, the intermediate valency also permits greater enzyme loading on each NC. In conjunction with enhanced NC delivery, this resulted in a significant increase in the number of ASM molecules transported across the BBB (11-fold increase in cell culture and mice), which is of great translational relevance for the treatment of type A NPD and other disorders.

While not demonstrated in this work, 1 μm anti-ICAM NCs with 4,100 anti-ICAM molecules/μm^2 (similar to the intermediate valency tested herein) were also found to efficiently target and remain bound to endothelial cells within the range of shear stresses experienced in small arteries, capillaries, and venules [259]. Further, previous work has demonstrated that perfusion prior to organ harvesting does not significantly impact anti-ICAM NC accumulation in organs (~90% retention in the brain after perfusion) [61]. Therefore, the enhanced brain delivery observed in our study is not likely due to poorly bound NCs or retention of NCs in the circulation. Although capillary depletion could be used to verify transendothelial transport and localization of NCs within the brain parenchyma, anti-ICAM/enzyme NCs have been observed to cross the BBB with internalization by subjacent cells both by transmission electron microscopy and immunohistochemistry in a mouse model of NPD (*unpublished data; Muro Laboratory*).

Overall, this is the first time the influence of targeting valency on lysosomal trafficking and transcytosis has been examined mechanistically in a systematic manner. Hence, this work is of great importance to the rationale design of therapeutic carriers because it increases knowledge in the field of drug delivery about how targeted carriers crosstalk with cells, as well as provides insight into vascular biology. In fact, it has been

postulated that shedding of ICAM-1, other endothelial CAMs, and their leukocyte co-receptors may help disengage both cell types after extravasation [292]. Since MMP secretion and cleavage of the extracellular domain of other endothelial receptors is common to diverse pathological states [285, 298, 299], it is likely that proteolytic cleavage may not only impact transcytosis via the CAM pathway, but may also regulate cell detachment of other ligand-receptor complexes, thereby broadly impacting drug delivery across endothelial linings. It is also possible that alternative mechanisms may contribute to the later stages of transcytosis mediated via clathrin pits or caveoli, warranting further investigation.

Lastly, although an intermediate valency was found to be most effective in this work, the optimal valency is expected to be different for each particular drug carrier design, taking into consideration their size, shape, the receptor targeted, the affinity moiety, type and length of linkers coupling these moieties to the carrier surface, etc. [177, 300-307]. Therefore, the best valency must be empirically determined for an intended application.

4.5. Conclusions

In the context of using anti-ICAM NCs for treatment of type A NPD and other LSDs, sufficient binding and uptake needs to be balanced with maximum NC detachment after transendothelial transport and the level of trafficking to lysosomes. In **Figure 35**, the role of valency on each of these processes is summarized. Ultimately, we found anti-ICAM NCs with an intermediate valency to be the best option among the valencies tested. By lowering valency, enzyme loading could be increased, which enhanced therapeutic delivery into the brain. The combination of enhanced transcytosis and enzyme loading

make these NCs especially favorable for treating neurological LSDs, representing for the first time an effective means to tackle these disorders. Consequently, this strategy also offers an opportunity for less frequent doses, which is beneficial for minimizing immunogenicity and reducing treatment costs. To the best of our knowledge, this is also the first time the mechanism subsequent to transcytosis of any receptor-targeted drug carrier has been examined, which is highly significant and relevant to the drug delivery community. Ultimately, knowing the molecular regulation that enables receptor-bound carriers to effectively detach from the basolateral side of the endothelium after transcytosis will enable manipulation of the responsible cell-signaling molecules to enhance this outcome. Overall then, this work sheds critical insight into fundamental pathways and parameters ruling biological processes, as well as their potential translational applications to optimize therapeutic delivery.

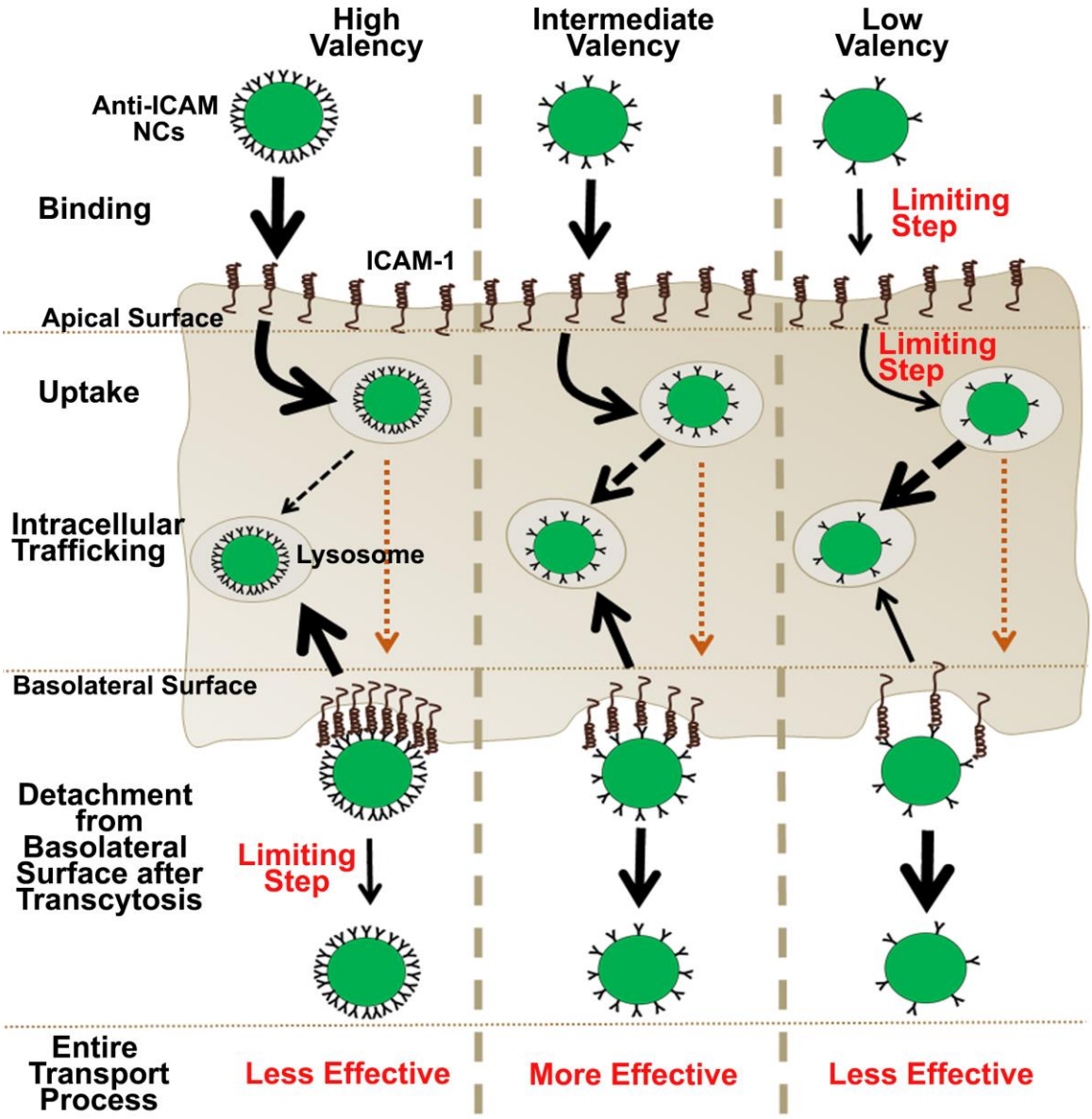

Figure 35. Model for the role of valency on NC transcytosis. The cartoon depicts the efficiency of anti-ICAM NC transport at each step: binding, uptake, lysosomal trafficking, and detachment from the basolateral surface after transcytosis. The thickness of each black arrow represents the efficiency of the step indicated, where increasing arrow thickness corresponds to greater efficiency. Black dashed arrows are the hypothesized efficiency of NC trafficking from the apical surface to lysosomes based on the comparison between lysosomal colocalization and binding/uptake data, although this was not assessed in the transwell model. Similarly, the orange dotted lines indicate that NCs are trafficked across the cell body, yet the effect of valency on the efficiency of this process was not assessed and, hence, the thickness of the arrows does not implicate the level of efficiency in this case. Although high valency NCs are efficient in binding and uptake, their high avidity impairs basolateral detachment, resulting in enhanced lysosomal trafficking. In contrast, the reduced avidity of low valency NCs hinders binding and uptake, while they are efficiently detached from the basolateral surface after transcytosis. Alternatively, an intermediate valency is optimal because it has sufficient avidity needed for binding and uptake, but does not limit basolateral detachment.

Chapter 5: Effect of ICAM-1-Targeted Carriers on Endothelial Release of an Inflammatory Mediator[4]

5.1. Introduction

Being at the interface between the circulation and subjacent tissues, vascular endothelial cells contribute to important physiological functions, including transport of metabolites and signaling molecules that communicate between these two compartments, regulation of vascular tone, hemostatic function, inflammatory response, and so on [308]. Hence, in many diseases, including LSDs, endothelial cells represent both an important target for therapeutic intervention, as well as a barrier to treatment of subjacent tissues, as previously discussed [10, 308]. An illustration of this relevance is the fact that numerous drug delivery strategies are being explored to target pharmaceuticals to the endothelium, either for endothelial-surface release into the circulation, uptake into endothelial cells to treat endothelial maladies, or transport across this lining [52, 309].

By contributing to the adhesion of leukocytes to the endothelium, their extravasation into sites of disease and other associated signaling cascades, ICAM-1 plays an important role in the inflammatory processes that underlie most maladies [66, 67, 73-75]. Interestingly, engagement of ICAM-1 by NCs coated with anti-ICAM antibodies or peptides, such as the case of liposomes, nanoparticles, dendrimers, micelles, protein conjugates, etc., induces a series of signal cascades and actin reorganization in endothelial cells, leading to vesicular transport both into and across these cells via the CAM pathway [68, 70, 71, 78]. As discussed in prior chapters, the CAM pathway is effective across a

[4]Chapter 5 text, table, and figures reproduced with permission from: Manthe, R.L. and Muro, S. *ICAM-1-targeted nanocarriers attenuate endothelial release of soluble ICAM-1, an inflammatory regulator*. Bioeng Transl Med, 2017. 2(1): p. 109-19; © 2017 Rachel L. Manthe and Silvia Muro.

broad spectrum of carrier sizes (from the nano- to the micro-scale), in contrast to clathrin- or caveolae-mediated pathways that associate with much smaller vesicles [62, 78]. This correlates well with the fact that ICAM-1 contributes to mobilization of leukocytes [310]. Similarly, the signal cascades that associate with endothelial uptake of anti-ICAM NCs involve PKC, Src kinases, Rho, Ca^{2+}, sphingomyelinase-mediated generation of ceramide, etc., which are reminiscent of those elicited upon leukocyte binding to endothelial cells during inflammation [68, 73, 78]. As well, the actin reorganization observed in both events are analogous and consist with mobilization of cortical into actin stress fibers [68, 73, 78]. Ultimately, endothelial targeting and vesicular-mediated transport via ICAM-1 has shown promise for diagnostic imaging and drug delivery applications in the context of cancer, LSDs, pulmonary, cardiovascular, and other diseases [61, 230-235].

However, due to the role of ICAM-1-mediated leukocyte adhesion and signaling in inflammation [66, 74, 75], the secondary effects of engaging this receptor and/or blocking it from its natural counterparts are not known. In fact, this aspect has not been carefully examined yet for most of the targeted drug delivery systems described in the literature. Given that cell-surface receptors and markers are typically involved in complex functions and/or signaling processes important to maintaining homeostasis, it is logical to assume that engagement by targeted drug carriers could lead to either beneficial or detrimental side effects, depending on their specific patho-physiological role. In the case of ICAM-1, it has been postulated that engagement by antibodies or drug carriers could lower the availability of this marker for engagement by its natural "ligands" (β_2 integrins, LFA-1 and Mac-1, present on the leukocyte surface) [74], therefore attenuating inflammation, which may render secondary benefits [311]. Conversely, it is also known that ICAM-1 binding by

leukocytes initiates pro-inflammatory cascades, including release of cytokines, generation of reactive oxygen species, expression of other CAMs, alteration of endothelial permeability, and so on [66, 75]; hence, ICAM-1 engagement by NCs could result in similar side effects.

In this context, an interesting biological process associated with ICAM-1 overexpression during inflammation and its engagement by leukocytes is that of endothelial release of the ectodomain of ICAM-1, which can then circulate as the "soluble" form of this molecule (sICAM-1) [75, 76]. Release of sICAM-1 is believed to occur via cleavage of the ICAM-1 ectodomain by proteases, such as MMP-9, as examined in **Chapter 4** for detachment of anti-ICAM NCs after transendothelial transport [288]. Additional proteases (*e.g.*, TNFα-converting enzyme (TACE/ADAM-17) and neutrophil elastase) may also be directly involved in ICAM-1 cleavage [312-314], or others may indirectly play a role in this process, such as in the case of MMP-2, which again is involved in cleavage of latent MMP-9 into its active form [293, 294].

The literature describes sICAM-1 as an inflammatory marker and regulator, which can promote the inflammatory response [75, 76]. Serum sICAM-1 appears to be low in healthy individuals, but its levels increase in many pathologies, associating with the disease progression and severity, as in the case of cancer, cardiovascular disease, immune syndromes and, generally, maladies involving chronic inflammation, including LSDs [75, 76, 315]. This association is not merely circumstantial, but sICAM-1 appears functionally involved in these diseases [76]. For instance, sICAM-1 aids in tumor progression by promoting angiogenesis and shielding tumors from cytotoxic lymphocytes, and it promotes

a pro-inflammatory phenotype by inducing the production of factors such as MIP-1α, IL-6, or TNFα [76, 316-319].

Therefore, in this chapter we began studying aspects relative to the potential secondary effects of endothelial ICAM-1 targeting, focusing on the influence of anti-ICAM NCs on endothelial release of sICAM-1. The results we obtained will help rationally inform the future design of drug carriers and selection of potential applications using this strategy.

5.2. Materials and Methods

5.2.1. Antibodies and Reagents

Monoclonal mouse anti-human ICAM-1 (clone R6.5) [243] was from American Type Culture Collection (Manassas, VA) and phycoerythrin-labeled monoclonal mouse anti-human ICAM-1 (clone LB-2) was from Santa Cruz Biotechnology (Dallas, TX). Alexa Fluor 350-labeled secondary antibodies were from Invitrogen (Carlsbad, CA). Non-specific mouse IgG was from Jackson ImmunoResearch (West Grove, PA). Green Fluoresbrite® 100 nm diameter polystyrene beads were from Polysciences (Warrington, PA). Porous transwell inserts (1.0 μm-pore) were from Thermo Fisher Scientific (Waltham, MA). Human sICAM-1 ELISA kits were from Invitrogen (Carlsbad, CA). ^{125}I and Iodogen pre-coated tubes were from PerkinElmer (Waltham, MA) and Thermo Fisher Scientific (Waltham, MA), respectively. MMP-9 Inhibitor I and MMP-2 Inhibitor I were from EMD Millipore (Billerica, MA). Unless specified, all other reagents were from Sigma-Aldrich (St. Louis, MO).

5.2.2. Preparation and Characterization of Anti-ICAM NCs

Model polymer NCs were prepared by coating via surface absorption unlabeled or ^{125}I-labeled anti-ICAM or non-specific IgG onto 100 nm, green fluorescent polystyrene beads (anti-ICAM NCs versus IgG NCs), as described in **Section 3.2.6**. The diameter of coated NCs was measured using particle tracking (Nanosight LM10, Malvern Instruments; Westborough, MA), while the PDI and ζ-potential were obtained by dynamic light scattering and electrophoretic mobility, respectively (Zetasizer Nano-S90; Malvern Instruments; Westborough, MA). The resulting antibody coat was assessed as described in **Section 4.2.3**.

5.2.3. Cell Cultures

HUVECs (Lonza Walkersville, Inc.; Walkersville, MD) were cultured in M-199 (Invitrogen; Carlsbad, CA) supplemented with 15% FBS, 2 mM L-glutamine, 15 μg/mL ECGS, 100 μg/mL heparin, 100 U/mL penicillin, and 100 μg/mL streptomycin. Cells were grown at 37°C, 5% CO_2, and 95% relative humidity on either 1% gelatin-coated coverslips or uncoated 1.0 μm-pore transwell inserts. Where indicated, cells were stimulated overnight with 10 ng/mL TNFα to induce endothelial activation, as found in LSDs [9, 239].

5.2.4. Binding and Uptake of Anti-ICAM NCs by Activated Endothelial Cells

TNFα-activated HUVECs grown on coverslips were incubated for 30 min at 37°C with green fluorescent anti-ICAM NCs or non-specific IgG NCs, followed by washing off non-bound carriers. The cells were fixed with 2% paraformaldehyde, stained with a Texas-Red secondary antibody to label carriers bound on the cell-surface (not internalized) [247],

and cell nuclei were stained blue with DAPI. Samples were visualized by fluorescence microscopy as described in prior sections. As in previous studies, the total number of NCs associated per cell (total green NC signal) and the number of NCs internalized within cells (total green signal minus green signal that colocalized with "surface" red signal) were quantified. This was achieved using an algorithm that normalizes the area of specific fluorescence (over a threshold background) to the number of pixels that correspond to the size of a single NC [247].

To assess NC interaction with TNFα-activated HUVECs in transwell models, ^{125}I-labeled anti-ICAM or IgG NCs were added to the apical chamber and incubated for 30 min at 37°C (pulse). Non-bound carriers were then removed by washing both chambers to eliminate any NCs that may have leaked across the cell monolayer. Cells were then incubated for additional time in carrier-free medium up to a total time of 5 h to allow transcytosis of bound NCs (chase). After both time points, ^{125}I-labeled anti-ICAM or IgG NCs associated with the endothelial layer were quantified using a gamma counter as described previously. Free ^{125}I was determined using TCA precipitation and subtracted from these measurements, to eliminate any contribution of free tracer [247].

5.2.5. Release of sICAM-1 by Endothelial Cells

Quiescent versus TNFα-activated HUVECs, grown on coverslips or transwells, were incubated at 37°C in the absence versus presence of anti-ICAM or non-specific IgG NCs. For transwell experiments, NCs were added to the apical chamber for 30 min (pulse), followed by washing to remove non-bound NCs, and incubation for additional time in carrier-free medium up to a total of 1 h or 5 h (chases). After each time, the cell medium

was collected and centrifuged at 3,000*g* for 5 min, followed by 1 min centrifugation at 17,000*g* to remove residual NCs, cells, and debris. The supernatants were used to quantify sICAM-1 by ELISA according to the manufacturer's instructions, followed by colorimetric detection using a SpectraMax M2e microplate reader (Molecular Devices; Sunnyvale, CA) at 450 nm. Similar experiments were performed in the presence of 3 mM amiloride, which inhibits CAM-mediated transport [68, 78], and 25 μM MMP-9 or MMP-2 inhibitors (MMP-9i; MMP2i), individually or in combination (Mixed MMPi).

5.2.6. Validation of sICAM-1 Differential Shedding versus Diffusion in Transwell Models

To verify lack of diffusion (indicative of differential release) of sICAM-1 across the endothelial cell monolayer, exogenous sICAM-1 was added to either the apical or basolateral chambers (2 ng/mL added) and incubated at 37°C for 4.5 h. The amount of sICAM-1 in each chamber was then measured by ELISA, as described above. To calculate the amount of sICAM-1 in each chamber as a percentage of sICAM-1 added, sICAM-1 that was released from activated endothelial cells during this time (obtained from control experiments where exogenous sICAM-1 was not added) was subtracted from the readings, and then the percentage was calculated.

5.2.7. Uptake of Membrane ICAM-1 versus sICAM-1 by Activated Endothelial Cells Incubated with Anti-ICAM NCs

TNFα-activated HUVECs grown on coverslips were incubated for 30 min at 37°C with green fluorescent anti-ICAM NCs. Then, the cells were washed to remove non-bound

NCs. The cells were fixed with 2% paraformaldehyde, stained with a blue Alexa Fluor 350-labeled secondary antibody to label NCs bound on the cell-surface (not internalized), and then permeabilized with 0.1% Triton X-100 and stained with a phycoerythrin-labeled anti-ICAM-1 (clone LB-2) antibody (pseudocolored red) to label both cell-surface and internalized NCs. Hence, cell-surface NCs appear white (green + blue + red), internalized membrane ICAM-1 complexed with NCs appear yellow (green + red), and internalized NCs without internalized membrane ICAM-1 appear green alone. Images were captured as described previously. Alternatively, after NC removal by washing, cells were lysed and the amount of sICAM-1 in these cell lysates was measured via ELISA, as described above.

5.2.8. Statistics

Experiments encompassed a total sample size of $n \geq 4$. Data were calculated as the mean ± SEM. Statistical significance was determined as $p < 0.1$ by Student's *t*-test or by the Mann-Whitney Rank Sum test, as indicated.

5.3. Results

5.3.1. Release of sICAM-1 by Endothelial Cells and Differential Apical versus Basolateral Distribution

Endothelial cells increase their release of sICAM-1 when activated during inflammation [76, 288, 316]. Hence, we first validated our detection of this phenomenon using endothelial cells grown on coverslips, the most common model used in prior sICAM-1 studies in cell culture. We incubated endothelial cells overnight with the pro-inflammatory cytokine TNFα (activation pulse), then removed TNFα and continued

incubations in fresh medium (release chase). As expected, TNFα enhanced sICAM-1 release by endothelial cells compared to non-activated counterparts: a 1.5-fold increase in a period of 30 min (**Figure 36A**). Then, we repeated this assay using endothelial cells grown as a monolayer on transwell inserts, a model that better reflects the natural status of endothelial cells by separating apical and basolateral compartments. Total sICAM-1 release in this model seemed similar or slightly enhanced to the coverslip model (1.4-fold at 30 min; **Figure 36A**). This setting also allowed us to independently examine sICAM-1 release from the apical versus basolateral sides of the endothelial cell monolayer. Unexpectedly, we observed a preferential release into the basolateral chamber underneath the cells (75% of total sICAM-1, 3-fold over the apical fraction; **Figure 36A**). The release of sICAM-1 continued increasing up to 1 h (2.7-fold over 30 min), then it seemed to saturate (at 5 h it was 1.1-fold over 1 h; **Figure 36B**). During all this time, the pattern of preferential basolateral release was maintained and, at saturation (5 h), basolateral sICAM-1 surpassed the apical fraction by 4.2-fold (**Figure 36B**).

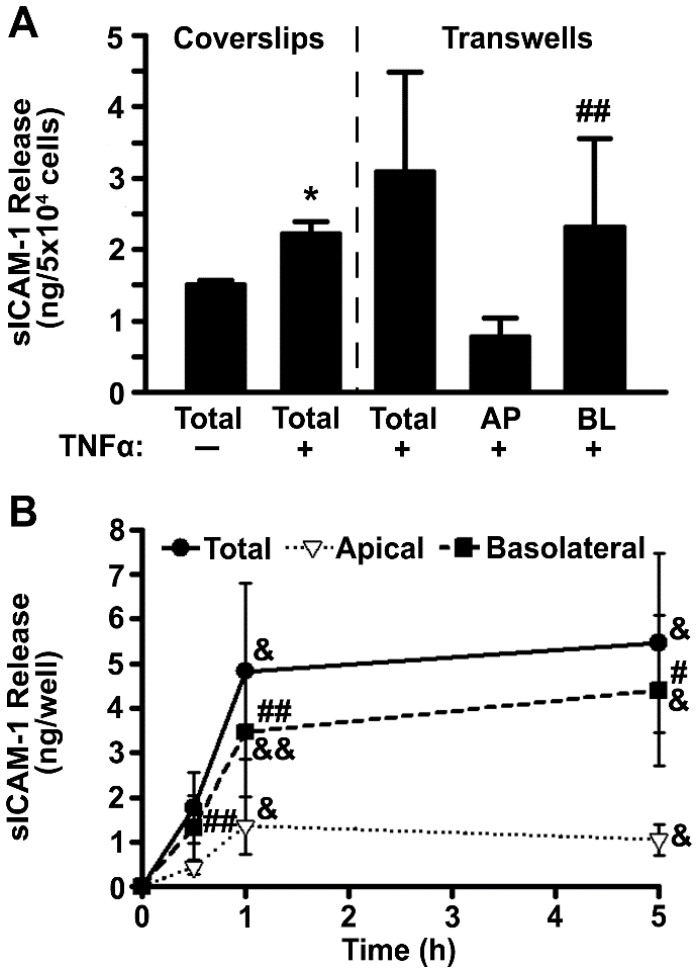

Figure 36. Release of sICAM-1 by endothelial cells. (A) HUVECs were grown on coverslips or transwell inserts in control medium versus medium containing TNFα (overnight; ~16 h). Cells were then washed and sICAM-1 release into the cell medium (apical (AP), basolateral (BL), and total (AP+BL)) was examined after 30 min, using ELISA. (B) Cumulative distribution of sICAM-1 release by TNFα-activated HUVECs grown on transwells was similarly measured at 30 min, 1 h, or 5 h. Data are the mean ± SEM. *Comparison to non-activated ECs; #comparison between apical and basolateral chambers at each time point; &comparison to 30 min (one symbol is $p < 0.1$ by Student's *t*-test and two symbols is $p < 0.1$ by Mann-Whitney Rank Sum test). Figure adapted from [291].

To validate the specificity of this differential pattern, we tested the passive permeability of the endothelial cell monolayer and the transwell filter (**Figure 37A**). In the absence of cells, addition of exogenous sICAM-1 to the apical chamber resulted in a similar distribution in both compartments (56% apical and 64% basolateral; **Figures 37A-B**). This indicates that sICAM-1 can diffuse through the filter pores, as expected. Then, we added

exogenous sICAM-1 to either the apical or basolateral chambers separated by endothelial cells, and sICAM-1 was measured in either chamber after 4.5 h. Opposite to the pattern of sICAM-1 release by cells, addition of exogenous sICAM-1 to the apical side resulted in a specific increase of the sICAM-1 level in this chamber, *i.e.*, 3.4-fold over the basolateral side (**Figures 37A-B**). This was 6.9-fold greater than the amount released by cells in this chamber, while detection in the basolateral chamber did not vary (1.2-fold over that of cells alone; **Figure 37C**). Conversely, exogenous sICAM-1 addition to the basolateral chamber resulted in an even greater enhancement in this chamber (24-fold over the apical side; **Figures 37A-B**). This addition rendered a minor increase in the level of sICAM-1 in the apical chamber (1.5-fold over cells alone) and a slightly greater increase in the basolateral fraction (2.3-fold; **Figure 37C**). Since cells alone release more sICAM-1 to the basolateral side, it was expected that adding exogenous sICAM-1 to this chamber would enhance sICAM-1 to a lesser extent than adding it to the apical side (**Figure 37C**). Yet, when comparing the absolute amount of exogenous sICAM-1 recovered from the basolateral versus apical chambers (middle bars in **Figure 37B**), it is clear that this corresponds to almost all sICAM-1 added. These results indicate that there is minimal (if any) passive leakage of sICAM-1 across endothelial cell monolayers and the levels of sICAM-1 detected in this model correspond to differential basolateral and apical release by endothelial cells.

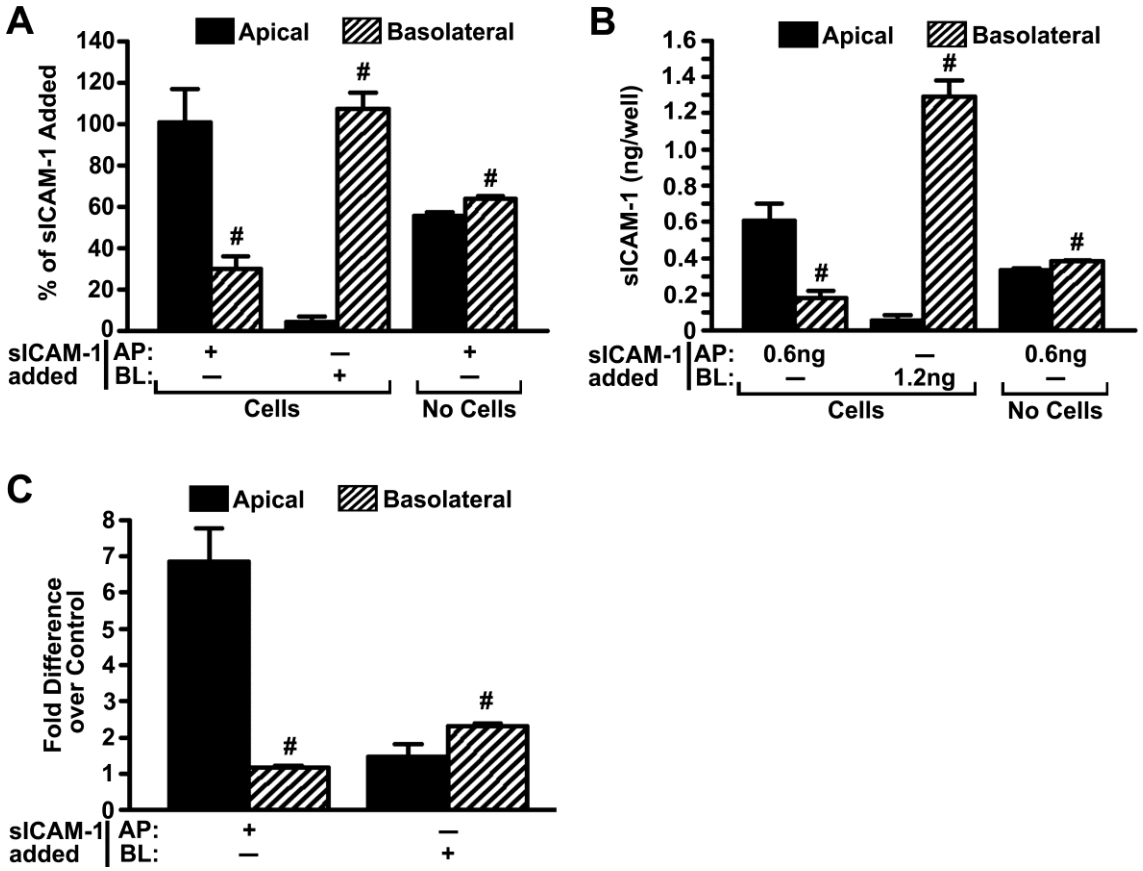

Figure 37. Validation of differential sICAM-1 release versus diffusion in the transwell model. Exogenous sICAM-1 was added to the apical (AP) or basolateral (BL) chambers of transwell inserts where TNFα-activated HUVEC monolayers had been grown, and sICAM-1 was measured in both chamber after 4.5 h at 37°C. Data show (A) relative distribution of exogenous sICAM-1 in the presence versus absence of cells, (B) exogenous sICAM-1 detected in these chambers (total sICAM-1 in each chamber minus sICAM-1 contributed to each chamber from cellular release) and (C) the fold difference in sICAM-1 detection over basal detection (no addition of exogenous sICAM-1) for each chamber. Data are the mean ± SEM. #Comparison between apical and basolateral chambers ($p < 0.1$ by Student's *t*-test). Figure adapted from [291].

5.3.2. MMP Mechanism of sICAM-1 Release by Endothelial Cells

It has been reported that release of sICAM-1 by endothelial cells may be in part contributed by shedding of ICAM-1 expressed at the cell-surface, a phenomenon also observed for other endothelial CAMs [76, 316-319]. This is believed to be mediated via cleavage of the ICAM-1 ectodomain by proteases, such as the case for MMP-9 [288]. Therefore, to examine if this mechanism contributes to the observed differential

distribution of sICAM-1 across activated endothelial cell monolayers, we measured release in the presence of MMP-9 and/or MMP-2 inhibitors, whereby MMP-2 was meant to serve as a control. We focused on the first 30 min after removal of the TNFα pulse, as this had shown active release rather than saturation (**Figure 36B**). As expected, MMP-9 inhibition led to a 37% decrease in total sICAM-1 by activated endothelial cells (**Figure 38A**). MMP-2 inhibition also reduced total sICAM-1 (by 22%, not significant), and simultaneous inhibition of MMP-9 and MMP-2 behaved as MMP-9 inhibition alone (34% reduction; **Figure 38A**).

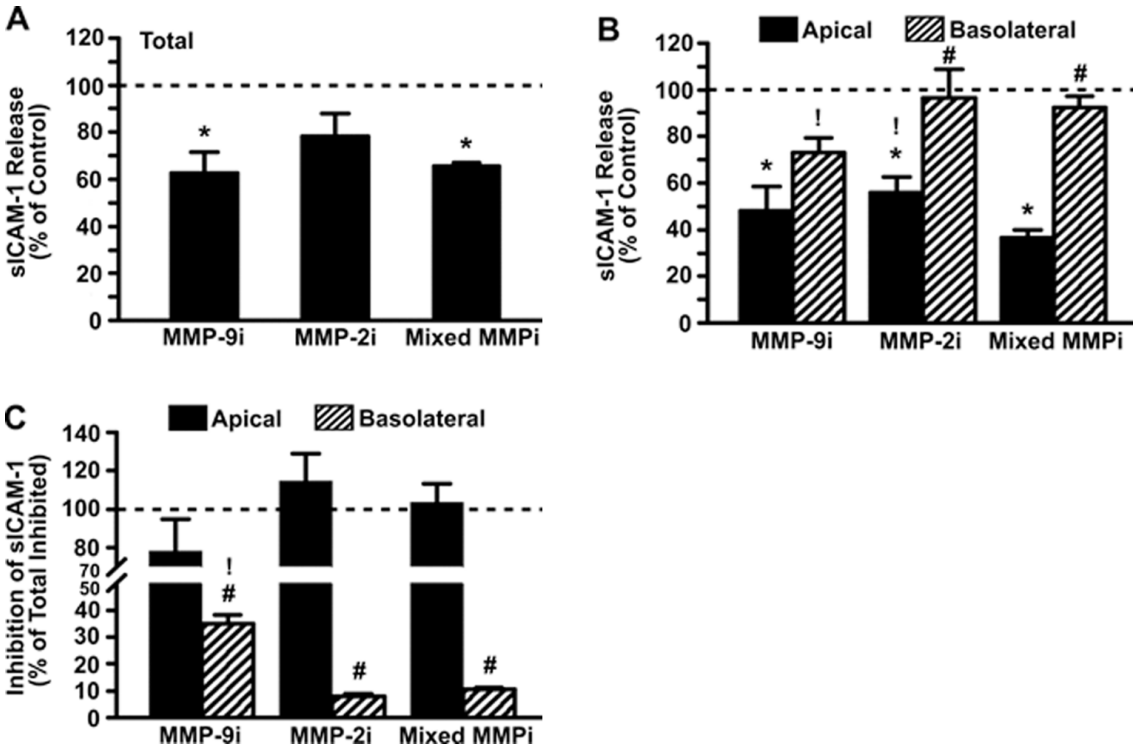

Figure 38. Effect of MMP inhibition on sICAM-1 release by activated endothelial cells. TNFα-activated HUVECs grown on transwell inserts were incubated in control medium or medium containing inhibitors of MMP-9 (MMP-9i), MMP-2 (MMP-2i), or a mixture of both (Mixed MMPi) for 30 min. (A) Total (apical + basolateral) and (B) apical versus basolateral release of sICAM-1, as measured by ELISA and expressed as the percentage of control without inhibitors (horizontal dashed lines). (C) Inhibition of apical or basolateral release of sICAM-1 relative to the total inhibition observed (horizontal dashed line). Data are the mean ± SEM. *Comparison to control for each condition and chamber; #comparison between apical and basolateral chambers; !comparison to mixed MMPi for each chamber ($p < 0.1$ by Student's *t*-test). Figure reproduced from [291].

Interestingly, compared with respective controls in each chamber, the effect caused by MMP-9 was greater in the apical versus basolateral chamber (48% versus 73% of respective chamber controls; **Figure 38B**). Comparing the absolute amount of sICAM-1 contributed by MMP-9 to either chamber (**Figure 38C**), we observed that inhibition of this proteinase more readily decreased sICAM-1 in the apical versus basolateral chamber (78% versus 35% contribution). MMP-2 inhibition also decreased apical sICAM-1 release (56% of control), although no effect was observed with regard to basolateral release (96% of control; **Figure 38B**). In fact, when comparing the absolute amount of sICAM-1 contributed by MMP-2 in these chambers, only apical activity was found (114% versus 8% contribution; **Figure 38C**). Despite observing MMP-9 and MMP-2 effects in the apical chamber, simultaneous inhibition of both proteinases did not render enhanced or additive effects on this side (37% of control, statistically similar to MMP-9 inhibition alone) and little inhibition arose in the basolateral chamber (92% of control; **Figure 38B**). Altogether, these results suggest that both MMPs are functionally involved in sICAM-1 release to the apical space, with MMP-9 contributing to a greater extent, while MMP-9 alone contributes to basolateral sICAM-1 release and this contribution is lower than that at the apical side. This finding correlates well with the role of MMP-9 in basolateral detachment of anti-ICAM NCs after transendothelial transport, while MMP-2 had no effect (**Figure 32**).

5.3.3. Effect of Anti-ICAM NCs on sICAM-1 Release by Endothelial Cells

In addition to pro-inflammatory factors alone, sICAM-1 release has been postulated to associate with other events. For instance, binding of leukocytes to endothelial CAMs is known to regulate leukocyte-endothelial interactions during inflammation, including

disengagement of both cell types after leukocyte extravasation [287-290, 292]. In this context, leukocyte binding to endothelial CAMs seems to result in both leukocyte and endothelial secretion of MMPs, as well as sICAM-1 release [73]. Therefore, it is plausible that binding of ICAM-1-targeted NCs to endothelial ICAM-1 may result in a similar effect.

To examine this, we used model polystyrene NCs coated with anti-ICAM (anti-ICAM NCs) versus non-specific IgG (IgG NCs). Although not biodegradable, these NCs allows us to examine ICAM-1 targeting and sICAM-1 release events without confounding results that may arise from simultaneous NC degradation. As described in prior chapters, these formulations are relatively stable (*i.e.*, lack of aggregation, antibody detachment, and albumin coating) [61] and render binding, endocytosis, intracellular trafficking, and *in vivo* circulation and biodistribution comparable to biodegradable PLGA carriers [58, 81]. The characterization data for anti-ICAM and IgG NCs can be seen below in **Table 5**.

Table 5. NC characterization.

	Size (nm)	PDI	Zeta Potential (mV)	Antibodies/NC
Uncoated NCs	109.3 ± 1.8	0.06 ± 0.01	-35.5 ± 1.2	N/A
Anti-ICAM NCs	156.8 ± 2.3	0.18 ± 0.01	-27.4 ± 0.3	267 ± 10
IgG NCs	158.0 ± 4.9	0.15 ± 0.01	-28.7 ± 0.4	193 ± 13

Data are the mean ± SEM. Table reproduced from [291].

As described previously [61, 68], fluorescence microscopy showed that anti-ICAM NCs specifically bound to and were internalized by activated endothelial cells grown on coverslips: 241-fold and 456-fold over non-specific IgG NCs, respectively, after only 30 min incubation (**Figure 39A**). In addition, radioisotope tracing of ^{125}I-labeled anti-ICAM NCs showed that this formulation also bound specifically to activated endothelial cells grown on transwell inserts, *e.g.*, 30-fold over ^{125}I-labeled IgG NCs after 30 min incubation

(**Figure 39B**). A similar specificity was found after 5 h incubation (31-fold over IgG NCs). Yet, at this time the absolute amount of NCs associated with cells decreased below that observed at 30 min (3.1-fold decrease for anti-ICAM NCs), which is consistent with transendothelial transport previously observed in this model (**Chapter 4** and [71]).

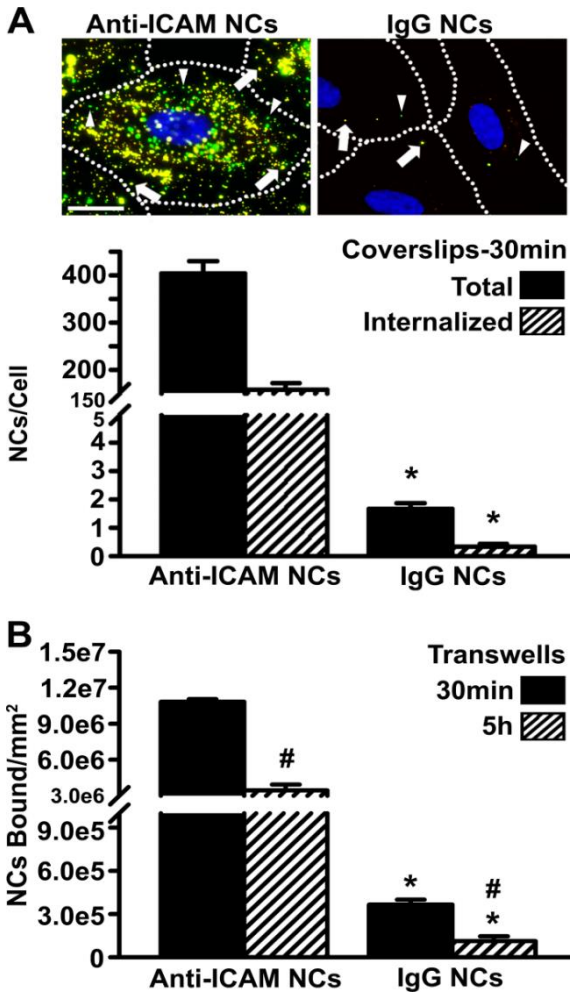

Figure 39. Specific interaction of anti-ICAM NCs with activated endothelial cells. (A) TNFα-activated HUVECs were incubated for 30 min at 37°C with green fluorescent anti-ICAM or IgG NCs. Non-bound NCs were removed by washing, and surface-bound NCs were immunostained using a Texas-Red secondary antibody, which renders non-internalized NCs in yellow (green + red; arrows) versus green internalized NCs (arrowheads). Images and quantification of total cell-associated (surface-bound + internalized) and internalized NCs are shown. Scale bar = 10 μm. (B) TNFα-activated HUVECs grown on transwell inserts were incubated for 30 min at 37°C with ^{125}I-labeled anti-ICAM or IgG NCs. Non-bound NCs were removed by washing both chambers, and cells were incubated in fresh medium up to 5 h total. NCs associated with the cell fraction were quantified using a gamma counter at both time points. Data are the mean ± SEM. *Comparison between anti-ICAM and IgG NCs; #comparison between 30 min and 5 h ($p < 0.1$ by Student's *t*-test). Figure reproduced from [291].

Next, we focused on the effect of anti-ICAM NCs on sICAM-1 release by activated endothelial cells. As in the absence of NCs (**Figure 36B**), preferential release of sICAM-1 to the basolateral versus apical side was also observed in the presence of anti-ICAM NCs (**Figure 40**). However, surprisingly, NCs significantly inhibited this process (**Figure 41**): after 30 min incubation, anti-ICAM NCs reduced total sICAM-1 release by 50% in the coverslip model and by 60% in the transwell model, which was specific compared to IgG NCs (13% and 24% reduction, respectively; **Figure 41A**). This effect persisted with time and was observed in both the apical and basolateral compartments (**Figures 41B-C** and **Figure 42**).

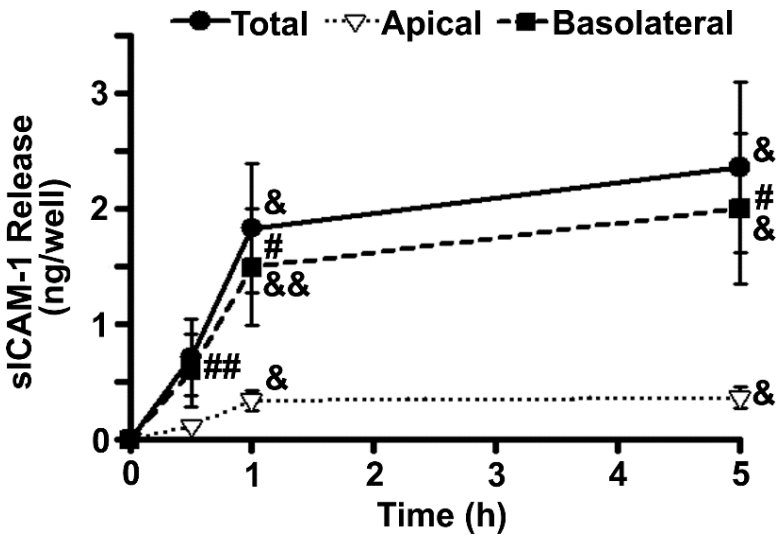

Figure 40. Release of sICAM-1 by activated endothelial cells incubated with anti-ICAM NCs. Cumulative distribution of sICAM-1 release by TNFα-activated HUVECs grown on transwell inserts and incubated with anti-ICAM NCs for 30 min (pulse), followed by removal of non-bound NCs and incubation in carrier-free medium for additional time up to 1 h or 5 h total. Data are the mean ± SEM. [#]Comparison between apical and basolateral chambers at each time point; [&]comparison to 30 min (one symbol is $p < 0.1$ by Student's *t*-test and two symbols is $p < 0.1$ by Mann-Whitney Rank Sum test). Figure reproduced from [291].

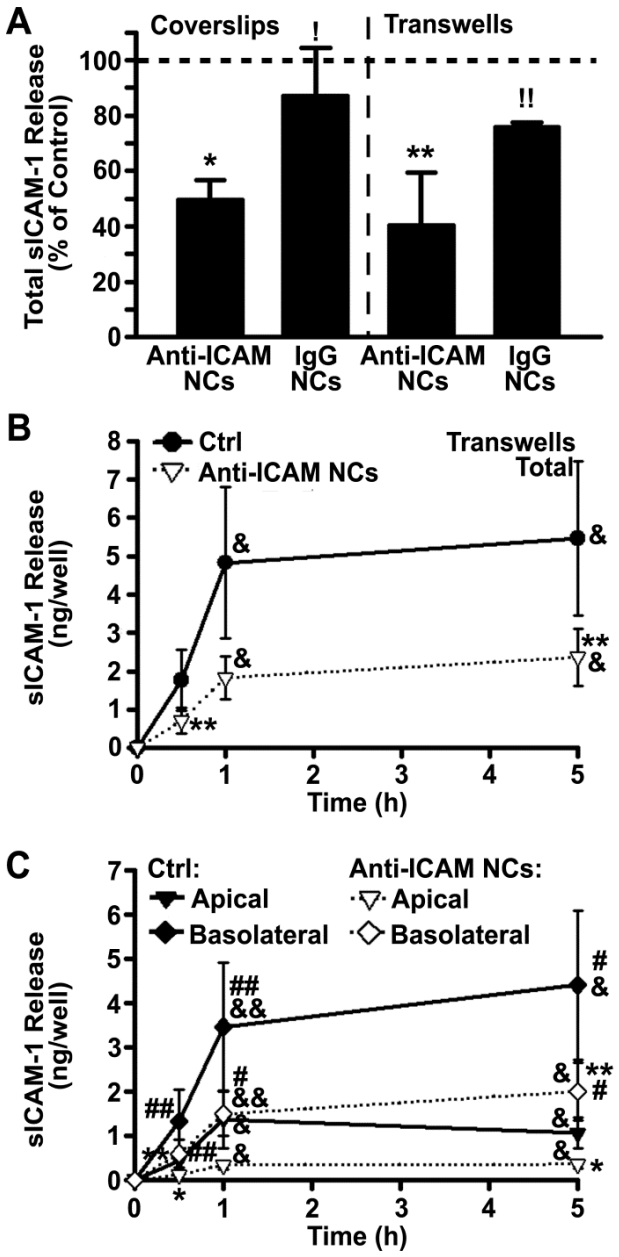

Figure 41. Attenuation of sICAM-1 release by anti-ICAM NCs. (A) Total sICAM-1 release by TNFα-activated HUVECs grown on coverslips or transwell inserts after incubation with anti-ICAM or non-specific IgG NCs for 30 min. Data are presented as a percentage of cells incubated in the absence of NCs (control; horizontal dashed line). (B, C) Cumulative distribution of sICAM-1 release by activated HUVECs grown on transwell inserts and incubated in control medium (Ctrl) or medium containing anti-ICAM NCs. Incubations were for 30 min (pulse), followed by NC removal and incubation in fresh medium for additional time up to 1 h or 5 h total. Total sICAM-1 in (A) and (B) represents the apical + basolateral fractions. Data are the mean ± SEM. *Comparison to control; [!]comparison between anti-ICAM and IgG NCs; [#]comparison between apical and basolateral chambers at each time point; [&]comparison to 30 min (one symbol is $p < 0.1$ by Student's *t*-test and two symbols is $p < 0.1$ by Mann-Whitney Rank Sum test). Figure reproduced from [291].

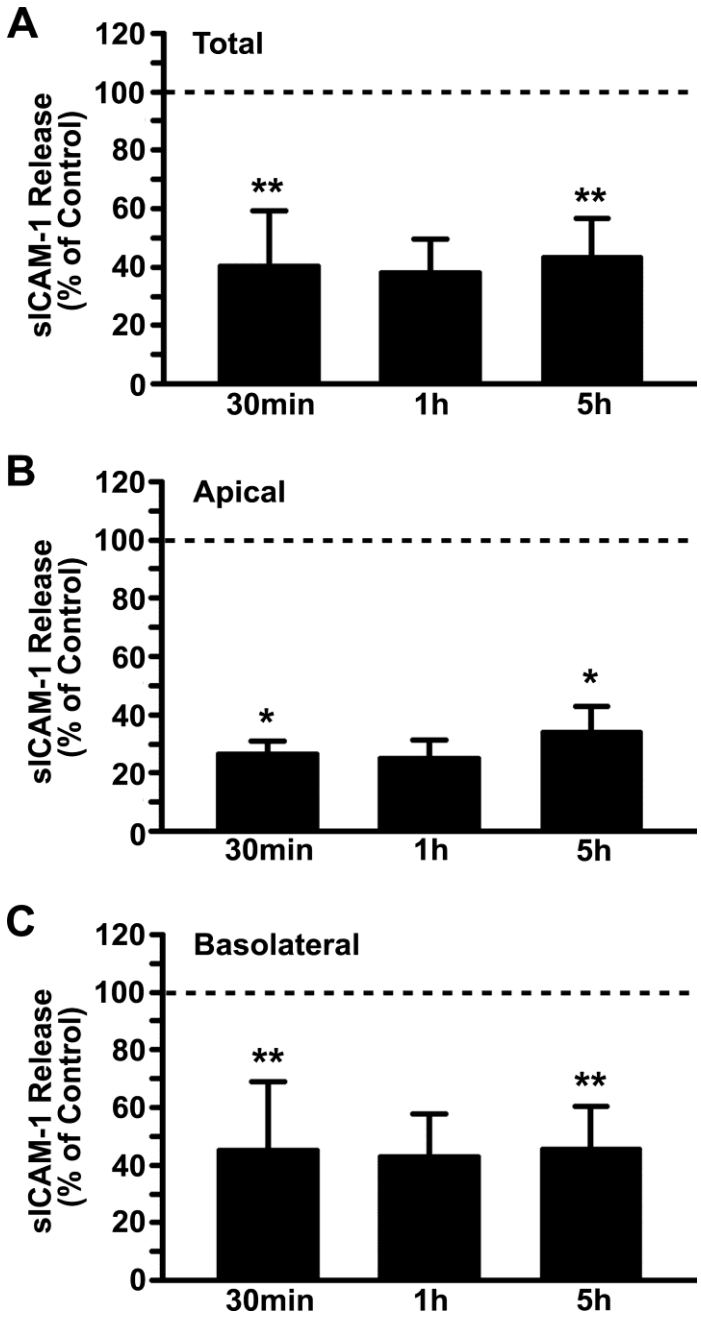

Figure 42. Reduction of sICAM-1 release by endothelial cells incubated with anti-ICAM NCs. Cumulative distribution of sICAM-1 release by TNFα-activated HUVECs grown on transwell inserts and incubated with anti-ICAM NCs for 30min (pulse), followed by removal of non-bound NCs and incubation in carrier-free medium for additional time up to 1 h or 5 h total. (A-C) Data show sICAM-1 release as a percentage of cells incubated in the absence of anti-ICAM NCs (control; horizontal dashed lines). Data are the mean ± SEM. *Comparison to control (one symbol is $p < 0.1$ by Student's *t*-test and two symbols is $p < 0.1$ by Mann-Whitney Rank Sum test). Figure reproduced from [291].

Reduction of sICAM-1 release by NCs was greater in the apical compartment versus the basolateral side: *e.g.*, at 30 min, respective reductions of 73% versus 55% were observed (**Figures 42B-C**). However, over time the inhibitory effect of anti-ICAM NCs was more balanced between the two chambers (66% apical and 55% basolateral reduction by 5 h; **Figures 42B-C**). Importantly, anti-ICAM NCs reduced release of sICAM-1 at a greater extent than MMP inhibitors (**Figure 43**). At 30 min when active sICAM-1 release was occurring, anti-ICAM NCs reduced total sICAM-1 by 60% compared to 37%, 22%, and 34% reductions rendered by inhibiting MMP-9, MMP-2, or both simultaneously. This was also the case for attenuation of sICAM-1 at the apical side (73% reduction by NCs versus 52%, 44%, and 63% decrease for inhibitors of MMP-9, MMP-2, and both) and the basolateral side (55% reduction by NCs versus 27%, 4%, and 8% decrease for inhibitors of MMP-9, MMP-2, and both).

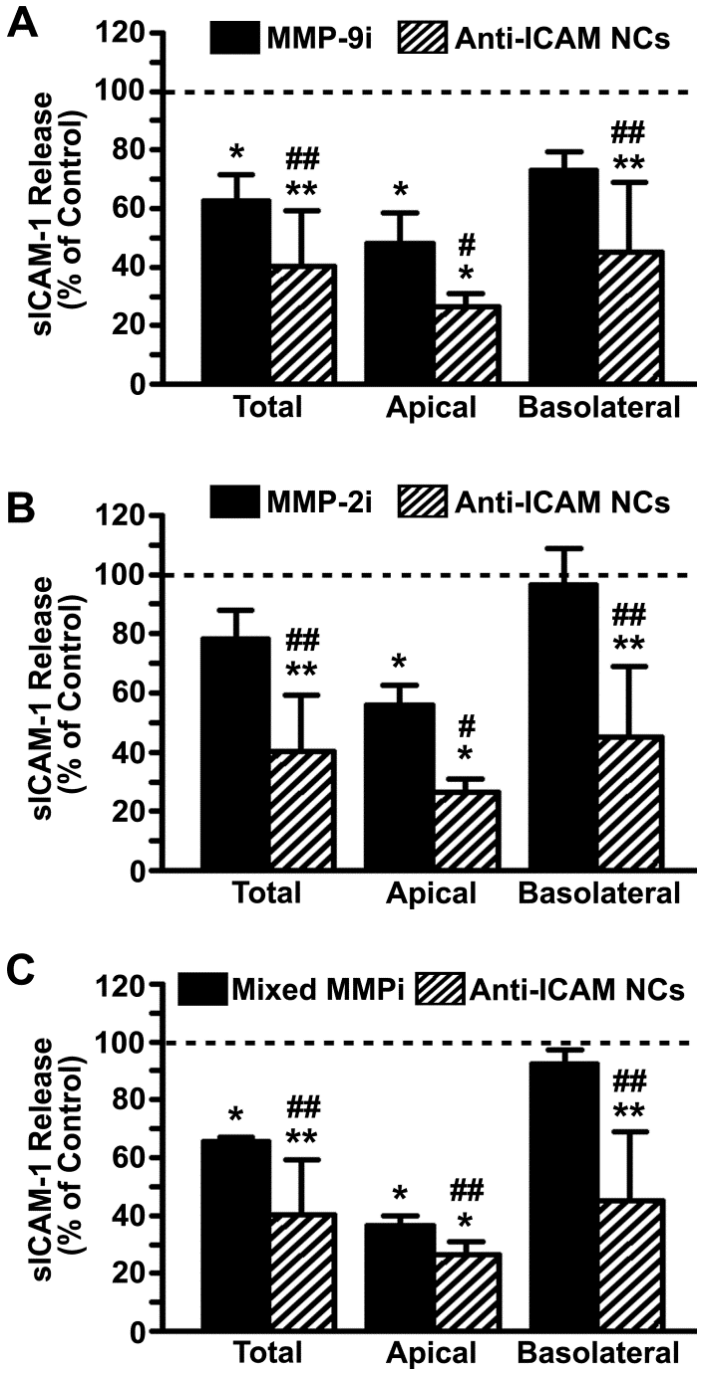

Figure 43. Comparative reduction of sICAM-1 by anti-ICAM NCs versus MMP inhibitors. Reduction in sICAM-1 release by TNFα-activated HUVECs grown on transwell inserts and incubated for 30 min with MMP inhibitors (MMP-9i, MMP-2i, or a mixture of both (Mixed MMPi)) or with anti-ICAM NCs. Data show sICAM-1 release as a percentage of controls (absence of inhibitors and NCs; indicated by the horizontal dashed lines). Data are the mean ± SEM. *Comparison to control; #comparison between anti-ICAM NCs and inhibitors (one symbol is $p < 0.1$ by Student's *t*-test and two symbols is $p < 0.1$ by Mann-Whitney Rank Sum test). Figure reproduced from [291].

5.3.4. Mechanism by which Anti-ICAM NCs Reduce sICAM-1 Release by Endothelial Cells

A possible explanation for the inhibitory effect observed is that sICAM-1 could be captured by anti-ICAM NCs. Binding of sICAM-1 to anti-ICAM NCs would outcompete NC binding to cells and these sICAM-1-bound NCs would remain in the cell medium. Subsequently, they would be removed by centrifugation prior to the ELISA measurement used to detect sICAM-1. To test this, we washed endothelial cells after the initial 30 min incubation with anti-ICAM NCs to remove the NCs that did not bind to cells (and may contain sICAM-1), and continued the incubation in NC-free medium for another 30 min (1 h data shown in **Figures 41B-C** and **Figure 42**). Despite the absence of anti-ICAM NCs in the milieu, the same reduction in sICAM-1 was observed in the total, apical, or basolateral chambers (compare the first 30 min to the second 30 min (1 h) in **Figure 42** or respective slopes in **Figures 41B-C**). For instance, 73% and 55% reductions were seen in the apical and basolateral sides in the presence of anti-ICAM NCs in the milieu (first 30 min), and 75% and 57% reductions were observed if removed from the milieu (second 30 min (1 h)). Since the number of NCs interacting with cells at 30 min is the same as at 1 h (no more binding was possible since NCs had been removed from the milieu), this indicates that reduction of sICAM-1 is not caused by anti-ICAM NCs in the milieu, but by NCs interacting with cells.

Supporting this, it has been shown that when anti-ICAM NCs bind to cell-membrane ICAM-1, this receptor-NC complex is internalized, which reduces the level of ICAM-1 displayed at the membrane [80] (**Figure 44A** also validates this previous finding). Co-uptake of membrane ICAM-1 with NCs could then, in turn, diminish the amount of

ICAM-1 available for shedding from the plasmalemma. To test this alternative, we examined the effect of anti-ICAM NCs on sICAM-1 release in the presence of amiloride (**Figures 44B-C**), an inhibitor of the CAM pathway [68, 78]. It was expected that inhibiting NC uptake would also inhibit uptake of membrane ICAM-1 and, hence, the inhibitory effect of NCs on sICAM-1 release would be lost. **Figure 44B** shows that this is the case: at 30 min when active uptake of anti-ICAM NCs occurred (see **Figure 39A**), amiloride enhanced apical sICAM-1 by 2.5-fold compared to cells incubated with anti-ICAM NCs in the absence of this inhibitor, while no effect of amiloride was found at 5 h (0.88-fold) when both active sICAM-1 release and NC endocytosis had saturated and these processes were no longer active. Instead, no increase was observed at the basolateral side at either time point (0.73-fold and 0.95-fold, respectively; **Figure 44C**). In addition, negligible amounts of sICAM-1 were found in the cell lysates after 30 min incubation with anti-ICAM NCs, implying that reduced sICAM-1 release by NCs is not due to uptake of the cleaved receptor (0.003 ± 0.001 ng/well internalized sICAM-1 versus 1.5 ± 0.3 ng/well sICAM-1 released into the cell medium). Therefore, attenuation of sICAM-1 release in the presence of anti-ICAM NCs is due to removal of surface ICAM-1 during uptake of the carrier-receptor complex.

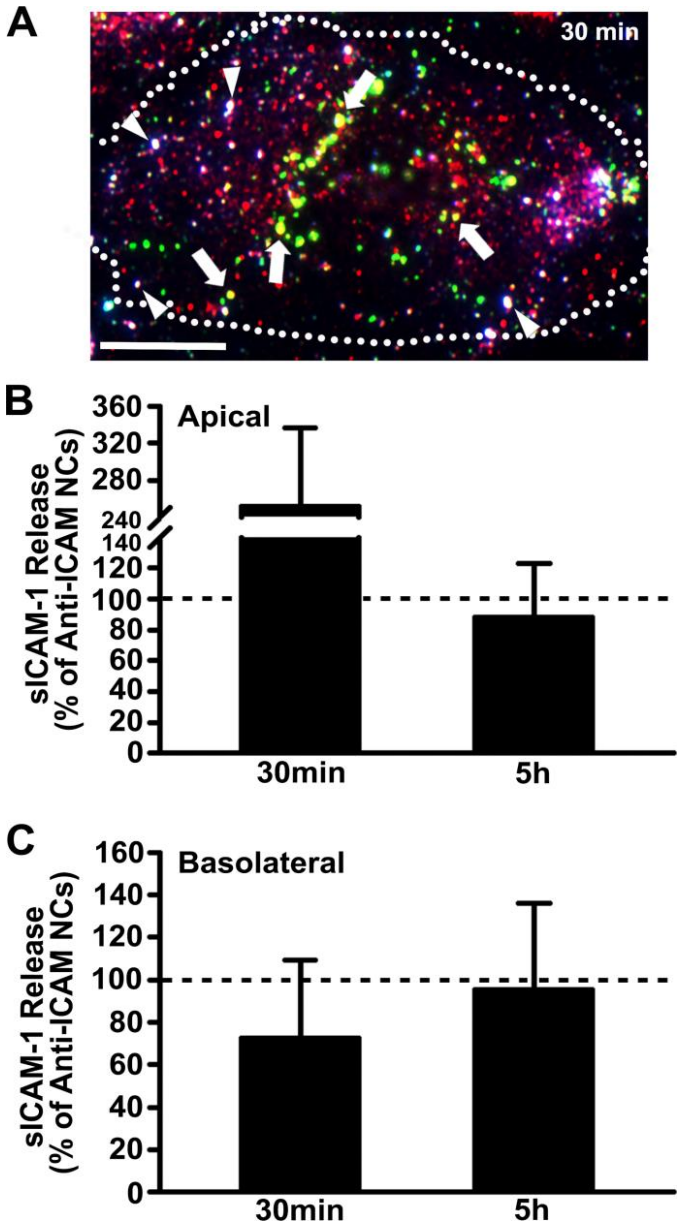

Figure 44. Inhibition of anti-ICAM NC uptake attenuates sICAM-1 release. (A) Image of TNFα-activated HUVECs grown on coverslips and incubated for 30 min at 37°C with green fluorescent anti-ICAM NCs. Non-bound NCs were removed by washing, and then the cells were fixed and immunostained (see **Section 5.2.7**) to render surface-bound NCs triple labeled in green + blue + red (white color; arrowheads). Instead, internalized membrane ICAM-1 complexed with NCs double labeled in green + red (yellow color; arrows) and internalized NCs without membrane ICAM-1 are labeled in green alone. Scale bar = 10 μm. (B) Apical and (C) basolateral release of sICAM-1 by TNFα-activated HUVECs grown on transwell inserts and incubated with anti-ICAM NCs in the presence of amiloride, an inhibitor of CAM endocytosis. Incubations were for 30 min (pulse), followed by anti-ICAM NC removal and incubation for additional time up to 5 h total. Data are expressed relative to the absence of amiloride (control; indicated by the horizontal dashed lines). Data are the mean ± SEM. Figure reproduced from [291].

5.4. Discussion

Targeting of imaging agents and drug NCs to endothelial ICAM-1 holds promise in the context of diagnostic and therapeutic interventions focused at the vascular endothelium [61, 230-235]. Binding of drug NCs to ICAM-1 on the endothelial surface induces signaling conducive to NC transport into and across this lining [68, 71, 78]. Although numerous cell culture and *in vivo* studies suggest that no acute toxicity associates with this strategy [61, 230-235], potential side effects must be carefully examined for further translational development. This work investigated the influence of ICAM-1 targeting on endothelial release of sICAM-1, a marker of inflammation that associates with a variety of maladies [76], revealing an unexpected benefit of anti-ICAM NCs.

During inflammation, which underlies most pathologies, including type A NPD and other LSDs, ICAM-1 becomes overexpressed on the surface of activated endothelial cells and, concomitantly, sICAM-1 levels increase in serum [76, 315]. TNFα and other pro-inflammatory factors (IL-1β, IL-6, IFN-γ, angiotensin II, etc.) induce such an outcome [76, 316, 320]. The mechanism for sICAM-1 release is not fully characterized, yet the soluble form of this molecule can arise from proteolytic cleavage of the ectodomain of cell-surface ICAM-1 [288, 316, 320]. We reproduced this by treating endothelial cells with TNFα, using both a solid-surface model and a transwell filter model. While the first model is commonly described [312-314, 320], sICAM-1 release on polarized linings has been predominantly reported for epithelial cells, not endothelial cells [321, 322]. From our study, it appears that activated endothelial cells separating apical and basolateral compartments released slightly greater levels of sICAM-1 than those not polarized (**Figure 36**), where basolateral levels surpassed apical ones. While we could not find direct

comparisons on both models in the literature, work showing independent experiments using solid-surface and transwells seems to support our finding [323]. Also, preferential basolateral secretion is supported by previous studies [324]. The fact that, *in vivo*, sICAM-1 has been found not only in serum but it has also been implicated in angiogenesis, migration of vascular smooth muscle cells, and other events involving the basolateral space [75], indicates that its differential distribution reflects a functional purpose. Hence, both apical and basolateral release events must be considered.

In accord with the results found in **Chapter 4**, MMP-9 was involved in endothelial release of sICAM-1 upon inflammatory stimulation (**Figure 38**), which is also in agreement with the literature [288]. It has been shown that ICAM-1 provides cell-surface docking for pro-MMP-9, the latent form of MMP-9 [288], and then the active enzyme can cleave ICAM-1 at its membrane-proximal domain [288]. Yet, our results also suggest that the contribution of MMP-9 to this event was partial and there must be other factors involved. Inhibition of MMP-2 seemed to influence sICAM-1 release and this could be an additional mechanism. However, simultaneous inhibition of MMP-9 and MMP-2 did not render an enhanced effect, ruling out this option, in accord with the fact that ICAM-1 is not known to be an MMP-2 substrate. Yet, MMP-2 may indirectly play a role in this process since it can cleave pro-MMP-9 into MMP-9 [293, 294]. This would explain why MMP-2 inhibition resulted in a reduction of sICAM-1 release similar to MMP-9 inhibition, but no additive effects were found when inhibiting both (**Figure 38**). Hence, additional factors must contribute to sICAM-1 release in our assays. Other studies have shown mRNA transcripts specifically encoding sICAM-1 [325, 326], but our assays involve pulse-chase experiments to examine release within 30 min, and *de novo* protein synthesis is unlikely to

play a major role. Other molecules that may be involved in this process include TNFα-converting enzyme (TACE/ADAM-17) and neutrophil elastase, as seen previously [288, 312-314].

While inhibiting MMPs was expected to decrease sICAM-1 release, the inhibitory effect of anti-ICAM NCs on this event (**Figures 41** and **42**) was unexpected, based on the fact that ICAM-1 binding by its natural ligands, leukocytes, elicits (instead of reduces) sICAM-1 release. This may help dynamic detachment of leukocyte-endothelial engagement in areas where the leukocyte "samples" the endothelial surface prior to extravasation [73, 287-290, 292]. It may also play a role in loosening leukocyte-endothelial attachment after extravasation and to subsequently downregulate cell-surface ICAM-1 [73, 287-290, 292]. Because the signaling cascades induced in endothelial cells by NC binding to ICAM-1 are reminiscent of those induced by leukocytes [73], an increase in sICAM-1 release was expected. However, the reduction observed can be understood based on the fact that anti-ICAM NCs are rapidly internalized by endothelial cells and, since they bind to ICAM-1, their internalization removes ICAM-1 from the plasmalemma, as we have previously shown [80]. In fact, we have observed that most cell-surface ICAM-1 is internalized during this event (as verified in **Figure 44A**) and then, once within cells, NCs traffic to lysosomes or are transcytosed, whereas a fraction of internalized ICAM-1 recycles back to the plasmalemma after 1 h [70, 71, 80]. Hence, by reducing the availability of membrane ICAM-1 on the cell-surface, anti-ICAM NCs reduced sICAM-1 release. This was demonstrated by the fact that inhibiting NC uptake with amiloride counteracted the inhibitory effects on sICAM-1 release (**Figures 44B-C**) and that only negligible amounts of sICAM-1 were found in cell lysates. In previous publications, we have shown that

amiloride decreased endocytosis of anti-ICAM NCs without affecting their binding [68, 78]; hence, validating this mechanism. In addition, the time and location of this inhibitory effect (predominant on the apical side at 30 min; **Figure 41**) pairs well with a role for anti-ICAM NC endocytosis in lowering surface ICAM-1 and sICAM-1 release.

5.5. Conclusions

Given that elevated sICAM-1 is considered a pathological marker implicated in the development of numerous pathologies (inflammation, atherosclerosis, cancers, neurological disorders, autoimmune diseases, LSDs, etc.) [75, 76, 315], attenuation of its release may benefit these conditions. Interestingly, inhibition of sICAM-1 release by anti-ICAM NCs surpassed that of MMP inhibitors in the apical and basolateral compartments (**Figure 43**), which suggests translational relevance. As said, multiple factors appear to contribute to sICAM-1 release from activated endothelial cells and their individual inhibition only partially reduces this event. Using a cocktail of inhibitors to improve their outcome requires knowing all factors involved in each pathological situation (currently unknown), and would pose serious risk as they regulate multiple processes apart from ICAM-1 cleavage. Instead, reducing sICAM-1 release may be a bonus of targeting ICAM-1 for drug delivery applications, whereby NCs may combine the action of their therapeutic cargo with this secondary effect. Anti-ICAM NCs reduce sICAM-1 by decreasing cell-surface ICAM-1 during endocytosis (**Figure 45**), regardless of the factors involved in ICAM-1 cleavage and without inhibiting their activity in other necessary functions. Therefore, this potentially beneficial effect deserves further attention.

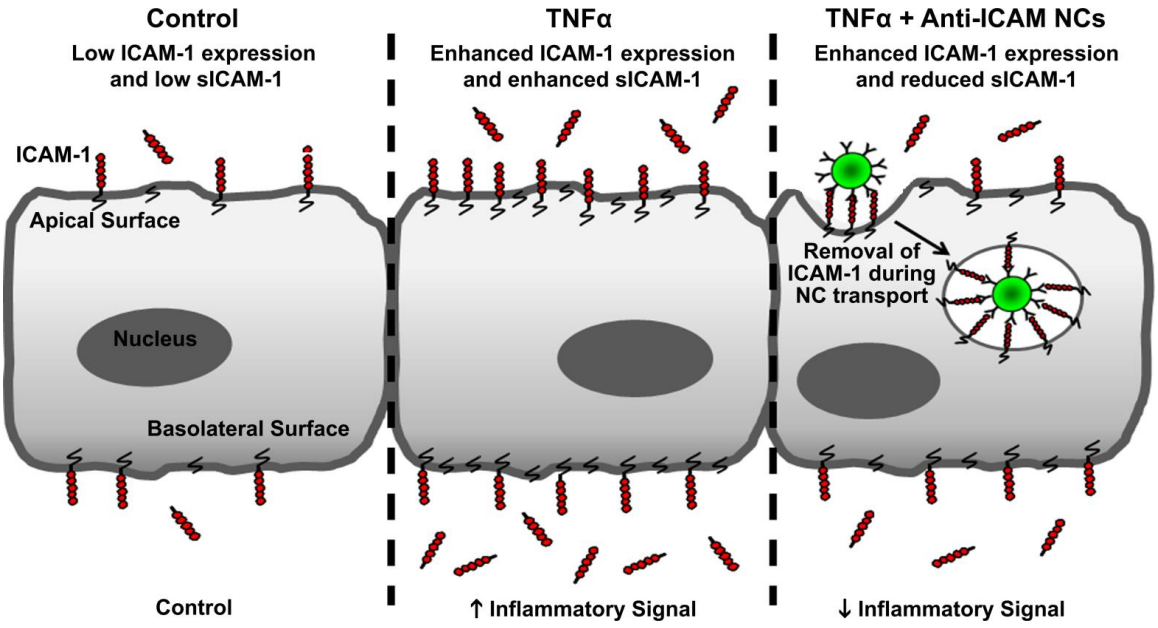

Figure 45. Endothelial release of sICAM-1 in the absence and presence of anti-ICAM NCs. During inflammation (*e.g.*, TNFα activation), endothelial cells overexpress ICAM-1 and undergo enhanced shedding of its "soluble" ectodomain (sICAM-1), which acts as an inflammatory regulator. Anti-ICAM NCs significantly reduce sICAM-1 release by mobilizing ICAM-1 from the cell-surface into intracellular vesicles during NC transport into the endothelium. Since elevated levels of sICAM-1 associate with numerous diseases, this effect may provide a secondary benefit of using ICAM-1-targeted carriers for drug delivery. Figure reproduced from [291].

Chapter 6: Final Remarks and Future Directions[5]

In summary, this dissertation examined (1) the status of vesicular-mediated transport in type A NPD, which indicates the CAM pathway is an advantageous route for therapeutic enzyme delivery; (2) the influence of targeting valency on regulation of the CAM pathway, thereby enabling us to optimize therapeutic enzyme delivery to the brain; and (3) the effect of ICAM-1 engagement by anti-ICAM NCs on reducing endothelial release of sICAM-1, which indicates a secondary anti-inflammatory effect of this approach.

With regard to the status of vesicular-mediated transport in type A NPD, we observed impaired caveolae-mediated endocytosis and EGF-induced macropinocytosis similar to that found previously for clathrin-mediated endocytosis [57]. Further, bulk fluid-phase uptake was altered, as well as fluid-phase uptake via the clathrin and caveolar pathways. In agreement, intracellular trafficking of ligands associated with these pathways was also distorted. However, anti-ICAM NC uptake via the CAM pathway was minimally impacted in diseased cells. Interestingly, transcytosis of model ligands for the clathrin, caveolar, and CAM pathways was relatively unaffected in the disease scenario. Ultimately though, the CAM pathway seems the most viable alternative to classical endocytic routes for lysosomal enzyme delivery given that it allows specific targeting, enhanced loading of an enzyme cargo, and is the least impaired pathway in regard to uptake and transcytosis.

[5]Chapter 6 contains text reproduced in part with permission from: (1) Rappaport, J., Manthe, R.L., et al., *Altered clathrin-independent endocytosis in type A Niemann-Pick disease cells and rescue by ICAM-1-targeted enzyme delivery.* Mol Pharm, 2015. 12(5): p. 1366-76; © 2015 American Chemical Society. (2) Manthe, R.L.* and Rappaport, J.*, et al., *A comparative study on the alterations of endocytic pathways in multiple lysosomal storage disorders.* Mol Pharm, 2016. 13(2): p. 357-68; © 2015 American Chemical Society. (3) Manthe, R.L.* and Serrano, D.*, et al. *How carrier size and valency modulate receptor-mediated signaling: understanding the link between binding and endocytosis of ICAM-1-targeted carriers.* Biomacromolecules, 2016. 17(10): p. 3127-37; © 2016 American Chemical Society. (4) Manthe, R.L. and Muro, S. *ICAM-1-targeted nanocarriers attenuate endothelial release of soluble ICAM-1, an inflammatory regulator.* Bioeng Transl Med, 2017. 2(1): p. 109-19; © 2017 Rachel L. Manthe and Silvia Muro.

As well, this strategy has been demonstrated to provide delivery to lysosomes, resulting in enhanced enzyme accumulation and substrate reduction [57, 60-64, 69, 252, 257].

While we examined alterations in endocytic behavior in type A NPD, this work and others [21, 115, 117-120, 252, 257] indicate endocytic function occurs rather widely in LSDs. In particular, endocytic pathways may be affected differently in LSDs that are characterized by different genetic defects and primary storage materials [257]. As such, advancing treatment of each LSD will require thorough characterization of their endocytic activity for more informed selection of appropriate therapeutic approaches. This applies to enzyme replacement, including administration of recombinant enzymes and viral vectors [16, 21, 57] that rely on receptor-mediated uptake to gain entry into cells, as well as other agents that may rely on pinocytic uptake.

Moreover, this work highlighted the implications of lysosomal storage and endocytic/trafficking dysfunction, as lysosomal dysfunction arising from drugs and materials employed in drug delivery may render a similar phenotype. For example, non-degradable drug carrier materials, such as quantum dots, gold, titanium dioxide, and others, have been shown to accumulate and impact lysosomal/autophagic compartments [327-331]. Intracellular delivery of lipids or slow-degrading polymers used in liposomes and other carrier formulations could also render side effects consistent with lysosomal storage [328, 332]. As an alternative, combining such therapies with strategies to decrease lysosomal storage or restore endocytic trafficking by other means may be beneficial. For example, induction of lysosomal exocytosis via treatment with the minor vitamin E species, δ-tocopherol, has shown to be a promising strategy to alleviate storage of undigested metabolites in LSDs [148, 149]. In addition to the work presented herein, I contributed to

a study in our laboratory examining the effect of δ-tocopherol on vesicles internalized via different endocytic pathways [333]. We found that induction of lysosomal exocytosis to remove substrate storage temporarily impairs several endocytic routes, resulting in reduced uptake of therapeutic ASM, which is an important finding in regard to utility of this approach in combination therapies for LSD treatment [333]. Ultimately, awareness of lysosome function in regulating vesicular-mediated transport will improve therapeutic efficacy and diminish the toxicity of future drug carriers, including not only those aimed at treating LSDs, but also other diseases requiring endocytic entry within and across cells.

The second part of this dissertation significantly enhanced our understanding of the effects of targeting valency on regulation of the CAM pathway. In regard to ICAM-1 targeting, valency density appears to be the main parameter controlling the cell-associated signaling conducive to CAM-mediated endocytosis [79]. In future work, it will be important to examine this regulation for other receptors and their associated pathways in order to extract more general conclusions. However, other routes associated with signaling common to the CAM pathway, including ceramide and PKC enrichment, are key to multiple events for phagocytic and macropinocytic pathways, intracellular invasion of pathogens, leukocyte adhesion and extravasation, and certain events of transcytosis [265, 334-338]. Therefore, the findings presented herein [79] may broadly apply to the use of other routes for drug delivery.

In regard to NC transcytosis, there was an inverse linear relationship with valency, but since this process depends on the preceding events of binding and uptake, an intermediate valency was found to be most efficient. In contrast, there was an inverted trend in lysosomal colocalization since NCs that do not efficiently detach from the

basolateral endothelium after transcytosis are trafficked to lysosomes. In addition to lysosomal transport from the basolateral cell-surface after transcytosis (scenario C in **Figure 25**), NC transport to lysosomes from the apical surface independent of transcytosis is also possible (scenario A in **Figure 25**). However, since the bell-shaped curves for lysosomal trafficking and transcytosis are inverted suggests scenario C contributes more to the observed differences in these processes for anti-ICAM NCs with different valencies. Nevertheless, since these two processes seem to influence NC trafficking to lysosomes, this may also explain why lysosomal transport is slightly faster than transcytosis. Further, since NC transport to lysosomes and transcytosis are independent processes, we deduced they may be independently influenced by valency as well. However, this should be verified experimentally in future work. Further, independent lysosomal and transcellular transport could explain why minimal differences were found in **Chapter 3** for examination of altered transcytosis via the clathrin, caveolar, and CAM pathways in diseased cells. Therefore, defects associated with the endo-lysosomal route that impair ligand uptake may not significantly influence the transcytosis pathway.

In addition to elucidating the role of targeting valency on carrier binding, cell-signaling conducive to endocytic uptake, as well as lysosomal trafficking and transcytosis, this work described for the first time a mechanism for detachment of targeted carriers from their bound receptor following transendothelial transport. Specifically, proteolytic cleavage of MMP-9 was found to influence the release of sICAM-1, which correlated well with modulation of anti-ICAM NC transcytosis by MMP-9 inhibition or addition of active MMP-9 to the cell culture medium. While we did not provide direct evidence that valency influences detachment of NCs from the basolateral endothelium, other data demonstrating

the effects of high valency on anti-ICAM NC transcytosis and brain delivery support this claim. However, for additional validation, transcytosis of anti-ICAM NCs with different valencies in the presence of MMP inhibitors or recombinant MMPs could be tested. Further, in contrast to using pharmacological inhibitors, siRNA for gene silencing of MMP-9 or MMP-2 may be a better method to clarify the role of these molecules in this process. As further validation, anti-ICAM NC biodistribution could be examined in MMP-9 or MMP-2 knockout mice. Additionally, it is worth testing other proteases that may be involved in ICAM-1 cleavage, such as TACE/ADAM-17 [314], in order to expose all potential players involved in detachment of anti-ICAM NCs following transcytosis.

Since MMP-9 and MMP-2 are also involved in degrading the extracellular matrix (ECM) of the vascular wall [339], these molecules may also permit NC penetration for access to subjacent tissues. While anti-ICAM NCs have been observed to accumulate in tissues such as the lungs and brain (*unpublished data; Muro Laboratory*), how these and other drug carriers traverse the ECM is not understood, representing an important and novel question. Therefore, further exploration of ECM penetration by anti-ICAM NCs may enable the design of drug carriers capable of greater tissue accumulation.

Apart from valency, a number of other parameters can influence the efficacy of therapeutic carriers and warrant investigation [47, 59, 62, 78, 79, 176, 259]. For example, work by our laboratory has found increasing anti-ICAM carrier size enhances transcytosis and reduces lysosomal trafficking [62, 305]. Therefore, effects of modulating both carrier size and valency should be elucidated in order to design carriers that are more amenable for specific disorders, such as those requiring enhanced accumulation in the vascular endothelium (for inflammation, arthrosclerosis, thrombosis, anti-oxidant protection, etc.)

[229] versus therapeutic delivery across biological barriers (for LSDs and other neurological disorders). Importantly, studies to assess phenotypic changes in type A NPD or other LSDs (*e.g.*, motor skills, cognition, survival, etc.) in animal models following enzyme therapy via anti-ICAM NCs is necessary to further prove utility of this strategy. These findings could also be further validated by examination of lysosomal storage and other morphological features in tissues and organs primarily affected.

To further improve anti-ICAM carriers for clinical use, targeting moieties that are smaller and/or are derived from human components, such as antibody fragments, peptides (γ3 derived from fibrinogen), etc. could be used to reduce immune recognition and associated toxicity that limits utilization of whole antibodies [305, 340]. Along similar lines, anti-ICAM NCs coupled with CD47, a self-recognition marker that signals "don't eat me" to phagocytic cells, could improve enzyme delivery by diminishing immune recognition and clearance ([47] and *unpublished data; Muro Laboratory*). Overall, additional cell culture and *in vivo* work is necessary to determine the extent of immunogenicity and toxicity associated with different anti-ICAM carrier formulations.

For the purposes of this work, we assessed CAM-mediated transport using non-degradable polystyrene NCs to avoid confounding effects of carrier degradation. Yet, for clinical use, carriers should be composed of biodegradable materials based on the potential for undesirable lysosomal accumulation as described above. Apart from being biodegradable and FDA-approved, PLGA is an ideal material for LSD treatment since its degradation enhances the acidic environment in lysosomes [341, 342] and, consequently, aids in proper lysosomal enzyme activity and restoration of lysosomal acidification found to be impacted in some LSDs [90, 91, 341, 342]. Furthermore, lysosomal enzymes could

be encapsulated in porous or hollow PLGA carriers, providing the opportunity to control the rate of enzyme release, and further reduce the potential immunogenicity associated with these recombinant enzymes [25, 38-40].

Additionally, since ICAM-1 binding by natural ligands (leukocyte integrins) results in release of sICAM-1, an inflammatory regulator, we investigated the influence of anti-ICAM NCs on this process in the third aim. In the absence of NCs, endothelial cells released sICAM-1 when treated with the pro-inflammatory cytokine, TNFα. This was reduced by inhibiting MMP-9 or MMP-2, yet inhibiting both did not render additive effects. Overall, additional molecules involved in this process need to be investigated. Interestingly, anti-ICAM NCs reduced sICAM-1 to a greater extent than MMP inhibition, both at the apical and basolateral sides. This effect was enhanced with time, although NCs had been removed after binding to cells, ruling out a "trapping" effect of NCs. Instead, inhibiting anti-ICAM NC endocytosis counteracted their inhibition on sICAM-1 release. Hence, anti-ICAM NCs inhibited sICAM-1 release by mobilizing ICAM-1 from the cell-surface into intracellular vesicles. Therefore, it would worth testing whether valency of anti-ICAM NCs could be used to control the extent of sICAM-1 release. Nevertheless, since elevated sICAM-1 levels associate with numerous diseases, this effect represents a secondary benefit of using ICAM-1-targeted NCs for drug delivery. As such, this potentially beneficial effect deserves further attention and careful examination in animal models of disease such as LSDs.

Lastly, peripheral or brain endothelial cell monolayers grown in transwell inserts represent a simple, yet valuable model to evaluate transcytosis as it permits separation of the apical and basolateral compartments consistent with the natural status of endothelial

cells. Since the degree of barrier restriction is higher *in vivo*, we used the pulse-chase technique in our experiments to mitigate any potential leakage. As observed in **Chapter 5**, even sICAM-1 (< 110 kDa) did not freely diffuse across these cell monolayers. As such, this method provides good evaluation of transcytosis for only cell-bound cargos and NCs. Further, our *in vivo* findings in **Chapter 4** were consistent with those obtained in our cell culture model of the BBB and, hence, we trust the results obtained in this work. However, *in vivo*, the barrier function of the BBB encompasses additional features [343, 344], and future work may focus on incorporating these features in order to best mimic the physiological situation. For example, recently developed dynamic, three-dimensional and microfluidic-based BBB models allow inclusion of subendothelial cell types, such as astrocytes and pericytes that influence the formation, integrity, and function of the endothelial barrier, and these systems also permit evaluation of the effects of flow/shear stress [343-346]. As well, the polarization status of the cells in these models warrants investigation since this may influence the localization, distribution, and/or function of cellular components (*e.g.*, tight junction proteins, receptors, lipid raft domains, PKC and other signaling molecules, transporters, enzymes, etc.) [344, 346, 347] that regulate transcytosis and other events, such as the release of sICAM-1.

Overall, this dissertation has rendered significant knowledge pertaining to the utility and optimization of anti-ICAM NCs for therapeutic delivery. Specifically, this research will guide translational enzyme replacement strategies for treatment of type A NPD and other LSDs, as well as many other disorders that require similar delivery. While these carriers and application are relevant, the work shown herein can be taken as an illustration of the importance of studying the parameters of any receptor-targeted carriers

for therapeutic applications. In the field of drug delivery, chemical and physical parameters of therapeutic carriers are somewhat understood, but very limited work has examined biological crosstalk between carriers and cells/tissues. In this work, we demonstrated that modulating just one parameter (valency) markedly influences cellular interaction and transport of NCs, resulting in significant differences in therapeutic delivery. While improving binding and uptake with higher valency, the ability to cross the BBB is diminished. In contrast, although lowering valency correlates with more effective transcytosis *per se*, this process depends on binding/uptake and, consequently, too much of a reduction in valency can decrease the chance to traverse this barrier. Therefore, a balance must be achieved for optimal effects and will likely differ for each receptor-targeted drug carrier given differences in expression and distribution of the targeted receptor, associated cell-signaling, mechanism(s) of transport, and mechanism(s) of carrier detachment. Therefore, this work is highly relevant for identifying parameters regulating carrier-cell communication and highlights the importance of empirically tuning these parameters for optimal efficacy. Ultimately, studies pertaining to these aspects will help advance the field of drug delivery by aiding rationale design of more effective drug carriers.

Appendix

Publications

The text and data presented in this dissertation are from the following publications (* authors contributed equally):

Manthe, R.L. and Muro, S. *Role of valency on intra- and transcellular transport of ICAM-1-targeted nanocarriers in the brain endothelium.* (Awaiting submission).

Manthe, R.L. and Muro, S. *ICAM-1-targeted nanocarriers attenuate endothelial release of soluble ICAM-1, an inflammatory regulator.* Bioengineering and Translational Medicine, 2017. 2(1): p. 109-19.

Manthe, R.L.*, Serrano, D.*, Paul, E., Chadha, R., and Muro, S. *How carrier size and valency modulate receptor-mediated signaling: understanding the link between binding and endocytosis of ICAM-1-targeted carriers.* Biomacromolecules, 2016. 17(10): p. 3127-37.

Manthe, R.L.*, Rappaport, J.*, Solomon, M., Garnacho, C., and Muro, S. *A comparative study on the alterations of endocytic pathways in multiple lysosomal storage disorders.* Molecular Pharmaceutics, 2016. 13(2): p 357-68.

Rappaport, J., Manthe, R.L., Garnacho, C., and Muro, S. *Altered clathrin-independent endocytosis in type A Niemann-Pick disease cells and rescue by ICAM-1-targeted enzyme delivery.* Molecular Pharmaceutics, 2015. 12(5): p. 1366-76.

Manthe, R.L. and Muro, S. *Lysosomes and nanotherapeutics: diseases, treatments, and side effects.*, in *Handbook of Nanobiomedical Research*, V. Torchilin, Editor. 2014, World Scientific Publishing Co.: Singapore. Vol. 2, Chapter 8: p. 261-305.

Additional publications not contained within this dissertation:

Manthe, R.L.*, Rappaport, J.*, Long, Y., Marugan, J., Zheng, W., Muro, S. *Therapeutic exocytosis via δ-tocopherol diminishes classical endocytic pathways in a Niemann-Pick disease model: a role for non-classical ICAM-1-mediated transport.* (Awaiting submission).

International and National Conference Abstracts and Proceedings

Indicates presenting author(s)

R.L. Manthe* and S. Muro. (September 2016). Attenuation of soluble ICAM-1 release by ICAM-1-targeted nanocarriers used for drug delivery. *4th International Nanomedicine & Drug Delivery Symposium (NanoDDS)*, Johns Hopkins University, Baltimore, MD. Poster Presentation.

M.A. Solomon*, R. Moscoso, R. Bautista, R.L. Manthe, and S. Muro. (September 2016). Altered status of transcytosis pathways in lysosomal storage diseases: implications for targeted enzyme replacement therapy. *4th International Nanomedicine & Drug Delivery Symposium (NanoDDS)*, Johns Hopkins University, Baltimore, MD. Poster Presentation.

R.L. Manthe*, E.H. Schuchman, and S. Muro. (March 2016). Enhanced lysosomal enzyme delivery across the blood-brain barrier by modulating the valency of ICAM-1-targeted nanocarriers. *12th Annual WORLD Symposium*, San Diego, CA. Poster and Oral Presentation.

R.L. Manthe*, J. Hsu, and S. Muro. (October 2015). Role of valency on transcytosis of ICAM-1-targeted nanocarriers into the brain. *5th Annual Meeting of the American Society for Nanomedicine*, Arlington, VA. Poster and Oral Presentation.

J. Rappaport, R.L. Manthe*****, C. Garnacho, and S. Muro. (May 2015). Comparative study reveals alterations in several endocytosis routes in various lysosomal storage disorders. *17th Barrier and Transporter Meeting*, Bad Herrenalb, Germany. Poster Presentation.

R.L. Manthe* and S. Muro. (July 2014). Mechanism of nanocarrier release from the abluminal endothelium. *Controlled Release Society Annual Meeting 2014*, Chicago, IL. Oral Presentation.

I. Villanueva*, R.L. Manthe, and K. Knapstein. (June 2013). Development of a design- and project-based framework to include scientific reasoning in an undergraduate, introductory-level bioengineering laboratory course. *120th ASEE Annual Conference and Exposition*, Atlanta, GA. Oral Presentation and Conference Proceeding.

Local Symposium Abstracts and Proceedings

Indicates presenting author(s)

R.L. Manthe*, J. Rappaport, Y. Long, J. Marugan, W. Zheng, and S. Muro. (June 2016) Therapeutic exocytosis by δ-tocopherol diminishes uptake of therapeutic enzymes: optimizing combination therapy for lysosomal storage disorders. *ResearchFest 2016*, University of Maryland, College Park, MD. Poster Presentation.

R.L. Manthe*, J. Hsu, and S. Muro. (November 2015). Role of valency on transcytosis of ICAM-1-targeted nanocarriers into the brain. *Bioscience Day 2015*, University of Maryland, College Park, MD. Poster Presentation.

J. Rappaport, R.L. Manthe*, C. Garnacho, and S. Muro. (June 2015). Comparative study reveals alterations in several endocytosis routes in various lysosomal storage disorders. *ResearchFest 2015*, University of Maryland, College Park, MD. Poster Presentation.

R.L. Manthe* and S. Muro. (November 2014). Mechanism enabling necessary detachment of ICAM-1-targeted nanocarriers from endothelial barriers after transcytosis. *Bioscience Day 2014*, University of Maryland, College Park, MD. Poster Presentation.

R.L. Manthe* and S. Muro. (April 2014). Mechanism of abluminal release of receptor-bound nanocarriers after transcytosis. *GRID-Graduate Research Interaction Day*, University of Maryland, College Park, MD. Oral Presentation.

R.L. Manthe* and S. Muro. (February 2014). Investigating the role of matrix metalloproteinases in mediating ICAM-1-targeted nanocarrier transport through endothelial barriers. *Bioengineering Graduate Student Society-RAP Session*, Fischell Department of Bioengineering, University of Maryland, College Park, MD. Oral Presentation.

R.L. Manthe* and S. Muro. ICAM-1-targeted nanocarriers attenuate the release of inflammatory mediators. Presented at *ResearchFest 2013*, University of Maryland, College Park, MD (July 2013); *Maryland Nanomedicine Day 2013*, University of Maryland School of Pharmacy, Baltimore, MD (July 2013); *Bioscience Day 2013*, University of Maryland, College Park, MD (November 2013). Poster Presentation.

I. Villanueva*, K. Knapstein*, and R.L. Manthe*. (April 2013). Use of problem-based learning and electronic journals to assist undergraduate freshmen and sophomore bioengineering students navigate through the scientific method. *Innovations in Teaching and Learning Conference*, University of Maryland, College Park, MD. Poster Presentation.

Fellowships and Awards

Third Place, Best Poster ($500 Award) October 2015
5th Annual Meeting of the American Society for Nanomedicine

NIH Ruth L. Kirschstein NRSA Individual Pre-Doctoral Fellowship July 2015 - 2017
National Institutes of Health: National Heart, Lung, and Blood Institute

Third Place, Best Poster-Bioengineering Category November 2014
Bioscience Day, University of Maryland, College Park

First Place, Best Presentation-Science of the Cell Category ($500 Award) April 2014
Graduate Student Interaction Day (GRID), University of Maryland, College Park

Honorable Mention March 2014
Ford Foundation Pre-Doctoral Fellowship Program

Future Faculty Program ($3,000 Travel Award) January 2014 - May 2015
James A. Clark College of Engineering, University of Maryland, College Park

Best Paper Award-Biomedical Education Division June 2013
American Society for Engineering Education Annual Conference

Distinguished Graduate Teaching Assistant 2012 - 2013
Center for Teaching Excellence, University of Maryland, College Park

Flagship Research Fellowship September 2011 - 2015
Graduate School of the University of Maryland, College Park

National Science Foundation Graduate Research Fellowship September 2011 - 2014

References

1. Futerman, A.H. and G. van Meer, *The cell biology of lysosomal storage disorders.* Nat Rev Mol Cell Biol, 2004. 5(7): p. 554-65.
2. Ballabio, A., *Disease pathogenesis explained by basic science: lysosomal storage diseases as autophagocytic disorders.* Int J Clin Pharmacol Ther, 2009. 47 Suppl 1: p. S34-8.
3. Lieberman, A.P., et al., *Autophagy in lysosomal storage disorders.* Autophagy, 2012. 8(5): p. 719-30.
4. Platt, F.M., B. Boland, and A.C. van der Spoel, *The cell biology of disease: lysosomal storage disorders: the cellular impact of lysosomal dysfunction.* J Cell Biol, 2012. 199(5): p. 723-34.
5. Andrews, N.W., *Regulated secretion of conventional lysosomes.* Trends Cell Biol, 2000. 10(8): p. 316-21.
6. Luzio, J.P., P.R. Pryor, and N.A. Bright, *Lysosomes: fusion and function.* Nat Rev Mol Cell Biol, 2007. 8(8): p. 622-32.
7. McNeil, P.L. and T. Kirchhausen, *An emergency response team for membrane repair.* Nat Rev Mol Cell Biol, 2005. 6(6): p. 499-505.
8. Sabatini, D. and M.B. Adesnik, *The biogenesis of membranes and organelles.*, in *The Metabolic and Molecular Bases of Inherited Disease*, C. Scriver, et al., Editors. 2001, McGraw-Hill: New York City, NY. p. 433-520.
9. Muro, S., *Strategies for delivery of therapeutics into the central nervous system for treatment of lysosomal storage disorders.* Drug Deliv Transl Res, 2012. 2(3): p. 169-86.
10. Ballabio, A. and V. Gieselmann, *Lysosomal disorders: from storage to cellular damage.* Biochim Biophys Acta, 2009. 1793(4): p. 684-96.
11. Desnick, R.J. and E.H. Schuchman, *Enzyme replacement and enhancement therapies: lessons from lysosomal disorders.* Nat Rev Genet, 2002. 3(12): p. 954-66.
12. Schultz, M.L., et al., *Clarifying lysosomal storage diseases.* Trends Neurosci, 2011. 34(8): p. 401-10.
13. Begley, D.J., C.C. Pontikis, and M. Scarpa, *Lysosomal storage diseases and the blood-brain barrier.* Curr Pharm Des, 2008. 14(16): p. 1566-80.
14. Hsu, J. and S. Muro, *Nanomedicine and drug delivery strategies for treatment of genetic diseases.*, in *Human Genetic Diseases*, D. Plaseska-Karafilska, Editor. 2011, InTech.: Rijeka, Croatia. p. 241-66.
15. Jeyakumar, M., et al., *Storage solutions: treating lysosomal disorders of the brain.* Nat Rev Neurosci, 2005. 6(9): p. 713-25.
16. Muro, S., *New biotechnological and nanomedicine strategies for treatment of lysosomal storage disorders.* Wiley Interdiscip Rev Nanomed Nanobiotechnol, 2010. 2(2): p. 189-204.

17. Parenti, G., et al., *New strategies for the treatment of lysosomal storage diseases (review).* Int J Mol Med, 2013. 31(1): p. 11-20.

18. Ratko, T.A., et al., in *Enzyme-Replacement Therapies for Lysosomal Storage Diseases*. Rockville (MD): Agency for Healthcare Research and Quality (US), 2013. Publication No. 12(13)-EHC154-EF.

19. Manthe, R.L. and S. Muro, *Lysosomes and nanotherapeutics: diseases, treatments, and side effects.*, in *Handbook of Nanobiomedical Research*, V. Torchilin, Editor. 2014, World Scientific Publishing Co.: Singapore. Vol. 2, Chapter 8: p. 261-305.

20. Seregin, S.S. and A. Amalfitano, *Gene therapy for lysosomal storage diseases: progress, challenges and future prospects.* Curr Pharm Des, 2011. 17(24): p. 2558-74.

21. Dhami, R. and E.H. Schuchman, *Mannose 6-phosphate receptor-mediated uptake is defective in acid sphingomyelinase-deficient macrophages: implications for Niemann-Pick disease enzyme replacement therapy.* J Biol Chem, 2004. 279(2): p. 1526-32.

22. Furbish, F.S., et al., *Uptake and distribution of placental glucocerebrosidase in rat hepatic cells and effects of sequential deglycosylation.* Biochim Biophys Acta, 1981. 673(4): p. 425-34.

23. LeBowitz, J.H., et al., *Glycosylation-independent targeting enhances enzyme delivery to lysosomes and decreases storage in mucopolysaccharidosis type VII mice.* Proc Natl Acad Sci U S A, 2004. 101(9): p. 3083-8.

24. Lee, K.O., et al., *Improved intracellular delivery of glucocerebrosidase mediated by the HIV-1 TAT protein transduction domain.* Biochem Biophys Res Commun, 2005. 337(2): p. 701-7.

25. Matzner, U., et al., *Non-inhibitory antibodies impede lysosomal storage reduction during enzyme replacement therapy of a lysosomal storage disease.* J Mol Med (Berl), 2008. 86(4): p. 433-42.

26. Orii, K.O., et al., *Defining the pathway for Tat-mediated delivery of beta-glucuronidase in cultured cells and MPS VII mice.* Mol Ther, 2005. 12(2): p. 345-52.

27. Prince, W.S., et al., *Lipoprotein receptor binding, cellular uptake, and lysosomal delivery of fusions between the receptor-associated protein (RAP) and alpha-L-iduronidase or acid alpha-glucosidase.* J Biol Chem, 2004. 279(33): p. 35037-46.

28. Zhang, X.Y., et al., *Cellular uptake and lysosomal delivery of galactocerebrosidase tagged with the HIV Tat protein transduction domain.* J Neurochem, 2008. 104(4): p. 1055-64.

29. Zhu, Y., et al., *Dexamethasone-mediated up-regulation of the mannose receptor improves the delivery of recombinant glucocerebrosidase to Gaucher macrophages.* J Pharmacol Exp Ther, 2004. 308(2): p. 705-11.

30. Aviezer, D., et al., *A plant-derived recombinant human glucocerebrosidase enzyme--a preclinical and phase I investigation.* PLoS One, 2009. 4(3): p. e4792.

31. Harmatz, P., et al., *Enzyme replacement therapy for mucopolysaccharidosis VI: a phase 3, randomized, double-blind, placebo-controlled, multinational study of recombinant human N-acetylgalactosamine 4-sulfatase (recombinant human arylsulfatase B or rhASB) and follow-on, open-label extension study.* J Pediatr, 2006. 148(4): p. 533-39.

32. Lyseng-Williamson, K.A., *Elosulfase Alfa: a review of its use in patients with mucopolysaccharidosis type IVA (Morquio A syndrome).* BioDrugs, 2014. 28(5): p. 465-75.

33. McGovern, M.M., et al., *Novel first-dose adverse drug reactions during a phase I trial of olipudase alfa (recombinant human acid sphingomyelinase) in adults with Niemann-Pick disease type B (acid sphingomyelinase deficiency).* Genet Med, 2016. 18(1): p. 34-40.

34. Wraith, J.E., et al., *Enzyme replacement therapy for mucopolysaccharidosis I: a randomized, double-blinded, placebo-controlled, multinational study of recombinant human alpha-L-iduronidase (laronidase).* J Pediatr, 2004. 144(5): p. 581-8.

35. Zimran, A., *Velaglucerase alfa: a new option for Gaucher disease treatment.* Drugs Today (Barc), 2011. 47(7): p. 515-29.

36. Zimran, A., D. Elstein, and E. Beutler, *Low-dose therapy trumps high-dose therapy again in the treatment of Gaucher disease.* Blood, 2006. 108(3): p. 802-3.

37. Barton, R.W. and E.F. Neufeld, *The Hurler corrective factor. Purification and some properties.* J Biol Chem, 1971. 246(24): p. 7773-9.

38. Brooks, D.A., R. Kakavanos, and J.J. Hopwood, *Significance of immune response to enzyme-replacement therapy for patients with a lysosomal storage disorder.* Trends Mol Med, 2003. 9(10): p. 450-3.

39. Kishnani, P.S., et al., *Immune response to enzyme replacement therapies in lysosomal storage diseases and the role of immune tolerance induction.* Mol Genet Metab, 2016. 117(2): p. 66-83.

40. Wang, J., et al., *Neutralizing antibodies to therapeutic enzymes: considerations for testing, prevention and treatment.* Nat Biotechnol, 2008. 26(8): p. 901-8.

41. Boado, R.J., et al., *Pharmacokinetics and brain uptake in the rhesus monkey of a fusion protein of arylsulfatase a and a monoclonal antibody against the human insulin receptor.* Biotechnol Bioeng, 2013. 110(5): p. 1456-65.

42. Boado, R.J., et al., *Genetic engineering of a lysosomal enzyme fusion protein for targeted delivery across the human blood-brain barrier.* Biotechnol Bioeng, 2008. 99(2): p. 475-84.

43. Bockenhoff, A., et al., *Comparison of five peptide vectors for improved brain delivery of the lysosomal enzyme arylsulfatase A.* J Neurosci, 2014. 34(9): p. 3122-9.

44. Osborn, M.J., et al., *Targeting of the CNS in MPS-IH using a nonviral transferrin-alpha-L-iduronidase fusion gene product.* Mol Ther, 2008. 16(8): p. 1459-66.

45. Langer, R., *Drug delivery and targeting.* Nature, 1998. 392(6679 Suppl): p. 5-10.

46. Moghimi, S.M., A.C. Hunter, and J.C. Murray, *Nanomedicine: current status and future prospects.* FASEB J, 2005. 19(3): p. 311-30.

47. Muro, S., *Challenges in design and characterization of ligand-targeted drug delivery systems.* J Control Release, 2012. 164(2): p. 125-37.

48. Parveen, S., R. Misra, and S.K. Sahoo, *Nanoparticles: a boon to drug delivery, therapeutics, diagnostics and imaging.* Nanomedicine, 2012. 8(2): p. 147-66.

49. Sahoo, S.K., S. Parveen, and J.J. Panda, *The present and future of nanotechnology in human health care.* Nanomedicine, 2007. 3(1): p. 20-31.

50. Torchilin, V.P., *Multifunctional nanocarriers.* Adv Drug Deliv Rev, 2006. 58(14): p. 1532-55.

51. Bareford, L.M. and P.W. Swaan, *Endocytic mechanisms for targeted drug delivery.* Adv Drug Deliv Rev, 2007. 59(8): p. 748-58.

52. Chrastina, A., K.A. Massey, and J.E. Schnitzer, *Overcoming in vivo barriers to targeted nanodelivery.* Wiley Interdiscip Rev Nanomed Nanobiotechnol, 2011. 3(4): p. 421-37.

53. Conner, S.D. and S.L. Schmid, *Regulated portals of entry into the cell.* Nature, 2003. 422(6927): p. 37-44.

54. Duncan, R. and S.C. Richardson, *Endocytosis and intracellular trafficking as gateways for nanomedicine delivery: opportunities and challenges.* Mol Pharm, 2012. 9(9): p. 2380-402.

55. Grabrucker, A.M., et al., *Nanoparticle transport across the blood brain barrier.* Tissue Barriers, 2016. 4(1): p. e1153568.

56. Hillaireau, H. and P. Couvreur, *Nanocarriers' entry into the cell: relevance to drug delivery.* Cell Mol Life Sci, 2009. 66(17): p. 2873-96.

57. Rappaport, J., C. Garnacho, and S. Muro, *Clathrin-mediated endocytosis is impaired in type A-B Niemann-Pick disease model cells and can be restored by ICAM-1-mediated enzyme replacement.* Mol Pharm, 2014. 11(8): p. 2887-95.

58. Garnacho, C., et al., *Delivery of acid sphingomyelinase in normal and niemann-pick disease mice using intercellular adhesion molecule-1-targeted polymer nanocarriers.* J Pharmacol Exp Ther, 2008. 325(2): p. 400-8.

59. Hsu, J., et al., *Enhancing biodistribution of therapeutic enzymes in vivo by modulating surface coating and concentration of ICAM-1-targeted nanocarriers.* J Biomed Nanotechnol, 2014. 10(2): p. 345-54.

60. Hsu, J., et al., *Enhanced delivery of alpha-glucosidase for Pompe disease by ICAM-1-targeted nanocarriers: comparative performance of a strategy for three distinct lysosomal storage disorders.* Nanomedicine, 2012. 8(5): p. 731-9.

61. Hsu, J., et al., *Enhanced endothelial delivery and biochemical effects of alpha-galactosidase by ICAM-1-targeted nanocarriers for Fabry disease.* J Control Release, 2011. 149(3): p. 323-31.

62. Muro, S., et al., *Control of endothelial targeting and intracellular delivery of therapeutic enzymes by modulating the size and shape of ICAM-1-targeted carriers.* Mol Ther, 2008. 16(8): p. 1450-8.

63. Muro, S., E.H. Schuchman, and V. Muzykantov, *Immunotargeting to ICAM-1 provides binding, internalization and lysosomal delivery of acid sphinomyelinase.* Am J Hum Genet, 2004. 75: p. PN268.

64. Muro, S., E.H. Schuchman, and V.R. Muzykantov, *Lysosomal enzyme delivery by ICAM-1-targeted nanocarriers bypassing glycosylation- and clathrin-dependent endocytosis.* Mol Ther, 2006. 13(1): p. 135-41.

65. Papademetriou, J., et al., *Comparative binding, endocytosis, and biodistribution of antibodies and antibody-coated carriers for targeted delivery of lysosomal enzymes to ICAM-1 versus transferrin receptor.* J Inherit Metab Dis, 2013. 36(3): p. 467-77.

66. Muro, S., *Intercellular adhesion molecule-1 and vascular adhesion molecule-1.*, in *Endothelial Biomedicine*, W.C. Aird, Editor. 2007, Cambridge University Press: New York City, NY. p. 1058-70.

67. Rothlein, R., et al., *A human intercellular adhesion molecule (ICAM-1) distinct from LFA-1.* J Immunol, 1986. 137(4): p. 1270-4.

68. Muro, S., et al., *A novel endocytic pathway induced by clustering endothelial ICAM-1 or PECAM-1.* J Cell Sci, 2003. 116(Pt 8): p. 1599-609.

69. Hsu, J., J. Hoenicka, and S. Muro, *Targeting, endocytosis, and lysosomal delivery of active enzymes to model human neurons by ICAM-1-targeted nanocarriers.* Pharm Res, 2015. 32(4): p. 1264-78.

70. Ghaffarian, R., T. Bhowmick, and S. Muro, *Transport of nanocarriers across gastrointestinal epithelial cells by a new transcellular route induced by targeting ICAM-1.* J Control Release, 2012. 163(1): p. 25-33.

71. Hsu, J., J. Rappaport, and S. Muro, *Specific binding, uptake, and transport of ICAM-1-targeted nanocarriers across endothelial and subendothelial cell components of the blood-brain barrier.* Pharm Res, 2014. 31(7): p. 1855-66.

72. Papademetriou, I.T., et al., *In vivo performance of polymer nanocarriers dually-targeted to epitopes of the same or different receptors.* Biomaterials, 2013. 34(13): p. 3459-66.

73. Serrano, D. and S. Muro, *Endothelial cell adhesion molecules and drug delivery applications.*, in *Mechanobiology of the Endothelium*, H. Aranda-Espinoza, Editor. 2015, CRC Press: Boca Raton, FL. p. 4100-32.

74. Springer, T.A., *Adhesion receptors of the immune system.* Nature, 1990. 346(6283): p. 425-34.

75. Lawson, C. and S. Wolf, *ICAM-1 signaling in endothelial cells.* Pharmacol Rep, 2009. 61(1): p. 22-32.

76. Witkowska, A.M. and M.H. Borawska, *Soluble intercellular adhesion molecule-1 (sICAM-1): an overview.* Eur Cytokine Netw, 2004. 15(2): p. 91-8.

77. Ansar, M., et al., *Biological functionalization of drug delivery carriers to bypass size restrictions of receptor-mediated endocytosis independently from receptor targeting.* ACS Nano, 2013. 7(12): p. 10597-611.

78. Serrano, D., et al., *Intercellular adhesion molecule 1 engagement modulates sphingomyelinase and ceramide, supporting uptake of drug carriers by the vascular endothelium.* Arterioscler Thromb Vasc Biol, 2012. 32(5): p. 1178-85.

79. Serrano, D., et al., *How carrier size and valency modulate receptor-mediated signaling: understanding the link between binding and endocytosis of ICAM-1-targeted carriers.* Biomacromolecules, 2016. 17(10): p. 3127-37.

80. Muro, S., et al., *ICAM-1 recycling in endothelial cells: a novel pathway for sustained intracellular delivery and prolonged effects of drugs.* Blood, 2005. 105(2): p. 650-8.

81. Muro, S., et al., *Endothelial targeting of high-affinity multivalent polymer nanocarriers directed to intercellular adhesion molecule 1.* J Pharmacol Exp Ther, 2006. 317(3): p. 1161-9.

82. Meikle, P.J., et al., *Prevalence of lysosomal storage disorders.* JAMA, 1999. 281(3): p. 249-54.

83. Mellman, I., R. Fuchs, and A. Helenius, *Acidification of the endocytic and exocytic pathways.* Annu Rev Biochem, 1986. 55: p. 663-700.

84. Holtzman, E., Historical fragments; methods; some terminology., in *Lysosomes*, P. Siekevitz, Editor. 1989, Plenum Press: New York City, NY. p. 1-24.

85. Kornfeld, S., et al., *Steps in the phosphorylation of the high mannose oligosaccharides of lysosomal enzymes.* Ciba Found Symp, 1982(92): p. 138-56.

86. Rosenfeld, M.G., et al., *Biosynthesis of lysosomal hydrolases: their synthesis in bound polysomes and the role of co- and post-translational processing in determining their subcellular distribution.* J Cell Biol, 1982. 93(1): p. 135-43.

87. Neufeld, E.F., *The uptake of enzymes into lysosomes: an overview.* Birth Defects Orig Artic Ser, 1980. 16(1): p. 77-84.

88. Eskelinen, E.L., Y. Tanaka, and P. Saftig, *At the acidic edge: emerging functions for lysosomal membrane proteins.* Trends Cell Biol, 2003. 13(3): p. 137-45.

89. Mancini, G.M., A.C. Havelaar, and F.W. Verheijen, *Lysosomal transport disorders.* J Inherit Metab Dis, 2000. 23(3): p. 278-92.

90. Pearce, D.A., et al., *Action of BTN1, the yeast orthologue of the gene mutated in Batten disease.* Nat Genet, 1999. 22(1): p. 55-8.

91. Raychowdhury, M.K., et al., *Molecular pathophysiology of mucolipidosis type IV: pH dysregulation of the mucolipin-1 cation channel.* Hum Mol Genet, 2004. 13(6): p. 617-27.

92. Mijaljica, D., M. Prescott, and R.J. Devenish, *V-ATPase engagement in autophagic processes.* Autophagy, 2011. 7(6): p. 666-8.

93. Sobota, J.A., et al., *Inhibitors of the V0 subunit of the vacuolar H+-ATPase prevent segregation of lysosomal- and secretory-pathway proteins.* J Cell Sci, 2009. 122(Pt 19): p. 3542-53.

94. Kloska, A., A. Tylki-Szymanska, and G. Wegrzyn, *Lysosomal storage diseases--an overview.* Postepy Biochem, 2011. 57(2): p. 128-32.

95. Schmidt, B., et al., *A novel amino acid modification in sulfatases that is defective in multiple sulfatase deficiency.* Cell, 1995. 82(2): p. 271-8.

96. Verity, C., et al., *The epidemiology of progressive intellectual and neurological deterioration in childhood.* Arch Dis Child, 2010. 95(5): p. 361-4.

97. Schuchman, E.H. and R.J. Desnick, *Types A and B Niemann-Pick disease.* Mol Genet Metab, 2017. 120(1-2): p. 27-33.

98. Gal, A.E., et al., *A practical chromogenic procedure for the detection of homozygotes and heterozygous carriers of Niemann-Pick disease.* N Engl J Med, 1975. 293(13): p. 632-6.

99. He, X., et al., *A fluorescence-based, high-performance liquid chromatographic assay to determine acid sphingomyelinase activity and diagnose types A and B Niemann-Pick disease.* Anal Biochem, 2003. 314(1): p. 116-20.

100. Jones, I., et al., *Characterization of common SMPD1 mutations causing types A and B Niemann-Pick disease and generation of mutation-specific mouse models.* Mol Genet Metab, 2008. 95(3): p. 152-62.

101. Irun, P., et al., *Identification of seven novel SMPD1 mutations causing Niemann-Pick disease types A and B.* Clin Genet, 2013. 84(4): p. 356-61.

102. Toth, B., et al., *Molecular genetic characterization of novel sphingomyelin phosphodiesterase 1 mutations causing niemann-pick disease.* JIMD Rep, 2012. 3: p. 125-9.

103. Simonaro, C.M., et al., *The demographics and distribution of type B Niemann-Pick disease: novel mutations lead to new genotype/phenotype correlations.* Am J Hum Genet, 2002. 71(6): p. 1413-9.

104. Acuna, M., et al., *Epidemiological, clinical and biochemical characterization of the p.(Ala359Asp) SMPD1 variant causing Niemann-Pick disease type B.* Eur J Hum Genet, 2016. 24(2): p. 208-13.

105. Zhang, H., et al., *Identification of a distinct mutation spectrum in the SMPD1 gene of Chinese patients with acid sphingomyelinase-deficient Niemann-Pick disease.* Orphanet J Rare Dis, 2013. 8: p. 15.

106. Genetics, A.C.o., *ACOG Committee Opinion No. 442: Preconception and prenatal carrier screening for genetic diseases in individuals of Eastern European Jewish descent.* Obstet Gynecol, 2009. 114(4): p. 950-3.

107. Settembre, C., et al., *A block of autophagy in lysosomal storage disorders.* Hum Mol Genet, 2008. 17(1): p. 119-29.

108. Fraldi, A., et al., *Lysosomal fusion and SNARE function are impaired by cholesterol accumulation in lysosomal storage disorders.* EMBO J, 2010. 29(21): p. 3607-20.

109. Levine, B., N. Mizushima, and H.W. Virgin, *Autophagy in immunity and inflammation.* Nature, 2011. 469(7330): p. 323-35.

110. Martinez-Vicente, M., et al., *Cargo recognition failure is responsible for inefficient autophagy in Huntington's disease.* Nat Neurosci, 2010. 13(5): p. 567-76.

111. Nixon, R.A. and D.S. Yang, *Autophagy failure in Alzheimer's disease--locating the primary defect.* Neurobiol Dis, 2011. 43(1): p. 38-45.

112. Sanchez-Perez, A.M., et al., *Parkinson's disease and autophagy.* Parkinsons Dis, 2012. 2012: p. 429524.

113. Yang, Z.J., et al., *The role of autophagy in cancer: therapeutic implications.* Mol Cancer Ther, 2011. 10(9): p. 1533-41.

114. Zhang, L., R. Sheng, and Z. Qin, *The lysosome and neurodegenerative diseases.* Acta Biochim Biophys Sin (Shanghai), 2009. 41(6): p. 437-45.

115. Aby, E., et al., *Mutations in palmitoyl-protein thioesterase 1 alter exocytosis and endocytosis at synapses in Drosophila larvae.* Fly (Austin), 2013. 7(4): p. 267-79.

116. Hortsch, R., et al., *Glycolipid trafficking in Drosophila undergoes pathway switching in response to aberrant cholesterol levels.* Mol Biol Cell, 2010. 21(5): p. 778-90.

117. Liscum, L. and J.R. Faust, *Low density lipoprotein (LDL)-mediated suppression of cholesterol synthesis and LDL uptake is defective in Niemann-Pick type C fibroblasts.* J Biol Chem, 1987. 262(35): p. 17002-8.

118. Marks, D.L. and R.E. Pagano, *Endocytosis and sorting of glycosphingolipids in sphingolipid storage disease.* Trends Cell Biol, 2002. 12(12): p. 605-13.

119. Puri, V., et al., *Clathrin-dependent and -independent internalization of plasma membrane sphingolipids initiates two Golgi targeting pathways.* J Cell Biol, 2001. 154(3): p. 535-47.

120. Tecedor, L., et al., *CLN3 loss disturbs membrane microdomain properties and protein transport in brain endothelial cells.* J Neurosci, 2013. 33(46): p. 18065-79.

121. Cardone, M., et al., *Abnormal mannose-6-phosphate receptor trafficking impairs recombinant alpha-glucosidase uptake in Pompe disease fibroblasts.* Pathogenetics, 2008. 1(1): p. 6.

122. Malatack, J.J., D.M. Consolini, and E. Bayever, *The status of hematopoietic stem cell transplantation in lysosomal storage disease.* Pediatr Neurol, 2003. 29(5): p. 391-403.

123. Sands, M.S. and B.L. Davidson, *Gene therapy for lysosomal storage diseases.* Mol Ther, 2006. 13(5): p. 839-49.

124. Rastall, D.P. and A. Amalfitano, *Recent advances in gene therapy for lysosomal storage disorders.* Appl Clin Genet, 2015. 8: p. 157-69.

125. Ellinwood, N.M., C.H. Vite, and M.E. Haskins, *Gene therapy for lysosomal storage diseases: the lessons and promise of animal models.* J Gene Med, 2004. 6(5): p. 481-506.

126. Gritti, A., *Gene therapy for lysosomal storage disorders.* Expert Opin Biol Ther, 2011. 11(9): p. 1153-67.

127. Doerr, J., et al., *Arylsulfatase A overexpressing human iPSC-derived neural cells reduce CNS sulfatide storage in a mouse model of Metachromatic Leukodystrophy.* Mol Ther, 2015. 23(9): p. 1519-31.

128. Griffin, T.A., H.C. Anderson, and J.H. Wolfe, *Ex vivo gene therapy using patient iPSC-derived NSCs reverses pathology in the brain of a homologous mouse model.* Stem Cell Reports, 2015. 4(5): p. 835-46.

129. Gurda, B.L., et al., *Evaluation of AAV-mediated gene therapy for central nervous system disease in canine Mucopolysaccharidosis VII.* Mol Ther, 2016. 24(2): p. 206-16.

130. Murrey, D.A., et al., *Feasibility and safety of systemic rAAV9-hNAGLU delivery for treating mucopolysaccharidosis IIIB: toxicology, biodistribution, and immunological assessments in primates.* Hum Gene Ther Clin Dev, 2014. 25(2): p. 72-84.

131. Tardieu, M., et al., *Intracerebral administration of adeno-associated viral vector serotype rh.10 carrying human SGSH and SUMF1 cDNAs in children with mucopolysaccharidosis type IIIA disease: results of a phase I/II trial.* Hum Gene Ther, 2014. 25(6): p. 506-16.

132. Worgall, S., et al., *Treatment of late infantile neuronal ceroid lipofuscinosis by CNS administration of a serotype 2 adeno-associated virus expressing CLN2 cDNA.* Hum Gene Ther, 2008. 19(5): p. 463-74.

133. Platt, F.M., et al., *Prevention of lysosomal storage in Tay-Sachs mice treated with N-butyldeoxynojirimycin.* Science, 1997. 276(5311): p. 428-31.

134. Porto, C., et al., *The pharmacological chaperone N-butyldeoxynojirimycin enhances enzyme replacement therapy in Pompe disease fibroblasts.* Mol Ther, 2009. 17(6): p. 964-71.

135. Coutinho, M.F., J.I. Santos, and S. Alves, *Less is more: substrate reduction therapy for lysosomal storage disorders.* Int J Mol Sci, 2016. 17(7): p. 1065-86.

136. Cherqui, S., *Cysteamine therapy: a treatment for cystinosis, not a cure.* Kidney Int, 2012. 81(2): p. 127-9.

137. Gahl, W.A., J.G. Thoene, and J.A. Schneider, *Cystinosis.* N Engl J Med, 2002. 347(2): p. 111-21.

138. Camargo, F., et al., *Cyclodextrins in the treatment of a mouse model of Niemann-Pick C disease.* Life Sci, 2001. 70(2): p. 131-42.

139. Matsuo, M., et al., *Effects of intracerebroventricular administration of 2-hydroxypropyl-beta-cyclodextrin in a patient with Niemann-Pick Type C disease.* Mol Genet Metab Rep, 2014. 1: p. 391-400.

140. Tanaka, Y., et al., *Efficacy of 2-hydroxypropyl-beta-cyclodextrin in Niemann-Pick disease type C model mice and its pharmacokinetic analysis in a patient with the disease.* Biol Pharm Bull, 2015. 38(6): p. 844-51.

141. Sawkar, A.R., et al., *Gaucher disease-associated glucocerebrosidases show mutation-dependent chemical chaperoning profiles.* Chem Biol, 2005. 12(11): p. 1235-44.

142. Suzuki, Y., *Chemical chaperone therapy for GM1-gangliosidosis.* Cell Mol Life Sci, 2008. 65(3): p. 351-3.

143. Yam, G.H., C. Zuber, and J. Roth, *A synthetic chaperone corrects the trafficking defect and disease phenotype in a protein misfolding disorder.* FASEB J, 2005. 19(1): p. 12-8.

144. Narita, K., et al., *Protein transduction of Rab9 in Niemann-Pick C cells reduces cholesterol storage.* FASEB J, 2005. 19(11): p. 1558-60.

145. Chen, F.W., C. Li, and Y.A. Ioannou, *Cyclodextrin induces calcium-dependent lysosomal exocytosis.* PLoS One, 2010. 5(11): p. e15054.

146. Medina, D.L., et al., *Transcriptional activation of lysosomal exocytosis promotes cellular clearance.* Dev Cell, 2011. 21(3): p. 421-30.

147. Strauss, K., et al., *Exosome secretion ameliorates lysosomal storage of cholesterol in Niemann-Pick type C disease.* J Biol Chem, 2010. 285(34): p. 26279-88.

148. Xu, M., et al., *delta-Tocopherol reduces lipid accumulation in Niemann-Pick type C1 and Wolman cholesterol storage disorders.* J Biol Chem, 2012. 287(47): p. 39349-60.

149. Long, Y., et al., *Induced pluripotent stem cells for disease modeling and evaluation of therapeutics for Niemann-Pick disease type A.* Stem Cells Transl Med, 2016. 5(12): p. 1644-55.

150. Brady, R.O., *Enzyme replacement therapy: conception, chaos and culmination.* Philos Trans R Soc Lond B Biol Sci, 2003. 358(1433): p. 915-9.

151. Wasserstein, M.P., et al., *Successful within-patient dose escalation of olipudase alfa in acid sphingomyelinase deficiency.* Mol Genet Metab, 2015. 116(1-2): p. 88-97.

152. Bangham, A.D., M.M. Standish, and J.C. Watkins, *Diffusion of univalent ions across the lamellae of swollen phospholipids.* J Mol Biol, 1965. 13(1): p. 238-52.

153. Beija, M., et al., *Colloidal systems for drug delivery: from design to therapy.* Trends Biotechnol, 2012. 30(9): p. 485-96.

154. Musacchio, T. and V.P. Torchilin, *Recent developments in lipid-based pharmaceutical nanocarriers.* Front Biosci (Landmark Ed), 2011. 16: p. 1388-412.

155. Betigeri, S., et al., *Non-viral systemic delivery of siRNA or antisense oligonucleotides targeted to Jun N-terminal kinase 1 prevents cellular hypoxic damage.* Drug Deliv Transl Res, 2011. 1(1): p. 13-24.

156. Moghimi, S.M. and J. Szebeni, *Stealth liposomes and long circulating nanoparticles: critical issues in pharmacokinetics, opsonization and protein-binding properties.* Prog Lipid Res, 2003. 42(6): p. 463-78.

157. Discher, D.E. and A. Eisenberg, *Polymer vesicles.* Science, 2002. 297(5583): p. 967-73.

158. Duncan, R. and M.J. Vicent, *Polymer therapeutics-prospects for 21st century: the end of the beginning.* Adv Drug Deliv Rev, 2013. 65(1): p. 60-70.

159. Kabanov, A.V. and T. Okano, *Challenges in polymer therapeutics: state of the art and prospects of polymer drugs.* Adv Exp Med Biol, 2003. 519: p. 1-27.

160. Panyam, J. and V. Labhasetwar, *Biodegradable nanoparticles for drug and gene delivery to cells and tissue.* Adv Drug Deliv Rev, 2003. 55(3): p. 329-47.

161. Ghandehari, H., *Materials for advanced drug delivery in the 21st century: a focus area for Advanced Drug Delivery Reviews.* Adv Drug Deliv Rev, 2008. 60(9): p. 956.

162. Kayser, O., A. Lemke, and N. Hernandez-Trejo, *The impact of nanobiotechnology on the development of new drug delivery systems.* Curr Pharm Biotechnol, 2005. 6(1): p. 3-5.

163. Mundargi, R.C., et al., *Nano/micro technologies for delivering macromolecular therapeutics using poly(D,L-lactide-co-glycolide) and its derivatives.* J Control Release, 2008. 125(3): p. 193-209.

164. Moghimi, S.M., A.C. Hunter, and J.C. Murray, *Long-circulating and target-specific nanoparticles: theory to practice.* Pharmacol Rev, 2001. 53(2): p. 283-318.

165. Agnihotri, S.A., N.N. Mallikarjuna, and T.M. Aminabhavi, *Recent advances on chitosan-based micro- and nanoparticles in drug delivery.* J Control Release, 2004. 100(1): p. 5-28.

166. Schmaljohann, D., *Thermo- and pH-responsive polymers in drug delivery.* Adv Drug Deliv Rev, 2006. 58(15): p. 1655-70.

167. Jain, T.K., et al., *Magnetic nanoparticles with dual functional properties: drug delivery and magnetic resonance imaging.* Biomaterials, 2008. 29(29): p. 4012-21.

168. Probst, C.E., et al., *Quantum dots as a platform for nanoparticle drug delivery vehicle design.* Adv Drug Deliv Rev, 2013. 65(5): p. 703-18.

169. Shubayev, V.I., T.R. Pisanic, 2nd, and S. Jin, *Magnetic nanoparticles for theragnostics.* Adv Drug Deliv Rev, 2009. 61(6): p. 467-77.

170. Vasir, J.K. and V. Labhasetwar, *Targeted drug delivery in cancer therapy.* Technol Cancer Res Treat, 2005. 4(4): p. 363-74.

171. Maeda, H., et al., *Tumor vascular permeability and the EPR effect in macromolecular therapeutics: a review.* J Control Release, 2000. 65(1-2): p. 271-84.

172. Suk, J.S., et al., *Gene delivery to differentiated neurotypic cells with RGD and HIV Tat peptide functionalized polymeric nanoparticles.* Biomaterials, 2006. 27(29): p. 5143-50.

173. Hilgenbrink, A.R. and P.S. Low, *Folate receptor-mediated drug targeting: from therapeutics to diagnostics.* J Pharm Sci, 2005. 94(10): p. 2135-46.

174. Pardridge, W.M., *Biopharmaceutical drug targeting to the brain.* J Drug Target, 2010. 18(3): p. 157-67.

175. Jones, A.T., *Gateways and tools for drug delivery: endocytic pathways and the cellular dynamics of cell penetrating peptides.* Int J Pharm, 2008. 354(1-2): p. 34-8.

176. Calderon, A.J., et al., *Optimizing endothelial targeting by modulating the antibody density and particle concentration of anti-ICAM coated carriers.* J Control Release, 2011. 150(1): p. 37-44.

177. Fakhari, A., et al., *Controlling ligand surface density optimizes nanoparticle binding to ICAM-1.* J Pharm Sci, 2011. 100(3): p. 1045-56.

178. Guo, Y., et al., *Compact, polyvalent mannose quantum dots as sensitive, ratiometric FRET probes for multivalent protein-ligand interactions.* Angew Chem Int Ed Engl, 2016. 55(15): p. 4738-42.

179. Wiley, D.T., et al., *Transcytosis and brain uptake of transferrin-containing nanoparticles by tuning avidity to transferrin receptor.* Proc Natl Acad Sci U S A, 2013. 110(21): p. 8662-7.

180. Zern, B.J., et al., *Reduction of nanoparticle avidity enhances the selectivity of vascular targeting and PET detection of pulmonary inflammation.* ACS Nano, 2013. 7(3): p. 2461-9.

181. Trollet, C., D. Scherman, and P. Bigey, *Delivery of DNA into muscle for treating systemic diseases: advantages and challenges.* Methods Mol Biol, 2008. 423: p. 199-214.

182. Varkouhi, A.K., et al., *Endosomal escape pathways for delivery of biologicals.* J Control Release, 2011. 151(3): p. 220-8.

183. Sahay, G., D.Y. Alakhova, and A.V. Kabanov, *Endocytosis of nanomedicines.* J Control Release, 2010. 145(3): p. 182-95.

184. Rappaport, J., I. Papademetriou, and S. Muro, *Endocytosis and the endolysosomal route in drug delivery.*, in *Drug Delivery across Physiological Barriers.*, S. Muro, Editor. 2016, Pan Standford Publishing: Singapore. p. 313-39.

185. McMahon, H.T. and E. Boucrot, *Molecular mechanism and physiological functions of clathrin-mediated endocytosis.* Nat Rev Mol Cell Biol, 2011. 12(8): p. 517-33.

186. Nichols, B., *Caveosomes and endocytosis of lipid rafts.* J Cell Sci, 2003. 116(Pt 23): p. 4707-14.

187. McIntosh, D.P., et al., *Targeting endothelium and its dynamic caveolae for tissue-specific transcytosis in vivo: a pathway to overcome cell barriers to drug and gene delivery.* Proc Natl Acad Sci U S A, 2002. 99(4): p. 1996-2001.

188. Gong, Q., C. Huntsman, and D. Ma, *Clathrin-independent internalization and recycling.* J Cell Mol Med, 2008. 12(1): p. 126-44.

189. Stan, R.V., *Endocytosis pathways in endothelium: how many?* Am J Physiol Lung Cell Mol Physiol, 2006. 290(5): p. L806-8.

190. Dautry-Varsat, A., *Receptor-mediated endocytosis: the intracellular journey of transferrin and its receptor.* Biochimie, 1986. 68(3): p. 375-81.

191. Ding, B.S., et al., *Advanced drug delivery systems that target the vascular endothelium.* Mol Interv, 2006. 6(2): p. 98-112.

192. Dejana, E., *Endothelial cell-cell junctions: happy together.* Nat Rev Mol Cell Biol, 2004. 5(4): p. 261-70.

193. Stevens, T., et al., *Mechanisms regulating endothelial cell barrier function.* Am J Physiol Lung Cell Mol Physiol, 2000. 279(3): p. L419-22.

194. Azmin, M.N., et al., *The effect of non-ionic surfactant vesicle (niosome) entrapment on the absorption and distribution of methotrexate in mice.* J Pharm Pharmacol, 1985. 37(4): p. 237-42.

195. Hanig, J.P., J.M. Morrison, Jr., and S. Krop, *Ethanol enhancement of blood-brain barrier permeability to catecholamines in chicks.* Eur J Pharmacol, 1972. 18(1): p. 79-82.

196. Kitchens, K.M., M.E. El-Sayed, and H. Ghandehari, *Transepithelial and endothelial transport of poly (amidoamine) dendrimers.* Adv Drug Deliv Rev, 2005. 57(15): p. 2163-76.

197. Kobiler, D., et al., *Sodium dodecylsulphate induces a breach in the blood-brain barrier and enables a West Nile virus variant to penetrate into mouse brain.* Brain Res, 1989. 496(1-2): p. 314-6.

198. Oh, P., et al., *Live dynamic imaging of caveolae pumping targeted antibody rapidly and specifically across endothelium in the lung.* Nat Biotechnol, 2007. 25(3): p. 327-37.

199. Pardridge, W.M., *Blood-brain barrier delivery.* Drug Discov Today, 2007. 12(1-2): p. 54-61.

200. Muro, S., M. Koval, and V. Muzykantov, *Endothelial endocytic pathways: gates for vascular drug delivery.* Curr Vasc Pharmacol, 2004. 2(3): p. 281-99.

201. Braidman, I.P. and G. Gregoriadis, *Rapid partial purification of placental glucocerebroside beta-glucosidase and its entrapment in liposomes.* Biochem J, 1977. 164(2): p. 439-45.

202. Gregoriadis, G. and B.E. Ryman, *Lysosomal localization of -fructofuranosidase-containing liposomes injected into rats.* Biochem J, 1972. 129(1): p. 123-33.

203. Patel, H. and B.E. Ryman, *Alpha-mannosidase in zinc-deficient rats: possibility of liposomal therapy in mannosidosis.* Biochemical Society Transations 1974. 2(5): p. 1014-17.

204. Steger, L.D. and R.J. Desnick, *Enzyme therapy. VI: Comparative in vivo fates and effects on lysosomal integrity of enzyme entrapped in negatively and positively charged liposomes.* Biochim Biophys Acta, 1977. 464(3): p. 530-46.

205. Takada, G., H. Onodera, and K. Tada, *Delivery of fungal beta-galactosidase to rat brain by means of liposomes.* Tohoku J Exp Med, 1982. 136(2): p. 219-29.

206. Umezawa, F., et al., *Enzyme replacement with liposomes containing beta-galactosidase from Charonia lumpas in murine globoid cell leukodystrophy (twitcher).* Biochem Biophys Res Commun, 1985. 127(2): p. 663-7.

207. Schmitz, J., L.W. Poll, and S. vom Dahl, *Therapy of adult Gaucher disease.* Haematologica, 2007. 92(2): p. 148-52.

208. Moore, D.F., et al., *Enzyme replacement therapy in orphan and ultra-orphan diseases: the limitations of standard economic metrics as exemplified by Fabry-Anderson disease.* Pharmacoeconomics, 2007. 25(3): p. 201-8.

209. Rohrbach, M. and J.T. Clarke, *Treatment of lysosomal storage disorders : progress with enzyme replacement therapy.* Drugs, 2007. 67(18): p. 2697-716.

210. Rombach, S.M., et al., *Cost-effectiveness of enzyme replacement therapy for Fabry disease.* Orphanet J Rare Dis, 2013. 8: p. 29.

211. Alexis, F., et al., *Factors affecting the clearance and biodistribution of polymeric nanoparticles.* Mol Pharm, 2008. 5(4): p. 505-15.

212. Amoozgar, Z. and Y. Yeo, *Recent advances in stealth coating of nanoparticle drug delivery systems.* Wiley Interdiscip Rev Nanomed Nanobiotechnol, 2012. 4(2): p. 219-33.

213. Mumtaz, S. and B.K. Bachhawat, *Enhanced intracellular stability and efficacy of PEG modified dextranase in the treatment of a model storage disorder.* Biochim Biophys Acta, 1994. 1199(2): p. 175-82.

214. Ansari, N.H., et al., *Delivery of liposome-sequestered hydrophobic proteins to lysosomes of normal and Batten disease cells.* J Neurosci Res, 1997. 47(3): p. 341-7.

215. Weissmann, G., et al., *A general method for the introduction of enzymes, by means of immunoglobulin-coated liposomes, into lysosomes of deficient cells.* Proc Natl Acad Sci U S A, 1975. 72(1): p. 88-92.

216. Koshkaryev, A., et al., *Targeting of lysosomes by liposomes modified with octadecyl-rhodamine B.* J Drug Target, 2011. 19(8): p. 606-14.

217. Meerovich, I., et al., *Screening and optimization of ligand conjugates for lysosomal targeting.* Bioconjug Chem, 2011. 22(11): p. 2271-82.

218. Thekkedath, R., A. Koshkaryev, and V.P. Torchilin, *Lysosome-targeted octadecyl-rhodamine B-liposomes enhance lysosomal accumulation of*

glucocerebrosidase in Gaucher's cells in vitro. Nanomedicine (Lond), 2013. 8(7): p. 1055-65.

219. Cabrera, I., et al., *alpha-Galactosidase-A loaded-nanoliposomes with enhanced enzymatic activity and intracellular penetration.* Adv Healthc Mater, 2016. 5(7): p. 829-40.

220. Barrias, C.C., et al., *Biological evaluation of calcium alginate microspheres as a vehicle for the localized delivery of a therapeutic enzyme.* J Biomed Mater Res A, 2005. 74(4): p. 545-52.

221. Corchero, J.L., et al., *Enzymatic characterization of highly stable alpha-galactosidase A displayed on magnetic particles.* Biochemical Engineering Journal, 2012. 67(15): p. 20-27.

222. Sarrazin, S., et al., *Guanidinylated neomycin mediates heparan sulfate-dependent transport of active enzymes to lysosomes.* Mol Ther, 2010. 18(7): p. 1268-74.

223. Dekiwadia, C.D., A.C. Lawrie, and J.V. Fecondo, *Peptide-mediated cell penetration and targeted delivery of gold nanoparticles into lysosomes.* J Pept Sci, 2012. 18(8): p. 527-34.

224. Giannotti, M.I., et al., *pH-responsive polysaccharide-based polyelectrolyte complexes as nanocarriers for lysosomal delivery of therapeutic proteins.* Biomacromolecules, 2011. 12(7): p. 2524-33.

225. Salvalaio, M., et al., *Targeted polymeric nanoparticles for brain delivery of high molecular weight molecules in lysosomal storage disorders.* PLoS One, 2016. 11(5): p. e0156452.

226. Lee, H.J., et al., *alpha-Galactosidase delivery using 30Kc19-human serum albumin nanoparticles for effective treatment of Fabry disease.* Appl Microbiol Biotechnol, 2016. 100(24): p. 10395-402.

227. Muro, S., et al., *Control of intracellular trafficking of ICAM-1-targeted nanocarriers by endothelial Na+/H+ exchanger proteins.* Am J Physiol Lung Cell Mol Physiol, 2006. 290(5): p. L809-17.

228. Garnacho, C., et al., *Differential intra-endothelial delivery of polymer nanocarriers targeted to distinct PECAM-1 epitopes.* J Control Release, 2008. 130(3): p. 226-33.

229. Muro, S., et al., *Slow intracellular trafficking of catalase nanoparticles targeted to ICAM-1 protects endothelial cells from oxidative stress.* Am J Physiol Cell Physiol, 2003. 285(5): p. C1339-47.

230. Anselmo, A.C., et al., *Exploiting shape, cellular-hitchhiking and antibodies to target nanoparticles to lung endothelium: Synergy between physical, chemical and biological approaches.* Biomaterials, 2015. 68: p. 1-8.

231. Choi, K.S., et al., *Inflammation-specific T1 imaging using anti-intercellular adhesion molecule 1 antibody-conjugated gadolinium diethylenetriaminepentaacetic acid.* Mol Imaging, 2007. 6(2): p. 75-84.

232. Hamilton, A.J., et al., *Intravascular ultrasound molecular imaging of atheroma components in vivo.* J Am Coll Cardiol, 2004. 43(3): p. 453-60.

233. Park, S., et al., *Self-assembled nanoplatform for targeted delivery of chemotherapy agents via affinity-regulated molecular interactions.* Biomaterials, 2010. 31(30): p. 7766-75.

234. Weller, G.E., et al., *Targeted ultrasound contrast agents: in vitro assessment of endothelial dysfunction and multi-targeting to ICAM-1 and sialyl Lewisx.* Biotechnol Bioeng, 2005. 92(6): p. 780-8.

235. Zhang, N., et al., *PLGA nanoparticle--peptide conjugate effectively targets intercellular cell-adhesion molecule-1.* Bioconjug Chem, 2008. 19(1): p. 145-52.

236. Fukuda, T., et al., *Dysfunction of endocytic and autophagic pathways in a lysosomal storage disease.* Ann Neurol, 2006. 59(4): p. 700-8.

237. Parkinson-Lawrence, E.J., et al., *Lysosomal storage disease: revealing lysosomal function and physiology.* Physiology (Bethesda), 2010. 25(2): p. 102-15.

238. Simons, K. and J. Gruenberg, *Jamming the endosomal system: lipid rafts and lysosomal storage diseases.* Trends Cell Biol, 2000. 10(11): p. 459-62.

239. Schuchman, E.H. and R. Desnick, *Niemann-Pick diseases types A and B: acid sphingomyelinase deficiencies.*, in *The Metabolic and Molecular Bases on Inherited Disease*, C. Scriver, et al., Editors. 2001, McGraw-Hill: New York City, NY. p. 3589-610.

240. Stan, R.V., *Structure and function of endothelial caveolae.* Microsc Res Tech, 2002. 57(5): p. 350-64.

241. Pelkmans, L. and A. Helenius, *Endocytosis via caveolae.* Traffic, 2002. 3(5): p. 311-20.

242. Pelkmans, L., J. Kartenbeck, and A. Helenius, *Caveolar endocytosis of simian virus 40 reveals a new two-step vesicular-transport pathway to the ER.* Nat Cell Biol, 2001. 3(5): p. 473-83.

243. Marlin, S.D. and T.A. Springer, *Purified intercellular adhesion molecule-1 (ICAM-1) is a ligand for lymphocyte function-associated antigen 1 (LFA-1).* Cell, 1987. 51(5): p. 813-9.

244. Hurwitz, R., K. Ferlinz, and K. Sandhoff, *The tricyclic antidepressant desipramine causes proteolytic degradation of lysosomal sphingomyelinase in human fibroblasts.* Biol Chem Hoppe Seyler, 1994. 375(7): p. 447-50.

245. Orlandi, P.A. and P.H. Fishman, *Filipin-dependent inhibition of cholera toxin: evidence for toxin internalization and activation through caveolae-like domains.* J Cell Biol, 1998. 141(4): p. 905-15.

246. Schlegel, R., et al., *Amantadine and dansylcadaverine inhibit vesicular stomatitis virus uptake and receptor-mediated endocytosis of alpha 2-macroglobulin.* Proc Natl Acad Sci U S A, 1982. 79(7): p. 2291-5.

247. Muro, S., V.R. Muzykantov, and J.C. Murciano, *Characterization of endothelial internalization and targeting of antibody-enzyme conjugates in cell cultures and in laboratory animals.* Methods Mol Biol, 2004. 283: p. 21-36.

248. Meier, O., et al., *Adenovirus triggers macropinocytosis and endosomal leakage together with its clathrin-mediated uptake.* J Cell Biol, 2002. 158(6): p. 1119-31.

249. West, M.A., M.S. Bretscher, and C. Watts, *Distinct endocytotic pathways in epidermal growth factor-stimulated human carcinoma A431 cells.* J Cell Biol, 1989. 109(6 Pt 1): p. 2731-9.

250. Kirkham, M. and R.G. Parton, *Clathrin-independent endocytosis: new insights into caveolae and non-caveolar lipid raft carriers.* Biochim Biophys Acta, 2005. 1746(3): p. 349-63.

251. Torgersen, M.L., et al., *Internalization of cholera toxin by different endocytic mechanisms.* J Cell Sci, 2001. 114(Pt 20): p. 3737-47.

252. Rappaport, J., et al., *Altered clathrin-independent endocytosis in type A Niemann-Pick disease cells and rescue by ICAM-1-targeted enzyme delivery.* Mol Pharm, 2015. 12(5): p. 1366-76.

253. Damke, H., et al., *Clathrin-independent pinocytosis is induced in cells overexpressing a temperature-sensitive mutant of dynamin.* J Cell Biol, 1995. 131(1): p. 69-80.

254. Mayor, S. and R.E. Pagano, *Pathways of clathrin-independent endocytosis.* Nat Rev Mol Cell Biol, 2007. 8(8): p. 603-12.

255. Singh, R.D., et al., *Selective caveolin-1-dependent endocytosis of glycosphingolipids.* Mol Biol Cell, 2003. 14(8): p. 3254-65.

256. Zhang, Y., et al., *Different contributions of clathrin- and caveolae-mediated endocytosis of vascular endothelial cadherin to lipopolysaccharide-induced vascular hyperpermeability.* PLoS One, 2014. 9(9): p. e106328.

257. Rappaport, J., et al., *A comparative study on the alterations of endocytic pathways in multiple lysosomal storage disorders.* Mol Pharm, 2016. 13(2): p. 357-68.

258. Bhowmick, T., et al., *Effect of flow on endothelial endocytosis of nanocarriers targeted to ICAM-1.* J Control Release, 2012. 157(3): p. 485-92.

259. Calderon, A.J., et al., *Flow dynamics, binding and detachment of spherical carriers targeted to ICAM-1 on endothelial cells.* Biorheology, 2009. 46(4): p. 323-41.

260. Mellman, I., *Endocytosis and molecular sorting.* Annu Rev Cell Dev Biol, 1996. 12: p. 575-625.

261. Damm, E.M., et al., *Clathrin- and caveolin-1-independent endocytosis: entry of simian virus 40 into cells devoid of caveolae.* J Cell Biol, 2005. 168(3): p. 477-88.

262. Samie, M.A. and H. Xu, *Lysosomal exocytosis and lipid storage disorders.* J Lipid Res, 2014. 55(6): p. 995-1009.

263. Falkow, S., R.R. Isberg, and D.A. Portnoy, *The interaction of bacteria with mammalian cells.* Annu Rev Cell Biol, 1992. 8: p. 333-63.

264. Fernandes, M.C., et al., *Trypanosoma cruzi subverts the sphingomyelinase-mediated plasma membrane repair pathway for cell invasion.* J Exp Med, 2011. 208(5): p. 909-21.

265. Grassme, H., et al., *Ceramide in bacterial infections and cystic fibrosis.* Biol Chem, 2008. 389(11): p. 1371-9.

266. Grassme, H., J. Riethmuller, and E. Gulbins, *Biological aspects of ceramide-enriched membrane domains.* Prog Lipid Res, 2007. 46(3-4): p. 161-70.

267. Miller, M.E., et al., *Ebolavirus requires acid sphingomyelinase activity and plasma membrane sphingomyelin for infection.* J Virol, 2012. 86(14): p. 7473-83.

268. Moulder, J.W., *Comparative biology of intracellular parasitism.* Microbiol Rev, 1985. 49(3): p. 298-337.

269. Zeidan, Y.H., R.W. Jenkins, and Y.A. Hannun, *Remodeling of cellular cytoskeleton by the acid sphingomyelinase/ceramide pathway.* J Cell Biol, 2008. 181(2): p. 335-50.

270. Kruth, H.S., et al., *Macropinocytosis is the endocytic pathway that mediates macrophage foam cell formation with native low density lipoprotein.* J Biol Chem, 2005. 280(3): p. 2352-60.

271. Ghaffarian, R. and S. Muro, *Distinct subcellular trafficking resulting from monomeric vs multimeric targeting to endothelial ICAM-1: implications for drug delivery.* Mol Pharm, 2014. 11(12): p. 4350-62.

272. Braulke, T. and J.S. Bonifacino, *Sorting of lysosomal proteins.* Biochim Biophys Acta, 2009. 1793(4): p. 605-14.

273. Pelkmans, L., *Secrets of caveolae- and lipid raft-mediated endocytosis revealed by mammalian viruses.* Biochim Biophys Acta, 2005. 1746(3): p. 295-304.

274. Yu, Y.J., et al., *Boosting brain uptake of a therapeutic antibody by reducing its affinity for a transcytosis target.* Sci Transl Med, 2011. 3(84): p. 84ra44.

275. Li, W., et al., *Endogenous ceramide contributes to the transcytosis of oxLDL across endothelial cells and promotes its subendothelial retention in vascular wall.* Oxid Med Cell Longev, 2014. 2014: p. 823071.

276. Simionescu, M., D. Popov, and A. Sima, *Endothelial transcytosis in health and disease.* Cell Tissue Res, 2009. 335(1): p. 27-40.

277. McGovern, M.M., et al., *Lipid abnormalities in children with types A and B Niemann Pick disease.* J Pediatr, 2004. 145(1): p. 77-81.

278. Saslowsky, D.E., et al., *Ganglioside GM1-mediated transcytosis of cholera toxin bypasses the retrograde pathway and depends on the structure of the ceramide domain.* J Biol Chem, 2013. 288(36): p. 25804-9.

279. Abdel Shakor, A.B., et al., *Cell surface ceramide controls translocation of transferrin receptor to clathrin-coated pits.* Cell Signal, 2012. 24(3): p. 677-84.

280. Schnitzer, J.E., *Caveolae: from basic trafficking mechanisms to targeting transcytosis for tissue-specific drug and gene delivery in vivo.* Adv Drug Deliv Rev, 2001. 49(3): p. 265-80.

281. Ghaffarian, R., et al., *Intra- and trans-cellular delivery of enzymes by direct conjugation with non-multivalent anti-ICAM molecules.* J Control Release, 2016. 238: p. 221-30.

282. Dautry-Varsat, A., A. Ciechanover, and H.F. Lodish, *pH and the recycling of transferrin during receptor-mediated endocytosis.* Proc Natl Acad Sci U S A, 1983. 80(8): p. 2258-62.

283. Brown, V.I. and M.I. Greene, *Molecular and cellular mechanisms of receptor-mediated endocytosis.* DNA Cell Biol, 1991. 10(6): p. 399-409.

284. Lodish, H., Berk, A., Zipursky, S.L., et al., *Receptor-mediated endocytosis and sorting of internalized proteins.*, in *Molecular Cell Biology*. 2000, W.H. Freeman: New York City, NY.

285. Hayashida, K., et al., *Molecular and cellular mechanisms of ectodomain shedding.* Anat Rec (Hoboken), 2010. 293(6): p. 925-37.

286. Jacob, M.P., *Extracellular matrix remodeling and matrix metalloproteinases in the vascular wall during aging and in pathological conditions.* Biomed Pharmacother, 2003. 57(5-6): p. 195-202.

287. Faveeuw, C., G. Preece, and A. Ager, *Transendothelial migration of lymphocytes across high endothelial venules into lymph nodes is affected by metalloproteinases.* Blood, 2001. 98(3): p. 688-95.

288. Fiore, E., et al., *Matrix metalloproteinase 9 (MMP-9/gelatinase B) proteolytically cleaves ICAM-1 and participates in tumor cell resistance to natural killer cell-mediated cytotoxicity.* Oncogene, 2002. 21(34): p. 5213-23.

289. Manicone, A.M. and J.K. McGuire, *Matrix metalloproteinases as modulators of inflammation.* Semin Cell Dev Biol, 2008. 19(1): p. 34-41.

290. Vu, T.H. and Z. Werb, *Matrix metalloproteinases: effectors of development and normal physiology*. Genes Dev, 2000. 14(17): p. 2123-33.

291. Manthe, R.L. and S. Muro, *ICAM-1-targeted nanocarriers attenuate endothelial release of soluble ICAM-1, an inflammatory regulator.* Bioeng Transl Med, 2017. 2(1): p. 109-19.

292. Hyun, Y.M., et al., *Uropod elongation is a common final step in leukocyte extravasation through inflamed vessels.* J Exp Med, 2012. 209(7): p. 1349-62.

293. Fridman, R., et al., *Activation of progelatinase B (MMP-9) by gelatinase A (MMP-2).* Cancer Res, 1995. 55(12): p. 2548-55.

294. Toth, M., et al., *Pro-MMP-9 activation by the MT1-MMP/MMP-2 axis and MMP-3: role of TIMP-2 and plasma membranes.* Biochem Biophys Res Commun, 2003. 308(2): p. 386-95.

295. Jevnikar, A.M., et al., *Differing regulation and function of ICAM-1 and class II antigens on renal tubular cells.* Kidney Int, 1990. 38(3): p. 417-25.

296. Bien-Ly, N., et al., *Transferrin receptor (TfR) trafficking determines brain uptake of TfR antibody affinity variants.* J Exp Med, 2014. 211(2): p. 233-44.

297. Aoudjit, F., E.F. Potworowski, and Y. St-Pierre, *Bi-directional induction of matrix metalloproteinase-9 and tissue inhibitor of matrix metalloproteinase-1 during T lymphoma/endothelial cell contact: implication of ICAM-1*. J Immunol, 1998. 160(6): p. 2967-73.

298. Navaratna, D., et al., *Proteolytic degradation of VE-cadherin alters the blood-retinal barrier in diabetes.* Diabetes, 2007. 56(9): p. 2380-7.

299. Witkowska, A.M., *Soluble ICAM-1: a marker of vascular inflammation and lifestyle.* Cytokine, 2005. 31(2): p. 127-34.

300. Gunawan, R.C. and D.T. Auguste, *Immunoliposomes that target endothelium in vitro are dependent on lipid raft formation.* Mol Pharm, 2010. 7(5): p. 1569-75.

301. Herd, H., et al., *Nanoparticle geometry and surface orientation influence mode of cellular uptake.* ACS Nano, 2013. 7(3): p. 1961-73.

302. Kawano, K. and Y. Maitani, *Effects of polyethylene glycol spacer length and ligand density on folate receptor targeting of liposomal Doxorubicin in vitro.* J Drug Deliv, 2011. 2011: p. 160967.

303. Mitragotri, S., *In drug delivery, shape does matter.* Pharm Res, 2009. 26(1): p. 232-4.

304. Rudnick, S.I. and G.P. Adams, *Affinity and avidity in antibody-based tumor targeting.* Cancer Biother Radiopharm, 2009. 24(2): p. 155-61.

305. Serrano, D., *Role of ICAM-1-mediated endocytosis in endothelial function and implications for carrier-assisted drug delivery*, in *Department of Cell Biology and Molecular Genetics*. 2014, University of Maryland, College Park. p. 1-205.

306. Simone, E.A., T.D. Dziubla, and V.R. Muzykantov, *Polymeric carriers: role of geometry in drug delivery.* Expert Opin Drug Deliv, 2008. 5(12): p. 1283-300.

307. Stefanick, J.F., et al., *A systematic analysis of peptide linker length and liposomal polyethylene glycol coating on cellular uptake of peptide-targeted liposomes.* ACS Nano, 2013. 7(4): p. 2935-47.

308. Aird, W.C., *Endothelium in health and disease.* Pharmacol Rep, 2008. 60(1): p. 139-43.

309. Howard, M., et al., *Vascular targeting of nanocarriers: perplexing aspects of the seemingly straightforward paradigm.* ACS Nano, 2014. 8(5): p. 4100-32.

310. Carman, C.V. and T.A. Springer, *A transmigratory cup in leukocyte diapedesis both through individual vascular endothelial cells and between them.* J Cell Biol, 2004. 167(2): p. 377-88.

311. Muzykantov, V.R., *Targeted therapeutics and nanodevices for vascular drug delivery: quo vadis?* IUBMB Life, 2011. 63(8): p. 583-5.

312. Champagne, B., et al., *Proteolytic cleavage of ICAM-1 by human neutrophil elastase.* J Immunol, 1998. 161(11): p. 6398-405.

313. Lyons, P.D. and E.N. Benveniste, *Cleavage of membrane-associated ICAM-1 from astrocytes: involvement of a metalloprotease.* Glia, 1998. 22(2): p. 103-12.

314. Tsakadze, N.L., et al., *Tumor necrosis factor-alpha-converting enzyme (TACE/ADAM-17) mediates the ectodomain cleavage of intercellular adhesion molecule-1 (ICAM-1).* J Biol Chem, 2006. 281(6): p. 3157-64.

315. DeGraba, T., et al., *Profile of endothelial and leukocyte activation in Fabry patients.* Ann Neurol, 2000. 47(2): p. 229-33.

316. Becker, J.C., et al., *Shedding of ICAM-1 from human melanoma cell lines induced by IFN-gamma and tumor necrosis factor-alpha. Functional consequences on cell-mediated cytotoxicity.* J Immunol, 1991. 147(12): p. 4398-401.

317. Becker, J.C., et al., *Soluble intercellular adhesion molecule-1 inhibits MHC-restricted specific T cell/tumor interaction.* J Immunol, 1993. 151(12): p. 7224-32.

318. Gho, Y.S., et al., *Stimulation of tumor growth by human soluble intercellular adhesion molecule-1.* Cancer Res, 2001. 61(10): p. 4253-7.

319. Gho, Y.S., H.K. Kleinman, and G. Sosne, *Angiogenic activity of human soluble intercellular adhesion molecule-1.* Cancer Res, 1999. 59(20): p. 5128-32.

320. Leung, K.H., *Release of soluble ICAM-1 from human lung fibroblasts, aortic smooth muscle cells, dermal microvascular endothelial cells, bronchial epithelial cells, and keratinocytes.* Biochem Biophys Res Commun, 1999. 260(3): p. 734-9.

321. Arendshorst, W.J. and E. Bello-Reuss, *Kidney.*, in *Intercelluar Signaling in Development and Disease*, E.A. Dennis and R.A. Bradshaw, Editors. 2011, Academic Press: Cambridge, MA. p. 141-66.

322. Kinjyo, S., et al., *Polarized secretion of chemokine RANTES and sICAM-1 from a bronchial epithelial cell line BEAS-2B.* J Allergy Clin Immunol., 2000. 105(1): p. S294-5.

323. Kasper, J., et al., *Inflammatory and cytotoxic responses of an alveolar-capillary coculture model to silica nanoparticles: comparison with conventional monocultures.* Part Fibre Toxicol, 2011. 8(1): p. 6.

324. Snyder-Talkington, B.N., et al., *Multi-walled carbon nanotubes induce human microvascular endothelial cellular effects in an alveolar-capillary co-culture with small airway epithelial cells.* Part Fibre Toxicol, 2013. 10: p. 35.

325. Wakatsuki, T., et al., *A distinct mRNA encoding a soluble form of ICAM-1 molecule expressed in human tissues.* Cell Adhes Commun, 1995. 3(4): p. 283-92.

326. Whiteman, S.C., et al., *Human rhinovirus selectively modulates membranous and soluble forms of its intercellular adhesion molecule-1 (ICAM-1) receptor to promote epithelial cell infectivity.* J Biol Chem, 2003. 278(14): p. 11954-61.

327. Ding, F., et al., *Overendocytosis of gold nanoparticles increases autophagy and apoptosis in hypoxic human renal proximal tubular cells.* Int J Nanomedicine, 2014. 9: p. 4317-30.

328. Frohlich, E., *Cellular targets and mechanisms in the cytotoxic action of non-biodegradable engineered nanoparticles.* Curr Drug Metab, 2013. 14(9): p. 976-88.

329. Li, R., et al., *Interference in autophagosome fusion by rare earth nanoparticles disrupts autophagic flux and regulation of an interleukin-1beta producing inflammasome.* ACS Nano, 2014. 8(10): p. 10280-92.

330. Stearns, R.C., J.D. Paulauskis, and J.J. Godleski, *Endocytosis of ultrafine particles by A549 cells.* Am J Respir Cell Mol Biol, 2001. 24(2): p. 108-15.

331. Stern, S.T., P.P. Adiseshaiah, and R.M. Crist, *Autophagy and lysosomal dysfunction as emerging mechanisms of nanomaterial toxicity.* Part Fibre Toxicol, 2012. 9: p. 20.

332. Song, W., et al., *Ceria nanoparticles stabilized by organic surface coatings activate the lysosome-autophagy system and enhance autophagic clearance.* ACS Nano, 2014. 8(10): p. 10328-42.

333. Manthe, R.L., et al., *Therapeutic exocytosis via δ-tocopherol diminishes classical endocytic pathways in a Niemann-Pick disease model: a role for non-classical ICAM-1-mediated transport.* Awaiting submission.

334. Canals, D., et al., *Differential effects of ceramide and sphingosine 1-phosphate on ERM phosphorylation: probing sphingolipid signaling at the outer plasma membrane.* J Biol Chem, 2010. 285(42): p. 32476-85.

335. Cardone, M.H., et al., *Phorbol myristate acetate-mediated stimulation of transcytosis and apical recycling in MDCK cells.* J Cell Biol, 1994. 124(5): p. 717-27.

336. Cheeseman, K.L., et al., *Targeting of protein kinase C-epsilon during Fcgamma receptor-dependent phagocytosis requires the epsilonC1B domain and phospholipase C-gamma1.* Mol Biol Cell, 2006. 17(2): p. 799-813.

337. Holopainen, J.M., M. Subramanian, and P.K. Kinnunen, *Sphingomyelinase induces lipid microdomain formation in a fluid phosphatidylcholine/sphingomyelin membrane.* Biochemistry, 1998. 37(50): p. 17562-70.

338. Lopes Pinheiro, M.A., et al., *Acid sphingomyelinase-derived ceramide regulates ICAM-1 function during T cell transmigration across brain endothelial cells.* J Immunol, 2016. 196(1): p. 72-9.

339. Vihinen, P. and V.M. Kahari, *Matrix metalloproteinases in cancer: prognostic markers and therapeutic targets.* Int J Cancer, 2002. 99(2): p. 157-66.

340. Garnacho, C., D. Serrano, and S. Muro, *A fibrinogen-derived peptide provides intercellular adhesion molecule-1-specific targeting and intraendothelial transport of polymer nanocarriers in human cell cultures and mice.* J Pharmacol Exp Ther, 2012. 340(3): p. 638-47.

341. Baltazar, G.C., et al., *Acidic nanoparticles are trafficked to lysosomes and restore an acidic lysosomal pH and degradative function to compromised ARPE-19 cells.* PLoS One, 2012. 7(12): p. e49635.

342. Bourdenx, M., et al., *Nanoparticles restore lysosomal acidification defects: Implications for Parkinson and other lysosomal-related diseases.* Autophagy, 2016. 12(3): p. 472-83.

343. Cecchelli, R., et al., *Modelling of the blood-brain barrier in drug discovery and development.* Nat Rev Drug Discov, 2007. 6(8): p. 650-61.

344. He, Y., et al., *Cell-culture models of the blood-brain barrier.* Stroke, 2014. 45(8): p. 2514-26.

345. Haseloff, R.F., et al., *In search of the astrocytic factor(s) modulating blood-brain barrier functions in brain capillary endothelial cells in vitro.* Cell Mol Neurobiol, 2005. 25(1): p. 25-39.

346. McConnell, H.L., et al., *The translational significance of the neurovascular unit.* J Biol Chem, 2017. 292(3): p. 762-70.

347. Stamatovic, S.M., R.F. Keep, and A.V. Andjelkovic, *Brain endothelial cell-cell junctions: how to "open" the blood brain barrier.* Curr Neuropharmacol, 2008. 6(3): p. 179-92.